Dynamic Analysis and Control of String-Stiffened Flexible Robotic Manipulators

A thesis submitted in partial fulfillment of the requirements

for the degree of

Doctor of Philosophy

by

Rajesh Ranjan

Roll No: 136103006

Department of Mechanical Engineering

Indian Institute of Technology Guwahati

Guwahati-781039

India

August 2023

Declaration

I declare that this thesis entitled 'Dynamic Analysis and Control of String-Stiffened Flexible Robotic Manipulators' submitted by me is a presentation of original research work done under the guidance of Dr. Santosha Kumar Dwivedy, Professor, Department of Mechanical Engineering, Indian Institute of Technology Guwahati, Guwahati, Assam, India. This work has not been submitted elsewhere for the award of any degree, diploma, associateship, fellowship, or title in this institute or any other university or institution of higher learning.

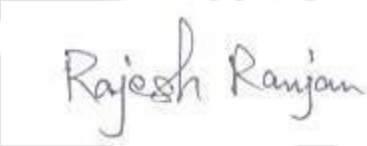

August 2023
Place: IIT Guwahati, Guwahati,
Assam, India, PIN-781039.

Rajesh Ranjan,
Department of Mechanical Engineering,
Indian Institute of Technology Guwahati,
Guwahati, Assam, India, PIN-781039.
Email-ID: rajesh.2013@iitg.ac.in

Certificate

This is to certify that this thesis entitled 'Dynamic Analysis and Control of String-Stiffened Flexible Robotic Manipulators' submitted by 'Rajesh Ranjan' in partial fulfillment of the requirement for the award of the degree of Doctorate of Philosophy, by the Indian Institute of Technology Guwahati, Assam, India, is a record of the *bona fide* research work carried out by him under my guidance and supervision at the Department of Mechanical Engineering, Indian Institute of Technology Guwahati, Guwahati, Assam, India. To the best of my knowledge and belief, no part of the work reported in this thesis has been presented for the award of any degree, diploma, associateship, fellowship, or title in this institute or any other university or institution of higher learning.

August 2023
Place: IIT Guwahati, Guwahati,
Assam, India, PIN-781039.

Dr. Santosha K. Dwivedy
Professor,
Department of Mechanical Engineering,
Indian Institute of Technology Guwahati,
Guwahati, Assam, India, PIN-781039.
Email-ID: dwivedy@iitg.ac.in
Phone: 91-361-2582670

Dedicated to my parents Shrimati (Mrs.) Mira Devi and Shri (Mr.) Mukund Narayan Singh, and my Grandmother Swargiya (Late) Kumudini Devi.

Acknowledgments

First and foremost, I would like to express my wholehearted and sincere gratitude to my advisor Prof. Santosha K. Dwivedy, for his kind support, guidance, encouragement, compassion, and patience throughout this journey. I am grateful to him for all the discussions and the knowledge he imparted and the academic freedom that he has given to me.

I am grateful to my Doctoral committee chairman, Prof. Debabrata Chakraborty, for his critical assessment during the entire period of progress. I extend my sincere thanks to my Doctoral committee members, Prof. Harshal B. Nemade and Prof. Dibakar Bandopadhya for their helpful suggestions.

I extend my sincere thanks to Dr. Basireddy Sandeep Reddy, Dr. Chayan Bhawal, and Dr. Uday Shanker Dixit for their readiness and prompt help in intellectual discussion during my research. The helping and encouraging approach of Dr. Pankaj Biswas towards me is gratefully acknowledged.

I want to express my immense gratitude and heartfelt thanks to my parents Shrimati Meera Devi and Shri Mukund Narayan Singh for their teachings, support, encouragement, and kind blessings. I am deeply indebted to my mother for her sacrifice, selfless service, and nurturing, and for enabling me to focus on and devote my maximum time to my study. I owe my knowledge of Mathematics, Physics, and the English language to my father Shri Mukund Narayan Singh. I offer my heartfelt thanks to my father for his special care in building, guiding, and shaping my knowledge, expertise, and career path. I am grateful to my grandmother Late Kumudini Devi for her tender care, upbringing in my childhood, and for her blessings. I express my gratitude and high regard for my spiritual Guru (Sanskrit words ‘Gu’ means Darkness and ‘Ru’ means light, Guru means a person who takes one from darkness or ignorance to enlightenment) Shri Mangal Kishore Prasad Singh for showing me the path to follow and my destiny in advance at times. I am grateful to my uncle Shri Nripendra Prasad Singh for his guardianship and for cultivating good habits in my childhood. I hold my uncle Late Madhav Prasad Singh in high esteem and owe my gratitude to him. I offer my due respect to my both aunties. I express my sincere thanks and gratitude to my maternal grandfathers Late Dineshwar Prasad Singh and Late Ram Lagan Prasad Singh, my maternal grandmother, maternal uncles Shri Bhanu Pratap Singh, Shri Gyanendra (aka, Mantu)

Prasad Singh, Shri Jainendra (aka, Fantu) Prasad Singh and Ashok Vardhan (aka, Santu) Azad. I am grateful to my Uncle Late Ashoke Prasad Singh and my aunt Smt. Kiran Devi for their kind help and for taking pain in my education. I acknowledge that I have learned the art and pursuit of perseverance and endeavor from my elder brother Mr. Rajesh Kumar Singh. I really enjoyed the company of Mr. Jay Shanker Singh in my childhood. I extend my sincere gratitude to my brother Shri Manish Kumar, sister-in-law Smt. Shalini Singh, sister Smt. Versha Kumari and brother-in-law Shri Nilamber Kumar Singh for their support during my Ph. D. work. I am thankful to my father-in-law Late Bishnu Deo Singh, mother-in-law Smt. Sunita Devi, brother-in-law Shri Rahul Prasad Singh for their support and patience. Last but not least, I thank my wife Smt. Sujata Singh for her patience, care, and standing with me through thick and thin.

I sincerely thank all whose expressed or unexpressed well wishes helped me to move forward in the journey. I also extend my gratitude towards the vital elements, the surroundings with their scenic beauty and lush greenery, the fresh breeze, space, fire, and sweet water which provide thriving support and opportunities to the student community inside the IIT Guwahati campus which is situated at the bank of the mighty Brahmaputra river. Also, I would like to express my thanks to all the workers, managers, and administrators who are part of the institute system for their constant efforts to keep the system running efficiently.

I am grateful to the divine God ‘Shiv’ who is the source of all divine energy, without whose grace, nothing can be achieved. I recite 108 times ‘Om Namah Shivay’, (I bow my head before the God Shiv).

Finally, salutation to his holiness, whose divine grace has always guided me and filled me with a sense of deep understanding.

Rajesh Ranjan

August 2023
Place: Guwahati

Rajesh Ranjan
Department of Mechanical Engineering,
IIT Guwahati, Guwahati, India-781039.

Abstract

Flexible link manipulators (FLMs) although have many advantages over rigid link manipulators like low weight, less power consumption, increased maneuverability, and swift action, they exhibit inherent structural deformation which makes them oscillatory. The oscillatory behavior of the manipulator is exhibited even after the end of the motion. This is called residual vibration of the link. This affects the accuracy and settling time of the end-effector which, in turn, limits the repeatability of the manipulator in high-speed engineering applications. So, in order to carry out any task satisfactorily, it is necessary to control the tip deflection of FLMs. This requires accurate dynamic modeling of flexible manipulators. Although the model-free control method also is gaining popularity in recent years, without accurate dynamic modeling, it may be unstable and may pose difficulty in ensuring precise control of the complex robots in the actual working environments. It also needs extensive experience. Therefore, the accurate dynamic model is still an important step in the precision control of a flexible manipulator which exhibits highly coupled and nonlinear dynamic behaviors. However, the dynamics of the system are highly nonlinear and complex which, in turn, complicates control of the end-effector. The effective inertia of the system changes as a nonlinear function of robot configuration. Flexural dynamics application complicates the problem much further which leads to serious problems in the modeling and control of the system.

To tackle the problem of suppression of residual vibrations, various types of control techniques are being applied by different researchers, such as shape optimization of links, passive damping using viscoelastic damping layer on the links in conjunction with active damping using piezoelectric sensors and actuators, trajectory optimization, variable stiffness actuators, etc.

In all these attempts by different researchers, the main aim is to control the tip deflection of an FLM. However, the same can also be achieved by using a pair of strings. The fact that the axial stiffness of a string is much larger than the bending stiffness of a cantilever beam of the same material and area of cross-section, can be effectively utilized to significantly increase the stiffness of an FLM if arranged in the proper configuration.

The theoretical analysis in the present thesis shows that through stiffening by a pair of strings, the tip deflection can be reduced significantly without adding much weight to the manipulator. Therefore, string-stiffened flexible link manipulators (SSFLMs) seek the attention of current researchers for the systematic study of its behavior during operations. In the present study, systematic mathematical modeling, analysis, and control of a string-stiffened flexible-joint flexible-link manipulator have been carried out.

In the present thesis, kinematic and dynamic analyses of a manipulator with a rigid link and flexible joint, a manipulator with flexible links, and manipulators with both link and joint flexibilities have been studied. Kinematic and dynamic modeling of flexible manipulators with the finite element method and assumed mode method both have been done.

First of all, it has been determined that how the dynamic behavior of a flexible link manipulator depends on various parameters of the manipulator. Transverse deflection, axial deflection, and flexural rotation in the modeling of the flexible link have been considered using both the finite element method and the assumed mode method. Thorough investigations of a string-stiffened flexible link manipulator have been done. Passive and active, both types of control have been applied to minimize the tip deflection of a flexible link manipulator.

Planar as well as three-dimensional manipulators have been studied. Both single and multilink manipulators have been studied in the present work. In the study on coordinating manipulators for handling hazardous chemicals, motion synchronization of coordinating manipulators with respect to time and position has been considered.

In this research work, five problems related to flexible manipulators have been investigated. In the first work, parametric studies of a two-link flexible manipulator both the links of which are flexible, are studied. Kinematic and dynamic modeling has been done using the finite element method. The effects of different parameters of the manipulators like link length ratio, link diameter ratio, ratio of payload mass to the total mass of both links as well as the effect of different input torque profiles on the tip deflections, slopes at the tips, angular displacements and velocities of both the links of the manipulator have been investigated. The effects of torques due to gravity and centrifugal and Coriolis forces also have been studied. Time versus tip deflection and joint response plots are obtained for different parameter ratios which will help a designer to decide the optimal values of parameters of the manipulator for obtaining minimum tip deflection.

In the second problem dynamic analysis of a single-link flexible manipulator has been carried out using the finite element method. Control and elimination of residual vibration of the tip of the manipulator have been achieved using the linear quadratic regulator (LQR) optimal control technique.

In the third and fourth problems, the tip deflections of a single-link and a rigid-flexible double-link flexible manipulator have been increased with the help of a pair of strings tied on both sides of the flexible link. Kinematic and dynamic analyses of the string-stiffened flexible link manipulators are carried out in these works. The assumed mode method has been applied for the discretization of the flexible link. Mode shapes of a cantilever beam with axial load have been used. The dynamic behavior of cables during the operation of the manipulator and their effect on the link vibration are obtained. The effects of pulling of link tip by the pair of cables on the joint of the manipulator have also been investigated. The axial deformation of the flexible link was taken care of. The buckling strength of the flexible link also has been considered. The effect of tension in the pair of strings on the tip deflection has been ascertained. The effect of geometric nonlinearities on the dynamic responses of the string-stiffened flexible link manipulators (SSFLMs) is found. Although the string-stiffening of the flexible manipulator decreased the tip deflections of the flexible links, residual vibration of the links still persisted which has been eliminated by applying robust PID and impedance control.

In the fifth and the last problem, kinematic and dynamic analyses of two three-dimensional robotic manipulators of 3 joint axes each employed in cooperative handling of a job are carried out. Synchronization of motions of these manipulators with respect to time of motion and position of their end-effector (tip) has been carried out. Path planning of these robots also has been done. Jerks at the start and end of the trajectories of the manipulators are minimized.

Keywords**:** rigid link manipulators, 3R manipulators, coordinating manipulators, path planning, flexible link manipulators, flexible joint manipulators, string-stiffened flexible link manipulators, parametric study, finite element analysis, assumed mode method, kinematic and dynamic analyses, position control, force control, vibration control, PID control, impedance control, LQR control, optimal control

Contents

Declaration . . . . . **i**

Certificate . . . . . **iii**

Dedication of the Present Work . . . . . **v**

Acknowledgements . . . . . **vii**

Abstract . . . . . **ix**

Contents . . . . . **xiii**

List of Figures . . . . . **xix**

List of Tables . . . . . **xxv**

Abbreviations . . . . . **xxvii**

Chapter 1: Introduction **1**

1.1 Background 1
1.2 Rigid Manipulators 2
1.3 Flexible Manipulators 2
1.4 Cooperative Manipulators 4
1.5 Control of Flexible Manipulators 5
1.6 Applications of Flexible and Cooperative Manipulators 6
1.7 Need of the Present Investigation 8
1.8 Thesis Organization 10

Chapter 2: Literature Review **11**

2.1 Introduction 11
2.2 Modelling and Control of Flexible Link Manipulators 11
2.2.1 Single Link Manipulators 12
2.2.2 Two and Multilink Manipulators 12

2.2.3 Parallel Manipulators 15
2.3 Mathematical and Experimental Studies of Flexible Joint and Flexible Link Manipulators 15
2.3.1 Modeling of Flexible Manipulators 16
2.3.2 Kinematic Analysis of Flexible Manipulators 19
2.3.3 Dynamic Analysis of Flexible Manipulators 19
2.3.4 Numerical Studies of Flexible Manipulators 22
2.3.5 Trajectory Planning of Flexible Manipulators 23
2.3.6 Experimental Studies on Flexible Manipulators 24
2.4 Control of Flexible Manipulators 25
2.4.1 Proportional, Integral and Derivative Control 25
2.4.2 Optimal Control Methods 25
2.4.3 Sliding Mode Control 26
2.4.4 Adaptive Control 26
2.4.5 Fuzzy Logic Control 27
2.4.6 Neural Network Control 28
2.4.7 Miscellaneous Types of Control Methods 29
2.5 Application of Flexible Manipulators 32
2.6 Cooperative Manipulators 35
2.6.1 Historical Review of Cooperative Manipulators 35
2.6.2 Kinematic Analysis of Cooperative Manipulators 37
2.6.3 Dynamic Analysis and Control of Cooperative Manipulators 39
2.6.4 Modeling and Control of Flexible Cooperative Manipulators 41
2.7 Modeling and Control of Manipulators Working in Coordination 42
2.8 Summary and Identification of Research Gap 43
2.8.1 Summary of Research Work 43
2.8.2 Identification of Research Gap 46
2.9 Objective of the Present Work (Problem Formulation) 49

Chapter 3: Parametric Study of a Two-Link Flexible Manipulator 51

3.1 Introduction 51
3.2 Finite Element Modelling of the Manipulator 51
3.3 Kinematic Analysis 52
3.4 Dynamic Analysis 56
3.4.1 Dynamic Equation of Motion 60
3.4.2 Boundary Conditions 61
3.4.3 Rayleigh Damping 62
3.4.4 Torques Applied at Joints 62
3.5 Results and Discussions 64
3.6 Verification of Results 79
3.7 Conclusions 81

Chapter 4: Dynamic Analysis and Control of a Single-Link Flexible Manipulator Using Finite Element Method 83

4.1 Introduction 83
4.2 Finite Element Modelling of the Manipulator 84
4.2.1 Boundary Conditions 89
4.2.2 Application of Damping 89
4.2.3 Final Equation of Motion of the System 90
4.3 Control of the FLM and FJFLM 90
4.3.1 Stability Analysis 93
4.4 Results and Discussions 94
4.4.1 Verification of Results 94
4.4.2 Control of Tip Vibration 103
4.5 Conclusions 107

Chapter 5: Dynamic Analysis and Control of a String-Stiffened Single-Link Flexible Manipulator 109

5.1 Introduction 109
5.2 Modelling 109

5.2.1 Force Consideration 110
5.2.2 General Equation of Motion of a String-Stiffened Flexible Link . . . 112
5.2.3 Dynamic Equation of Motion of the Single-Link Flexible Manipulator . 120
5.3 Control of the Flexible-Joint and Flexible-Link Manipulator 124
5.3.1 Control of the SSSLFM When Joint Flexibility is Not Considered . . . 125
5.3.2 Control of the SSSLFM When Joint Flexibility is Considered 126
5.4 Results and Discussions 129
5.4.1 Taking the Effect of String Vibration 132
5.4.2 Verification of Results 135
5.4.3 The Effect of Axial Displacement and Load and Geometric Nonlinearity 143
5.4.4 Control of Tip Vibration 145
5.4.4.1 Control of the SSSLFM When Joint Flexibility is Not Considered. 145
5.4.4.2 Flexible Joint Control 146
5.4.4.3 Flexible Joint and Flexible Link Control 148
5.5 Conclusion 150

Chapter 6: Dynamic Analysis and Control of a String-Stiffened Rigid-Flexible Two-Link Manipulator 151

6.1 Introduction 151
6.2 Modelling 151
6.2.1 Dynamic Equation of Motion of the Two-Link Rigid-Flexible Manipulator 153
6.3 Control of Tip Vibration 156
6.3.1 Flexible Link Control 156
6.3.2 Flexible-Link and Flexible-Joint Control 157
6.4 Results and Discussions 159
6.4.1 Tip Deflection of the Manipulator without any String Attachment . . . 161
6.4.2 Tip Deflection of the String-Stiffened Manipulator without Considering String Vibration 162

6.4.3 Tip Deflection of the String-Stiffened Manipulator when String Vibration is Also Considered 162
6.4.4 Verification of Results 166
6.4.5 Control of Tip Vibration 171
6.4.5.1. Flexible Link Control 171
6.4.5.2. Flexible Joint and Flexible Link Control 174
6.5 Conclusions 176

Chapter 7: Kinematic and Dynamic Analyses of Two 3R Co-ordinating Manipulators 177

7.1 Introduction 177
7.2 Kinematics of the Manipulators 178
7.2.1 Inverse Kinematics 180
7.3 Dynamic Equations 180
7.3.1 Effect of Joint Flexibility 181
7.4 Results and Discussion 183
7.4.1 Trajectory Planning 183
7.4.2 Calculation of External Load M_i on Wrist 185
7.4.3 Kinematics and Dynamics of the Manipulators without Considering Joint Flexibility 186
7.4.4 Effect of Joint Flexibility 190
7.5 Conclusion 190

Chapter 8: Conclusions and Scope of Future Work 191

8.1 Introduction 191
8.2 General Conclusions 191
8.3 Specific Conclusions 193
8.3.1 Parametric Study of a Two-Link Flexible Manipulator 193
8.3.1.1 Effect of link length ratio δ on the dynamic response of the manipulator 193

8.3.1.2 Effect of link diameter ratio ν on the dynamic response of the manipulator 193
8.3.1.3 Effect of payload mass (at the tip of 2nd link) on dynamic response of the manipulator 194
8.3.1.4 Effect of torque profile on the dynamic response of the manipulator. 194
8.3.1.5 Effect of torque due to gravity and the Coriolis and centrifugal forces on the dynamic response of the manipulator 195
8.3.1.6 Effects of different parameters on the dynamic response of the manipulator 195
8.3.2 Dynamic Analysis and Control of a Single-Link Flexible Manipulator Using Finite Element Method 196
8.3.3 Dynamic Analysis and Control of String-Stiffened Flexible Manipulator with Flexible Joint 197
8.3.4 Kinematic and Dynamic Analysis of Two 3R Coordinating Manipulators 198
8.5 Scope of Future Work 199

Bibliography 201

List of Publications 245

List of Figures

1.1 Schematic representation of a rigid manipulator. 3

1.2 Schematic representation of a flexible manipulator with flexible joint and rigid link. 3

1.3 Schematic representation of a flexible link manipulator with a rotary joint . . 3

1.4 Schematic representation of a flexible manipulator with flexible joint and flexible link. 3

1.5 Cooperative handling of an object. 4

1.6 Flexible manipulators: **(a)** Canadarm2 **[**Source: http://www.asc-sa.gc.ca/eng/iss/mobile-base/default.asp], and **(b)** Dextre, [Source:http://en.wikipedia.org/wiki/Dextre#mediaviewer/File:Dextrereally hasnohead.jpg]. 7

1.7 Use of robots in construction: **(a)** robotic manipulator used for ceramic fitting, **(b)** an example of a carpentry aid wearable robot under, **(c)** ROCCO project brick assembly robot, **(d)** an example of a wearable welding robot under development [Source: http://cdn.intechopen.com/pdfs-wm/5555.pdf]. . 8

3.1 A two-link flexible manipulator. 52

3.2 Effect of link-length ratio on the dynamic behavior: **(a)** torque on the hub, **(b)** torque on 2nd joint, **(c)** angular displacement of the hub, **(d)** angular displacement of joint 2, **(e)** joint 1 angular speed, **(f)** joint 2 angular speed **(g)** tip deflection of link 1, **(h)** tip deflection of link 2, **(i)** flexural rotation of link 1 and **(j)** flexural rotation of link 2. 68

3.3 Effect of link-diameter ratio on the dynamic behavior: **(a)** torque on the hub, **(b)** torque on 2nd joint, **(c)** angular displacement of the hub, **(d)** angular displacement of joint 2, **(e)** joint 1 angular speed, **(f)** joint 2 angular speed **(g)** tip deflection of link 1, **(h)** tip deflection of link 2, **(i)** flexural rotation of link 1 and **(j)** flexural rotation of link 2. 71

3.4 Effect of mass ratio of payload to manipulator on dynamic behavior: **(a)** torque on hub, **(b)** torque on 2nd joint, **(c)** angular displacement of hub, **(d)** angular displacement of joint 2, **(e)** joint 1 angular speed, **(f)** joint 2 angular speed **(g)** tip deflection of link 1, **(h)** tip deflection of link 2, **(i)** flexural rotation of link 1 and **(j)** flexural rotation of link 2. 73

3.5 Effect of torque profiles on the dynamic behavior: **(a)** torque on hub, **(b)** torque on 2nd joint, **(c)** angular displacement of hub, **(d)** angular displacement of joint 2, **(e)** joint 1 angular speed, **(f)** joint 2 angular speed **(g)** tip deflection of link 1, **(h)** tip deflection of link 2, **(i)** flexural rotation of link 1 and **(j)** flexural rotation of link 2. 75

3.6 Effect of link-length ratio on the dynamic behavior for **(a)** angular displacement of the hub, **(b)** angular displacement of joint 2, **(c)** tip deflection of link 1, **(d)** tip deflection of link 2. 76

3.7 Effect of link-length ratio on dynamic behavior: **(a)** angular displacement of the hub, **(b)** angular displacement of joint 2, **(c)** tip deflection of link 1, **(d)** tip deflection of link 2. 77

3.8 Dynamic response for the damping ratio: **(a)** angular displacement of the hub, **(b)** angular displacement of joint 2, **(c)** tip deflection of link 1, and **(d)** tip deflection of link 2. 79

3.9 Angular displacement **(a)** joint 1, **(b)** joint 2 **(c)** tip deflections of link1 and link 2, and **(d)** slopes at the tips of links 1 and 2. 80

4.1 Finite element modeling of the manipulator: **(a)** Discretization scheme of the manipulator and **(b)** position of the manipulator with time. 84

4.2 Input given to the manipulator's joint: **(a)** angular displacement, **(b)** angular velocity, and **(c)** angular acceleration. 96

4.3 Tip motion of the FLM: **(a)** axial displacement, **(b)** transverse displacement **(c)** slope at the tip **(d)** axial velocity, **(e)** transverse velocity **(f)** time rate of change of slope at the tip **(g)** axial acceleration, **(h)** transverse acceleration **(i)** differentiation of slope at the tip twice with respect to time. 98

4.4 The trapezoidal angular velocity profile of the motor. 100

4.5 The motion of FJFLM at different points on the flexible link in transverse direction: **(a)** displacement at sensor point, **(b)** velocity at sensor point, **(c)** acceleration at sensor point, **(d)** displacement at payload point, **(e)** velocity at payload point and **(f)** acceleration at payload point. 102

4.6 Modal response for **(a)** FLM, and **(b)** FJFLM. 103

4.7 Motion control of the tip of the FLM using LQR optimal control: **(a)** axial displacement, **(b)** axial velocity, **(c)** transverse displacement, **(d)** transverse velocity, **(e)** slope at the tip, and **(f)** rate of change of slope at the tip. . . . 105

.

4.8 Motion control of the Tip of the FJFLM using LQR optimal control: **(a)** axial displacement, **(b)** axial velocity, **(c)** transverse displacement, **(d)** transverse velocity, **(e)** slope at the tip and **(f)** rate of change of slope at the tip. 106

5.1 A schematic diagram of the SSSLFM: **(a)** as viewed from the top **(b)** as viewed from the front. 110

5.2 CAD model of the SSSLFM in Solidworks 2019 as viewed from **(a)** the front and **(b)** the top. 111

5.3 Forces acting on the flexible link with the payload. 112

5.4 Modeling of string oscillations: **(a)** boundary conditions at the end of the stiffening string **(b)** deflection of the string. 117

5.5 A single-link flexible manipulator. 122

5.6 Input given to the manipulator joint: **(a)** angular displacement, **(b)** angular velocity, and **(c)** angular acceleration. 131

5.7 Tip deflection of the SSSLFM in **(a)** Case 1, **(b)** Case 2, and **(c)** Case 3. . . 133

5.8 Tip deflections of the SSFLM in **(a)** Case 4, **(b)** Case 5, and **(c)** Case 6. . . 134

5.9 Tip deflection of the flexible link manipulator without any string stiffening. 134

5.10 Input profile: **(a)** angular displacement, **(b)** angular velocity, and **(c)** angular acceleration of input given to the motor. 137

5.11 Link tip deflection and rate of change of the deflection when no payload is applied and the link is without any string attachment: **(a)** link tip deflection **(b)** time rate of change of the tip deflection. 138

5.12 Link tip deflection and its rate of change when a payload of 180×10^{-3} kg is applied and the link is without any string attachment: **(a)** link tip deflection **(b)** time-rate of change of the tip deflection. 138

5.13 Modal analysis results of ANSYS for the FLM without string-stiffening . . 139

5.14 Tip deflections when boundary conditions I(a) of Case I have been applied to Eq. (5.49) when: (a) $T_1 = T_2 = 0.25P_{Cr}$, (b) $T_1 = T_2 = 0.29P_{Cr}$, (c) $T_1 = T_2 = 0.30P_{Cr}$, (d) $T_1 = T_2 = 0.40P_{Cr}$, (e) $T_1 = T_2 = 0.50P_{Cr}$ and (f) $T_1 = T_2 = 0.60P_{Cr}$. 141

5.15 Tip deflections of the link for different values of tensions in strings when the tip is free to move: (a) $T_1 = T_2 = 0.25P_{Cr}$, (b) $T_1 = T_2 = 0.50P_{Cr}$, (c) $T_1 = T_2 = 0.60P_{Cr}$, (d) $T_1 = T_2 = 0.61P_{Cr}$, (e) $T_1 = T_2 = 0.62P_{Cr}$ and (f) $T_1 = T_2 = 0.65P_{Cr}$. 142

5.16 Tip deflection of the SSSLFM when few of the above-mentioned factors are not considered. 144

5.17 Tip deflection and joint motion control of the string stiffened flexible link manipulator **(a)** tip deflection, **(b)** rate of change of tip deflection, **(c)** joint angular displacement, and **(d)** joint angular speed. 146

5.18 Tip deflection control of the flexible joint-flexible link string stiffened manipulator: **(a)** tip deflection, **(b)** rate of change of tip deflection, **(c)** joint angular displacement, and **(d)** joint angular speed. 147

5.19 Tip deflection control of the flexible joint-flexible link string-stiffened single link manipulator: **(a)** tip deflection, **(b)** rate of change of tip deflection, **(c)** joint angular displacement, and **(d)** joint angular speed. 149

6.1 A schematic diagram of the string-stiffened rigid-flexible two-link manipulator (SSRFTLM) as viewed from (a) the top and (b) the front. . . 152

6.2 The 3D CAD model of the SSRFTLM obtained using SOLIDWORKS 2019. 152

6.3 A two-link rigid-flexible manipulator. 153

6.4 The motion of joint 1 and joint 2: **(a)** angular displacement, **(b)** angular velocity, and **(c)** angular acceleration. 161

6.5 Tip deflection of the SSRFTLM with a payload but without any string-stiffening. 162

6.6 Tip deflection of the SSRFTLM in **(a)** Case 2, **(b)** Case 3, and **(c)** Case 4 . . 164

6.7 Tip deflections of the SSRFTLM in **(a)** Case 5, **(b)** Case 6, and **(c)** Case 7. . 165

6.8 The motion of joint 1 and joint 2: **(a)** angular displacement, **(b)** angular velocity, and **(c)** angular acceleration. 168

6.9 Tip deflection $w_{Tip\,2}$ when tensions T_1 and T_2 in the strings are: **(a)** $T_1 = T_2 = 0.10P_{Cr}$, **(b)** $T_1 = T_2 = 0.20P_{Cr}$, **(c)** $T_1 = T_2 = 0.25P_{Cr}$, **(d)** $T_1 = T_2 = 0.30P_{Cr}$, **(e)** $T_1 = T_2 = 0.40P_{Cr}$, **(f)** $T_1 = T_2 = 0.50P_{Cr}$, **(g)** $T_1 = T_2 = 0.55P_{Cr}$, and **(h)** $T_1 = T_2 = 0.60P_{Cr}$.. 170

6.10 Tip deflection control of the SSRFTLM: **(a)** tip deflection of link 2 $w_{Tip\,2}$, **(b)** rate of change of tip deflection of link 2 $\dot{w}_{Tip\,2}$ w.r.t. time, **(c)** joint angular displacement of link 1, **(d)** joint angular displacement of link 2, **(e)** joint angular speed of link 1, and **(f)** joint angular speed of link 2. 173

6.11 Tip deflection control of the SSRFTLM: **(a)** tip deflection of link 2 $w_{Tip\,2}$, **(b)** rate of change of tip deflection of link 2 $\dot{w}_{Tip\,2}$ w.r.t. time, **(c)** joint angular displacement of link 1, **(d)** joint angular displacement of link 2, **(e)** joint angular speed of link 1, and **(f)** joint angular speed of link 2. 175

7.1 Schematic diagram of cooperative manipulators A and B handling hazardous chemicals. 178

7.2 Link coordinate system for the two manipulators up to gripper. 179

7.3 Two manipulators cooperatively handling hazardous chemicals (There is a 4 mm of gap between the two containers at the time of pouring). 185

7.4 Joint angle of manipulator A before torque smoothening. 187

7.5 Joint angle of manipulator A after torque smoothening. 187

7.6 Joint angle of manipulator B before torque smoothening. 187

7.7 Joint angle of manipulator B after torque smoothening. 187

7.8 Joint velocity of manipulator A before torque smoothening. 188

7.9 Joint velocity of manipulator A after torque smoothening. 188

7.10 Joint velocity of manipulator B before torque smoothening. 188

7.11 Joint velocity of manipulator B after torque smoothening. 188

7.12 Joint angular acceleration of manipulator A before torque smoothening. . . 188

7.13 Joint angular acceleration of manipulator A after torque smoothening. . . 188
7.14 Joint angular acceleration of manipulator B before torque smoothening. . . 189
7.15 Joint angular acceleration of manipulator B after torque smoothening. . . 189
7.16 Joint torque of manipulator A before torque smoothening. 189
7.17 Joint torque of manipulator A after torque smoothening. 189
7.18 Joint torque of manipulator B before torque smoothening. 189
7.19 Joint torque of manipulator B after torque smoothening. 189
7.20 Variation of joint torque with time for manipulator A. 190
7.21 Variation of joint torque with time for manipulator B. 190

List of Tables

3.1	Inertial and elastic properties of the links of the manipulator	65
3.2	Maximum values of tip deflections	66
3.3	Rayleigh damping coefficients	79
3.4	Inertial parameters of the FLM [Usoro et al. (1986)]	80
4.1	Description of finite element modeling of the system	85
4.2	Numerical values of the parameters used for FJFLM	94
4.3	Frequencies and tip deflection values of FLM and FJFLM	98
4.4	Analytical constants, dimensions, and material properties of FJFLM [Malgaca et al. (2016)]	99
5.1	Dimensions and material properties of SSSLFM	130
5.2	The Maximum tip deflection at the steady state and natural frequencies of the oscillations of the link and the strings	136
5.3	Dimensions and material properties of SSSLFM [Dixit and Kumar (2016)]	137
5.4	Deflection and frequency without any string attachment	139
5.5	Values of tip deflections at steady state and first natural frequencies of vibration of the flexible link	144
5.6	Controller gains	145
5.7	Joint properties	148
5.8	Controller gains for controlling both joint and link flexibility	148
6.1	Dimensions and material properties of the SSRFTLM	159
6.2	Values of tip deflections and first natural frequencies of vibration of the SSRFTLM	166
6.3	Dimensions and material properties of SSSLFM [Dixit and Kumar (2016)]	167
6.4	Values of tip deflections and frequencies of vibrations of the manipulator for different values of tensions in the pair of strings	170
6.5	Controller gains	172
6.6	Joint properties	174
7.1	Arm link coordinate parameters	179
7.2	Link mass and center of gravity	183

7.3 Actuator and link Inertia 183

Abbreviations

3-D	three dimensional
AMM	assumed mode method
APID	adaptive proportional-integral-derivative
DoF	degrees of freedom
FE	finite element
FEA	finite element analysis
FEM	finite-element method
FJFLM	flexible-joint flexible-link manipulator
FLM	flexible link manipulator
FLMs	flexible link manipulators
LQ	Linear Quadratic
LQR	linear quadratic regulator
PID	proportional-integral-derivative
RRR	revolute-revolute-revolute
SLFJFLM	single-link flexible-joint flexible-link manipulator
SLFM	single-link flexible manipulator
SSFLMs	string-stiffened flexible link manipulators
SSRFTLM	string-stiffened rigid-flexible two-link manipulator
SSSLFM	string-stiffened single-link flexible manipulator

Chapter 1

Introduction

1.1 Background

A robotic manipulator arm is defined as a reprogrammable multifunctional mechanical device used for moving material, parts, objects, or tools through programmed motions in order to perform various tasks. These human arm-like mechanical devices are composed of an assembly of links and joints. Links are defined as the rigid or flexible sections that make up the mechanism and joints are defined as the connection between two links.

Robotic manipulators may have one to ten axes of motion. Six-axis robotic manipulators are the most common since their range of motion is similar to the human arm. This provides the flexibility required to automate many industrial processes with robots.

Links and joints may be rigid or flexible. A link is said to be flexible if it exhibits flexural deformations while in motion. Similarly, a flexible joint has oscillatory rotational motion. Depending upon the nature of joints and links manipulators are composed of, they can be of the following types:

1. Manipulators with rigid joints and rigid links
2. Manipulators with flexible joints and rigid links
3. Manipulators with rigid joints and flexible links
4. Manipulators with flexible joints and flexible links

It is desired to design lighter robots with large payload-to-weight ratios that can also operate at higher speeds which makes them a subject of intensive research. Additional degrees of freedom are added when the flexibility of joints and links is considered. So, the major challenge is to control their end-point deflections in order to effectively utilize their advantages. Here, in the present research work, an innovative method of controlling their end-point precision by way of stiffening their flexibility using strings while retaining their advantage of being lightweight has been presented. The present thesis deals with manipulators with flexible joints and rigid links,

manipulators with rigid joints and flexible links, as well as manipulators with both flexible joints and flexible links.

1.2 Rigid Manipulators

Fig. 1.1 shows the schematic diagram of a single link rigid manipulator with a rigid joint at 'O' and a rigid link AB. There is a payload at point B at the tip of the manipulator. When torque τ is applied at the joint, the manipulator moves from position AB at an angle θ_i and time t_i to position AC at an angle θ_f with respect to the axis OX of the inertial frame of reference XOY at the time t_f.

1.3 Flexible Manipulators

For engineers, there is no such thing as a rigid body. According to Hayden (1965), all materials have finite stiffness and hence deform elastically under normally applied forces and moments. There are two kinds of flexibilities found in a serial manipulator: joint flexibility and link flexibility. Manipulators with any one or more numbers of either flexible joints or flexible links or with a combination of flexible joints and flexible links are called flexible manipulators.

When the joint of a manipulator that consists of a drive and gear assembly can be considered as torsional spring, the manipulator is called as flexible joint manipulator. The schematic diagram of the manipulator is shown in Fig. 1.2. XOY represents the inertial frame of reference. xoy is the reference frame at the root of the link axes which are parallel to the base frame. θ_m is the angular displacement of the driving motor at the joint and τ_m is motor torque applied by the motor on the joint of the manipulator. Let M_p be the mass of the payload and J_p be the rotational inertia of the payload. The link has planar motion. The motor at the joint is modeled as a torsional spring of spring constant K_T.

Fig. 1.3 shows the schematic diagram of a single link flexible manipulator in which the link is flexible and is shown in deformed condition while in operation. XOY is the immovable base frame while xoy is body attached rotating frame at the trailing end of the link AB. R_H is the radius of the hub of the manipulator. $\theta_l(t)$ is the angular displacement of the rigid joint at time t. $u(s,t)$ is the deflection of the link at s and time t in the axial direction. $w(s,t)$ is the deflection

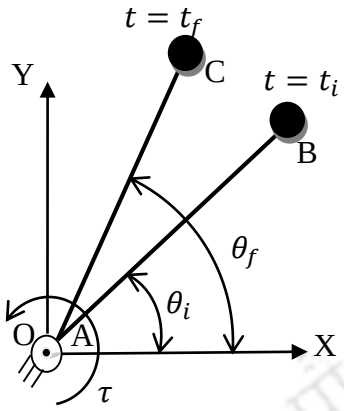

Figure 1.1: Schematic representation of a rigid manipulator.

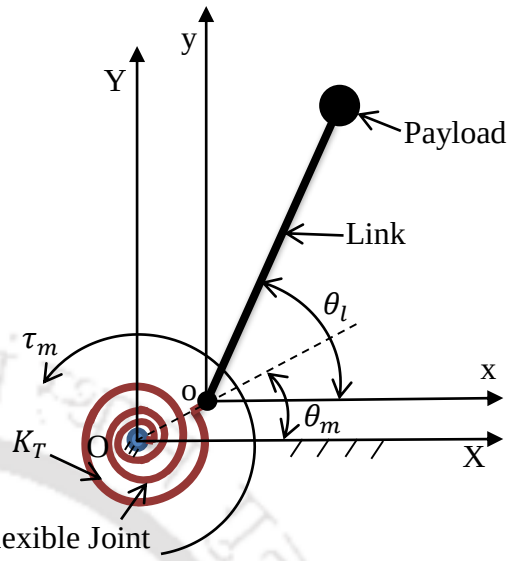

Figure 1.2: Schematic representation of a flexible manipulator with flexible joint and rigid link.

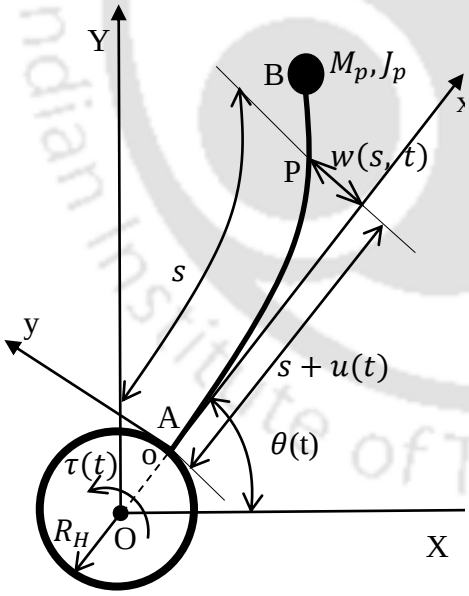

Figure 1.3: Schematic representation of a flexible link manipulator with a rotary joint.

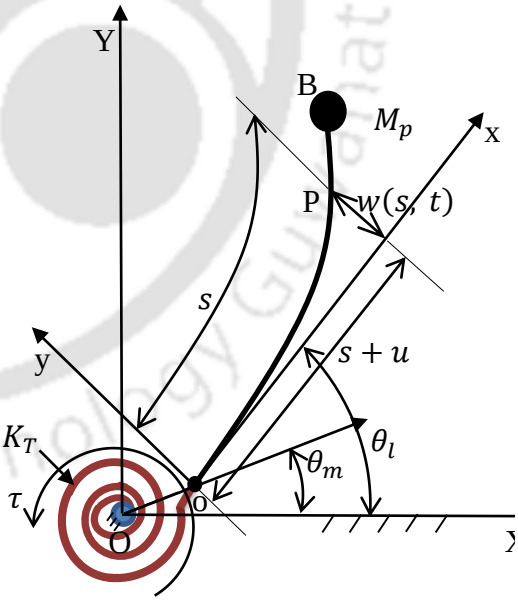

Figure 1.4: Schematic representation of a flexible manipulator with flexible joint and flexible link.

of the link in the transverse direction at any point P on the link. $\tau(t)$ is the motor torque applied on the joint.

At the tip B of the link, there is a payload of mass M_p and rotational inertia J_p. If the joint of the manipulator is also flexible then it can be represented as shown in Fig. 1.4. The flexible joint of the manipulator has been modeled as a torsional spring of spring constant K_T. The torque supplied by the motor is τ_m. Here, θ_m and θ_l represent respectively the angular displacements of the motor and the link of the manipulator.

1.4 Cooperative Manipulators

Many tasks that are difficult or even impossible to execute by a single robot can become affordable when two or more manipulators are employed in a cooperative manner. Not only this, keeping in view the lack of skilled manpower or limitations of human operators, robots in the near

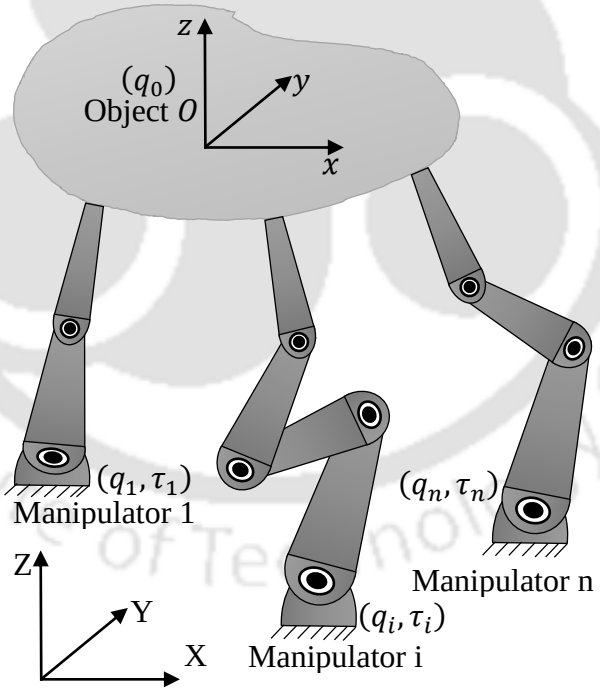

Figure 1.5: Cooperative handling of an object.

future will perform tasks together with humans. The use of two or more independent arms for manipulation tasks has several advantages over conventional robots. For instance, a cooperative

system can reduce the need for custom fixtures, permit the use of a simpler tool, and handle flexible objects. Furthermore, heavy objects can be manipulated by sharing the load among many robots. Cooperative manipulators are a group of two or more robotic arms that carry out together the task of cooperative manipulation of a common object. But the use of cooperative manipulators requires more advanced modeling and control techniques. Fig. 1.5 shows cooperative handling of an object by a group of manipulators. The tasks performed by cooperative manipulators can be achieved in teleoperated, semi-autonomous, or autonomous ways. The benefits of cooperative manipulators are help in load distribution between manipulators, an increase of manipulation dexterity, and integration of different team member skills.

1.5 Control of Flexible Manipulators

The dynamic model of FLMs is nonlinear and coupled with differential equations. Strong coupling exists between the rigid body motion and the elastic modes. The primary objective of control for an FLM is to compute the input torque required to drive the system to a desired trajectory and minimize the oscillation of the link tip. Both types of control can be applied to FLMs: open-loop control and closed-loop control. In open loop control, the input signal is computed based on reference trajectory, and tip oscillation is controlled by modifying the input signal considering the flexural properties of FLMs. The command shaping technique, time optimal control, computed torque method based on model inversion, etc. are the open loop control methods. The advantage of the command shaping technique is that it computes the input signal to minimize the residual vibrations without measurement data by solving a set of linear equations. In the computed torque method, the input torque is computed using model inversion law based on the desired output trajectory. Feedforward control is developed based on the inverse dynamic model. The dynamic model is derived in the form of differential-algebraic equations. The open loop control methods are simple and require less measurement but they are very sensitive to modeling errors, system parameter variation, and uncertainty in the implementation of desired trajectory. To overcome these drawbacks, feedback is required to monitor the system behavior to improve the performance of the controller and ensure the stability of the system. Control systems with feedback loops are called closed-loop control systems. The feedback linearization method, singular perturbation method, robust control, adaptive control, sliding mode control, pole placement method, and intelligent control methods such as fuzzy logic control, neural network control, etc.

are examples of closed-loop control that are applied in vibration control of FLMs. In PID feedback control, the errors in joint angular position and velocity with respect to reference trajectory are used in a feedback loop with constant gains. The gains are calculated based on the dynamic equation of motion of the vibrating system. The stability of the closed-loop control system is analyzed using the Lyapunov theorem or root locus method. Using the singular perturbation method, the system dynamics are divided into slow and fast dynamics, and a two-stage controller is developed to tackle system oscillations and trajectory tracking. Slow dynamics are used mainly to control the rigid body motion along the predefined trajectory in joint space. Fast dynamics are responsible for the stability of the vibrating system along the joint trajectory. Fast dynamics and slow dynamics are controlled separately. In this approach, the spillover problem in the fast dynamics is bounded by a perturbation parameter. The robust controllers are used for accurate trajectory tracking of FLMs in the presence of parameter uncertainties due to stiffness, damping, unknown payload mass, and unmodelled disturbances such as joint friction. When the model uncertainties are large and the bounds of uncertainty cannot be estimated, then robust controllers may not guarantee stability. To overcome these difficulties and to make the controller stable in the presence of unknown parameter uncertainty, adaptive controllers are used. Adaptive control for FLMs is designed mainly for accurate trajectory tracking and stabilizing vibrating system dynamics for large unknown payload mass. The nonlinear dynamic system of a flexible manipulator can be expressed in the fixed parameter form, which is the product of regression term and an unknown constant parameter. In addition to adaptive controllers, intelligent soft computing techniques such as fuzzy logic, neural networks, and reinforcement learning are also applied in the control of FLMs. Control with some intelligence is sometimes required to tackle unknown environments and to improve the whole performance of the system. These techniques are employed to choose suitable gains in feedforward compensation, feedback loop, or both.

1.6 Applications of Flexible and Cooperative Manipulators

Applications of flexible link manipulators (FLMs) can be found in many areas of operations. They can be employed in unstructured environments, for example in drones and underwater robots. Lightweight manipulators are also preferred for space applications. They can be used to perform a variety of tasks such as the launch of satellites, retrieval of spacecraft for inspection, maintenance and repair, movement of cargo, etc. All these missions require extreme

precision. However, because of carrying cost, manipulators' arms are usually very light and flexible, and their motion involves significant structural vibrations, especially after a grasping maneuver. Manipulators with long arms can also help perform hazardous tasks, for example, in fire-fighting, rescue operations, removing high levels of nuclear contamination, reactor decommissioning, landmine, and explosive ordinance disposal, etc. Deactivation and decommissioning (DandD) of defunct facilities where nuclear radiation or toxicity hazards preclude human presence employ manipulators with long arms that can be remotely controlled and regulated. But their long arm makes them highly flexible which poses problems in handling tasks smoothly and swiftly. So, to take advantage of FLMs, one needs to apply some suitable techniques to contain their oscillations.

Figs. 1.6(a-b) show a space manipulator named Dextre by the Canadian space agency and its details onboard the international space station (ISS). Many of the ISS's robotic arms and experiments can be operated from the Earth.

Applications of flexible cooperative manipulators in construction works range from painting, and plastering to carpentry. Figs. 1.7(a-d) show different applications of the manipulators in construction works. Cooperative flexible manipulators can also be used for agriculture and forestry purposes for the operations such as picking fruits and vegetables, sowing, weeding, etc.

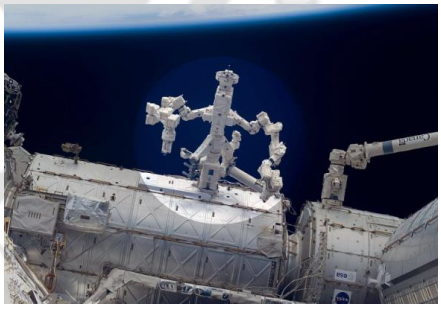

(a) **(b)**

Figure 1.6: Flexible manipulators: **(a)** Canadarm2 **[**Source: http://www.asc-csa.gc.ca/eng/iss/mobile-base/default.asp], and **(b)** Dextre, [Source:http://en.wikipedia.org/wiki/Dextre#mediaviewer/File:Dextrereallyhasnohead.jpg].

(a) **(b)** **(c)** **(d)**

Figure 1.7: Use of robots in construction: **(a)** robotic manipulator used for ceramic fitting, **(b)** an example of a carpentry aid wearable robot under, **(c)** ROCCO project brick assembly robot, **(d)** an example of a wearable welding robot under development [Source: http://cdn.intechopen.com/pdfs-wm/5555.pdf].

Some of the applications where cooperative manipulators can successfully be employed in industrial robotics are manipulation (pick-and-place), assembly, spray painting and coating, arc welding, laser cutting, mechanical finishing operations (deburring, grinding) etc. Robotic technologies are currently being employed in coordination tasks in driver assistance systems such as collision avoidance systems, lane keeping and parking assistance, and driver monitoring technologies [Siciliano and Khatib (2008)]. Some companies, for example, Google, have already developed fully autonomous vehicles. Rehabilitation and healthcare robots assist persons with disability in their necessary activities or provide therapy for persons seeking to improve physical or cognitive functions. [Krebs et al. (2003), Dellon and Matsuoka (2007)]. Cooperative medical robots can be employed in robotized surgery [Taylor, (2001, 2003)]. Cooperative manipulators can be used for cooking, aftercare, etc. in domestic applications.

1.7 Need of the Present Investigation

Research on the control of flexible manipulators has received overwhelming attention due to their several advantages over rigid robots: they require less material, are lighter in weight, consume less power, require smaller actuators, are swift in action, are more maneuverable and transportable, have less overall cost and higher payload to robot weight ratio. These manipulators, however, exhibit flexible deformation, which causes the position and orientation of the end-effector to deviate from its desired trajectory. The oscillatory behavior of the manipulator is exhibited even after the end of the motion. This is called residual vibration of the link. Flexible

manipulators cannot successfully perform their tasks before dampening their vibrations, which limits their effectiveness, especially in high-speed applications. However, control of flexible manipulators to maintain accurate positioning is an extremely challenging task. Due to the flexible nature of the system, the dynamics are highly non-linear and complex.

Flexible manipulators are effectively infinite dimensional systems and suitable approximations are made in order to analyze their behavior to a satisfactory degree of accuracy. There are many discretization methods namely the finite element method, assumed mode method, collocation method, etc. to discretize a continuous system into a finite number of degrees of freedom to ease the analytical solution of a continuous system.

Although the model-free control method also is gaining popularity in recent years, without accurate dynamic modeling, it may be unstable and may pose difficulty in ensuring precise control of the complex robots in the actual working environments. It also needs extensive experience. Therefore, accurate dynamic modeling is still an important step in the precision control of a flexible manipulator which exhibits highly coupled and nonlinear dynamic behaviors [Zheng et al. (2020)]. However, the dynamics of the system are highly nonlinear and complex which, in turn, complicates control of the end-effector. The effective inertia of the system changes as a nonlinear function of robot configuration. Flexural dynamics application complicates the problem much further which leads to serious problems in modeling and control of the system [Usoro et al. (1986)]. It is desired to design lighter robots with large payload-to-weight ratios that can also operate at higher speeds which makes them a subject of intensive research. In the present research work in this thesis, an attempt has been made to address the above-mentioned problems in the dynamic modeling and control of an FLM by applications of passive and active vibration controls of the tip deflection of the manipulator.

Due to the lightweight and flexible nature of FLMs, a single manipulator cannot handle heavy payloads without tip oscillations. Many tasks that require handling heavy payloads can become affordable when two or more FLMs are employed in a cooperative manner. There is a need for synchronization of motion of these manipulators and time of occurrence of processes involved in the job handling. An attempt has been made to carry out kinematic and dynamic analyses of two rigid manipulators working in coordination to handle a job at the end of this thesis which can be extended to a group of flexible manipulators.

1.8 Thesis Organization

The present thesis is comprised of a total of eight chapters. Chapter 1 presents the introduction of flexible manipulators and cooperative manipulators. Chapter 2 contains a literature survey of the work done on these topics by different researchers. Chapter 3 presents the finite element modeling of a two-link flexible manipulator for its parametric study. Chapter 4 consists of dynamic analysis using the finite element method and linear quadratic regulator (LQR) control of a single-link flexible manipulator. Chapter 5 comprises of dynamic analysis of a string-stiffened single-link flexible manipulator using Lagrange-Euler formulation and assumed mode method and control of its tip deflection using adaptive proportional-integral-derivative controller along with impedance control. Chapter 6 contains dynamic analysis and control of a rigid-flexible double-link string-stiffened flexible manipulator. Chapter 7 comprises kinematic and dynamic analyses of a three-dimensional revolute-revolute-revolute (RRR) joint-type rigid manipulators doing a cooperative task. Chapter 8 contains the conclusion and scope of future work.

Chapter 2

Literature Review

2.1 Introduction

In this chapter literature survey has been carried out related to the works that have been done by different researchers in the field of flexible manipulators and cooperative manipulators. The survey is divided into several aspects related to flexible manipulators such as types of flexible manipulators based on a number of links, modeling of flexible joint manipulators, kinematic and dynamic analysis, numerical studies, trajectory planning, experimental studies, control, and applications of flexible manipulators. A literature survey on cooperative manipulators also has been done with respect to modeling and control of these manipulators. Sections 2.2 to 2.4 describe different types of flexible manipulators and their modeling and control while section 2.5 mentions the works by different researchers on the modeling and control of flexible link manipulators (FLMs) applied in various real-world applications. Section 2.6 gives details of work done on cooperative manipulators regarding their modeling and control which is still a relatively less explored area. Section 2.7 describes the modeling and control of manipulators that work in coordination. Section 2.8 presents the summary of the literature review done in the present work as well as the technical gap which motivates to carry out present research work. Objectives of the present research work have been given in section 2.9.

The following section discusses the work done on modeling and control of manipulators with link flexibility.

2.2 Modelling and Control of Flexible Link Manipulators

Flexible manipulators may be planar or spatial. Spatial manipulators have a three-dimensional workspace. Planar manipulators may have a single link or more than one link. Spatial flexible link manipulators are multilink manipulators which also may consist of one or more flexible links.

Research done on modeling and control of such manipulators can be divided on the basis of the number of flexible links which has been mentioned in sections 2.2.1 and 2.2.2.

2.2.1 Single Link Manipulators

Ahmad et al. (2008) modeled the vibration of a constrained planar single-link flexible manipulator using assume mode method and proposed a Delayed Feedback Signal (DFS) and Proportional-Derivative (PD) controller to actively control the vibrations of flexible structure. Reddy, and Ghosal (2015) studied the nonlinear dynamics of a rotating wind turbine blade modeled as a one-dimensional beam, undergoing large deformation and with geometric nonlinearities using method of multiple scales. Dwivedy et al. (2009) analyzed a fiber-reinforced composite laminate-made single-link flexible manipulator with harmonic drive using the finite element method considering Euler-Bernoulli beam theory for a given acceleration profile. Bandopadhya et al. (2006) carried out a numerical and experimental investigation of the active vibration control of a single link planar flexible manipulator composed of magnetostrictive material (Terfenol-D) as smart active material. Payo et al. (2005) validated the nonlinear dynamic model for single-link very flexible arms experimentally. Ramalingam et al. (2021) applied a quadratic optimal regulator for the control of a single flexible-link manipulator made of hybrid polymer composite material of carbon fiber, glass fiber, and Kevlar fiber. Feliu-Talegon, and Feliu-Batlle (2022) used the singular perturbation theory combined with the input-state linearization technique to design fractional-order controllers for a single-link flexible manipulator.

2.2.2 Two and Multilink Manipulators

Wasfy and Noor (2003) reviewed papers related to the modeling of flexible multibody systems. Zavrazhina (2007) studied the influence of the flexibility of links on the dynamics of a multilink robot manipulator. Heidari et al. (2013) applied the nonlinear finite element method for the dynamic analysis of a three-dimensional highly flexible-link manipulator for determining the optimal trajectory using Pontryagin's minimum principle. Halalchi et al. (2014) considered the Linear Parameter Varying (LPV) modeling to control flexible-link robot manipulators using Euler-Lagrange equations. Qian et al. (2013) formulated the dynamics of spatial manipulator arms consisting of *n* flexible links and *n* flexible joints using 4 by 4 homogenous transformation matrices

and found transversal, longitudinal, and torsional deformation of its tip. Giorgio and Vescovo (2019) modeled a planar multilink flexible manipulator using a discrete Hencky bar-chain model to avoid the requirement of decomposing a nonlinear system using the assumed mode method into two slow and fast subsystems for its linearization. Celentano and Coppola (2011) and Celentano (2012) presented the dynamic model of a realistic flexible robot with flexible links having varying cross-sections using wavelet theory. Sun et al. (2009) presented the recursive finite segment multibody dynamics method for flexible systems. Zhao et al. (2010) carried out a kineto-static stiffness mapping derived by means of the general equation of dynamics for robot manipulators which takes into account the kinematic influence on the stiffness matrix. Qian and Zhang (2012) studied the impact dynamics of multi-link robots with link and joint flexibility. Qian et al. (2018) analyzed the nonlinear dynamics of the frictional impact of a flexible multilink manipulator arm with the target for several normal contact and friction models using the regularized approach in which stretching, bending, and torsional deformations of the flexible links in addition to the flexibility and mass of the joint were considered.

Zhang and Mei (2011) carried out the optimization of dimension parameters of delta manipulators based on natural frequency. Zhu et al. (2008) built a virtual prototype of a parallel machine tool using the multibody software package ADAMS considering links as flexible and carried out stress analysis using ANSYS to find the stress distribution in the flexible links for shape design, structural optimization, and fatigue examination.

Liu et al. (2012) used Hamilton's principle for the dynamic modeling of a manipulator handling a flexible payload and designed a position controller based on the Lyapunov function related to the total energy of the system. Sawada and Itamiya (2012) carried out position control of 2 DOF flexible link robot arms based on computed torque method. Zhang and Liu, (2012) designed a nonlinear PDE observer for a flexible two-link manipulator. Castri and Messina (2012) presented the dynamic modeling and active vibration control of planar multilink manipulators having flexible links through a full-state linear quadratic regulator controller by optimally placing collocated sensor/actuator pairs. Yu et al. (2007) established a 3-D dynamic model for a free-swimming flexible multi-link robot, which can predict the mechanics and behavior of the robot and accordingly aid the synthesis of locomotion control. Njeri et al. (2018.a) combined a filtered inverse feedforward controller to minimize the transient vibrations due to the sudden starting and

stopping of a 3D 2-link flexible manipulator and strain feedback controller to ensure rapid decay of residual vibrations of the manipulator. Njeri et al. (2018.b) developed filter-augmented augmented inverse controller for vibration control of a 3D 2-link flexible manipulator in which the link velocities were dependent on the value of the filter time constant whose careful choice could yield high operation speeds and minimal link vibrations, and also, compared to classical input shaping methods in which the trajectory is not fixed. Grandinetti et al. (2012) experimentally controlled the vibration of a three-degree-of-freedom cylindrical flexible macro-manipulator with a micro-manipulator. Esakki et al. (2013) worked on robust control of two three-link collaborative planar rigid manipulators handling a flexible object in the prescribed trajectory using the singular perturbation technique.

Boscariol et al. (2010) validated the result of a simulator, named FLiMHILS (Flexible Link Mechanisms HIL (hardware in loop) Simulator) by comparing the dynamic behavior of a real mechanism with the corresponding response of the simulator subject to the same stimuli and controller parameters. Cappelli et al. (2013) also used the hardware-in-the-loop (HIL) principle for designing dynamic controllers. Garg et al. (2014) designed and simulated a 4DOF–in vivo robot manipulator for stomach biopsy and performed the kinematic and dynamic analysis of the robot where they used Matlab for workspace analysis. Filaretov et al. (2014) used a multilink manipulator with a 3D vision system for cutting a flexible object without fixing it. Peng et al. (2012) designed and simulated the kinematic and dynamic behaviors of an inspection robot named flexible in-vessel inspection robot (FIVIR) for inner inspection of experimental advanced superconducting Tokamak (EAST) using ADAMS. Peng et al. (2021) designed, developed, and mathematically analyzed a multilink cable-driven hyper-redundant manipulator fitted with a camera at its tip for inspection of complex and unstructured environments like nuclear power plants and oil and gas pipelines. Liang et al. (2014) worked on the visual servoing of robot manipulators considering the full motor dynamics.

Sections 2.2.1 to 2.2.2 are comprised of research works on manipulators that are serial manipulators. Parallel manipulators may also have flexible links. Some of the works done on parallel manipulators are mentioned in section 2.2.3.

2.2.3 Parallel Manipulators

Zi et al. (2007a) established the inverse dynamic formulation of a cable-driven parallel manipulator (CPM) based on the inverse kinematics analysis using Lagrange's equations. Li et al. (2009) carried out elastodynamic optimization of a 2-DOF planar parallel pick-and-place robot with flexible links. Zhengsheng et al. (2013) applied the assumed mode method (AMM)-based substructure technique and the Lagrange principle to formulate the dynamic modeling of a 2-degrees of freedom (DoF) flexible link parallel manipulator to achieve real-time control by applying the singular perturbation technique (SPT) to divide the nonlinear dynamic system into two subsystems for the design of a reduced-order controller. The SPT transforms the nonlinear differential algebraic equation (DAE) constraints into explicit ordinary differential equations (ODEs). Raţ and Neagoe (2009) compared the dynamics of rigid and flexible links of a 3-DOF parallel robot. Du et al. (2007) carried out the finite element analysis for determining the dynamic stress of planar flexible-links parallel robots using the Kineto-Elastodynamics theory and the Timoshenko beam theory. Vidoni et al. (2012) carried out the kinematic and dynamic analysis of flexible-link parallel robots by means of an ERLS approach. Zhang et al. (2010) investigated axial forces on the dynamic properties of a flexible 3-PRR planar parallel manipulator moving with high speed.

The following section describes the research work carried out by different researchers on manipulators with flexible joints or flexible links or both.

2.3 Mathematical and Experimental Studies of Flexible Manipulators

There are flexible manipulators that may have flexible joints with either rigid links or flexible links. Research works on such types of manipulators can be mentioned under various headings, like kinematic analysis, dynamic analysis, numerical modelings, experimental works, control, etc. depending on the stress given in these works. However, the field of flexible manipulators has become so advanced that any work on these manipulators consists of all the types of analyses and control mentioned above. It is not possible to put any single work solely in a particular category. For example, control of an FLM by conventional methods cannot be possible

without its dynamic modeling, and dynamic modeling cannot be done without kinematic modeling. However, depending on the stress given in these works, these works have been mentioned in the following sections from 2.4.1 to 2.4.6.

2.3.1 Modeling of Flexible Manipulators

In this section, various types of methods that have been used by different researchers to find dynamic equations of motion are described. Mordfin and Tadikonda (2000) developed closed form solution for the small elastic motions of a planar, flexible, multilink system in which links connected by pin joints were represented as Euler-Bernoulli bars in transverse vibration. Jeleni and Crisfield (2001) presented the master-slave dynamic formulation for 3D beams considering large rotation and non-linear kinematics of arbitrary types of joints using Hamilton's principle. Lee (2005) proposed a trajectory control scheme for a horizontal two-link rigid/flexible robot having a payload at the free end by derived distributed-parameter dynamic model, consisting of two ordinary differential equations and one partial differential equation using the extended Hamilton's principle, and then designed a trajectory-tracking control scheme based on the distributed-parameter dynamic model, where the Lyapunov stability theorem was used as a mathematical tool that was a collocated control, free from the so-called spillover instability. The proposed control consisted of a PD control for the rigid dynamics, proportional control for the flexible dynamics, and feed-forward and dynamics compensation. Dado et al. (2001) developed a mathematical model based on the principle of virtual work that coupled the flexible drive shaft motion of the drive joints with the rigid body motion of the links for a mixed-loop robot with servo-motor drives present. Martins et al. (2002) modeled robotic manipulators with structural flexibility which was capable of reproducing nonlinear dynamic effects, such as the beam stiffening due to the centrifugal forces induced by the rotation of the joints, giving it the capability to predict reliable dynamic behaviors for a wide range of applications based on the assumptions of the Euler-Bernoulli hypothesis of inextensibility of the neutral fiber, and moderate rotations of the cross sections in order to account for the foreshortening of the beam due to bending.

Bascetta and Rocco (2002) developed a recursive model of a flexible manipulator with motors at the joints by a mixed Eulerian and Lagrangian formulation of the equations of a flexible body using both a time domain analysis and a frequency domain analysis, in order to show the

relevance of gyroscopic effects in modeling flexible robots. Kang and Mills (2002) formulated equations of motion for the planar parallel manipulator by applying the Lagrangian equation of the first type and Lagrangian multipliers that simplifies the complexities that arise due to multiple closed loop chains of the parallel manipulator and the structurally flexible linkages. Kalyoncu (2008) studied the dynamics of a flexible arm tracing a multi-straight-line path under the action of an external driving torque and an axial force using Euler-Bernoulli beam theory and Lagrange's equation of motion. Callegari et al. (2009) designed a mini-spherical wrist exploring the realization of mini-devices for the orientation of parts or tools for small-scale application in the space characterized by a spherical motion whose joints were suitable to be realized by the techniques of flexures. Mechefske et al. (2010) provided a method to determine the variable flexible joint parameters which are dependent on configurations of a parallel robot. Rognant et al. (2010) presented a systematic procedure for the elastodynamic modeling of industrial robots consisting of flexible links and joints that applies to either serial or parallel manipulators based on a 3-D space generalization of the equivalent rigid link system (ERLS) description, the finite-element method (FEM), and the Lagrange principle. Tian and Wang (2011) developed a dynamic model of a manipulator with three degrees of freedom using Newton-Euler formulation through which they obtained automatically kinematic and dynamic parameters of the manipulator as well as simulation equations concurrently. Chen et al. (2011) obtained dynamic behaviors, including kinematics output response, dynamic stress of driving limbs, and natural frequency of a 4-UPS-RPS (universal joints-prismatic pairs-spherical joints)- (revolution joints-prismatic pairs-spherical joints) high-speed spatial 5-Degree of freedom parallel robot in which the driving limbs and spherical joints were treated as flexible bodies, the moving platform, stationary platform and other joints of parallel robot were treated as rigid bodies. Liu et al. (2011) presented the design and control of spring-assisted modular and reconfigurable robots (MRR), which has a spring embedded in each joint module. Korayem et al. (2012) proposed a method for decreasing jerk and increasing the Maximum Allowable Load (MAL) of a nonholonomic Wheeled Mobile Manipulator (WMM) considering the flexibility of joints in singular conditions. Korayem et al. (2012) studied the dynamic modeling of nonholonomic wheeled mobile robotic manipulators, which consist of a serial manipulator with elastic joints and an autonomous wheeled mobile platform. To avoid computing the Lagrange multipliers associated with the nonholonomic constraints, they adopted the approach of Gibbs-Appell (G-A) formulation in recursive form. Vakil et al. (2012) analyzed a

flexible joint-flexible link manipulator by assumed mode method and Lagrange's method by considering the whole system as a combination of two subsystems, one with flexible link but without joints' flexibility and another with joints' flexibility and rotor's moment of inertias. Zhang and Qiang et al. (2012) modeled the joint flexibility as the torsional spring of an industrial robot with rigid links and flexible joints and derived the dynamic equations for this robot by using Lagrange's method. Wang et al. (2012), in order to ascertain the effect of stiffness on the slipping collision of a flexible arm, established a contact-impact model by using the Hertz impact theory and nonlinear spring-damper theory and derived collision dynamics of the flexible arm through Lagrange equations and solved the dynamic equation by the fourth-order Runge-Kutta method. Boscariol et al. (2012) designed and implemented a simulator for 3D flexible-link serial robots adopting the method based on an Equivalent Rigid Link System (ERLS). Vidoni et al. (2013) did dynamic modeling of systems with large displacements and small elastic deformation which was based on an Equivalent Rigid Link System (ERLS) that enables to decouple of the kinematic equations of the Equivalent Rigid Link System from the compatibility equations of the displacements at the joints. Niu (2013) discussed the identification and compensation of torque ripples in the drive train after an in-depth analysis of the root causes of the vibration excitation resulting in the parasitic torque pulsation due to characteristics of drive train components, misalignment in assembly and mechanical tolerance of castings. Wang and Xia (2013) considered the flexibility of joints with rigid links by Lagrange's method for the design of the controller. Zhang (2013) developed a dynamic model of planar 3-RRR flexible parallel robots by the finite element method, the floating frame of reference, the Lagrange equation, and the principle of virtual work and established the nonlinear dynamic equation with rigid-elastic coupling in which they considered lumped masses and moments of inertia of each joint and the moving platform. Hussain et al. (2017) tried to determine suitable joint stiffness of soft joints of fingers using rapid prototyping techniques based on the mechanics of tendon-driven hands and on a compliant system exploiting beam theory for the fingers to track a certain predefined trajectory in an underactuated tendon-driven soft hand to improve its grasping capabilities.

Modeling of an FLM is of two types: Kinematic modeling and Dynamic modeling. The following next two sections mention the different works for the kinematic as well as dynamic analyses of flexible manipulators.

2.3.2 Kinematic Analysis of Flexible Manipulators

In this section, works in which efforts were done to find position/displacements, velocities, and accelerations of joints and end-effectors either by using direct kinematics or inverse kinematics have been mentioned.

Ubertini (2000) applied a method to the inverse kinematics problem of flexible link systems that is based upon a nonlinear compensation scheme and makes use of the Grobner basis method to avoid the kinematic singularities. Hwang (2006) developed a nonlinear recursive formulation in terms of a set of time-invariant scalars, vectors, and matrices that depend on the spatial coordinates as well as the assumed displacement fields for the kinematic and dynamic analyses of robotic manufacturing systems which are used for open-loop flexible manipulators that undergo large translational and rotational displacements. Sun et al. (2011) carried out a kineto-static analysis of a high-speed parallel manipulator with rigid-flexible coupled links used in parallel kinematic machines to gain the high velocity and acceleration of the end-effector, which can be applied in the production line of Pick-and-Place and improve the production efficiency. Zhang et al. (2011) employed a quadratic programming (QP)-based method, as a remedy for joint angle drifts for redundant robot manipulators with physical constraints (e.g., joint-angle limits and joint-velocity limits). Ata et al. (2012) compared the Kinematic analysis of a single link flexible manipulator using a tangential coordinate system (TCS) and virtual link coordinate system (VLCS), also called Equivalent Rigid Link Coordinates (ERLC) and found that TCS analysis gives better results in terms of frequency and deflection. The next section describes the dynamic modeling of flexible manipulators.

2.3.3 Dynamic Analysis of Flexible Manipulators

This section mentions the various techniques used by different investigators to carry out dynamic analysis. Dwivedy and Eberhard (2006) carried out an extensive survey of literature related to dynamic analyses of flexible robotic manipulators wherein they considered both joint and link flexibility. Low and Vidyasagar (1988) derived the dynamic equations of motion of a rigid-flexible link manipulator using Hamilton's principle. Jeleni and Crisfield (2001) presented the master-slave dynamic formulation for 3D beams considering large rotation and non-linear kinematics of arbitrary types of joints using Hamilton's principle. Ata and Johar (2005) used the extended

Hamilton's principle and assumed modes method for analyzing a nonlinear rigid-flexible manipulator with zero tip deformation constraint. Hwang (2003) applied the Newton-Euler method for flexible bodies to obtain large, loosely coupled system equations of motion for an open-loop flexible multibody system. Hwang (2008) developed a method using generalized Newton-Euler equations for decoupling joint and elastic accelerations while maintaining the nonlinear inertia coupling between rigid body motion and elastic body deformation. Vakil et al. (2008) studied a planar flexible link manipulator by assumed mode method (AMM) using Lagrange's equation and validated the result with a full nonlinear finite element method. Sun et al. (2004) did the dynamic modeling of a flexible manipulator system consisting of a flexible link and a rigid link based on the assumed mode method using the Lagrange dynamic model. Naganathan and Soni (1987) presented a finite element-based nonlinear model of flexible link manipulators. They found the governing equations of motion of the manipulators using Timoshenko beam theory. Ashrafiuon and Nataraj (1991) developed variational equations of motion for flexible serial manipulators using the finite element method which accounted for full coupling between the rigid body motion and link deformation. Korayem et al. (2009) employed the finite element method (FEM) for modeling and deriving the dynamic equations of the manipulator with flexible links and joints and investigated the effect of a carried payload on the residual vibration magnitude. Zhang et al. (2012) investigated the planar 3-RRR flexible parallel robot and presented the rigid-flexible coupling dynamic model based on the floating frame of reference. Zhang and Zhang (2012) also used the same method to study RRR and 3-PRR flexible parallel robot systems.

Nataraj (1993) performed a nondimensional parametric analysis of a single link flexible manipulator and accounted for the coupling between axial and flexural deformations. Basher (2000) developed an analytical model of the beam, characterized by an infinite number of modes, using the Euler-Bernoulli beam equation and modal expansion method. Reshmin (2001) used averaging method to study the dynamic problem of controlling manipulator robots whose links are connected by flexible joints with elastic compliance and investigated the case when the stiffness of the elastic elements and the gear ratios of the reducers of the electric drive are large. Franitza (2002) performed the dynamic analysis of non-linear elastically deformable mechanisms considering loads related to mass inertial terms besides the quasi-static case that changed the original first-order set of linear differential equations into non-linear second-order partial differential equations. He et al. (2005) found through the nonlinear dynamic analysis of a planar

two-links flexible under-actuated manipulator that the internal resonance of the multi-modal nonlinear dynamic mechanical system influenced the vibration of the system considerably. He and Lu (2005) studied the influence of passive joints on the dynamics of planar flexible underactuated 2-link manipulators and proposed a vibration reduction method based on the internal resonance phenomenon of a multi-degree nonlinear dynamic system. Suzuki et al. (2005) analyzed the casting and winding dynamics of an inelastic hyper-flexible multi-link manipulator with strings, ropes, or wires to capture a distant target object. Zhang and Angeles (2005) established the complete mathematical model for dealing with the case of an n-flexible-joint and n-rigid link manipulator colliding with its environments by using the concept of impulse potential energy and the generalized impulse momentum equations. Theingi et al. (2006) presented the dynamics of planar parallel manipulators with joint coupling. To take into account the backlash effect one may refer to the works of Dentsoras and Aspragathos [1991] and Yang et. al. [2016]. In the latter work, the backlash effect on planetary gear systems has been studied. Lu et al. (2015) evaluated the effect of backlash in the planetary gear reducer at the joint on the dynamic response of a single-link flexible manipulator and found that the dynamic response of the system is sensitive to the backlash and the excitation frequency simultaneously. Zhicheng (2006) analyzed experimentally the control of contact force response of a single-degree manipulator with its environment with the help of acceleration sensors and force sensors. Persad et al. (2010) performed the dynamic stress analysis on a single link manipulator with payload, subjected to high joint acceleration and deceleration where actuation was achieved with a linear extension spring. Gao and Bian (2012) investigated the factors that result in the resonance of the flexible manipulator with both link flexibility and joint flexibility based on the flexible dynamics equations and verified with numerical simulations.

Zhang and Zhou (2006) focused on the dynamics of flexible robots with N number of links and N number of joints where they modeled each flexible joint as a linearly elastic torsional spring and applied the assumed mode method to describe the deformation of the flexible link considering the link as Euler-Bernoulli's beam. The complete governing equations of motion of the flexible-link-joint robots were derived by Kane's method.

Liu et al. (2012) analyzed the pneumatic elastomer of flexible joints considering the uniform distributed mass of pneumatic artificial muscle (PAM). Huang et al. (2013) used two pneumatic flexible actuators as actuating drivers to drive a bending joint and established the angle dynamic model based on the first law of thermodynamics and joint dynamic equations. Guo and

Lee (2013) presented an equivalent pin model (EPM) of flexure finger dynamics by accounting for the moving rotation center and varying radius of a compliant joint and compared the maximum stress among different configurations. Modeling tolerance guidelines were derived by comparing the Euler–Bernoulli beam model against finite element analysis (FEA) without neglecting shear distortions. Hirschkorn and Kövecses's (2013) work is primarily concerned with the mass matrix and how it relates to the movement of a mechanism in a particular coordinate axis direction. The next section mentions the various types of numerical techniques applied in different studies to solve the dynamic equation of motion.

2.3.4 Numerical Studies of Flexible Manipulators

Na and Kim (2001) modeled a multi-link flexible structure as a Timoshenko beam and joint as a torsional spring and used Newmark time integration and Newton-Raphson iteration methods for solving the non-linear equations of motion for each time step. Hwang (2003) applied the Newton-Euler method for flexible bodies to obtain large, loosely coupled system equations of motion for an open-loop flexible multibody system formulated in terms of a set of time-invariant scalars, vectors, and matrices. Hwang (2006a) developed kinematic and force models using absolute reference, joint relative, and elastic coordinates as well as joint reaction forces. Hwang (2006b) developed a recursive formulation with the generalized Newton-Euler equations for the dynamic analysis of flexible bodies that undergo large translational and rotational displacements. They employed numerical methods, such as the Newton-Raphson, Runge-Kutta, and Adams-Bashforth-Moulton methods to correct for constraint violations. Le et al. (2012) dealt with Newmark time stepping methods and finite rotations for nonlinear finite element analysis of flexible beam structures. Hwang and Wei (2008) developed a method for decoupling joint and elastic accelerations while maintaining the inertia coupling between rigid body motion and elastic body in multibody automation systems. Wang et al. (2010) modeled the robotic arm manipulating a load due to gravity taking spring mass damper-friction model based on human muscular characteristics considering variable impedance. Abe (2015) did mathematical modeling of a single-link flexible manipulator considering the axial displacement and nonlinear curvature due to large transverse deflections and tried to eliminate residual vibrations using the particle swarm optimization technique. Shitole and Sumathi (2015) introduced an estimation method based on sliding discrete Fourier transform (SDFT) integrated with a phase-locked loop for online

estimation of mode and frequency of vibration of a single-link flexible manipulator (SLFM) in the presence of noise and offset. Augustynek and Adamiec-Wójcik (2012) presented a mathematical model of the mechanism with flexible beam-like links, and rotary joints and assessed the assembly errors in finite element analysis to reduce the number of generalized coordinates, and therefore the number of equations of motion to a minimum. Travail et al. (2005) presented a non-linear mathematical model of telescopic flexible multi-link robotic manipulators undergoing large rigid body translations and rotations. They applied a non-linear, co-rotational finite element method to model the robotic manipulator. In the next section, research in trajectory planning for residual vibration suppression of tip of flexible manipulator has been mentioned.

2.3.5 Trajectory Planning of Flexible Manipulators

Farid and Salimi (2001) proposed an inverse dynamic approach to determine the required actuating torque and force for a planar flexible-link manipulator with revolute-prismatic joints such that its end-point follows a given trajectory. Ata (2012) analyzed a rigid/flexible manipulator considering it as Euler-Bernoulli's beam and using the Extended Hamilton's Principle and designed joints trajectory based on fifth-order polynomial trajectory and soft motion trajectory for the first three mode shapes of the flexible link. Ata (2010) did a dynamic analysis of a two-link rigid-flexible manipulator considering the flexible link as an Euler-Bernoulli beam by extending Hamilton's principle and compared the merits of a soft motion (SM) trajectory with that of a Linear segment with parabolic blends (LSPB) trajectory of tip motion. Pan et al. (2010) measured the torsional stiffness of the joint in the torsional stiffness testing platform and estimated the coefficients of the friction model from the test results of the performance testing instrument for the drive unit. Wang (2011) proposed a scheme to achieve the link-tip trajectory tracking control and vibration suppression of the flexible-link robot arm by using the inverse dynamic method and the Linear Quadratic (LQ) optimum control method. Ulrich et al. (2012) considered the vibration damping of a space manipulator joint and designed adaptive trajectory control. Yurkevich (2016) discussed a controller design for trajectory tracking control of a multilink manipulator in which two time-scale motions were used for a closed-loop system. Moghanni-Bavil-Olyaei et al. (2019) carried out a numerical simulation for backstepping control of the trajectory tracking of a single-link flexible-joint flexible-link manipulator (SLFJFLM) as an underactuated mechanical system.

Zhou and Yu (2011) derived the dynamic model parameters of modular robots with flexible joints using 3D motion measurement system and found the exciting trajectory based on the finite Fourier series function where the coefficients of the Fourier series were optimized with the self-adaptive genetic algorithm. Narula et al. (2017) controlled a single-link flexible-joint manipulator by a non-linear control technique i.e. a backstepping method which was tuned using a genetic algorithm (GA), cuckoo search algorithm (CSA) and teacher learning based optimization (TLBO) and assessed their control performances. Yan et al. (2021) presented a robust control method based on optimal control for motion control (i.e., position control and trajectory tracking control) of a single link flexible joint manipulator with parameter perturbations and external disturbances.

Hara et al. (2012) achieved improved efficiency in joint space motion for free-floating space robots and flexible-base robots. Tapia et al. (2010) presented a dynamical analysis and modeling of a robot with 5 dual joints (10 DoF) by dual algebra method giving only one solution for different robot topologies. Gao et al. (2011) put forward a vibration control strategy based on the controllable local degree of freedom in order to suppress the vibration of the flexible-joint manipulator. Chalon et al. (2010) studied the torque and stiffness behavior and suggested two quality measures: the safety margin concept and the sensitivity concepts.

In the following section, investigations carried out regarding the experimental validations of different algorithms for vibration control of FLMs have been mentioned.

2.3.6 Experimental Studies on Flexible Manipulators

Minakata et al. (2002) experimented with different forms of a biped robot to realize passive walking and thus minimize energy consumption by a biped. Mohan et al. (2010) experimentally determined the joint damping coefficient as well as the structural damping coefficient. Peza-Solis et al. (2022) carried out the experimental validation for the control of a single-link flexible manipulator with sliding mode control to tackle parametric uncertainty. Phung et al. (2011) pursued a model-based machine-learning approach in which the deflection of the end effector at the target pose was estimated from strain gauge signals and compensated in advance by a corresponding correction of the joint angles. Laffranchi et al. (2012**)** presented an analysis of the role of physical damping in compliant actuation systems. Xu et al. (2018) experimentally and analytically investigated the stability of the nonlinear dynamic system of a multilink flexible

manipulator for all admissible parameter uncertainties, unknown nonlinearities, and exogenous disturbances input by using a linear observer-based closed-loop system. Yamakawa et al. (2016) carried out an experimental investigation of whip manipulation of flexible objects by a robotic manipulator through a designed trajectory of the robot. In the next section, various attempts made by different researchers for the control of tip deflection of flexible manipulators have been given.

2.4 Control of Flexible Manipulators

Various types of control schemes have been successfully applied by different researchers to control tip deflections. Some of them are mentioned in the following subsections.

2.4.1 Proportional, Integral, and Derivative Control

Zi et al. (2007b) designed an immune PID controller with a fuzzy controller as an anti-body-suppressed function improving the self-tuning capability to control the wind-induced vibration. De Luca and Flacco (2011) designed a PD-type regulator for the cancellation of the gravity effect on robots with flexible joints. González-Vázquez and Moreno-Valenzuela (2013) presented control architectures that are continuous-time, smooth, and structured with PD terms in the trajectory tracking error and showed that controllers structured with a feedforward plus PD terms exhibit a time-scale separation. Feliu-Talegon et al. (2019) proposed a control system for a single link flexible manipulator that combined a fractional-order proportional-derivative (PD) controller for tip position with a feedforward force control which attained higher stability robustness and higher phase margin than a PD controller, which is the integer-order controller of similar complexity.

2.4.2 Optimal Control Methods

Jayasuriya and Choura (1991) controlled the tip oscillation of a flexible link manipulator by applying shaped input function based on minimum energy and bounded control criteria. Laub (1979) used the Schur method for obtaining the solution of the algebraic Riccati equation. Bossi et al. (2011) applied both MPC (Model Predictive Control) and LQR methods to control the vibration of a single link manipulator and concluded by experiment that the MPC method has a considerable advantage over the LQR method. Singla et al. (2015) developed a hybrid controller

with the combination of three different control schemes, namely inverse dynamics feedforward control by dynamic inversion for generating the nominal trajectory to obtain linearized models, command shaping, and linear state feedback control designed with a linear quadratic regulator (LQR) to ensure stabilization of a single link flexible manipulator. Ikizoğlu and Gürışık (2018) applied LQR-based optimal control for control of tip deflection of a flexible link manipulator. Crowe-Wright (2018) also applied the LQR control theory for the control of a double pendulum inverted on a cart.

2.4.3 Sliding Mode Control

Liu et al. (2012) proposed a sliding mode controller to realize system trajectory tracking performance and suppress the elastic vibration of a manipulator handling a flexible payload based on a distributed-parameter dynamic model and hence is free from the so-called spillover instability. Duarte et al. (2015) applied active vibration control using a sliding mode observer with active vibration sliding mode controller for residual vibration suppression of a single link flexible manipulator. Xu et al. (2013) derived the dynamic equations of the hydraulic rigid-flexible manipulator using the Lagrange principle and the assumed mode method and developed an adaptive sliding mode controller to simultaneously control the rigid motion and suppress vibration with uncertainties estimated by the adaptive law. Liu et al. (2013) proposed an adaptive sliding mode control method for the multivariable rigid-flexible coupling system of manipulators handling a flexible payload. Fareh (2019) presented sliding fractional order control for a single flexible link manipulator to utilize the advantage of the robustness of the fractional order control and the sliding mode technique.

2.4.4 Adaptive Control

Yoo et al. (2008) used adaptive motion/force control of multiple manipulators with joint flexibility. Zhu et al. (1998) used virtual decomposition, and Han et al. (2011) worked on robust adaptive dead zone and friction compensation using the RWCMAC network. Guo and Sun (2013) proposed nonlinear robust adaptive control for free-floating space manipulators. Jafarinasab et al. (2019) presented the model-based adaptive motion control algorithms for an underactuated aerial robotic manipulator comprised of an unmanned aerial vehicle (UAV) octocopter and a multilink

serial robotic arm. Jafarinasab et al. (2019) presented the model-based adaptive motion control algorithms for an underactuated aerial robotic manipulator comprised of a UAV octocopter and a multilink serial robotic arm. Abiko and Yoshida (2010) proposed adaptive control for a reactive system where the dynamic coupling between an actively operated part and a passively moving part in a multibody robotic system occurs to overcome nonlinear parameterization of the dynamic equation and uncertainties in coordinate mapping from Cartesian space to joint space.

2.4.5 Fuzzy Logic Control

Li et al. (2002) presented a method for the identification of joint parameters for a 9-DOF modular redundant robot using fuzzy theory and a genetic algorithm to avoid converging to locally optimal solutions.

Park and Cho (2003) presented the design of a robust adaptive fuzzy observer for uncertain nonlinear dynamic systems based on the Lyapunov synthesis approach to realize the minimal dynamic order of the observer. Green and Sasiadek (2005) gave an adaptive fuzzy logic control scheme for tracking the endpoint of a two-link flexible robot. Wai and Yang (2008) presented an adaptive fuzzy neural network control (AFNNC) design via a Takagi-Sugeno (T-S) dynamic fuzzy model with online learning ability to achieve high-precision position tracking by an n-link manipulator. Onen et al. (2010) proposed two adaptive networks-based fuzzy logic controllers (ANFLCs) for tracking control of the rigid link and the flexible link and tested the performances of ANFLCs for different types and different numbers of membership functions like triangular, trapezoidal, Gaussian, and Sigmoidal. Li et al. (2012) designed a fuzzy adaptive controller for a single-link robotic manipulator with immeasurable states by utilizing the back-stepping technique and the dynamic surface control (DSC) techniques to achieve good tracking performance. Li et al. (2013) proposed an adaptive fuzzy output feedback approach for a single-link robotic manipulator coupled to a brushed direct current (DC) motor with a flexible joint to achieve the output trajectory. Gao, and He (2017) applied fuzzy logic control for controlling the tip vibration of a single-link flexible manipulator. Chang et al. (2021) proposed an adaptive fuzzy tracking backstepping control method for control of the single-link robotic manipulator by combining the command-filter technique with the backstepping control technique. Diao et al. (2021) developed a finite-time adaptive fuzzy fault-tolerant control for the single-link flexible-joint robot system with an actuator fault.

Ni et al. (2012) proposed a novel robust controller which combines friction compensation and fuzzy-sliding mode controller for the nonlinear friction and uncertainty disturbance in the control system. Madhusoodanan and Ushakumari (2012) presented the method of the position control of a hydraulic three Degree of Freedom (DoF) revolute robot manipulator with Proportional Integral Sliding Mode Control (PISMC) and Fuzzy Logic Control (FLC).

Wai and Muthusamy (2013) proposed a fuzzy-neural-network inherited SMC (FNNISMC) scheme to relax the requirement of detailed system information and dealt with the chattering control efforts in the SMC system.

2.4.6 Neural Network Control

Asada and Asari (1988) applied the teaching of expert skill using curve fitting of data stored in a computer to the impedance control of a simple grinding robot. Krikochoritis and Tzafestas (2001) presented a method based on the feedback linearlization technique for the control of flexible joint robots using dynamic neural networks. Yoo et al. (2006) presented a control system based on a combination of the adaptive dynamic surface control (DSC) technique and self-recurrent wavelet neural network (SRWNN) for control of a three-link flexible joint robot for position tracking, payload uncertainties, and external disturbances. Maouche and Attari (2007) proposed a hybrid control strategy with nonlinear control and adaptive neural control to control the joint position and velocity as well as the deflection of the arm tip based on dynamics developed by Lagrange's formulation. Yoo et al. (2008) applied a robust output feedback control approach and the observer dynamic surface design technique to control the link and actuator velocity of a three-link flexible-joint robot with model uncertainties (payload uncertainties and external disturbances) using self-recurrent wavelet neural networks (SRWNNs). Sun et al. (2010) designed a control strategy using wavelet neural networks based on the Lyapunov function backstepping method for flexible joints to compensate for frictional and external disturbances with uncertain parameters. Gu and Liu (2011) proposed adaptive dynamic surface control (DSC) approach and recurrent Elman neural networks (RENNs) based on Lyapunov stability analysis to design a position-tracking control system in the joint space to provide good robustness against payload uncertainties and external disturbances. Park and Han (2011) proposed Robust-tracking control for robot manipulators with dead zone and friction using backstepping and RFNN controller based on Lyapunov stability

analysis to replace adaptive controller which requires information on the robot dynamics in advance. Daachi et al. (2012) proposed an adaptive neural controller in the Cartesian space for the redundant robot confronted with mobile obstacles. Yoo (2014) investigated a distributed adaptive containment control problem of networked uncertain flexible joint robots in the presence of multiple dynamic leaders under a directed graph topology using a neural network. Ouyang et al. (2017) employed reinforcement learning control of a single-link flexible using two radial basis function neural networks (NNs): actor NN for generating a policy and critic NN for evaluating the cost-to-go. Njeri et al. (2019) developed a self-tuning strain feedback gain controller for a 3D, two-link flexible manipulator using the artificial neural network for high-speed control. Ouyong et al. (2017) proposed the reinforcement learning control of a single-link flexible manipulator modeled using the assumed mode method (AMM) and Lagrange's equation in which the critic NN was employed to approximate the cost function of the system and actor NN was used to design a proper control input in combination with critic NN to control the manipulator. Amiri et al. (2008) compared Feed-Forward Neural Network (FFNN) and Diagonal Recurrent Neural Network (DRNN) methods to control a single-link flexible manipulator and found that the DRNN-based controller significantly improved the precision of the tip motion tracking, and the DRNN-based controller is more suitable in online control of the plant.

2.4.7 Miscellaneous Types of Control Methods

Chang and Fu (1997) investigated the dynamics of both the deburring process and the flexible manipulator and utilized a singular perturbation technique to separate the system into a slow subsystem and a fast subsystem. They developed an adaptive hybrid position/force controller for the slow subsystem and a dynamic feedback controller for the fast subsystem. Shi et al. (1999) did dynamic modeling of a rigid-flexible manipulator for constrained motion task control using Hamilton's principle and proposed a multivariable controller for the simultaneous motion and force control of the manipulator. Jiang et al. (2017) proposed a robust observer for a flexible single-link manipulator based on the partial differential equation (PDE) dynamic model to estimate the distributed spatiotemporally varying states with unknown boundary disturbance and spatially distributed disturbance.

McPhee et al. (2002) analyzed the dynamics of multibody systems using virtual work and symbolic Maple programming. Feliu et al. (2003) designed an inverse dynamics-based control system for a three-degree-of-freedom flexible light link arm with its mass concentrated at the tip using a two-nested control-loop scheme to control the tip position by using joint position and tip acceleration feedback. Taghirad and Khosravi (2003) designed and simulated robust composite controllers for flexible joint robots using fast and slow control algorithms. Jiang and Goldenberg (1999) used joint torque to compensate end-effector acceleration error of a flexible link. Ott et al. (2003) discussed decoupling-based cartesian impedance control of flexible joint robots that decouples the torque dynamics from the link dynamics. Korayem et al. (2006) proposed a method for feedback linearization of flexible joint manipulators to determine the dynamic load-carrying capacity of the manipulators. Ueda and Yoshikawa (2004) designed a mode-shape compensator with a constant gain matrix to improve the robustness of the arm configuration by inclining the dynamic manipulability ellipsoid's principal axes to change the coupling rigid body dynamics. Chen et al. (2006) analyzed the controllability of a planar 3DoF underactuated manipulator with one passive joint and the third flexible link based on the dynamic model using the assumed mode method and showed that the vibration controllability of an underactuated flexible manipulator is both joint-configuration-dependent and actuator-placement-dependent. Suzuki and Ebihara (2007) gave a casting control method for hyper-flexible manipulation assuming hyper-flexible elements as underactuated multi-link systems connected by nonelastic passive joints. Yoo et al. (2007) proposed a link position tracking dynamic surface controller for flexible joint robots without velocity measurements. Park et al. (2008) applied the observer dynamic surface design technique for position tracking of a flexible-joint arm. Choi et al. (2008) did the tolerance analysis of a robot manipulator having uncertainties in joint clearance and axis orientation through a general multibody dynamics sensitivity formulation that gave improved computational efficiency compared to the Monte Carlo procedure. Cascio et al. (2009) presented a smooth proximity computation technique for collision-free optimal control of multiple robotic manipulators based on Karush-Kuhn-Tucker (KKT) conditions. Chhabra and Emami (2009) discussed the concurrent synthesis of robot manipulators using modular hardware-in-loop simulation. Consolini et al. (2009) proposed a linear programming approach to the feed-forward minimum-time control of flexible joints. Du and Cai (2009) did dynamic modeling of a two-link flexible manipulator using the Lagrange principle and designed an active position controller using the nonlinear decoupling

feedback control method for joint torque of the PZT actuators. Gavriloiu et al. (2009) developed robust dynamical controllers based on the construction of a two-time scale dynamical motion of the closed-loop system for addressing the problems of tracking and regulation of flexible-link manipulators. Li et al. (2009) designed the decentralized robust control of robot manipulators with harmonic drive transmission and application to modular and reconfigurable serial arms based on Lyapunov's stability analysis and backstepping techniques where they considered each joint as an independent subsystem and the dynamical effects from the other links and joints as disturbances. Nikoobin and Haghighi (2009) proposed a Lyapunov-based nonlinear disturbance observer for serial n-link robot manipulators. Sun et al. (2009) presented the dynamic software flow of the rigid-flexible coupling system based on spatial operator algebra theory. Czarnetzki and Rohde (2010) presented an approach for simultaneous localization and modeling of dynamic elements of a robot's environment using a priori information using the Fast-SLAM (simultaneous localization and mapping) algorithm which is a kind of particle filter algorithm. Martin and Emami (2011) designed a hardware-in-loop simulator to emulate nonlinear and coupled dynamic loads to the joint actuators. Choi et al. (2011) proposed a numerical method to identify a set of independent parameters based on the dependency analysis of the regressors using measured motion trajectory data of a robot manipulator to compute the required joint torque for a desired trajectory. Hashemi et al. (2013) proposed a force/motion control scheme employing a combined linear parameter varying (LPV) gain-scheduled and inverse dynamics controller for the motion control of a 6-DoF robotic manipulator. Jia et al. (2013) proposed a dynamic surface control (DSC) method based on an extended state observer (ESO) for trajectory tracking of flexible joints that eliminates the calculation explosion of back-stepping. Cambera, and Feliu-Batlle (2017) used a fractional-order compensator to minimize the vibrations of a single-link manipulator based on combining a feedforward term and a feedback fractional order controller. Chen et al. (2019) presented methods for controlling the vibrations of a single-link flexible manipulator governed by the single-mode Duffing oscillator, and the multi-mode Duffing oscillators. Feliu-Talegon, and Feliu-Batlle (2019) designed and experimentally verified the effectiveness of a passivity-based fractional order controller for single-link flexible robots which had robust stability to parametric uncertainties and spill-over effects in addition to enhanced phase margin robustness. Yavuz (2019) applied the input shaping method for the suppression of residual vibrations of a single-link flexible glass fabric-reinforced epoxy-glass composite manipulator and also carried out experimental verifications. Sun

et al. (1999) applied different methods like shifting torques towards manipulator end-effectors to emulate a collocated scenario, minimizing the elastic accelerations, and minimizing the strain energy to control to reduce elastic vibrations of flexible-link cooperating manipulators. Tan et al. (2001) derived the dynamic model of joint flexibility of a direct-drive robot based on the Lagrangian method and thereafter carried out its stability analysis based on singular perturbation theory. Chen et al. (2013) analyzed the influence of end position addition mass and drive joint rotary inertia on the elastic motion stability of the end position of the manipulator's arm based on Routh's stability criterion. The following section mentions some of the applications of flexible manipulators or principles of flexible manipulators found in the literature.

2.5 Application of Flexible Manipulators

Martin et al. (1998) developed a general technique to model a space manipulator with flexible joints and suggested control schemes that reduce the undesirable effects of dynamic interactions between the attitude controller of a spacecraft and the flexible modes of a space manipulator mounted on it, as well as thruster fuel consumption. Tan (2003) presented a formulation for dynamic simulations of space manipulators with flexible links. They also derived governing equations of motion with full sets of inertial, gyro, and elastic restoring terms. The mid-point rule was used to integrate the governing equations which exhibit good accuracy and long-term numerical stabilities. Lee and Lee (2003) analyzed tendon-driven robotic mechanisms with flexible tendons which can only exert tension i.e., force is transmitted only in a unidirectional sense. Chu et al. (2008) studied the dynamic characteristic of a space flexible manipulator driven by a harmonic retarder fixed in a joint. Carpenter and Peck (2009) performed numerical simulations for a general control-moment gyroscopes (CMGs) system and investigated how the choices of an operation concept and actuation method influence base reactions and power consumption while orienting a camera on a spacecraft-mounted imaging payload. Chen and Chen (2011) discussed the dynamic modeling and singular perturbation control of a free-floating space robot with normal flexible joints and an uncontrolled base. Zhao and Bai (2011) studied the effects of joint clearance on the dynamic characteristics of a space robot manipulator where they established the contact dynamics model of the clearance using the nonlinear spring-damp model and considered the friction effect using the Coulomb friction model. Chen and Chen (2012) developed dynamic equations of a flexible-joint space robot system using the Lagrange method

with the linear and angular momentum of the system conserved. They decompose the flexible-joint space robot system into two subsystems using the singular perturbation approach then stabilized the fast subsystem by using a torque differential feedback controller and tracked the expected trajectory of the slow subsystem in joint space under the effects of uncertain parameters using a robust neural network control scheme. Chen and Chen (2012) discussed the robust control problem of a free-floating flexible-joint space robot with an uncontrolled base to track the desired trajectory in the workspace. Walsh and Forbes (2012) presented modeling of a two-link flexible manipulator with rotary joints and flexible telescopic booms, such as the Next Generation Large Canadarm under investigation by the Canadian Space Agency where they discretized each link's displacement by using the Rayleigh-Ritz method. The equations of motion were derived using Lagrange's equation. The two links were initially assumed to be free floating; their motion is constrained appropriately using a technique known as the null-space method. Guo and Sun (2013) tackled the problem of vibration suppression by approximating the flexible link on the assumed mode method and then with the second Lagrange approach and the linear momentum conservation and applied nonlinear robust control and nonlinear robust adaptive control schemes for the coordinated motion of the free-floating flexible space manipulator system. Tian et al. (2013) studied the coupling dynamics and control of a satellite capturing flexible robot and solar panel system using the Absolute Nodal Based (ACB) method and proposed the stability of the satellite attitude. Xu and Sun (2013) established a dynamic model of a three-dimensional four-link flexible-joint space manipulator with revolute joints considering the different values of nonlinear stiffness coefficient of the torsion-spring and inertia coupling by the Lagrange method and verified the model by PD controller.

Ollero et al. (2021) presented a review paper on aerial robotic manipulators. Ding et al. (2019) carried out a literature review of aerial manipulation using rotorcraft-mounted manipulators with respect to mechanical structure design, and modeling and control for the period of 2008-2017. Sharifi et al. (2015) developed a nonlinear robust adaptive impedance controller for unmanned aerial vehicles equipped with a robot manipulator.

Orlowski, and Girard (2012) presented a review of flight dynamics, stability, and control of flapping wing micro-air vehicles. Abas et al. (2016) presented a review paper on numerical analysis of flapping wing biomimetic aerial vehicles from the Nanoscale to the micro-scale. He et al. (2018) proposed the boundary control for undesired vibrations of flapping-wing robotic aircraft.

Dong et al. (2020) developed a three-wing flapping wing rotor micro aerial vehicle that could perform controlled flight.

Abo-Shanab and Sepehri (2002) studied the dynamic stability of planar movements of a Caterpillar excavator-based log-loader as virtual links to reformulate the modeling of the non-fixed base manipulator in terms of a fixed-base manipulator with one degree of freedom joints that not only took into account the dynamics of the base that can potentially roll back-and-forth but also accounted for the flexibility of the contact between the base and the ground. Erkaya, S. (2012) studied the effects of joint clearance on a welding robot manipulator. Rafieian et al. (2009) studied the chatter vibrations in robotic grinding operations considering the grinding robot with flexible joints and rigid links and obtained dynamic equations by Lagrange's method. Chen et al. (2010) designed the collision-detecting sensor based on the difference between the reference torque calculated according to the dynamic model and the factual torque. Huang et al. (2011) designed the joint torque sensor of an assistive robotic manipulator to detect the collision by applying the finite element analysis method, optimized the pasted position of a strain gauge, developed a signal processing circuit with high disturbance-resisting capacity, and performed the experiment to ascertain higher sensitivity and real-time performance of the proposed design.

Simaan et al. (2009) carried out the design, development, and analysis of a continuum telerobotic system for minimally invasive surgery of the throat. Li et al. (2016) carried out the design, development, and analysis of a wire-driven snake-like continuum robotic flexible manipulator for minimally invasive surgery. Zhong et al. (2020) wrote a review paper on recent advances in the design and development of continuum robots for medical applications.

Li and Gao (2010) presented a mechanism based on flexible hinges and semi-cylindrical revolute joints to amplify the displacement of stack-type piezoelectric ceramic actuators. Ji and Hu (2011) designed a planar 2-DoF parallel four-bar manipulator modeled a 1-DoF flexure hinge and carried out static and dynamic analysis of the parallel four-bar manipulator.

Jensen-Segal et al. (2008) simulated and built a prototype of a bio-inspired vertical wall climbing pendular robot. Guo and Chen (2009) built a virtual model of a bionic cockroach robot with its coxa link made of flexible material and carried out kinematic simulation with Finite Element and Multi-body Dynamics software. Yu et al. (2006) studied the dynamic modeling of

robotic fish using Schiehlen's method. Yu et al. (2013) developed a small deployable agent (end-effector) vehicle connected by a smart cable to an underwater autonomous vehicle to manipulate a target with minimum collision risk. Svinin et al. (2006) studied the motion planning of human-like movements in the manipulation of flexible objects. Zhao (2010) designed and developed an anthropomorphic arm with 7 degrees of freedom and carried out an analysis with respect to its kinematics, workspace singularities, and self-motion. Geng et al. (2011) developed a new type of bidirectional controllable flexible bending joint based on elongation artificial muscles which can elongate axially and bend in two-dimension with two-way control in space and did the theoretical and experimental analysis on both axial elongation and bending deformation of joint and got the pressure-elongation relationship and bending moment-angle properties. Wang et al. (2012) conducted a dynamic analysis of the cable-driven humanoid arm (CDHA) based on Lagrange's method and validated it through several simulations in Matlab. In the next section, a literature review on cooperative manipulators has been carried out.

2.6. Cooperative Manipulators

Many tasks that are difficult or even impossible to execute by a single robot can become affordable when two or more manipulators are employed in a cooperative manner. Not only this, keeping in view, the lack of skilled manpower or limitations of human operators, robots in the near future will perform tasks together with humans. The use of two or more independent arms for manipulation tasks has several advantages over conventional robots. For instance, a cooperative system can reduce the need for custom fixtures, permit the use of a simpler tool, and handle flexible objects. Furthermore, heavy objects can be manipulated by sharing the load among many robots. But the use of cooperative manipulators requires more advanced modeling and control techniques. However, the research in this area is relatively new and cannot be said to be so adequate. The following section 2.6.1 depicts the evolution of research work in this field.

2.6.1 Historical Review of Cooperative Manipulators

Siciliano and Khatib (2008) have presented detailed accounts of the development of research works on cooperative manipulators in their handbook on robotics. Early works on cooperative manipulators can be traced to the work of Fujii and Kurono (1975), Nakano et al.

(1974), and Takase et al. (1974) who investigated the control of multi-arm robots, for example, master-slave control, force/compliance control and task space control. Fujii and Kurono (1975) and Takase et al. (1974) worked on force/compliance control that was implemented by exploiting the back-drivability of the actuators without using force/torque sensors, the importance of which was not recognized at the time and researchers were driven towards more complex approaches like using force/torque sensors in robotics. Nakano et al. (1974) proposed a master/slave force control approach for the coordination of two arms carrying an object cooperatively and stressed the necessity of force control for cooperative robots.

Uchiyama and Dauchez [(1988), (1993)], Walker et al. (1991), and Bonitz and Hsia (1994) solved these problems by force decomposition. William and Khatib (1993) devised geometrically clear parameterization of internal forces/moments acting on the object which was an important step in solving the problem of cooperative manipulation.

Several cooperative control schemes based on parameterizations have been designed including control of motion and force, for example, by Uchiyama and Dauchez [(1988), (1993)], Wen and Kreutz-Delgaudo (1992), Yoshikawa and Zheng (1993) and Perdereau and Drouin (1996) and impedance/compliance control by Bruhm et al. (1989), Schneider and Cannon Jr. (1992) and Bonitz and Hsia (1996). Other approaches include adaptive control by Hu et al. (1995) and Liu and Arimoto (1998), kinematic control by Chiacchio (1996), task-space regulation by Caccavale et al. (2000), joint-space control by Luecke and Lai (1997) and Caccavale et al. (1999) and coordinated control by Hsu (1993).

Also, the definition of user-oriented task-space variables for coordinated control by Caccavale et al. (2000) and the development of meaningful performance measures by Chiacchio et al. (1991) and Lee (1989) have been fruitfully investigated in the 1990s.

Orin and Oh (1981), Zheng and Luh (1988), Walker et al. (1989), Uchiyama (1990), and Munawar and Uchiyama (1997) worked on load sharing among the arms for optimal load distribution among the arms and robust holding of the object when the object is held by the arm without being grasped rigidly. So, this becomes a problem of optimization and can be solved by either heuristic [Uchiyama and Yamashita (1991)] or mathematical methods [Uchiyama and Kanamori (1992)]. Zhang and Chen (1993), Svinin and Uchiyama (1994) and Yukawa et al. (1996)

worked on the cooperative handling of the multibody and flexible objects. Uchiyama and Kanno (1996), Yamano et al. (2004), and Miyabe et al. (2004) studied the control of multi-flexible arm manipulators in cooperative manipulation.

In the 2000s, works on synchronization control of cooperative systems started in which the control problem is formulated accounting for the synchronization of motion of the manipulators involved in a cooperative task. Sun and Mills (2002) and Rodriguez-Angeles and Nizmeijer (2004) worked on synchronization control of cooperative systems. Lian et al. (2002) and Gueaieb et al. (2003) employed nonlinear intelligent control to mitigate parametric uncertainties, unmodeled dynamics, and external disturbances. Gudino-Lau et a. (2004) investigated control strategies for cooperative manipulators in the presence of partial state feedback. Researchers' communities started taking a heightened interest in applying cooperative control strategies on conventional industrial robots.

In the next section research on cooperative manipulators have been categorized under various domain of modeling and control and it has been tried to include more recent works in this area. A literature review on kinematic and dynamic analyses and on the control of cooperative manipulators has been presented.

2.6.2 Kinematic Analysis of Cooperative Manipulators

Munasinghe et al. (1999) worked on off-line trajectory generation that guarantees high-speed and precise end-effector point-to-point (positioning) control of industrial robot arms within the bounds of the most relevant constraints. Nakamura et al. (2002) worked on the control of trajectory generation by applying a method based on nonlinear separation that decomposes the nonlinear dynamics from the nonlinear static parts and linear dynamic parts. The controller was constructed for separation of trajectory generation and taught data generation for better performance under the speed and torque constraints imposed by the hardware of the robot arm. Chung and Slotine (2009) studied cooperative control and global exponential synchronization of groups of Lagrangian systems, such as mechanical robots. Dong and Farrell (2009) considered the cooperative control of multiple nonholonomic systems with dynamics and uncertainty and proposed cooperative control laws based on backstepping techniques such that the state of each system converges to a target point that moves along a desired trajectory. Samiei and Shafiee (2010)

developed a dynamic model of two cooperative rigid-flexible link manipulators and an object, based on the Lagrange equation and assumed mode method and obtained minimal constraint equations of the system. Matei (2012) used the Petri-net methodology to model a flexible manufacturing system that involved a team of different robots that worked together to make all the moulds of liquid aluminum. Fratu and Ilea (2012) developed a control algorithm for the avoidance of collision between two robots working in the same environment. Ouyang et al. (2012) proposed the method of position domain PD control instead of time domain PD control for tracking the contour of the end effector by which they claim to get zero tracking error for the master motion while the errors in controlling slave motion still persisted and contributed to the overall errors in tracking contour. According to the authors, the benefit of position domain PD control is that this ensures the synchronization of multiaxes motions between the reference motion and slave motions with respect to not only position but also velocity. Jazi et al. (2012) addressed the dynamic analysis by considering a new formulation for frictional contact used in dynamic modeling. Zhiguo et al. (2012) formulated the dynamics and the vibration of a flexible payload such as a solar panel of an artificial satellite by FEM and Lagrange's equation and carried out adaptive backstepping observer-control of a dual-manipulator cooperative system handling a flexible payload. Guidali et al. (2013) developed a method comprehensively to estimate the patient's contribution by combining kinematic measures and the motor assistance applied. They also carried out experiments to validate the method they developed. Bonarini et al. (2013) proposed R2P (Rapid Robot Prototyping), a modular approach. Ma and Tang (2013) suppressed the vibration for two manipulators handling a flexible payload using observer-based control theory where he used Lyapunov stability theory. Aghili (2013) worked on a technique that updated the kinematic parameters pertaining to the relative position/orientation uncertainties of the interconnected manipulators online by two cascaded estimators in order to tune a cooperative controller for achieving accurate motion tracking with minimum-norm actuation force that eliminated the need for high precision end-point sensing or force measurements. Long et al. (2014) studied the selection of feasible actuation schemes for the NAO robot with both arms engaged in a cooperative task by using screw theory. Dong, and Zhu (2018) planned the dynamic trajectory of a robotic manipulator in real-time at each sampling instant, based on the visual feedback and performed validation experiments for a predictive visual servo kinematic control scheme for the manipulator with the eye-in-hand configuration to perform autonomous capture of a non-cooperative space

target. Kim et al. (2019) applied a linear quadratic regulator and proportional-integral-derivative controller for trajectory tracking in cooperative transportation of an object by T3-multi rotors.

2.6.3 Dynamic Analysis and Control of Cooperative Manipulators

Lee and Kim (1990) presented dual redundant arm system operational quality measures to quantify the efficiency and capability of generating Cartesian accelerations by two cooperative arms based on the analysis of dual-arm dynamic interactions. Murphy et al. (1991) analyzed cooperative robot manipulators on a mobile platform. Pin et al. (1992) proposed a general conceptual architecture for enhancing the synergy between humans and machines of cooperative systems and investigated the implementation of the concept to the synergistic integration of the teleoperated and autonomous operation of a manipulator's arm for the execution of sequential tasks. Sarkar et al. (1994) designed nonlinear feedback for maintaining rolling contact between a robot arm and a moving object. Khatib et al. (1996a) studied the coordination and decentralized cooperation of multiple mobile manipulators. In another paper, Khatib et al. (1996b) developed an approach to control redundant systems of vehicle/arm coordination and multiple mobile manipulator decentralized cooperation operations based on the augmented object and virtual linkage concept. Casalino and Turetta (2003) dealt with the problem of suitably coordinating the maneuverings of a non-holonomic vehicle and the motion of a supported manipulation system (composed of one or two arms) when the overall system is commanded to execute a given grasping or manipulation task. Zeng and Sepehri (2004) designed a nonlinear position regulator for cooperating hydraulic manipulators handling a rigid object using Lyapunov's second method. Sujan and Meggiolaro (2004) addressed the problem of disturbance compensation for the successful assembly of structures by mobile field robots using a control architecture, consisting of a linear PID joint controller with model predictive feed-forward compensation for mobile base motions and interactive-force disturbance rejection. Zeng and Sepehri (2005) described the dynamic model of two or more hydraulic robots to coordinately regulate an object’s position/orientation while maintaining specified load sharing between the manipulators. Tinos et al. (2006) studied the motion and force control of cooperative robotic manipulators with passive joints. Chen and Li (2006) studied a group of mobile manipulators transporting an object with some mass and designed a leader-follower type control by applying a decentralized NN control law to model robot dynamics online. Setoodeh et al. (2006) studied discrete-time multi-model

control for cooperative teleoperation under time delay. Zhao (2011) studied the stability of a humanoid robot named YIREN using the zero moment point for the waist cooperative motion to compensate for the moment generated by the trajectory of the arms. Aghili (2011) addressed the problem of adaptive control of cooperative manipulators carrying an object in the presence of geometric uncertainties in the closed-kinematic loop. Panwar et al. (2012) designed an adaptive neural controller for a cooperative multiple-robot manipulator system manipulating a single rigid object. Zi et al. (2012) studied the kinematics and dynamics of cooperative cable parallel manipulators for multiple mobile cranes (CPMMCs) using the geometric methodology and d' Alembert's principle and simulated the results for triple mobile cranes with 6 Degrees of Freedom. Abdelhedi et al. (2013) designed a controller by incorporating the cross-coupling technology into the sliding mode control for a nonlinear system of multiple networked robot manipulators. Esakki et al. (2013) worked on robust control of two three-link collaborative planar rigid manipulators handling a flexible object in the prescribed trajectory using the singular perturbation technique. Kasi et al. (2014) applied disturbance observer-based position control in the robot manipulator maneuver and cooperative control in cooperative drilling operations to maintain the alignment of the drill bit during the bone drilling experiment. For a robotic system of systems (SoS) consisting of m number of distributed, cooperative, and heterogenous manipulators, Incremona et al. (2015) proposed a supervisory sliding mode (SM) control with a modular and composable approach relying on basic modules featuring a multilevel functional architecture, including a supervisor and a couple of hybrid position/force control schemes associated with a couple of cooperative robotic manipulators and verified it experimentally. Ficuciello et al. (2014) experimentally investigated the region of stability in the impedance parameter space of Cartesian impedance control of a redundant robot arm executing a cooperative task with a human. Casalino et al. (2015) carried out the kinematic and dynamic modeling, and the cooperative control of the transportation of large objects in underwater scenarios using two free-floating vehicles each one endowed with a 7 degrees of freedom redundant manipulator. Baigzadehnoe et al. (2017) proposed an adaptive fuzzy backstepping position tracking control scheme for position and force control of multi-robot manipulator systems handling a common object cooperatively. Zhan et al. (2020) presented an RBFNN-based collision-free detumbling strategy (CFDS) for a space manipulator to detumble a non-cooperative target while avoiding collisions in a static or dynamic environment using an acceleration potential field (AccPF) method. Kabanov, and Kramar (2021) implemented the

suboptimal feedback cooperative control based on state dependent Riccati Equations (SDRE) in which a common controller for the entire cooperative system in an underwater environment has been used. Zhang et al. (2021) applied recurrent neural network (RNN) control to avoid the mutual collision of dual robot manipulators while doing collaboration tasks of cup-stacking. Zhai et al. (2022) proposed an adaptive neural synchronized impedance controller (ANSIC) to achieve and guarantee the desired movement trajectory and manufacturing force in the cooperation task by cooperative manipulators processing under uncertain environments.

2.6.4 Modeling and Control of Flexible Cooperative Manipulators

Matsuno and Hatayama (1995) presented quasi-static cooperative control of two two-link flexible manipulators. Kim and Uchiyama (2000) did dynamic modeling of cooperating flexible manipulators handling a rigid object by using lumped parameters. Dou and Yu (2002) did dynamic modeling of flexible cooperative manipulators by using the finite element method and the Lagrange equation. They applied the predictive and compensative control algorithm to complete the inverse dynamic task of the system based on the compensation of the nominal rigid configuration of flexible manipulators. Liu and Yu (2003) using FEM studied the dynamic model of two 4R redundant flexible robots cooperating with a rigid payload. Zhang and Yu (2003) did the dynamic modeling and analysis of the cooperative flexible manipulators and proposed the inverse dynamic model by the force distribution method to track a desired trajectory accurately. Zhang and Yu (2004) carried out the dynamic analysis of planar cooperative manipulators with link flexibility. Trivailo (2006) presented non-linear dynamic modeling of composite systems of multiple flexible robotic manipulators. Esakki et al. (2013) worked on robust control of two three-link collaborative planar rigid manipulators handling a flexible object in the prescribed trajectory using the singular perturbation technique. Stolfi et al. (2018) optimized control gains of the impedance and proportional-derivative control using a cost function strategy against the interaction between rigid and elastic dynamics during the impact phase between a space manipulator and a target satellite.

2.7 Modeling and Control of Manipulators Working in Coordination

There are many jobs that need not be handled by a group of cooperative robots. But, they need coordination with the ambient environment as well as among the robots that are involved in such types of jobs. For example, autonomous vehicles don't need cooperative handling but they are needed to be operated in coordination with the other vehicles and passengers in their vicinity. The modeling and control strategies that are involved in such types of jobs are also required to be applied in the case of cooperative manipulators. Here, a few of the works done in coordinated or coordinating robots have been mentioned. Seo et al. (2009) proposed a reinforcement learning method with a cascade Support Vector Machine based on structural risk minimization and distributed genetic algorithms for behavior learning and the evolution of collective autonomous mobile robots. Duchon et al. (2012) presented a concept paper that dealt with the different aspects of developing an autonomous intelligent vehicle. Bertuccelli et al. (2012) tried to optimize the vehicle decisions, such as route planning and allocation of team resources while operating in a dynamic and uncertain environment using a robust adaptive Markov Decision Process (RAMDP) algorithm. Lai et al. (2008) modeled fuzzy belief with a plausibility degree to deal with the logical omniscience problem of belief modeling and to create new tools for intelligent systems modeling, like propositional modal logic and fuzzy propositional modal logic which are tools for belief modeling. Alexis et al. (2011) proposed a switching model predictive attitude controller for an unmanned quad-rotor helicopter subject to atmospheric disturbances. The proposed control scheme is computed based on a piecewise affine (PWA) model of the quad-rotor's attitude dynamics, where the effects of the atmospheric turbulence are taken into consideration as additive disturbances. The quadrotor rejects the induced wind disturbances while performing accurate attitude tracking. Bertrand et al. (2011) presented both design and stability analyses of a hierarchical controller for a miniature VTOL (vertical takeoff and landing) UAV and designed position and attitude controllers with a time scale separation of the translational dynamics and the orientation dynamics of a six degrees of freedom VTOL UAV model applying singular perturbation theory. Gkountas and Tzes (2021) presented the modeling and control of Unmanned Aerial Manipulators (UAMs) in a leader/follower configuration performing a cooperative manipulation task. Thapa et al. (2018) presented the force control of a group of aerial manipulators

collaboratively transporting a flexible payload. Chang and Fu (1997) proposed a novel framework of a hybrid system of multiagents with switching behaviors approach, random walk, formation, and obstacle avoidance to facilitate multiagents to search for a target and formation within an unknown indoor environment. Ko et al. (2011) proposed an intelligent surveillance system based on swarm robot technology that worked by invader enclosing techniques using swarm robots based on multiple distributed object environments. The proposed methods are composed of three main stages: location estimation of the object, specified object tracking, and decision on the cooperative behavior of the swarm robots. Couceiro et al. (2013) carried out a comparison of different swarm robotic algorithms like Robotic Darwinian Particle Swarm Optimization (RDPSO), Extended Particle Swarm Optimization (EPSO), Physically-embedded Particle Swarm Optimization (PPSO), Glowworm swarm optimization (GSO), and Aggregations of foraging swarm (AFS) for operations like search and rescue operations and found that RDPSO was the most effective one. Shuai et al. (2009) have controlled the various expressions of the face of a humanoid robot, like head movement and greeting action, with the help of the motion controller that controlled the action of different kinds of motors and sensors. Hatanaka and Fujita (2010) worked on an image-based control technique to estimate the target object's motion in 3D space from vision data and proved the stability by using passivity. Lee et al. (2009) introduced the method of visual imaging during pre- and intra-operative sessions of minimally invasive surgery which produced 3-dimensional images of tissues under surgery by biomechanical modeling. Zhao (2010) developed the waist of a humanoid robot and studied its dynamic behavior in tandem with manipulators for the overall stability of the robot.

With the last section, the literature review on FLMs and cooperative manipulators has become over. The next few sections present the summary of the review, the technical gap in the research work carried out so far, and the objectives of the present research work.

2.8 Summary and Identification of Research Gap

2.8.1 Summary of Research Work

In the present chapter, a literature survey for manipulators with flexible links and/or flexible joints as well as for cooperative types of manipulators has been done. From the literature

survey, it can be concluded that extensive study has been conducted on all types of flexible manipulators, whether it is flexible link manipulator or flexible joint manipulator, or flexible-joint and flexible-link manipulator. All types of flexible manipulators, single-link or multilink, planar or three dimensional are studied in the past. Different researchers worked intensively on kinematics, dynamics, numerical solutions, experimental validation, and control of flexible manipulators as well as cooperative manipulators. Different types of composite materials such as hybrid polymer composite material of carbon fiber, glass fiber, Kevlar fiber, etc., and active smart materials (PZT) have been used to fabricate the links of flexible manipulators in order to damp their vibrations. Also, different types of designs of links have been considered, for example, tapered beams, curved beams, etc. in order to obtain minimum tip deflections. Optimization of dimension parameters of a manipulator is also used by a few investigators to increase the natural frequency of flexible link manipulators.

In most of the cases, the flexible links of the manipulators have been modeled as Euler-Bernoulli's beam. In some cases, the Timoshenko beam also has been considered. In order to find the displacement of any point on a link, the assumed mode method, finite element method as well as finite segment method have been used for the discretization of links in the kinematic analysis of a manipulator. In some works, joints trajectory based on fifth-order polynomial trajectory and soft motion trajectory were designed to control the jerk which enhances the utilization of flexible manipulators in many tasks.

For dynamic analysis of the manipulator, use of different types of methods for finding the dynamic equation of motion of the manipulator, such as Newton-Euler formulation, Hamilton's method, extended Hamilton's method, Euler-Lagrange formulation and Gibbs-Appell (G-A) formulation of dynamic equation of motion have been found in the literature. A relatively new method of kinematic and dynamic analysis: Kane's method is also found in a few cases. In some cases, the dynamic modeling of systems with large displacements and small elastic deformation have been based on an Equivalent Rigid Link System (ERLS) that enables to decouple the kinematic equations of the Equivalent Rigid Link System from the compatibility equations of the displacements at the joints. A few formulated the dynamics of a spatial manipulator arm consisting of n number of flexible links and n number of flexible joints using 4 by 4 homogenous transformation matrices. Many authors used the floating frame of reference (FFR) formulation,

one of the most used methods for the dynamic modeling of multibody flexible-link mechanisms with large displacements and small deformations. Few of the investigators formulated the dynamics of a spatial manipulator arm to find out all types of deformation: transversal, longitudinal, and torsional deformations of its tip.

Solutions of dynamic equations of motion of the manipulator have been obtained by using various numerical integration methods such as Runge-Kutta 4^{th} and 5^{th} order methods, Newmark time integration method, and Adams-Bashforth-Moulton method.

Various types of open-loop and closed-loop control algorithms have been applied for attenuating the vibrations and tip deflections of a flexible manipulator. In open loop control, input shaping method have been used for the containment of vibration of the robotic arm by suitably planning joint trajectories of the manipulator. In closed loop control, PID control, sliding mode control, fuzzy control, neural network, and combinations of these and many more types of control have been applied to minimize the tip deflections. For example, control of vibration of a flexible manipulator can be found in literature where a non-linear control technique, such as, the backstepping method has been tuned using a genetic algorithm (GA), cuckoo search algorithm (CSA), and teacher learning-based optimization (TLBO) for obtaining the best control performance.

Lyapunov stability theorem was used as a mathematical tool to check the stability of the overall system. Various types of experimental designs have been developed to validate the efficacy of the developed modeling and control algorithms.

The use of two or more independent arms for manipulation tasks has several advantages over conventional robots. For instance, a cooperative system can reduce the need for custom fixtures, permit the use of a simpler tool, and handle flexible objects. Furthermore, heavy objects can be manipulated by sharing the load among many robots. But the use of cooperative manipulators requires more advanced modeling and control techniques.

The critical issue of parameterizing the constraint forces/moments on the object based on the dynamic model of the whole cooperative system led to the definition of task control variables which solved many problems like how to control simultaneously the trajectory of the object, mechanical stresses (internal forces/moments) acting on the object, load sharing among the arms,

and even the external forces/moments on the object. Investigations on the control of cooperative manipulators comprised of master-slave control, force/compliance control, and task space control of multi-arm robots. Intensive research on different aspects of multi-arm robots, like the definition of task vectors with respect to the object to be handled, the dynamics of closed kinematic chain formed by multi-arm robot, and the object and force control issues such as hybrid position force control, was carried out by different researchers which made the basis for further study on more advanced topics from 1990s to till date.

2.8.2 Identification of Research Gap

It is desired to design lighter robots with large payload-to-weight ratios that can also operate at higher speeds which makes them a subject of intensive research. As it is evident from the above literature survey in sections 2.1 to 2.3 that the main focus of most of the researchers was on kinematic and dynamic analyses as well as on the control of flexible manipulators. Stress is on precise modeling of the FLMs. Some used the finite element method while others used the assumed mode method. For controlling tip deflection, some researchers used passive control methods, like using viscoelastic material for the fabrication of the link of FLM while many used active controls. Some used open loop-like input shaping techniques while others used closed loop control.

Very few investigators tried to find out the root cause of vibration in flexible manipulators. It is important to identify the factors upon which tip deflections of a flexible manipulator depend. How and to what extent these factors affect the dynamic behavior of a flexible manipulator is still not investigated thoroughly. A few who tried to do the parametric study of FLMs found the effects of tip payload mass and joint actuator inertia on the behavior of a flexible arm robot. Some studied the effect of hub inertia and payload on the vibration of a flexible manipulator. Few evaluated the effect of link flexibility on the tip position of a single link robotic arm to find the limiting inertia for payload mass if the allowable tip deviation is constrained to a certain limit, say, 5%. Shape optimization of a single-link flexible manipulator was also carried out by varying the cross-sectional area of the link along its length keeping the constraint on the mass of the manipulator and static tip deflection in order to maximize the fundamental frequency of the beam. But, they considered the effect of diameter only, that too, for a single link manipulator which has a limited workspace. A few did parametric study of a 2-link flexible manipulator, but they have simplified

their system by linearizing the system. They have not considered the effect of centrifugal and Coriolis forces and acceleration due to gravity also. When a flexible manipulator consists of more than one flexible link then its dynamic behavior does not depend on the parameters of its individual link only. Rather, it depends on the combined effect of the parameters of all the links that the manipulator is composed of. So, it can be concluded that the parametric study of a multilink flexible manipulator is still required to find out the effects of various parameters, for example, link length ratio, link diameter ratio, the ratio of the mass of payload to that of total link mass, as well as effects of different torque profiles on the dynamic responses of the manipulator with regard to joint angles, static deflection, residual vibration, response and settling time, etc. An attempt has been made in the present work to conduct a parametric study of a two-link flexible manipulator in chapter 3 of this thesis to find the dependence of the dynamic behavior of the manipulator on its various parameters.

The extensive survey on the modeling and control of flexible link manipulators also depicts that researchers are studying the modeling and control of FLMs for a long time so that they can replace RLMs with FLMs. In order to achieve minimum tip deflection of the FLMs, applications of various types of optimization techniques for shape optimization of flexible links (e.g., link of the tapered beam or kidney-shaped curved beam) have been applied. Some researchers applied passive damping techniques by using composite materials of viscoelastic damping layer for vibration damping of a flexible link manipulator. Some used hybrid vibration control techniques of viscoelastic damping along with active damping using piezoelectric sensors and actuators. Many researchers applied active vibration control like proportional, integral, and derivative control, sliding mode control, nonlinear feedback control based on the inverse dynamic model, a full-state linear quadratic regulator, a second-order bandpass filter, intelligent control, etc. to damp the mechanical vibrations of flexible robots. Many investigators successfully used input quantization based on the partial differential equation of the system with input-shaping techniques to suppress residual vibrations of FLMs.

In all these attempts by different researchers, the main aim is to control the tip deflection of an FLM. However, the same can also be achieved by using a pair of strings. The fact that the axial stiffness of a string is much larger than the bending stiffness of a cantilever beam of the same material and area of cross-section, can be effectively utilized to significantly increase the stiffness

of a flexible link manipulator if arranged in the proper configuration. Therefore, string-stiffened FLMs seek the attention of current researchers for the systematic study of their behaviors during operations.

The concept of variable stiffness structures is being applied for the control of end effectors of flexible manipulators in various applications. A few researchers designed and developed a compact variable stiffness and damping magnetorheological joint device for the control of residual vibrations of a single-link flexible manipulator. A cable-driven flexible manipulator for its suitable bending profile was also designed, developed, and mathematically optimized in order to achieve the required contact force and avoid obstacles.

Cables are also being used to support and contain vibrations of structures. Elaborate studies of active tendon control of slender and flexible structural systems such as long arms of tower cranes, guyed masts, and cable-stayed bridges, have been widely found in the literature to support and contain their oscillations. Many investigators studied the nonlinear interactions between a beam and the cable dynamics of a cable-stayed structure; designed the feedback control to stabilize the oscillations of both cable and beam of a cable-supported beam structure. The coupling between local and global modes of vibrations in a cable-stayed beam is studied. A parametric model that analytically describes the geometric nonlinearities in the dynamics of the structural system composed of two vertical cantilever beams connected by a suspended sagged cable was also proposed.

Although elaborate studies regarding the use of cables to support and control of vibrations of flexible structural systems are widely found in the literature to contain their oscillations, very few studies have been found where cables have been used to control the vibration of a flexible robotic arm. Only one or two investigators analyzed and experimentally tried to control the vibration of a single-link flexible manipulator by stiffening the manipulator through a pair of cables. They used either the finite segment method or the assumed mode method and Hamilton's principle to analyze the manipulator. However, with regard to the earlier studies following points of consideration occur and need to be addressed properly: (1) Mode shapes of a cantilever beam without any axial force have been taken. This may lead to the overestimation of tip deflection. (2) A single link manipulator has a limited workspace so that it may not be suitable in many practical conditions. (3) The behavior of cables during the operation of the manipulator and their effect on

the link vibration have not been considered. As cables are highly flexible and slack in themselves they may destabilize the manipulator operations. (4) Moreover, due to the pulling of the link tip by the pair of cables, the joint of the manipulator will behave erratically, which has not been considered. (5) Although the property of axial stiffness of the cables has been used, the axial deformation of the flexible link has not been considered. (6) The buckling strength of the flexible link has not been taken into account that must be considered as due to buckling the link may be destabilized and the tip may flip to the other side leading to the collision with the environment. (7) The effect of geometric nonlinearities on the dynamic responses of the string-stiffened flexible link manipulator cannot be neglected when large bending deformations may occur due to snapping through of the link tip due to forces at the link tip in axial and transverse directions. However, the earlier studies on a cable-stiffened flexible link manipulator have not considered the effect of geometric nonlinearities. (8) although the use of cables to stiffen the flexible link considerably minimizes the tip deflection, the residual vibrations of the link still persist. No attempt has been made to attenuate the vibration to zero. Therefore, an attempt has been made in the present research work to consider all the above factors while studying string-stiffened flexible link manipulators.

Various types of control and trajectory planning have been used to carry out cooperative tasks smoothly. But, path planning considering the jerks in robot motions has not been addressed adequately. In the last chapter of this thesis, kinematic and dynamic analyses of manipulators involved in collaborative work have been presented.

2.9 Objective of the Present Work (Problem Formulation)

In the present work, it is planned to study flexible manipulators with both joint and link flexibility.The objectives of the present research work can be presented in the following points:

- To carry out systematic mathematical modeling, analysis, and control of flexible manipulators with either link-flexibility or joint-flexibility as well as with both link and joint flexibilities.
- To investigate the dynamic behavior of a two-link flexible manipulator using the finite element method.

- To perform dynamic analysis using finite element method and LQR control of a single-link flexible manipulator with flexible joint.
- To carry out mathematical modeling and control of string-stiffened flexible-joint flexible-link manipulators in order to provide extra stiffness to the flexible link without adding much weight to the overall system.
- To conduct kinematic and dynamic analyses of two RRR collaborative manipulators.

Chapter 3

Parametric Study of a Two-Link Flexible Manipulator

3.1 Introduction

In the present work, a parametric study is carried out to analyze the dynamic behavior of a two-link flexible manipulator in which both links are flexible. It is desired to design lighter robots with large payload-to-weight ratios that can also operate at higher speeds which makes them a subject of intensive research. The dynamic behavior of a two-link manipulator depends upon several parameters, such as link length, link diameter, payload, the mass of the link, etc. Section 3.2 contains the finite element modeling of the manipulator. Sections 3.3 and 3.4 present respectively the kinematic analysis and the dynamic analysis. The results are discussed in section 3.5 and one verification is illustrated in section 3.6. The chapter is concluded in section 3.7.

3.2 Finite Element Modelling of the Manipulator

The finite element method has been used to discretize links of the manipulator into a finite number of elements. The finite element (FE) model of the 2-link flexible manipulator is shown in Fig 3.1. The finite element modeling of the manipulator has been done based on the work of Usoro et al. (1986). The number of finite elements for each of the two links is n_e. In the figure, the number for n_e has been chosen as 2 for an explanation. The model can be extended to different numbers of finite elements. In the figure, 1, 2, and 3 in ellipses denote the node numbers on link 1 and link 2. At the first node of the first element, a hub is situated while at the 2nd node of the 2nd element of 1st link motor is attached. A payload is attached to the tip of 2nd link. M_h and I_h are respectively mass and moment of inertia of the hub. Similarly, M_m and I_m are respectively mass and moment of inertia of the motor at the tip of the first link while M_P and I_P are respectively the mass and moment of inertia of the payload. Origin O of the inertial frame of reference XOY is on the hub center. $X_1O_1Y_1$ is the body attached frame of reference at the hub which rotates with the rotation of link 1. Points O and O_1 are coinciding. At the tip of the 1st link where the motor is situated, $X_2O_2Y_2$ is another body-attached frame of reference that is attached to link 2 so that $X_2O_2Y_2$ rotates with the rotation of link 2.

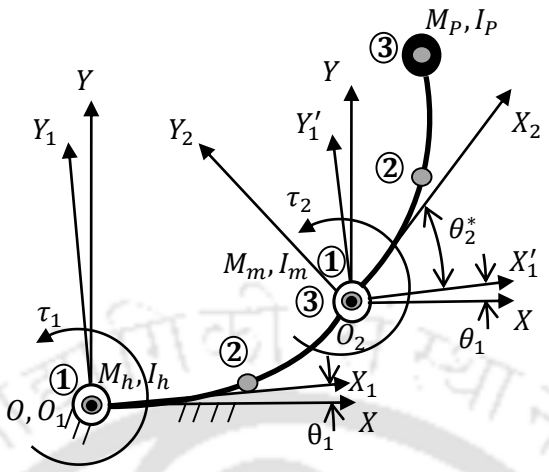

Figure 3.1: A two-link flexible manipulator

Each node has two degrees of freedom: flexural displacement and flexural rotation or slope. Thus there are four degrees of freedom per element which are denoted by $v_{1_{2j-1}}$, $v_{1_{2j}}$, $v_{1_{2j+1}}$ and $v_{1_{2j+2}}$ for the elements of 1st link and $v_{2_{2j-1}}$, $v_{2_{2j}}$, $v_{2_{2j+1}}$ and $v_{2_{2j+2}}$ for the elements of the 2nd link where 'j ' denotes the element number. The length of each element on link 1 is denoted by h_1 and that of each element on link 2 is by h_2. (x_{1_j}, y_{1_j}) and (x_{2_j}, y_{2_j}) are coordinates of a point on j^{th} element of link 1 and link 2 respectively in the body-attached local coordinate systems $X_1O_1Y_1$ and $X_2O_2Y_2$ that is attached to link 1 and link 2 respectively. τ_1 and τ_2 are the torques applied by respectively motor at the hub and that at the joint 2 at O_2. $\theta_1$is the angle subtended by link 1 in its deflected condition at any instant of time t. θ_2^* is the angle made by link 2 with the X-axis of the reference coordinate system? $X_1'O_2Y_1'$ where $\theta_2^* = \theta_2 + v_{1_{2n_1+2}}$. $v_{1_{2n_1+2}}$ is the slope of link 1 at its tip. $X_1'O_2Y_1'$ is parallel to the axis $X_1O_1Y_1$.

3.3 Kinematic Analysis

The links are considered as Euler-Bernoulli beams. The position vector of a point P_{1j} on j^{th} element of 1st link in the local coordinate system $X_1O_1Y_1$ is given by

$$\boldsymbol{r}_{\mathbf{1}_j}^{\mathbf{1}} = \begin{Bmatrix} (j-1)h_1 + x_{1_j} \\ y_{1_j} \end{Bmatrix} \tag{3.1}$$

y_{1_j} is given by $y_{1_j}(x_{1_j}, t) = \sum_{k=1}^{4} N_k(x_{1_j}) v_{1_{2j-2+k}}$ where $N_k(x_{1_j})$ are the Hermitian shape functions given by $N_1\left(x_{1_j}\right) = 1 - 3\frac{{x_{1_j}}^2}{{h_1}^2} + 2\frac{{x_{1_j}}^3}{{h_1}^3}$; $N_2\left(x_{1_j}\right) = x_{1_j} - 2\frac{{x_{1_j}}^2}{h_1} + \frac{{x_{1_j}}^3}{{h_1}^2}$; $N_3\left(x_{1_j}\right) = 3\frac{{x_{1_j}}^2}{{h_1}^2} - 2\frac{{x_{1_j}}^3}{{h_1}^3}$and $N_4\left(x_{1_j}\right) = -\frac{{x_{1_j}}^2}{h_1} + \frac{{x_{1_j}}^3}{{h_1}^2}$and $v_{1_{2j-2+k}}$ are the nodal variables of j^{th} element of link 1.

The position vector of the same point P_{1j} in inertial frame XOY can be given as

$$\boldsymbol{r_{1_j}^0} = T_1^0 \boldsymbol{r_{1_j}^1} \tag{3.2}$$

where $T_1^0 = \begin{bmatrix} cos\theta_1 & -sin\theta_1 \\ sin\theta_1 & cos\theta_1 \end{bmatrix}$ is the transformation matrix that transforms coordinates in the frame $X_1O_1Y_1$ to inertial frame XOY.

Similarly, the position vector of a point on j^{th}element of link 2 in inertial frame XOY is given by

$$\boldsymbol{r_{2_j}^0} = \boldsymbol{r_2^0} + T_1^0 T_2^1 \boldsymbol{r_{2_j}^2} \tag{3.3}$$

where $\boldsymbol{r_{2_j}^2} = \begin{Bmatrix} (j-1)h_2 + x_{2_j} \\ y_{2_j} \end{Bmatrix}$ is the position vector of a point on j^{th} element of link 2 in the body attached coordinate system $X_2O_2Y_2$. h_2 is the length of j^{th} element, $\left(x_{2_j}, y_{2_j}\right)$ are the coordinates of a point P_{2j} on j^{th} element of link 2 in the body attached coordinate system $X_{2_J}O_{2_J}Y_{2_J}$ at the junction of elements $(j-1)$ and j. The orientation of $X_{2_J}O_{2_J}Y_{2_J}$ and $X_2O_2Y_2$ has been supposed to be the same. $\boldsymbol{r_2^0}$ is the position vector of the origin $O_2$with respect to the origin of inertial frame O.

$$\boldsymbol{r_2^0} = T_1^0 \begin{Bmatrix} L_1 \\ v_{1_{2n_1+1}} \end{Bmatrix} \tag{3.4}$$

$$T_2^1 = \begin{bmatrix} cos(\theta_2 + v_{1_{2n_1+2}}) & -sin(\theta_2 + v_{1_{2n_1+2}}) \\ sin(\theta_2 + v_{1_{2n_1+2}}) & cos(\theta_2 + v_{1_{2n_1+2}}) \end{bmatrix} \tag{3.5}$$

and

$$y_{2_j}\left(x_{2_j}, t\right) = \sum_{k=1}^{4} N_k\left(x_{2_j}\right) v_{2_{2j-2+k}} \tag{3.6}$$

where $N_k(x_{2_j})$ are the Hermitian shape functions given by $N_1\left(x_{2_j}\right) = 1 - 3\frac{{x_{2_j}}^2}{{h_2}^2} + 2\frac{{x_{2_j}}^3}{{h_2}^3}$; $N_2\left(x_{2_j}\right) = x_{2_j} - 2\frac{{x_{2_j}}^2}{h_2} + \frac{{x_{2_j}}^3}{{h_2}^2}$; $N_3\left(x_{2_j}\right) = 3\frac{{x_{2_j}}^2}{{h_2}^2} - 2\frac{{x_{2_j}}^3}{{h_2}^3}$ and $N_4\left(x_{2_j}\right) = -\frac{{x_{2_j}}^2}{h_2} + \frac{{x_{2_j}}^3}{{h_2}^2}$ and $v_{2_{2j-2+k}}$ are the nodal variables of j^{th} element of link 2.

The velocity of point P_{1j} on j^{th} element of link 1 in the inertial frame of reference XOY in terms of Jacobean can be given as

$$\frac{d\boldsymbol{r}_{\boldsymbol{1_j}}^{\boldsymbol{0}}}{dt} = \frac{\partial \boldsymbol{r}_{\boldsymbol{1_j}}^{\boldsymbol{0}}}{\partial q_{1_j}}\dot{q}_{1_j} = \left[\frac{\partial \boldsymbol{r}_{\boldsymbol{1_j}}^{\boldsymbol{0}}}{\partial \theta_1} \quad \frac{\partial \boldsymbol{r}_{\boldsymbol{1_j}}^{\boldsymbol{0}}}{\partial v_{1_{2j-1}}} \quad \frac{\partial \boldsymbol{r}_{\boldsymbol{1_j}}^{\boldsymbol{0}}}{\partial v_{1_{2_j}}} \quad \frac{\partial \boldsymbol{r}_{\boldsymbol{1_j}}^{\boldsymbol{0}}}{\partial v_{1_{2j+1}}} \quad \frac{\partial \boldsymbol{r}_{\boldsymbol{1_j}}^{\boldsymbol{0}}}{\partial v_{1_{1_{2j+2}}}}\right]\dot{q}_{1_j} \tag{3.7}$$

where

$q_{1_j} = \left[\theta_1 \quad v_{1_{2j-1}} \quad v_{1_{2j}} \quad v_{1_{2j+1}} \quad v_{1_{2j+2}}\right]^T$ and $\dot{q}_{1_j} = \left[\dot{\theta}_1 \quad \dot{v}_{1_{2j-1}} \quad \dot{v}_{1_{2_j}} \quad \dot{v}_{1_{2j+1}} \quad \dot{v}_{1_{2j+2}}\right]^T$

where superscript T denotes the transpose of the vector and

$$\frac{d\boldsymbol{r}_{\boldsymbol{1_j}}^{\boldsymbol{0}\,T}}{dt} = \dot{q}_{1_j}{}^T\left[\frac{\partial \boldsymbol{r}_{\boldsymbol{1_j}}^{\boldsymbol{0}}}{\partial \theta_1}^T \quad \frac{\partial \boldsymbol{r}_{\boldsymbol{1_j}}^{\boldsymbol{0}}}{\partial v_{1_{2j-1}}}^T \quad \frac{\partial \boldsymbol{r}_{\boldsymbol{1_j}}^{\boldsymbol{0}}}{\partial v_{1_{2_j}}}^T \quad \frac{\partial \boldsymbol{r}_{\boldsymbol{1_j}}^{\boldsymbol{0}}}{\partial v_{1_{2j+1}}}^T \quad \frac{\partial \boldsymbol{r}_{\boldsymbol{1_j}}^{\boldsymbol{0}}}{\partial v_{1_{2j+2}}}^T\right]^T \tag{3.8}$$

Similarly, for point P_{2j} on j^{th} element of link 2, its velocity, and the transpose of velocity can be written in terms of Jacobean as follows

$$\begin{aligned}\frac{d\boldsymbol{r}_{\boldsymbol{2_j}}^{\boldsymbol{0}}}{dt} &= \frac{\partial \boldsymbol{r}_{\boldsymbol{2_j}}^{\boldsymbol{0}}}{\partial q_{2_j}}\dot{q}_{2_j} \\ &= \left[\frac{\partial \boldsymbol{r}_{\boldsymbol{2_j}}^{\boldsymbol{0}}}{\partial \theta_1} \quad \frac{\partial \boldsymbol{r}_{\boldsymbol{2_j}}^{\boldsymbol{0}}}{\partial \theta_2} \quad \frac{\partial \boldsymbol{r}_{\boldsymbol{2_j}}^{\boldsymbol{0}}}{\partial v_{1_{2n_1+1}}} \quad \frac{\partial \boldsymbol{r}_{\boldsymbol{2_j}}^{\boldsymbol{0}}}{\partial v_{1_{2n_1+2}}} \quad \frac{\partial \boldsymbol{r}_{\boldsymbol{2_j}}^{\boldsymbol{0}}}{\partial v_{2_{2j-1}}} \quad \frac{\partial \boldsymbol{r}_{\boldsymbol{2_j}}^{\boldsymbol{0}}}{\partial v_{2_{2_j}}} \quad \frac{\partial \boldsymbol{r}_{\boldsymbol{2_j}}^{\boldsymbol{0}}}{\partial v_{2_{2j+1}}} \quad \frac{\partial \boldsymbol{r}_{\boldsymbol{2_j}}^{\boldsymbol{0}}}{\partial v_{2_{2j+2}}}\right]\dot{q}_{2_j}\end{aligned} \tag{3.9}$$

where $q_{2_j} = \left[\theta_1 \quad \theta_2 \quad v_{1_{2n_1+1}} \quad v_{1_{2n_1+2}} \quad v_{2_{2j-1}} \quad v_{2_{2_j}} \quad v_{2_{2j+1}} \quad v_{2_{2j+2}}\right]^T$ and

$\dot{q}_{2_j} = \left[\dot{\theta}_1 \quad \dot{\theta}_2 \quad \dot{v}_{1_{2n_1+1}} \quad \dot{v}_{1_{2n_1+2}} \quad \dot{v}_{2_{2j-1}} \quad \dot{v}_{2_{2_j}} \quad \dot{v}_{2_{2j+1}} \quad \dot{v}_{2_{2j+2}}\right]^T$ so that

$$\frac{d\boldsymbol{r}_{\boldsymbol{2_j}}^{\boldsymbol{0}}{}^{T}}{dt}$$

$$= \dot{q}_{2_j}{}^{T}\left[\frac{\partial \boldsymbol{r}_{\boldsymbol{2_j}}^{\boldsymbol{0}}{}^{T}}{\partial \theta_1} \quad \frac{\partial \boldsymbol{r}_{\boldsymbol{2_j}}^{\boldsymbol{0}}{}^{T}}{\partial \theta_2} \quad \frac{\partial \boldsymbol{r}_{\boldsymbol{2_j}}^{\boldsymbol{0}}{}^{T}}{\partial v_{1_{2n_1+1}}} \quad \frac{\partial \boldsymbol{r}_{\boldsymbol{2_j}}^{\boldsymbol{0}}{}^{T}}{\partial v_{1_{2n_1+2}}} \quad \frac{\partial \boldsymbol{r}_{\boldsymbol{2_j}}^{\boldsymbol{0}}{}^{T}}{\partial v_{2_{2j-1}}} \quad \frac{\partial \boldsymbol{r}_{\boldsymbol{2_j}}^{\boldsymbol{0}}{}^{T}}{\partial v_{2_{2_j}}} \quad \frac{\partial \boldsymbol{r}_{\boldsymbol{2_j}}^{\boldsymbol{0}}{}^{T}}{\partial v_{2_{2j+1}}} \quad \frac{\partial \boldsymbol{r}_{\boldsymbol{2_j}}^{\boldsymbol{0}}{}^{T}}{\partial v_{2_{2j+2}}}\right]^{T} \tag{3.10}$$

The position vector of the motor at the tip of link 1 is given as

$$\boldsymbol{r}_{\boldsymbol{m}}^{\boldsymbol{0}} = T_1^0 \begin{Bmatrix} L_1 \\ y_{1_{n_1}}(x_{1_j} = h_1, t) \end{Bmatrix} \tag{3.11}$$

Putting $x_{1_j} = h_1$ in $y_{1_j}(x_{1_j}, t)$, where $j = n_1$ and $y_{1_j}\left(x_{1_j}, t\right) = v_{1_{2n_1+1}}$, Eq. (3.11) becomes

$$\boldsymbol{r}_{\boldsymbol{m}}^{\boldsymbol{0}} = T_1^0 \begin{Bmatrix} L_1 \\ v_{1_{2n_1+1}} \end{Bmatrix} \tag{3.12}$$

Similarly, the position vector of the payload at the tip of 2nd link is given by

$$\boldsymbol{r}_{\boldsymbol{p}}^{\boldsymbol{0}} = T_1^0 \begin{Bmatrix} L_1 \\ v_{1_{2n_1+1}} \end{Bmatrix} + T_1^0 T_2^1 \begin{Bmatrix} L_2 \\ v_{2_{2n_2+1}} \end{Bmatrix} \tag{3.13}$$

The translational velocity of the payload is given as $\frac{d\boldsymbol{r}_{\boldsymbol{p}}^{\boldsymbol{0}}}{dt}$ and translational velocity of the motor is given by $\frac{d\boldsymbol{r}_{\boldsymbol{m}}^{\boldsymbol{0}}}{dt}$. The angular velocity of the hub is written as $\omega_0^0 = \dot{\theta}_1 k$ where $k = [0 \quad 0 \quad 1]^T$; Angular velocity of the motor at the tip of 1st link is given by

$$\omega_2^0 = \dot{\theta}_1 k + \dot{\theta}_2 R_1^0 k = \dot{\theta}_1 \begin{Bmatrix} 0 \\ 0 \\ 1 \end{Bmatrix} + \dot{\theta}_2 \begin{bmatrix} cos\theta_1 & -sin\theta_1 & 0 \\ sin\theta_1 & cos\theta_1 & 0 \\ 0 & 0 & 1 \end{bmatrix} \begin{Bmatrix} 0 \\ 0 \\ 1 \end{Bmatrix} = (\dot{\theta}_1 + \dot{\theta}_2) \begin{Bmatrix} 0 \\ 0 \\ 1 \end{Bmatrix} \tag{3.14}$$

The angular velocity of the payload at the tip of 2nd link is given by

$$\omega_3^0 = \dot{\theta}_1 k + \dot{\theta}_2 R_1^0 k + \dot{\theta}_3 R_2^0 k = \dot{\theta}_1 \begin{Bmatrix} 0 \\ 0 \\ 1 \end{Bmatrix} + \dot{\theta}_2 \begin{bmatrix} cos\theta_1 & -sin\theta_1 & 0 \\ sin\theta_1 & cos\theta_1 & 0 \\ 0 & 0 & 1 \end{bmatrix} \begin{Bmatrix} 0 \\ 0 \\ 1 \end{Bmatrix} +$$

$$\dot{\theta}_3 \begin{bmatrix} cos(\theta_1 + \theta_2 + v_{1_{2n_1+1}}) & -sin(\theta_1 + \theta_2 + v_{1_{2n_1+1}}) & 0 \\ sin(\theta_1 + \theta_2 + v_{1_{2n_1+1}}) & \cos(\theta_1 + \theta_2 + v_{1_{2n_1+1}}) & 0 \\ 0 & 0 & 1 \end{bmatrix} \begin{Bmatrix} 0 \\ 0 \\ 1 \end{Bmatrix} = (\dot{\theta}_1 + \dot{\theta}_2) \begin{Bmatrix} 0 \\ 0 \\ 1 \end{Bmatrix} \tag{3.15}$$

$\dot{\theta}_3 = 0$, since the payload is assumed to be rigidly fixed to the tip of 2nd link. $R_i^0$is the rotation matrix that gives the orientation of i^{th}joint with respect to the inertial frame.

3.4 Dynamic Analysis

The kinetic energy T and potential energy V of the manipulator are given as follows

$$T(q,\dot{q}) = \sum_{i=1}^{m}\sum_{j=1}^{n_i} T_{i_j} + T_{hub} + T_{motor} + T_{payload} \tag{3.16}$$

$$V(q) = \sum_{i=1}^{m}\sum_{j=1}^{n_i} V_{i_j} + V_{hub} + V_{motor} + V_{payload} \tag{3.17}$$

Here $i = 1,2,\dots,m$, denotes the number of flexible links in the manipulator; $j = 1,2,\dots,n_i$, denotes the number of elements i^{th} link is divided into; q and $\dot{q}$ denote the generalized displacement and velocity vectors respectively. T_{i_j} and V_{i_j} denote the kinetic and potential energy of j^{th} element of i^{th}link respectively.

If $m_i$is the mass per unit length for i^{th}link, then the kinetic energy of j^{th}element of i^{th}link can be written as

$$T_{i_j} = \frac{1}{2}\int_0^{h_i} \frac{d\boldsymbol{r_{ij}^0}}{dt}^T m_i \frac{d\boldsymbol{r_{ij}^0}}{dt} dx_{i_j} = \frac{1}{2}\dot{q}_{i_j}{}^T \left(\int_0^{h_i} \frac{\partial \boldsymbol{r_{ij}^0}}{\partial q_{i_j}}^T m_i \frac{\partial \boldsymbol{r_{ij}^0}}{\partial q_{i_j}} dx_{i_j}\right)\dot{q}_{i_j} = \frac{1}{2}\dot{q}_{i_j}{}^T M_{i_j}\dot{q}_{i_j} \tag{3.18}$$

where $M_{i_j} = \int_0^{h_i} \frac{\partial \boldsymbol{r_{ij}^0}}{\partial q_{i_j}}^T m_i \frac{\partial \boldsymbol{r_{ij}^0}}{\partial q_{i_j}} dx_{i_j}$ is the mass matrix for j^{th} element of i^{th}link. On integration, for j^{th}element of 1st link, $M_{1_j}$is found to be

$$M_{1_j} = \begin{bmatrix} M_{1_j}(1,1) & M_{1_j}(1,2) & \cdots & M_{1_j}(1,5) \\ M_{1_j}(2,1) & & & \\ \vdots & & D_{1_j} & \\ M_{1_j}(5,1) & & & \end{bmatrix} \tag{3.19}$$

$$D_{1_j} = \frac{m_1 h_1}{420}\begin{bmatrix} 156 & 22h_1 & 54 & -13h_1 \\ 22h_1 & 4h_1^2 & 13h_1 & -3h_1^2 \\ 54 & 13h_1 & 156 & -22h_1 \\ -13h_1 & -3h_1^2 & -22h_1 & 4h_1^2 \end{bmatrix} \tag{3.20}$$

$$M_{1_j}(1,1) = \frac{m_1 h_1^3}{3}(3j^2 - 3j + 1) + \tilde{q}_{1_j}{}^T D_{1_j}\tilde{q}_{1_j} \tag{3.21}$$

where $\tilde{q}_{1_j} = [v_{1_{2j-1}} \quad v_{1_{2j}} \quad v_{1_{2j+1}} \quad v_{1_{2j+2}}]^T$;

$$M_{1_j}(1,2) = M_{1_j}(2,1) = \frac{m_1 h_1^2}{20}(10j - 7) \tag{3.22}$$

$$M_{1_j}(1,3) = M_{1_j}(3,1) = \frac{m_1 h_1^3}{60}(5j - 3) \tag{3.23}$$

$$M_{1_j}(1,4) = M_{1_j}(4,1) = \frac{m_1 h_1^2}{20}(10j - 3) \tag{3.24}$$

$$M_{1_j}(1,5) = M_{1_j}(5,1) = -\frac{m_1 h_1^3}{60}(5j - 2) \tag{3.25}$$

The total kinetic energy of link 1 can be found by summing over all the elements of link 1, i.e.,

$$T_1 = \sum_{j=1}^{n_1} T_{1_j} = \sum_{j=1}^{n_1} \frac{1}{2} \dot{q}_{1_j}^T M_{1_j} \dot{q}_{1_j} = \frac{1}{2} \dot{\hat{q}}_1^T M_1 \dot{\hat{q}}_1 \tag{3.26}$$

where

$$\dot{q}_{1_j} = \begin{bmatrix} \dot{\theta}_1 & \dot{v}_{1_{2j-1}} & \dot{v}_{1_{2j}} & \dot{v}_{1_{2j+1}} & \dot{v}_{1_{2j+2}} \end{bmatrix}^T \tag{3.27}$$

$$\dot{\hat{q}}_1 = [\dot{\theta}_1 \quad \dot{\bar{q}}_1]^T \tag{3.28}$$

$$\dot{\bar{q}}_1 = \begin{bmatrix} \dot{v}_{1_1} & \dot{v}_{1_2} & \dot{v}_{1_3} & \dot{v}_{1_4} & \cdots & \cdots & \dot{v}_{1_{2n_1-1}} & \dot{v}_{1_{2n_1}} & \dot{v}_{1_{2n_1+1}} & \dot{v}_{1_{2n_1+2}} \end{bmatrix}^T \tag{3.29}$$

Similarly, for j^{th}element of 2nd link, $M_{2_j}$is

$$M_{2_j} = \begin{bmatrix} M_{2_j}(1,1) & M_{2_j}(1,2) & M_{2_j}(1,3) & M_{2_j}(1,4) & M_{2_j}(1,5) & M_{2_j}(1,6) & M_{2_j}(1,7) & M_{2_j}(1,8) \\ M_{2_j}(2,1) & M_{2_j}(2,2) & M_{2_j}(2,3) & M_{2_j}(2,4) & M_{2_j}(2,5) & M_{2_j}(2,6) & M_{2_j}(2,7) & M_{2_j}(2,8) \\ M_{2_j}(3,1) & M_{2_j}(3,2) & M_{2_j}(3,3) & M_{2_j}(3,4) & M_{2_j}(3,5) & M_{2_j}(3,6) & M_{2_j}(3,7) & M_{2_j}(3,8) \\ M_{2_j}(4,1) & M_{2_j}(4,2) & M_{2_j}(4,3) & M_{2_j}(4,4) & M_{2_j}(4,5) & M_{2_j}(4,6) & M_{2_j}(4,7) & M_{2_j}(4,8) \\ M_{2_j}(5,1) & M_{2_j}(5,2) & M_{2_j}(5,3) & M_{2_j}(5,4) & & & & \\ M_{2_j}(6,1) & M_{2_j}(6,2) & M_{2_j}(6,3) & M_{2_j}(6,4) & & & & \\ M_{2_j}(7,1) & M_{2_j}(7,2) & M_{2_j}(7,3) & M_{2_j}(7,4) & & & & \\ M_{2_j}(8,1) & M_{2_j}(8,2) & M_{2_j}(8,3) & M_{2_j}(8,4) & & & & \end{bmatrix} = D_{2_j} \tag{3.30}$$

where $D_{2_j} = D_{1_j}$, is 4×4 matrix. Other elements of M_{2_j} can be found by integrating the respective terms of $M_{2_j} = \int_0^{h_2} \frac{\partial \boldsymbol{r_{2_j}^0}}{\partial q_{2_j}}^T m_2 \frac{\partial \boldsymbol{r_{2_j}^0}}{\partial q_{2_j}} dx_{2_j}$.

The total kinetic energy of link 2 can be found by summing over all the elements of link 2, i.e.,

$$T_2 = \sum_{j=1}^{n_2} T_{2_j} = \sum_{j=1}^{n_2} \frac{1}{2} \dot{q}_{2_j}^T M_{2_j} \dot{q}_{2_j} = \frac{1}{2} \dot{\hat{q}}_2^T M_2 \dot{\hat{q}}_2 \tag{3.31}$$

where

$$\dot{q}_{2_j} = \begin{bmatrix} \dot{\theta}_1 & \dot{\theta}_2 & \dot{v}_{1_{2n_1+1}} & \dot{v}_{1_{2n_1+2}} & \dot{v}_{2_{2j-1}} & \dot{v}_{2_{2j}} & \dot{v}_{2_{2j+1}} & \dot{v}_{2_{2j+2}} \end{bmatrix}^T \tag{3.32}$$

$$\dot{\hat{q}}_2 = \begin{bmatrix} \dot{\theta}_1 & \dot{\theta}_2 & \dot{v}_{1_{2n_1+1}} & \dot{v}_{1_{2n_1+2}} & \dot{\bar{q}}_2 \end{bmatrix}^T \tag{3.33}$$

$$\dot{\bar{q}}_2 = \begin{bmatrix} \dot{v}_{2_1} & \dot{v}_{2_2} & \dot{v}_{2_3} & \dot{v}_{2_4} & .. & .. & \dot{v}_{2_{2n_2-1}} & \dot{v}_{2_{2n_2}} & \dot{v}_{2_{2n_2+1}} & \dot{v}_{2_{2n_2+2}} \end{bmatrix}^T \tag{3.34}$$

The total kinetic energy of link 1 and link 2 can now be found by summing the kinetic energies of all the elements of both the links, i.e.,

$$T_L = \sum_{i=1}^{m} \sum_{j=1}^{n_i} T_{i_j} \tag{3.35}$$

T_L is the total kinetic energy of m number of flexible links. Here $m = 2$. Generalized variables $q =$

$$\begin{bmatrix} \theta_1, \theta_2, v_{1_1}, v_{1_2}, \dots, v_{1_{2n_1-1}}, v_{1_{2n_1}}, v_{1_{2n_1+1}}, v_{1_{2n_1+2}}, v_{2_1}, v_{2_2}, \dots, v_{2_{2n_2-1}}, v_{2_{2n_2}}, v_{2_{2n_2+1}}, v_{2_{2n_2+2}} \end{bmatrix}^T$$

$$T_{hub} = \frac{1}{2} \omega_0^{0^T} I_h \omega_0^0 \tag{3.36}$$

$$T_{motor} = \frac{1}{2} \frac{d\boldsymbol{r_m^0}}{dt}^T M_m \frac{d\boldsymbol{r_m^0}}{dt} + \frac{1}{2} \omega_1^{0^T} I_m \omega_1^0 \tag{3.37}$$

$$T_{payload} = \frac{1}{2} \frac{d\boldsymbol{r_p^0}}{dt}^T M_p \frac{d\boldsymbol{r_p^0}}{dt} + \frac{1}{2} \omega_2^{0^T} I_p \omega_2^0 \tag{3.38}$$

The potential energies of links are comprised of two parts: one due to the flexibility of the link and another due to gravity. Thus

$V_{i_j} = V_{i_{j_e}} + V_{i_{j_g}}$; where $V_{i_{j_e}}$ is the potential energy of elements due to the elasticity of links and $V_{i_{j_g}}$ is the potential energy of elements due to gravity.

$$V_{i_{j_e}} = \frac{1}{2}\int_0^{h_i} E_i I_i \frac{\partial^2 y_{i_j}}{\partial x_{i_j}^2} dx_{i_j} = \frac{1}{2}\bar{q}_{i_j}{}^T K_{i_j} \bar{q}_{i_j} \tag{3.39}$$

where $\bar{q}_{i_j} = [v_{i_{2j-1}} \quad v_{i_{2j}} \quad v_{i_{2j+1}} \quad v_{i_{2j+2}}]^T$; $K_{i_j} = \frac{E_i I_i}{h_i^3}\begin{bmatrix} 12 & 6h_i & -12 & 6h_i \\ 6h_i & 4h_i^2 & -6h_i & 2h_i^2 \\ -12 & -6h_i & 12 & -6h_i \\ 6h_i & 2h_i^2 & -6h_i & 4h_i^2 \end{bmatrix}$

$$V_{i_{j_g}} = m_i g[0\ 1]\boldsymbol{r_{ij}^0} \tag{3.40}$$

where i denotes the link number and j denotes the element number.

For any element of link 1, $V_{i_{j_g}}$ is given by

$$V_{1_{j_g}} = m_1 g[0\ 1]T_1^0 \begin{Bmatrix} \left(j-\frac{1}{2}\right)h_1^2 \\ \frac{h_1}{2}v_{1_{2j-1}} + \frac{h_1^2}{12}v_{1_{2j}} + \frac{h_1}{2}v_{1_{2j+1}} - \frac{h_1^2}{12}v_{1_{2j+2}} \end{Bmatrix} \tag{3.41}$$

And for any element of link 2, $V_{i_{j_g}}$ is given by

$$V_{2_{j_g}} = m_2 g[0\ 1]T_1^0 \begin{Bmatrix} L_1 \\ v_{1_{2j+1}} \end{Bmatrix} h_2 + m_2 g[0\ 1]T_1^0 T_2^1 \begin{Bmatrix} \left(j-\frac{1}{2}\right)h_2^2 \\ \frac{h_2}{2}v_{2_{2j-1}} + \frac{h_2^2}{12}v_{2_{2j}} + \frac{h_2}{2}v_{2_{2j+1}} - \frac{h_2^2}{12}v_{2_{2j+2}} \end{Bmatrix} \tag{3.42}$$

The total potential energy of each link can be found by summing up the potential energies of all elements of the link. Since link 1 comprises of $n_1$elements, its total potential energy is given by

$$V_1 = m_1 g[0\ 1]T_1^0 \begin{Bmatrix} \frac{1}{2}n_1^2 h_1^2 \\ \left[\frac{h_1}{2} \quad \frac{h_1^2}{12} \quad h_1 \quad 0 \quad h_1 \quad 0 \quad .. \quad .. \quad h_1 \quad 0 \quad \frac{h_1}{2} \quad -\frac{h_1^2}{12}\right]\bar{q}_1 \end{Bmatrix} + \frac{1}{2}\bar{q}_1^T \bar{K}_1 \bar{q}_1 \tag{3.43}$$

where $\bar{q}_1 = [v_{1_1} \quad v_{1_2} \quad v_{1_3} \quad v_{1_4} \quad v_{1_5} \quad v_{1_6} \quad .. \quad .. \quad v_{1_{2n_1-1}} \quad v_{1_{2n_1}} \quad v_{1_{2n_1+1}} \quad v_{1_{2n_1+2}}]^T$

Similarly, the total potential energy of link 2 that comprises of $n_2$elements can be given below

$$\begin{aligned} V_2 &= m_2 g[0\ 1]T_1^0 \begin{Bmatrix} L_1 \\ v_{1_{2j+1}} \end{Bmatrix} n_2 h_2 \\ &+ m_2 g[0\ 1]T_1^0 T_2^1 \begin{Bmatrix} \frac{1}{2}n_2^2 h_2^2 \\ \left[\frac{h_2}{2} \quad \frac{h_2^2}{12} \quad h_2 \quad 0 \quad h_2 \quad 0 \quad .. \quad .. \quad h_2 \quad 0 \quad \frac{h_2}{2} \quad -\frac{h_2^2}{12}\right]\bar{q}_2 \end{Bmatrix} \\ &+ \frac{1}{2}\bar{q}_2^T \bar{K}_2 \bar{q}_2 \end{aligned} \tag{3.44}$$

where

$\bar{q}_2 = [v_{2_1} \quad v_{2_2} \quad v_{2_3} \quad v_{2_4} \quad v_{2_5} \quad v_{2_6} \quad .. \quad .. \quad v_{2_{2n_2-1}} \quad v_{2_{2n_2}} \quad v_{2_{2n_2+1}} \quad v_{2_{2n_2+2}}]^T$

Since the datum of the inertial reference frame has been taken at the hub center, $V_{hub} = 0$.

$$V_{motor} = M_m g[0\ 1]\boldsymbol{r_m^0} \tag{3.45}$$

$$V_{payload} = M_p g[0\ 1]\boldsymbol{r_p^0} \tag{3.46}$$

3.4.1 Dynamic Equation of Motion

Once the total kinetic energy T and potential energy V of the whole system are known, the Lagrangian of the system can be given as

$$\mathcal{L} = T - V \tag{3.47}$$

Euler-Lagrange dynamic equation of motion is given as follows.

$$\frac{d}{dt}\left(\frac{\partial \mathcal{L}}{\partial \dot{\tilde{q}}_k}\right) - \frac{\partial \mathcal{L}}{\partial \tilde{q}_k} = Q_k \tag{3.48}$$

where $k = 1, 2, \dots, \tilde{N}$; $\tilde{N} = [2 + (2n_1 + 2) + (2n_2 + 2)]$ is the number of generalized variables $\tilde{q}$. $\tilde{q}_k$ is the k^{th} variable of generalized variable $\tilde{q}$, where

$$\tilde{q} = \left[\theta_1, \theta_2, v_{1_1}, v_{1_2}, \dots, v_{1_{2n_1-1}}, v_{1_{2n_1}}, v_{1_{2n_1+1}}, v_{1_{2n_1+2}}, v_{2_1}, v_{2_2}, \dots, v_{2_{2n_2-1}}, v_{2_{2n_2}}, v_{2_{2n_2+1}}, v_{2_{2n_2+2}}\right]^T$$

Time derivative of $\tilde{q}$ is $\dot{\tilde{q}}$.Using Eq. (3.47) in Eq. (3.48) dynamic equation of motion of the 2-link flexible manipulator can be obtained as

$$\tilde{M}(\tilde{q})\ddot{\tilde{q}} + \tilde{K}(q) + \tilde{H}(\tilde{q}, \dot{\tilde{q}}) + \tilde{G}(\tilde{q}) = \tilde{Q} \tag{3.49}$$

where $\tilde{M}_{\tilde{N}\times\tilde{N}}$ is the symmetric positive definite global mass matrix of the system of size $\tilde{N}$ by $\tilde{N}$, $\tilde{K}_{\tilde{N}\times\tilde{N}}$ is the symmetric positive definite global stiffness matrix of the system of size $\tilde{N}$ by $\tilde{N}$, $\tilde{H}_{\tilde{N}\times1}$is the force or torque on the system due to Coriolis and centrifugal force on the system, $\tilde{G}_{\tilde{N}\times1}$ is the force or torque on the system due to acceleration due to gravity, $\tilde{Q}_{\tilde{N}\times1}$ is the generalized force on the system given by $\tilde{Q} = \left[\tau_1 \quad \tau_2 \quad F_{1_1} \quad F_{1_2} \quad \dots \quad F_{1_{2n_1+1}} \quad F_{1_{2n_1+2}} \quad F_{2_1} \quad F_{2_2} \quad \dots \quad F_{2_{2n_2+1}} \quad F_{2_{2n_2+2}}\right]^T$ where τ_1 and τ_2 are the torque on joint 1 (hub) and joint 2 respectively other terms of $\tilde{Q}$ are external forces on respective nodes of link 1 and link 2.

3.4.2 Boundary Conditions

Link 1 is rigidly clamped to the hub while link 2 is rigidly clamped to the motor at the tip of 1st link. This makes the flexural displacements and slopes at the 1st nodes of both links equal to zero. That is,

$$v_{1_1} = v_{1_2} = v_{2_1} = v_{2_2} = 0 \tag{3.50}$$

Applying these boundary conditions to Eq. (3.49), the dynamic equation of motion of the system can be given as

$$M_{N\times N}\ddot{q} + K_{N\times N}q + H_{N\times1} + G_{N\times1} = Q_{N\times1} \tag{3.51}$$

where $N = 2n_1 + 2n_2 + 2$. The subscripts represent the size of the matrix. q is the generalized or global variables given as

$q_{N\times 1} =$

$$\left[\theta_1, \theta_2, v_{1_3}, v_{1_4}, \dots, v_{1_{2n_1-1}}, v_{1_{2n_1}}, v_{1_{2n_1+1}}, v_{1_{2n_1+2}}, v_{2_3}, v_{2_4}, \dots, v_{2_{2n_2-1}}, v_{2_{2n_2}}, v_{2_{2n_2+1}}, v_{2_{2n_2+2}}\right]^T;$$

$$Q_{N\times 1} = \begin{bmatrix} \tau_1 & \tau_2 & F_{1_3} & F_{1_4} & \dots & F_{1_{2n_1+1}} & F_{1_{2n_1+2}} & F_{2_3} & F_{2_4} & \dots & F_{2_{2n_2+1}} & F_{2_{2n_2+2}} \end{bmatrix}^T.$$

3.4.3 Rayleigh Damping

The motion of the two-link manipulator has been considered to be subjected to damping. The damping has been modeled as Rayleigh's damping which can be given as

$$C = \alpha M + \beta K \tag{3.52}$$

where α is the Rayleigh's mass damping coefficient and β is the stiffness damping coefficient. Considering damping the final dynamic equation of motion of the system can be given as

$$M_{N\times N}\ddot{q} + C_{N\times N}\dot{q} + K_{N\times N}q + H_{N\times 1} + G_{N\times 1} = Q_{N\times 1} \tag{3.53}$$

α and β have been calculated based on the work of Chowdhury and Dasgupta (2003) by considering 1st three modes of vibration as effective modes of vibration. The damping ratio ξ for 1st mode of vibration of links has been taken as $\xi_1 = 2\%$ and that for 3rd mode has been taken as $\xi_3 = 5\%$. From the modal analysis of flexible body motion, it is known that

$$\xi_k = \frac{\alpha}{2\omega_k} + \frac{\beta\omega_k}{2} \tag{3.54}$$

where $k = 1, 2, \dots, (N-2)$; the number of modes or degrees of freedom of non-rigid body (flexible) motion and $\omega_k$is the k^{th} frequency of vibration of the system. By solving the above system of equations, values of α and β can be found.

3.4.4 Torques Applied at Joints

Let δ, ν and η respectively, be defined as link length ratio, diameter ratio, and mass of payload to total link mass ratio such that $\delta = \frac{L_2}{L_1}$, $\nu = \frac{d_1}{d_2}$ and $\eta = \frac{M_P}{m}$ where L_1 and L_2 are respectively length of link 1 and link 2; d_1 and d_2 are respectively the diameter of link 1 and link 2 and m is the total mass of both the links. Let the mass of link 1 and link 2 per unit length be respectively m_1 and m_2 and I_1 and I_2 be their 2nd moment of area of cross-section. Mass of both

the links $m = m_1L_1 + m_2L_2$, the mass of the payload $M_p = \eta m$, the mass of the motor $M_m = \mu m$ where μ is a constant. Total moment of inertia of link 1 and link 2 about the hub axis

$$I_{hub}^{L} = \frac{1}{3}m_1L_1^3 + \frac{1}{12}m_2L_2^3 + m_2L_2\left(L_1 + \frac{L_2}{2}\right)^2 \tag{3.55}$$

Total moment of inertia of motor at the tip of link 1 and payload at the tip of link 2 about the hub axis

$$I_{hub}^{M_mM_p} = M_mL_1^2 + M_p(L_1 + L_2)^2 \tag{3.56}$$

Total moment of inertia of link 2 and payload about the axis of joint 2

$$I_{joint_2}^{L_2M_p} = \frac{1}{3}m_2L_2^3 + M_pL_2^2 \tag{3.57}$$

Total moment of inertia of the system (excluding hub inertia) about the hub axis

$$I_{hub}^{Sys} = I_{hub}^{L} + I_{hub}^{M_mM_p} \tag{3.58}$$

If the ratio of hub inertia about its own axis of rotation to the total moment of inertia of the system (excluding hub inertia) about the hub axis is taken to be $\mu_{I_{hub}}$ then hub inertia about its own axis of rotation is

$$I_{hub} = \mu_{I_{hub}} \times I_{hub}^{Sys} \tag{3.59}$$

If the ratio of inertia of the motor at the 2nd joint about its own axis of rotation to the total moment of inertia of the system (excluding hub inertia) about the hub axis is taken to be $\mu_{I_{motor}}$ then motor inertia about its own axis of rotation is

$$I_{motor} = \mu_{I_{motor}} \times I_{hub}^{Sys} \tag{3.60}$$

If the ratio of inertia of the payload at the tip of link 2 about its own axis of rotation to the total moment of inertia of the system (excluding hub inertia) about the hub axis is taken to be $\eta_{I_{payload}}$ then payload inertia about its own axis of rotation is

$$I_{payload} = \eta_{I_{payload}} \times I_{hub}^{Sys} \tag{3.61}$$

The total inertia of the system about the hub axis is

$$I_{hub}^{system} = I_{hub} + I_{hub}^{Sys} \tag{3.62}$$

Let the ratio of the amplitude of external torque applied on the hub to the total inertia of the system about the hub axis be ζ_1 and the ratio of that of external torque applied on joint 2 axes to the total moment of inertia of link 2 and payload about the axis of joint 2 be ζ_2, then the amplitude of torque on joint 1 and joint 2 are

$$\tau_{max_1} = \zeta_1 I_{hub}^{system} \text{ and } \tau_{max_2} = \zeta_2 I_{joint_2}^{L_2 M_p} \tag{3.63}$$

Sinusoidal torque profiles about the axes of rotation are applied according to the following equations for a time duration of $t = 0$ to t_m where t_m is the time duration for which torque is applied by the driving motor on joints and t_f is the final time up to when observation of the motion of the manipulator is made.

$$\left.\begin{matrix} \tau_k = \tau_{\max_k} sin\pi t, & 0 \le t < t_m \\ = 0, & t_m \le t < t_f \end{matrix}\right\}; k = 1,2. \tag{3.64}$$

3.5 Results and Discussions

Performances of the manipulator in terms of its joint and tip motions have been judged under different parameters of the manipulator, namely, link length ratio, link diameter ratio, payload to the mass of links ratio, and under different profiles of torque applied at joints of the manipulator. The inertial properties for both links have been given in Table 3.1. Sinusoidal torque profiles about the axes of rotation are applied for a time duration of $t = 0\ to\ 5$ seconds according to the following equations.

$$\left.\begin{matrix} \tau_k = \tau_{\max_k} \sin(\pi t), & 0 \le t < 2 \\ = 0, & 2 \le t < 5 \end{matrix}\right\}; k = 1,2. \tag{3.64.a}$$

Acceleration due to gravity g has been taken to be $g = 9.81 \text{m/s}^2$ and $g = 0\ \text{m/s}^2$ when the effect of gravity has not been considered. Also, when force or torque $H_{10\times1}$ due to Coriolis and centrifugal factor has not been considered, $H_{10\times1} = [0]_{10\times1}$. Rayleigh's damping coefficients corresponding to these set frequencies are found to be $\alpha = 2.3925$ and $\beta = 8.2036 \times 10^{-5}$.

Table 3.1: Inertial and elastic properties of the links of the manipulator

Properties	**Link 1**	**Link 2**
Length (in m)	$L_1 = 0.5$	$L_2 = \delta L_1$
Diameter of cross-section (in m)	$d_1 = \nu d_2$	$d_2 = 0.01$
Density of material (in kg/m^3)	$\rho_1 = 7850$	$\rho_2 = 7850$

For the present study, the constants mentioned in section 3.4.4 have been taken as follows:

$\mu = 0.05, \eta_{I_{payload}} = 0.001, \mu_{I_{motor}} = 0.002, \mu_{I_{hub}} = 0.05, \zeta_1 = 1, \zeta_2 = 0.2.$

Now, any one parameter of the manipulator out of its three parameters, namely, link length ratio, diameter ratio, and payload ratio, as well as joint torque profiles, is varied one by one at a time, and joint angular responses in terms of angular displacements and velocities, tip deflections of both the links as well as slopes at tips of these links have been observed. Through these observations, it has been tried to ascertain how these responses depend on the parameters of the manipulator. Studies have been done for whether acceleration due to gravity g and whether torques due to centrifugal and Coriolis forces H have been considered or not. Accordingly, the findings of the studies have been presented in the following cases:

Case (A): When the effect of gravity and torque due to Coriolis and centrifugal forces have been taken into account

A total of four cases arises in this case depending on the parameters that are varied, namely, case A(I) when the link-length ratio, A(II) when the link-diameter ratio, A(III) when ratio of payload mass to manipulator mass and A(IV) when torque profile, are varied. The findings have been presented below.

Sinusoidal torque profiles have been applied at joints as shown in Figs. 3.2 (a) and 3.2 (b). Here, It is to be noted that instead of applying constant torques at joints of manipulators with different link and payload ratios, the torques are applied in proportion to their inertia. This is to keep the justified torque limits. Otherwise, the manipulator with the least link and payload ratio

may experience (or be subjected to) the highest impacts of the torques giving higher values of displacement and deflections which may lead to erroneous inferences.

Table 3.2: Maximum values of tip deflections

Link length ratios $\boldsymbol{\delta = \frac{L_2}{L_1}}$	**Maximum values of tip deflection during the motion of the manipulator (in m)**	
	For time duration $0 \leq t < 2$ (in s)	For time duration $2 \leq t < 5$ (in s)
$\delta_1 = 1$	3.8609×10^{-5}	6.7879×10^{-6}
$\delta_2 = 0.75$	1.6454×10^{-5}	8.8628×10^{-7}
$\delta_3 = 0.5$	5.4611×10^{-6}	1.4657×10^{-7}

Case A (I): effect of link length ratio δ on the dynamic response of the manipulator

Taking the ratio of the mass of payload to that of links $\eta = 0.05$ and link diameter ratio $\nu = 1.5$ and keeping the length of the first link ($L_1 = 0.5$m) and diameter of 2nd link ($D_2 = 0.01$m) constant and varying length of 2nd link in ratios of $\delta = 1, 0.75, \text{and } 0.5$ one-by-one, various dynamic responses of the manipulator have been shown in Fig. 3.2 (c)-3.2 (j). It has been observed that the dynamic response of the manipulator depends on the ratio of lengths of links of the manipulator. The maximum values of tip deflections, in this case, have been shown in Table 3.2. Wherever the plots in the figures in the results and discussions section are not visible, they have been shown in the magnified view in the windows inside the figures. From Fig. 3.2 (c), it is seen that the joint angular displacement of the first joint is the highest for the manipulator with the least link length ratio $\delta_3$while that is the least for the manipulator with the 2nd highest δ, i.e., δ_2. This may be due to the lower weight on link 1 due to reduced δ. But after some value of δ, the inertia of link 1 may become higher which does not allow it to move to a larger angle. In case Fig. 3.2 (d), the angular displacement of joint 2 is the highest for δ_1 and the lowest for δ_2. Here, it is also

observed that the angular response of joint 2 is just opposite to that of joint 1. From Fig. 3.2 (e) and 3.2 (f), it is observed that joint angular velocities of both joints are higher for a lower link length ratio. This may be because of the lower inertia of the manipulators. From Fig. 3.2 (g) to 3.2 (j), it can be observed that tip deflections and slopes at the tips of link 1 and link 2 vary with the variation of δ in the same order. The reason for higher tip deflections and slopes of link 2 for higher δ is that higher δ increases the slenderness of the 2nd link which makes them more flexible and hence more tip deflection and slope. In the case of the 1st link, this may be due to higher loads on the tip of link 1 due to increased δ. The high frequency responses in the initial stages in Fig. 3.2 (g-j) are due to high inertia of the manipulator. Because of high inertia of the manipulator, it takes time to respond to the excitation given to the system. This causes dissipation of energy or redistribution of excitation energy in the form of transient vibration of the system with high frequency. This phenomenon can also be verified from the results of Usoro et al. (1986).

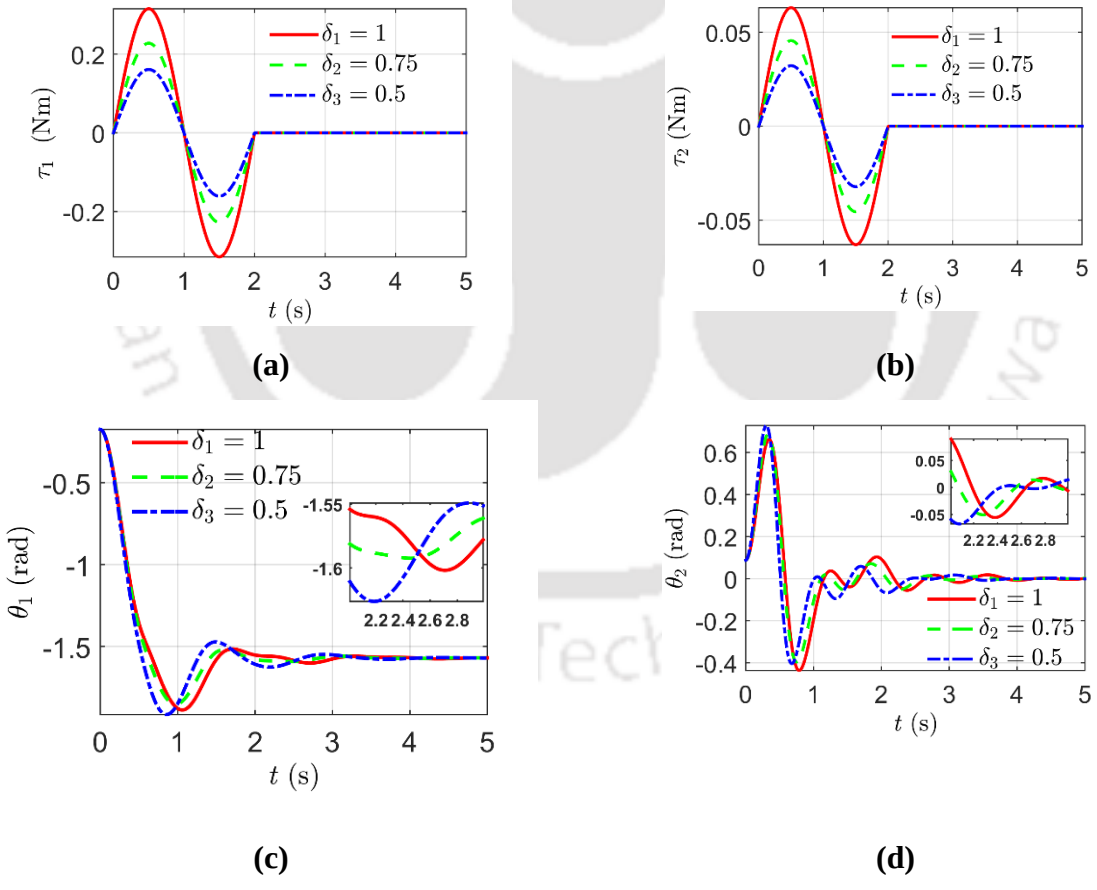

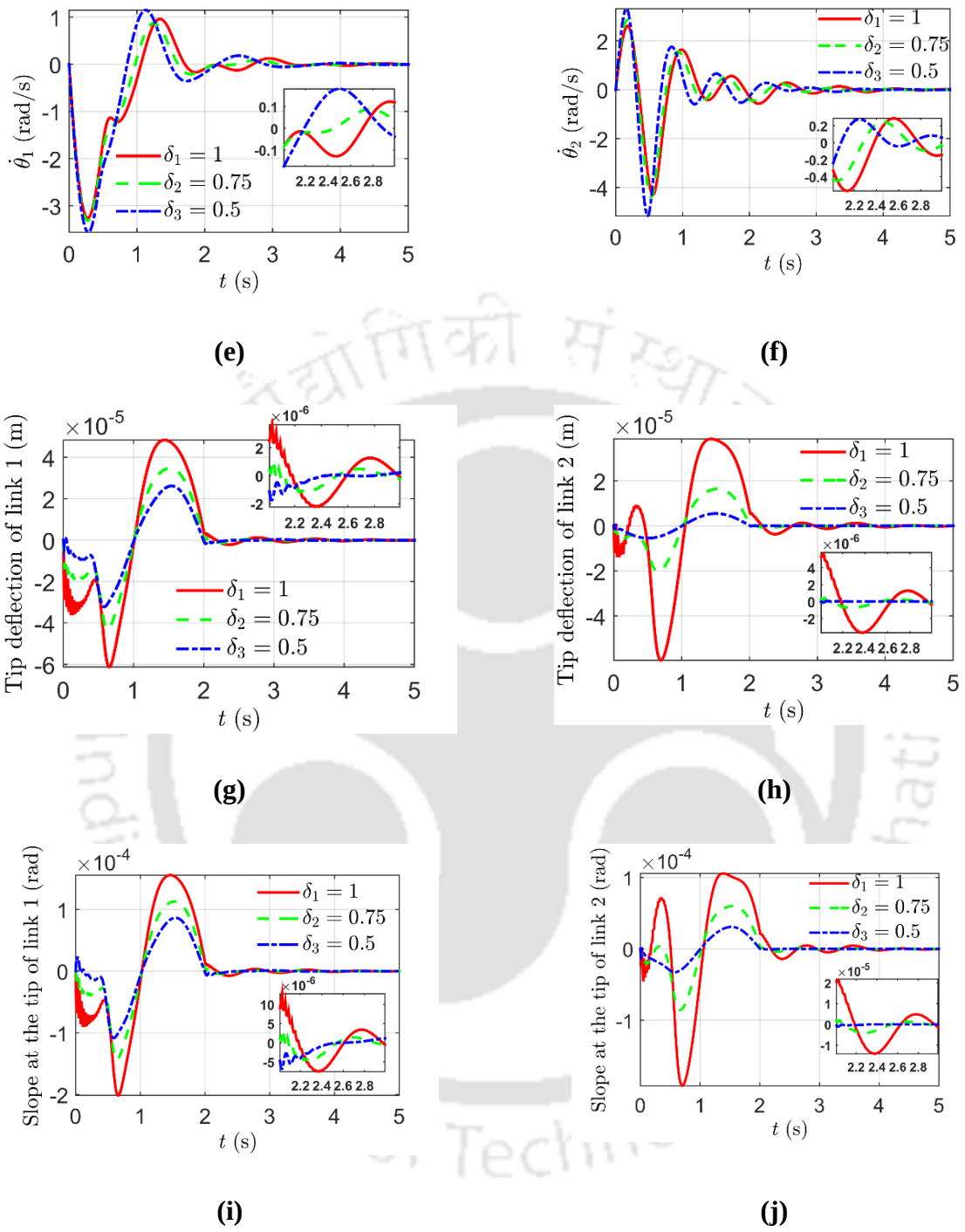

Figure 3.2: Effect of link-length ratio on the dynamic behavior: **(a)** torque on hub, **(b)** torque on 2nd joint, **(c)** angular displacement of hub, **(d)** angular displacement of joint 2, **(e)** joint 1 angular speed, **(f)** joint 2 angular speed **(g)** tip deflection of link 1, **(h)** tip deflection of link 2, **(i)** flexural rotation of link 1 and **(j)** flexural rotation of link 2.

Case A (II): effect of link diameter ratio ν on the dynamic response of the manipulator

Taking $\eta = 0.05,\ \delta = 0.75$ and keeping diameter of 2nd link ($D_2 = 0.01$ m) constant and varying diameter of 1st link in ratios of $\nu = 1.5, 1.25,$ and 1 one-by-one, it can be observed from Fig. 3.3 (a) to 3.3 (j) that dynamic response of the manipulator depends upon link diameters of the manipulator. Sinusoidal torque profiles are proportional to joint and link inertias have been applied at joints as shown in Figs. 3.3 (a) and 3.3 (b). Here, in Fig. 3.3 (c), it is seen that the joint angular displacement of the first joint is the highest for the manipulator with the link diameter ratio $\nu_2$while that is the least for the manipulator with the lowest ν, i.e., ν_3. This may be due to the same weight on link 1 due to the same δ and η in these three cases but the lowest torque applied at joint 1 of the manipulator with the least ν. In the case of Fig. 3.3 (d), the angular displacement of joint 2 is the highest for ν_1 and the lowest for ν_3.This is because the 2nd link of all the manipulators has the same link length and diameter so the mass of the 2nd link and payload mass to link mass ratio is the same while torque applied at the 2nd joint is proportional to the link diameter ratios ν. Similar explanations hold for the joint angular velocities at both joints shown in Fig. 3.3 (e) and 3.3 (f). In Figs. 3.3 (g) and 3.3 (i), it can be observed that tip deflections and slopes at tips of link 1 vary with the diameter ratios ν in reverse order. In Figs. 3.3 (h) and 3.3 (j), it can be observed that tip

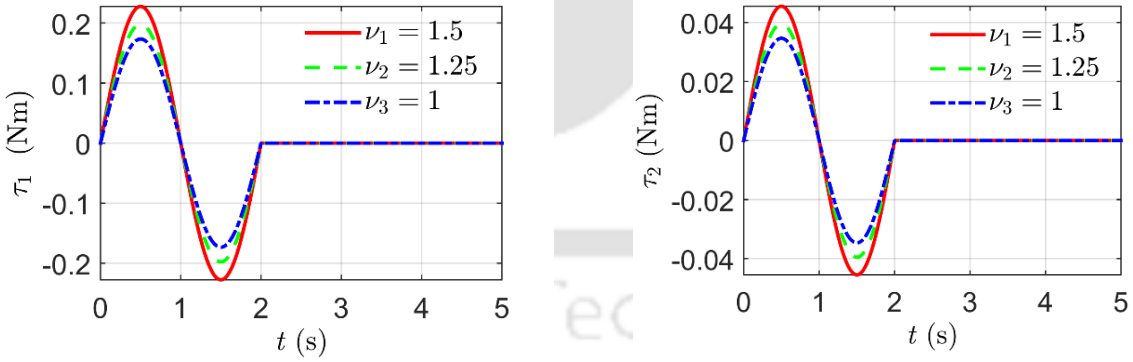

(a) **(b)**

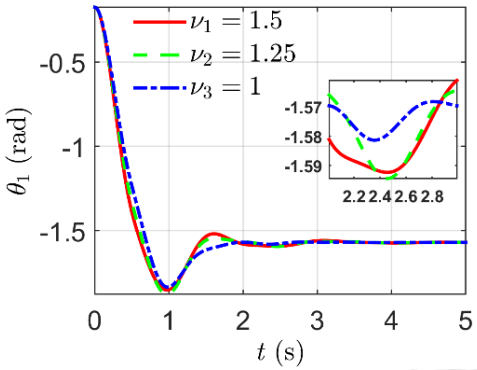
$\nu_1 = 1.5$
$\nu_2 = 1.25$
$\nu_3 = 1$
θ_1 (rad)
t (s)

(c)

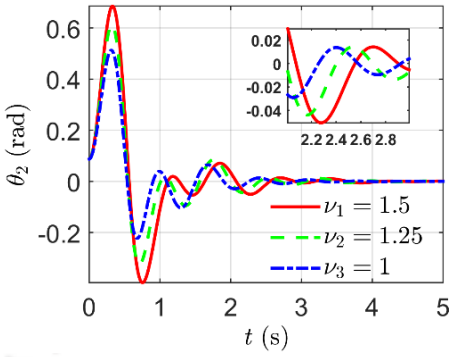
$\nu_1 = 1.5$
$\nu_2 = 1.25$
$\nu_3 = 1$
θ_2 (rad)
t (s)

(d)

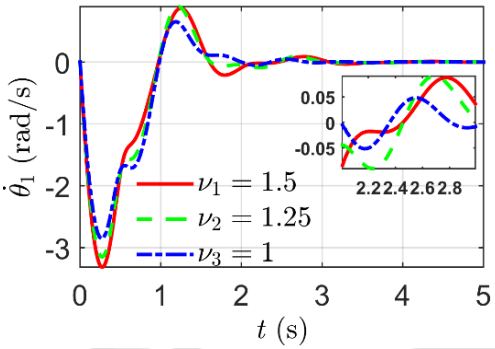
$\nu_1 = 1.5$
$\nu_2 = 1.25$
$\nu_3 = 1$
$\dot{\theta}_1$ (rad/s)
t (s)

(e)

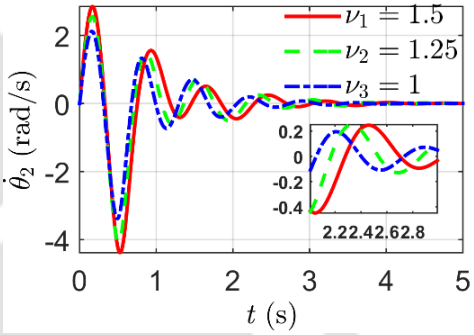
$\nu_1 = 1.5$
$\nu_2 = 1.25$
$\nu_3 = 1$
$\dot{\theta}_2$ (rad/s)
t (s)

(f)

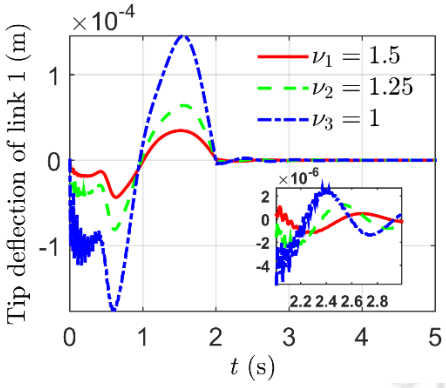
$\nu_1 = 1.5$
$\nu_2 = 1.25$
$\nu_3 = 1$
Tip deflection of link 1 (m)
t (s)

(g)

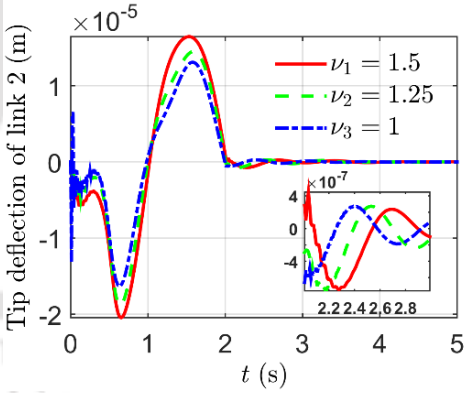
$\nu_1 = 1.5$
$\nu_2 = 1.25$
$\nu_3 = 1$
Tip deflection of link 2 (m)
t (s)

(h)

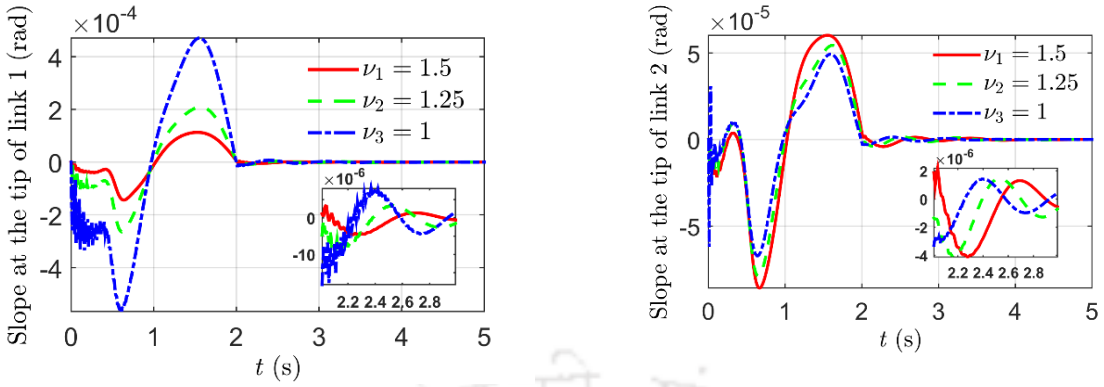

(i) **(j)**

Figure 3.3: Effect of link-diameter ratio on the dynamic behavior: **(a)** torque on hub, **(b)** torque on 2nd joint, **(c)** angular displacement of hub, **(d)** angular displacement of joint 2, **(e)** joint 1 angular speed, **(f)** joint 2 angular speed **(g)** tip deflection of link 1, **(h)** tip deflection of link 2, **(i)** flexural rotation of link 1 and **(j)** flexural rotation of link 2.

deflections and slopes at the tips of link 2 vary with the diameter ratios ν in the same order. This is because the 2nd links of these manipulators are having the same lengths and diameters but torques applied at the 2nd joint increase ν resulting in the inertia of payload in the direction opposite to the motion.

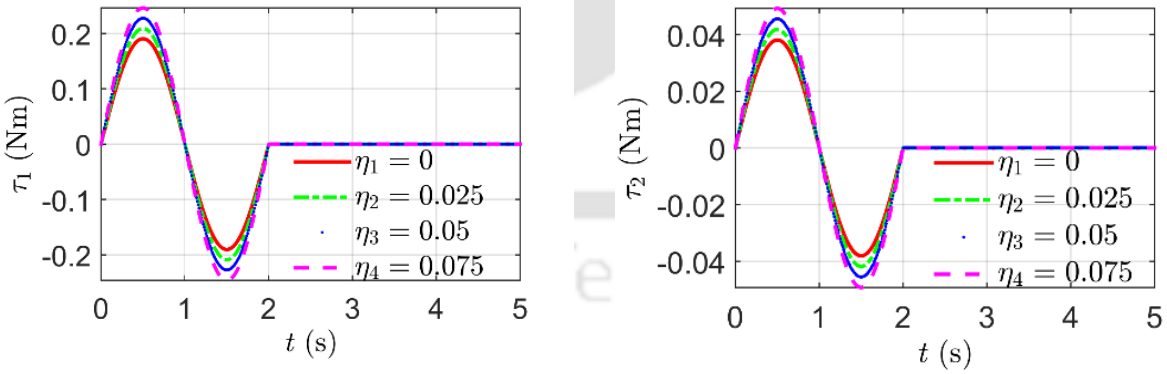

(a) **(b)**

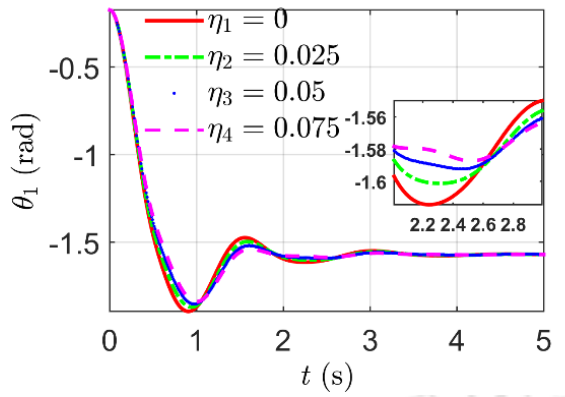
$\eta_1 = 0$
$\eta_2 = 0.025$
$\eta_3 = 0.05$
$\eta_4 = 0.075$
θ_1 (rad)
t (s)

(c)

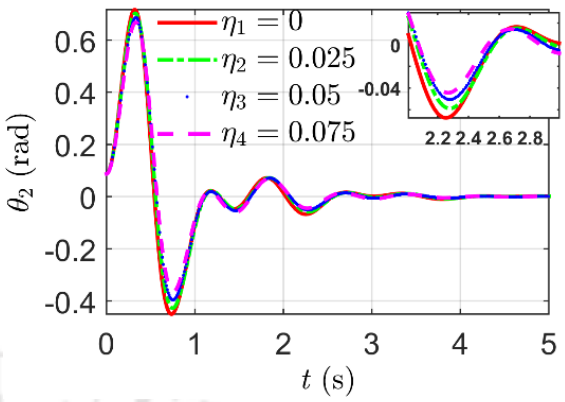
$\eta_1 = 0$
$\eta_2 = 0.025$
$\eta_3 = 0.05$
$\eta_4 = 0.075$
θ_2 (rad)
t (s)

(d)

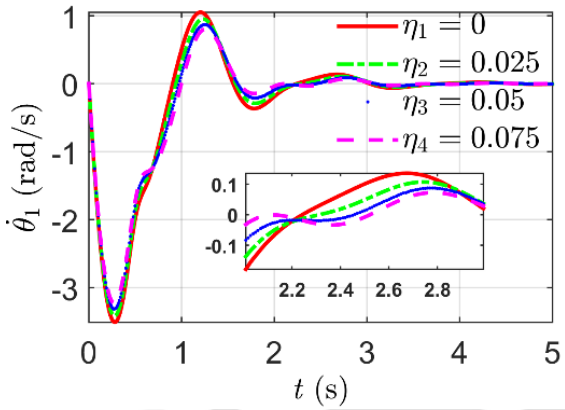
$\eta_1 = 0$
$\eta_2 = 0.025$
$\eta_3 = 0.05$
$\eta_4 = 0.075$
$\dot{\theta}_1$ (rad/s)
t (s)

(e)

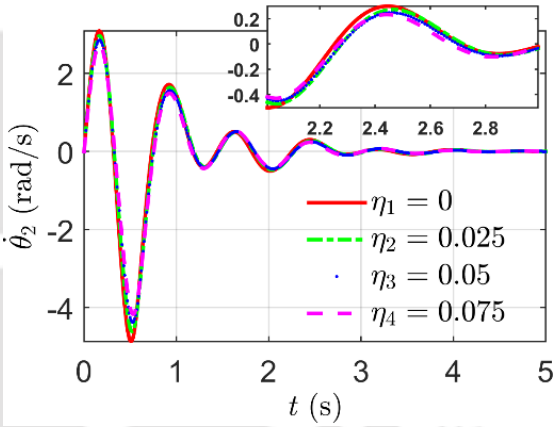
$\eta_1 = 0$
$\eta_2 = 0.025$
$\eta_3 = 0.05$
$\eta_4 = 0.075$
$\dot{\theta}_2$ (rad/s)
t (s)

(f)

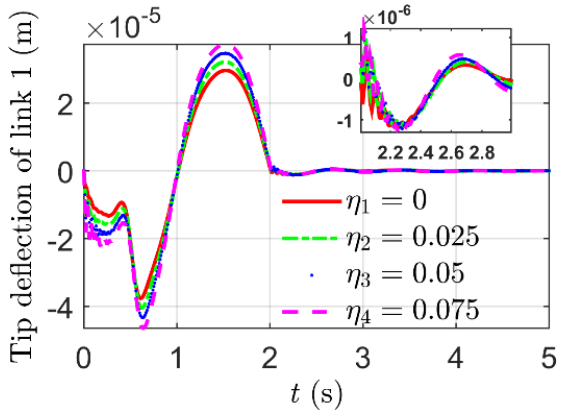
$\eta_1 = 0$
$\eta_2 = 0.025$
$\eta_3 = 0.05$
$\eta_4 = 0.075$
Tip deflection of link 1 (m)
t (s)

(g)

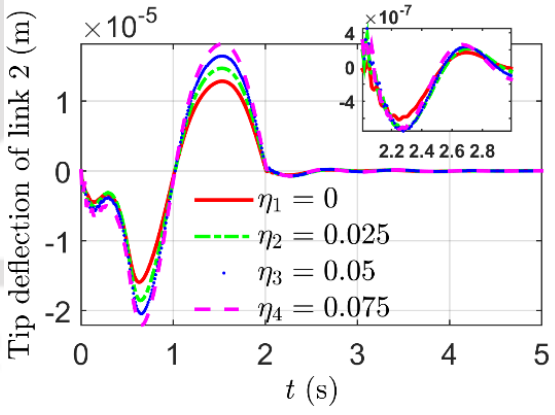
$\eta_1 = 0$
$\eta_2 = 0.025$
$\eta_3 = 0.05$
$\eta_4 = 0.075$
Tip deflection of link 2 (m)
t (s)

(h)

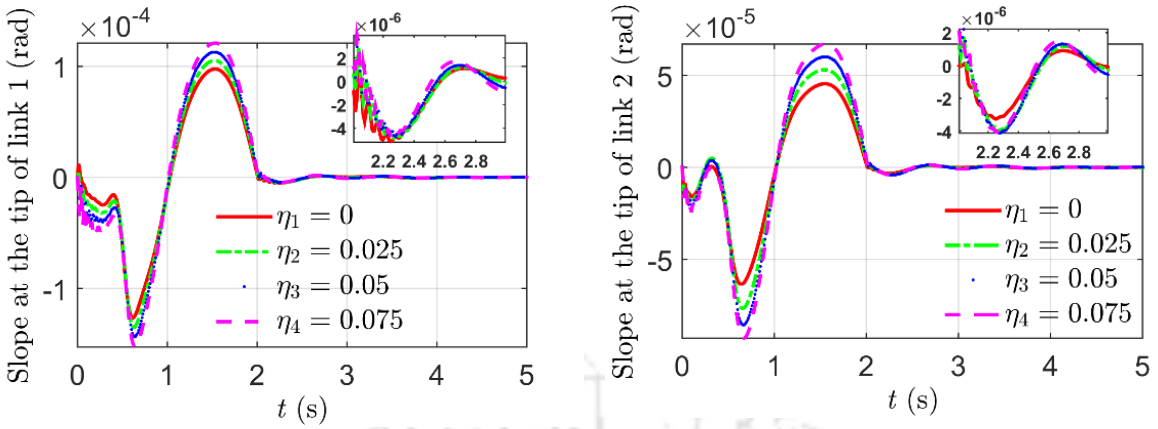

(i) **(j)**

Figure 3.4: Effect of mass ratio of payload to manipulator on dynamic behavior: **(a)** torque on hub, **(b)** torque on 2nd joint, **(c)** angular displacement of hub, **(d)** angular displacement of joint 2, **(e)** joint 1 angular speed, **(f)** joint 2 angular speed **(g)** tip deflection of link 1, **(h)** tip deflection of link 2, **(i)** flexural rotation of link 1 and **(j)** flexural rotation of link 2.

Case A (III): effect of the ratio of payload mass to the mass of links of the manipulator on its dynamic response

Taking $\nu = 1.5$ and $\delta = 0.75$ and varying mass of payload on the 2nd link in ratios of $\eta = 0, 0.025, 0.05,$ and 0.075 one-by-one, it has been observed from Figs. 3.4 (a) to 3.4 (j) that the dynamic response of the manipulator depends upon payload mass ratios. $\eta = 0$ denotes the condition when there is no payload on the tip of the 2nd link. Here, torques applied on joints 1 and 2 increase with η as shown in Figs. 3.4 (a) and 3.4 (b). From Figs. 3.4 (c) to 3.4 (f) it can be seen that angular responses of both the joints of the manipulator increase with the decrease in payload mass ratio. The corresponding links of these manipulators with different payload ratios are similar in lengths and diameters. So, this is due to less inertia offered by the links of the manipulator with less payload mass that tries to oppose any change in the state of motion of the links. But, the reverse conditions are found for tip deflections and slopes of both the links, i.e., these quantities increase with the increase in payload ratio.

Case A (IV): effect of torque profile on the dynamic response of the manipulator

Taking $\delta = 0.75$, $\nu = 1.5$ and $\eta = 0.025$ applying torques of different profiles but of the same amplitude and for the same duration of time from sinusoidal to trapezoidal, triangular, and

bang-bang one-by-one, it has been observed from Figs. 3.5 (a) to 3.5 (i) that the dynamic response of the manipulator depends upon the torque profile applied at joints. Figs. 3.5 (a) and 3.5 (b) show the torque profiles on the two joints. From Figs. 3.5 (c) to 3.5 (f), it can be seen that all the torque profiles give almost the same angular response profiles and amplitudes. However, the triangular torque profile gives the marginally highest joint angular displacements and velocities and the bang-bang torque profile gives the least joint displacements and velocities. From Figs. 3.5 (g) to 3.5 (j), it is observed that the sinusoidal torque profile gives the smoothest link tip motion while the bang-bang torque profile gives the jerky tip motion. This is because, in the bang-bang torque profile, an abrupt change in torque amplitude takes place which results in oscillatory behavior of link tip

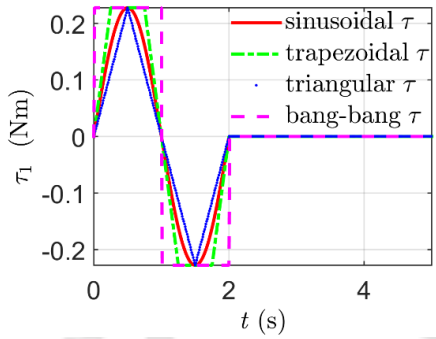

(a)

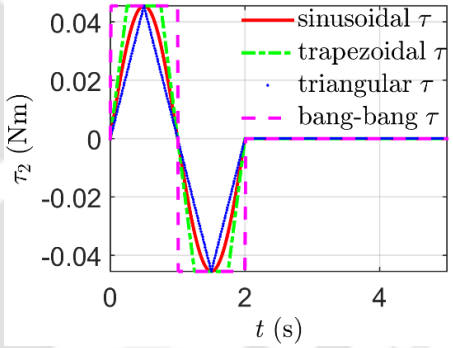

(b)

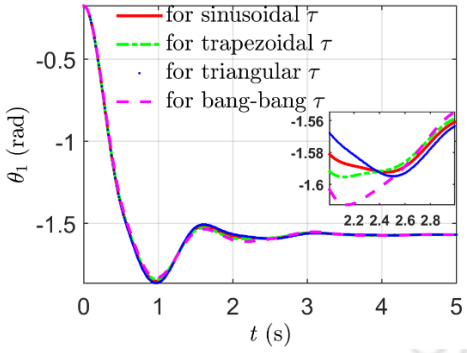

(c)

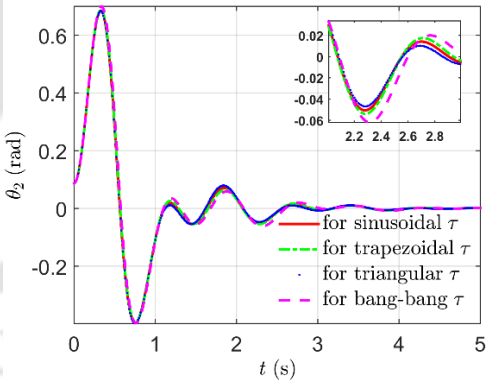

(d)

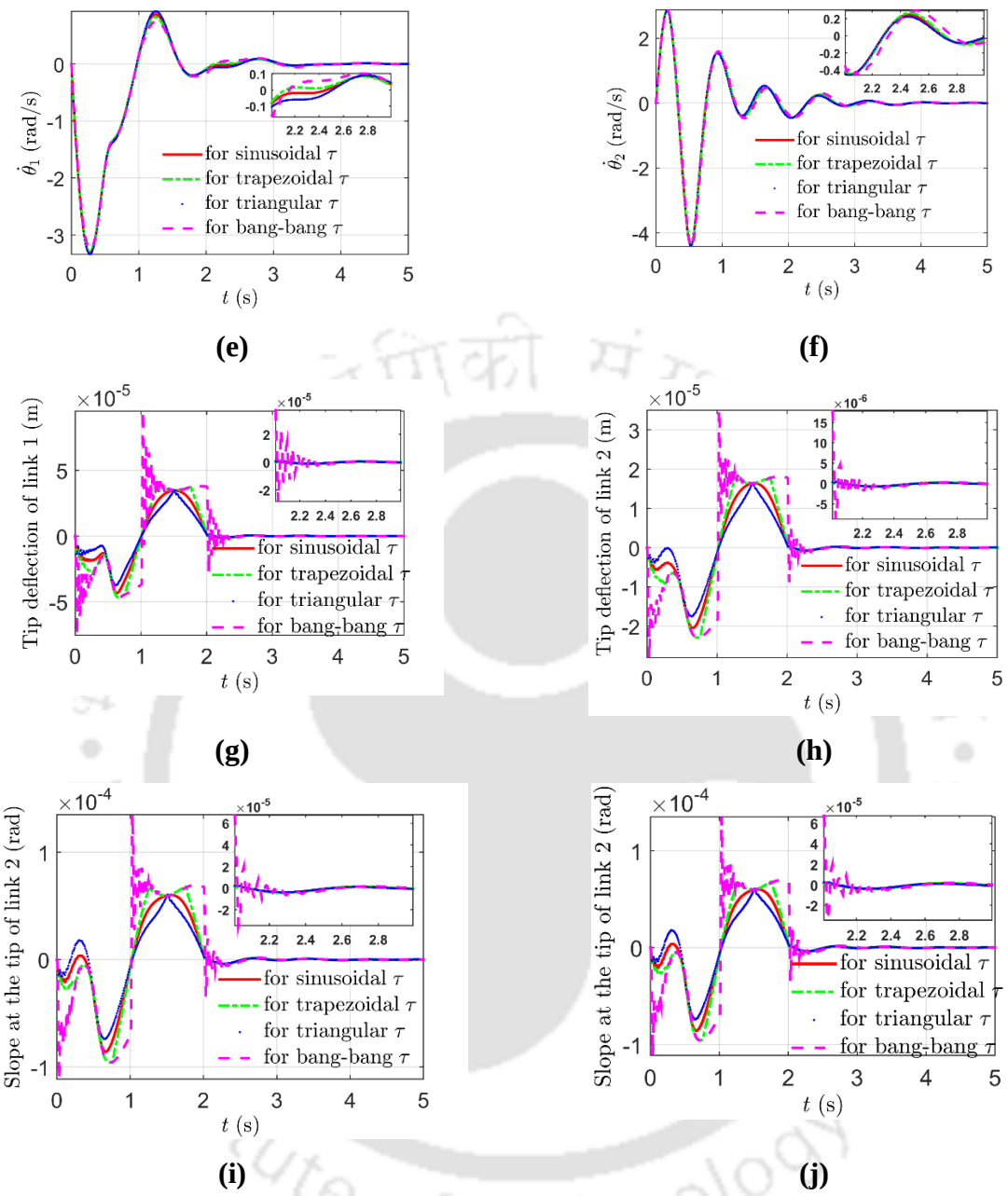

Figure 3.5: Effect of torque profiles on the dynamic behavior: **(a)** torque on hub, **(b)** torque on 2nd joint, **(c)** angular displacement of hub, **(d)** angular displacement of joint 2, **(e)** joint 1 angular speed, **(f)** joint 2 angular speed **(g)** tip deflection of link 1, **(h)** tip deflection of link 2, **(i)** flexural rotation of link 1 and **(j)** flexural rotation of link 2.

motion at every change in values of the torque profile. The bang-bang profile also gives very high overshoots which may lead the link tip to collide with the surroundings.

Case B: The effect of link-length ratios on the dynamic response of the manipulator when the effect of gravity has not been considered

The same values of η, ν D_2 and L_1 have been taken as in Case A (I) and δ is varied in the ratios of $\delta = 1, 0.75, \text{and } 0.5$ one by one. The magnitudes of joint torque are also taken to be the same for different δ as in Case A (I) that are shown in Figs. 3.2 (a) and 3.2 (b). The joint angular displacements of both the joints for different δ have been shown in Figs. 3.6 (a) and 3.6 (b). From Fig 3.6 (a), it is observed that the angular response of joint 1 increases with δ. In Fig. 3.6 (b) it is seen that the manipulator with the smallest δ has the highest joint 2 angular displacement. This may be due to the manipulator with the least rotational inertia about joint 2 having a maximum response to the torque applied in the absence of gravitational force. Also, the manipulator with $\delta = 0.5$ has angular displacement in a direction opposite to that of the remaining two. From Figs.

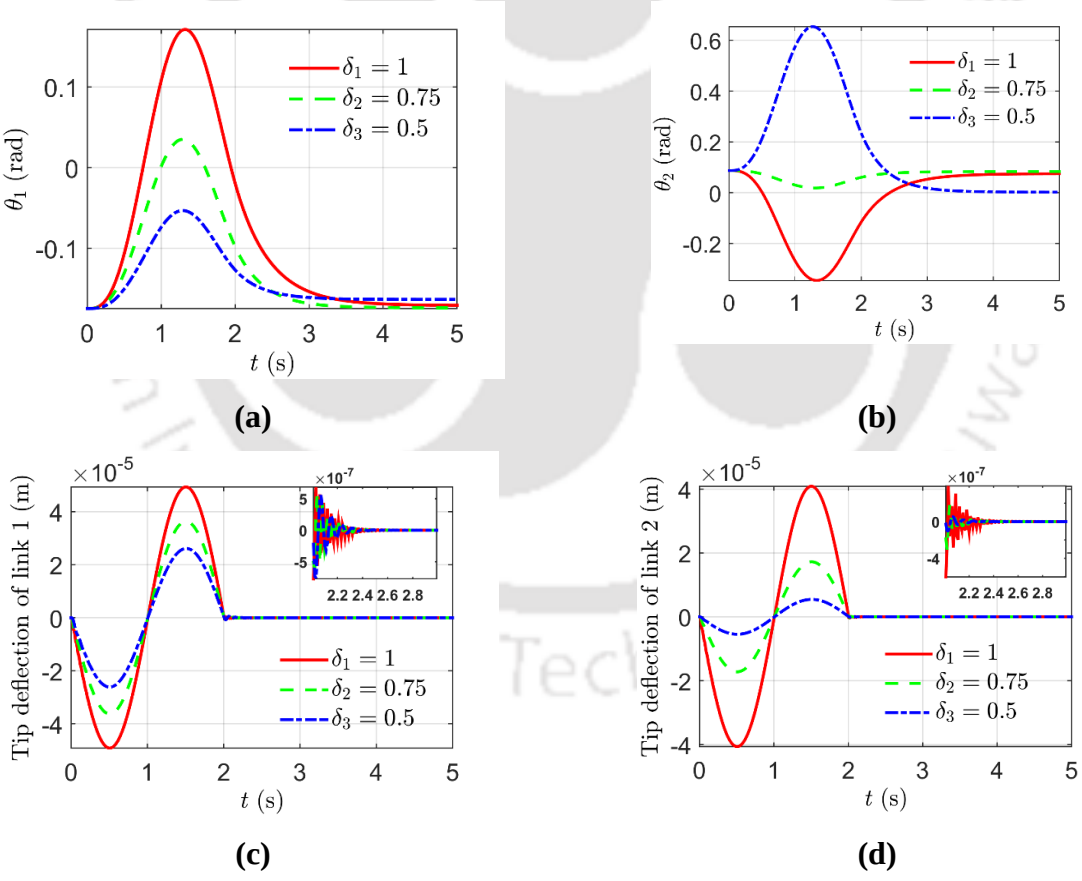

Figure 3.6: Effect of link-length ratio on dynamic behavior: **(a)** angular displacement of the hub, **(b)** angular displacement of joint 2, **(c)** tip deflection of link 1, **(d)** tip deflection of link 2.

3.6 (c) and 3.6 (d), it can be observed that tip deflections of both the links increase with the link length ratios δ. This may be due to the higher inertia experienced by these links. It is also noted that tip deflections in this case are lower than those in Case A (I). This is due to no link and payload weight acting on these links due to the absence of gravity.

Case C: Effect of link-length ratios on the dynamic response of the manipulator when effects due to both gravity and the Coriolis and centrifugal forces have not been considered

In this case, in addition to the effect of gravity, the effects of centrifugal and Coriolis forces have also not been considered. The same values of η, ν, D_2 and L_1 have been taken as in Case A

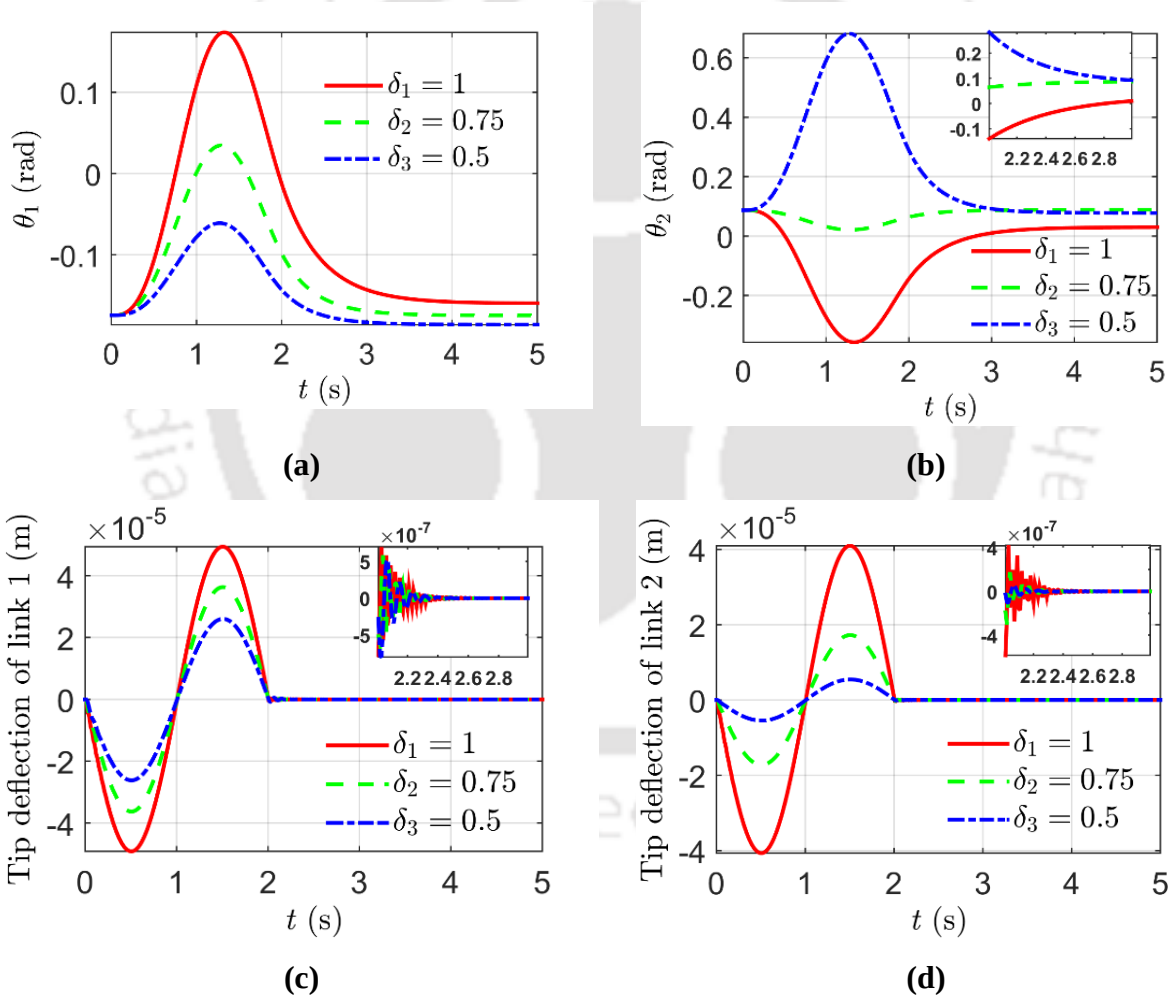

Figure 3.7: Effect of link-length ratio on the dynamic behavior: **(a)** angular displacement of the hub, **(b)** angular displacement of joint 2, **(c)** tip deflection of link 1, **(d)** tip deflection of link 2.

(I) and δ is varied in the ratios of $\delta = 1, 0.75, \text{and } 0.5$ one by one. The dynamic response of the manipulators with different δ can be observed from Figs. 3.7 (a) to 3.7 (d). From Figs. 3.7 (a) to 3.7 (d) it can be observed that the same kind of behavior of joint angular displacements and tip deflections are being observed as in the corresponding Figs. 3.6 (a) to 3.6 (d) of Case B. However, the differences, in this case, can be observed after 2 seconds of joint motion, wherein the levels of attainment of θ are different compared to Case B. This difference in behavior after 2 seconds of joint motion can be attributed to the fact that the torque due to centripetal and Coriolis forces is much less than the torque supplied by the motor which operates for 0 to 2 seconds. After 2 seconds of motion, the effects of centrifugal and Coriolis forces are clearly visible.

With regard to the offshoots and the settling time, it can be observed from the three cases A, B, and C that these values increase with the link length as can be seen from Figs. 3.2 (g) and 3.2 (h) of Case A (I), 3.6 (c) and 3.6 (d) of Case B, 3.7 (c) and 3.7 (d) of Case C. From Case A (II), it is seen that overshoots and settling time of the first link of the manipulator decrease with increase in diameters ratio while those for the 2nd link increase with the diameter ratio. In the case of Case A (III) it is observed that as the payload ratio increases, the offshoots and the settling time increase and response time decreases. From Case A (IV), it is seen that the sinusoidal and triangular torque profile gives the least overshoots, tip deflections, and settling time while the bang-bang torque profile gives the highest.

Since the dynamically calculated values of Rayleigh's damping coefficients $\alpha = 2.3925$ and $\beta = 8.2036 \times 10^{-5}$ in the case of Case A (I) seem to be very high as can be observed from Fig. 3.2 and also from the remaining figures, other values of these coefficients as given in Table 3.3 and available in the scientific literature [Chowdhury and Dasgupta (2003), Kandge (2007)] have also been tried to be applied. Among these results of the dynamic behavior of the manipulator for $\alpha = 0.2$ and $\beta = 2 \times 10^{-3}$ of the set (v) only have been presented in Fig. 3.8 (a) to 3.8 (d) for Case A (I) here, so that presentation should not be too lengthy.

The torques applied at joints are the same as in Figs. 3.2 (a) and 3.2 (b). Fig. 3.8 (a) and 3.8 (b) show the joint angular displacements while Figs 3.8 (c) and 3.8 (d) show tip deflections of the 1st and 2nd link respectively.

Table 3.3: Rayleigh damping coefficients

Rayleigh damping coefficients	Set of values				
	(i)	(ii)	(iii)	(iv)	(v)
α	0.001	0.0307	1.7355	0.75	0.2
β	0.005	3.8×10^{-4}	2×10^{-4}	2×10^{-4}	2×10^{-3}

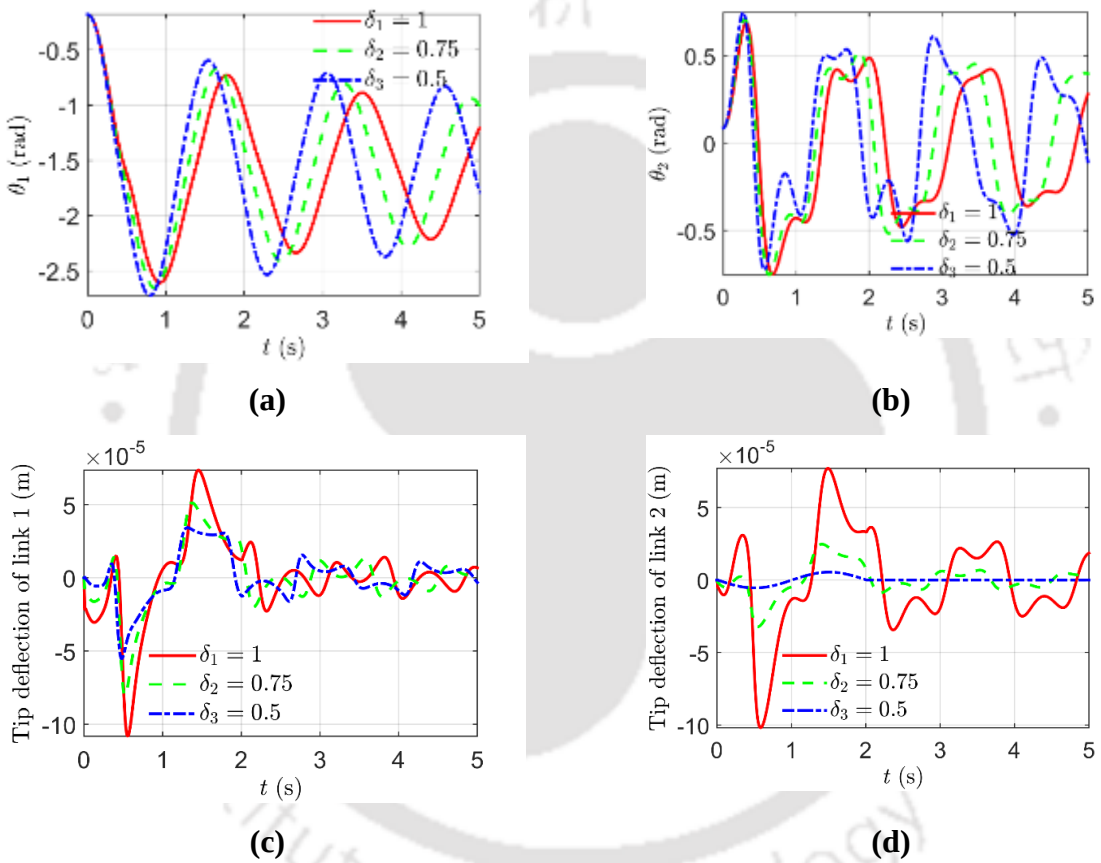

Figure 3.8: Dynamic response for the damping ratio: **(a)** angular displacement of the hub, **(b)** angular displacement of joint 2, **(c)** tip deflection of link 1, and **(d)** tip deflection of link 2.

3.6 Verification of Results

Theoretical analysis and the formulation of the problem mentioned in this chapter have been verified with the results of work done by Usoro et al. (1986). The parameters of the system taken by Usoro et al. (1986) are given in Table 3.4. The initial conditions taken are as given in the paper $\theta_1 = -90°$, and $\theta_2 = 5°$ and the other variables are set equal to zero. Torques applied to

Table 3.4: Inertial parameters of the FLM [Usoro et al. (1986)]

Inertial Parameters	**Link 1**	**Link 2**
Length of links (in m)	1	1
2nd moment of inertia of the cross section of the links (in m^4)	5×10^{-9}	5×10^{-9}
Mass per unit length (in kg/m)	5	5
Young modulus of elasticity (in N/m^2)	2.0×10^{11}	2.0×10^{11}

joints $\tau_1 = \tau_2 = 0$ Nm. The manipulator does not carry any payload. The results obtained using these conditions have been shown in Figs. 3.9 (a-d). Figs. 3.9 (a) and (b) give angular displacements of joints 1 and 2 respectively while Figs. 3.9 (c) and (d) present tip deflections of

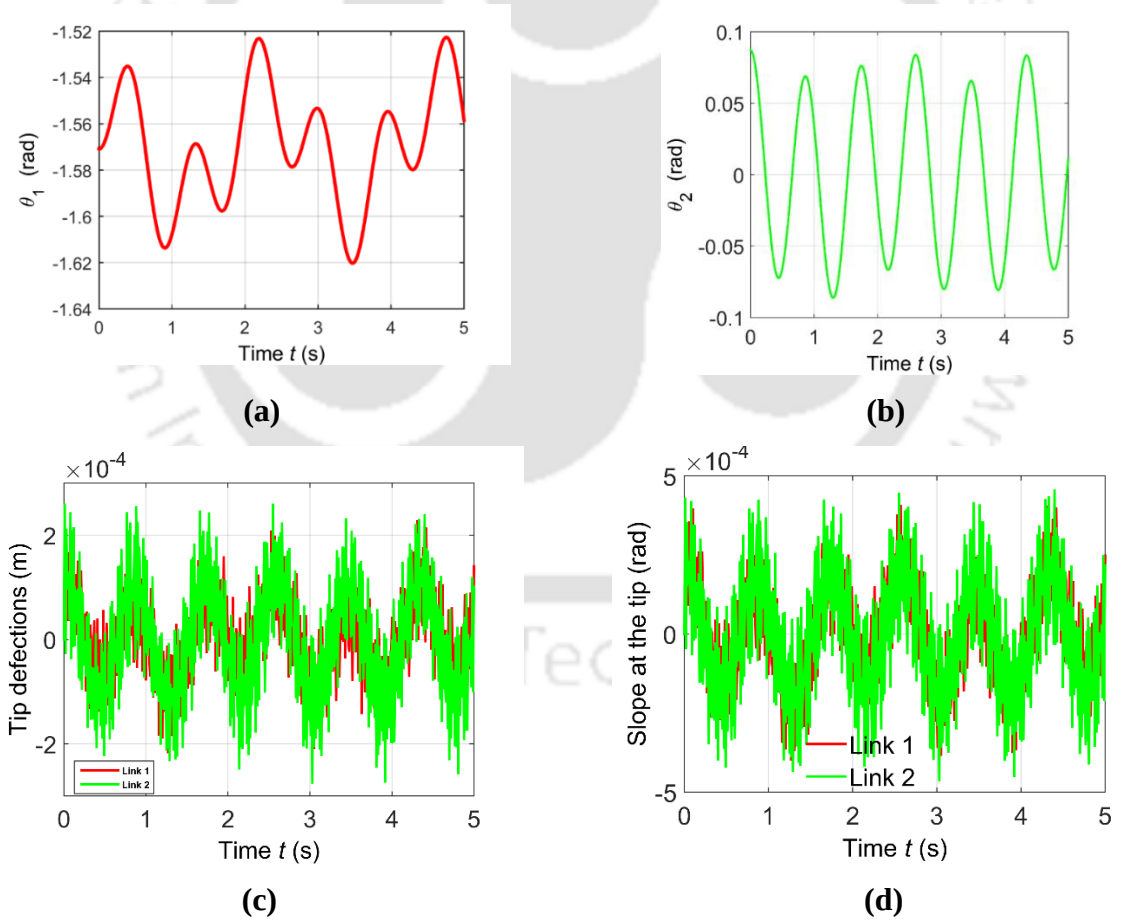

Figure 3.9: Angular displacement **(a)** joint 1, **(b)** joint 2 **(c)** tip deflections of link 1 and link 2, and **(d)** slopes at the tips of links 1 and 2.

link 1 and link 2 and slopes at their tips respectively. From Fig. 3.9 in the present work and Fig. 4 of Usoro et al. (1986) it can be observed that the results match well with each-other.

3.7 Conclusions

The joint angular displacements and velocities of the manipulator increase with a decrease in δ due to the lower inertia of the manipulators. Tip deflections and slopes at the tips of link 1 and link 2 vary with the variation of δ in the same order. This is because higher δ increases the slenderness of the 2nd link which makes them more flexible. In the case of the 1st link, this may be due to higher loads on the tip of link 1 due to increased δ. The overshoots and the settling time increase with the increase in link-length ratio δ.

With respect to the link-diameter ratio ν, the joint angular displacement θ_1 of the first joint depends on both the combined inertia of the manipulator and the amount of torque supplied that is proportional to ν. The angular displacement of joint 2 varies proportionally with ν. Tip deflections and slopes at the tip of link 1 vary with the diameter ratios ν in reverse order. This is because the lower ν makes the 1st links of these manipulators slender increasing the flexibilities of the links while the payloads on link 1 are the same. And at the tip of link 2, they vary with the diameter ratios ν in the same order because of the same mass of the 2nd links for all ν but torques applied at the 2nd joint increase proportionally with ν. The overshoots and the settling time for the first link and the 2nd link increase with the increase in diameter ratio.

Angular responses of both the joints of the manipulator increase with the decrease in payload mass ratio. The corresponding links of these manipulators with different payload ratios are similar in lengths and diameters. So, this is due to less inertia offered by the links of the manipulator with less payload mass that tries to oppose any change in the state of motion of the links. But, the reverse conditions are found for tip deflections and slopes of both the links, i.e., these quantities increase with the increase in payload ratio. The overshoots and the settling time increase with the increase in the payload ratio.

All the torque profiles give almost the same angular response profiles and their amplitudes. However, the triangular torque profile gives the marginally highest joint angular displacements and velocities and the bang-bang torque profile gives the least. It was also observed that the

sinusoidal torque profile gives the smoothest link tip motion while the bang-bang torque profile gives the jerky tip motion. This is because, in the bang-bang torque profile, an abrupt change in torque amplitude takes place which results in oscillatory behavior of link tip motion at every change in values of the torque profile. The bang-bang profile also gives very high overshoots which may lead the link tip to collide with the surroundings. The sinusoidal and triangular torque profile gives the least overshoots, tip deflections, and settling time while the bang-bang torque profile gives the highest.

In the absence of gravity, it is observed that the angular response of joint 1 increases with δ while that for joint 2 depends on the rotational inertia of joint 2. Tip deflections of both the links increase with the link length ratios δ. This may be due to the higher inertia experienced by these links. It is also noted that tip deflections in this case are lower than those in the presence of gravity. This is due to no link and payload weight acting on these links due to the absence of gravity.

When both gravitational force and Coriolis and centrifugal forces are not considered, the same kind of behavior of joint angular displacements and tip deflections are displayed in the absence of gravity. However, the differences, in this case, can be observed after 2 seconds of joint motion, wherein the levels of attainment of θ are different compared to the earlier case.

Chapter 4

Dynamic Analysis and Control of a Single-Link Flexible Manipulator Using Finite Element Method

4.1 Introduction

In the present study, the dynamic equation of motion of a single-link flexible manipulator (SLFM) has been obtained using the finite element method. The finite element modeling of the SLFM is based on the work of Malgaca et al. (2016). The numerical solutions have been obtained using the Newmark method.

Malgaka et al. (2016) applied a command shaping technique for control of the tip vibration which is very sensitive to system modeling errors. In the present work, an LQR controller has been used for the vibration control of the SLFM. LQR is an optimal control technique that provides practical feedback gains based on some performance measure function. The advantages of using the LQR technique are the simplicity to design an LQR controller using the cost function minimization technique and its versatility of use in multivariable systems with the same design procedure as for a single-input-single-output (SISO) system. The LQR controller shows a better transient response compared to the PID controller in vibration reduction. This produces better settling time, less overshoot for the reference tracking response, and smaller aberration in controlling the tip of an FLM compared to a PID controller [Alandoli and Lee (2020)].

This chapter is composed of total 5 sections. Section 4.1 consists of an introduction. In section 4.2 dynamic modeling of the SLFM using finite element method has been presented. Section 4.3 describes the method of control of tip deflection of the SLFM. Section 4.4 presents results and discussion, and section 4.5 concludes the chapter.

4.2 Finite Element Modelling of the Manipulator

The finite element model of the single-link flexible manipulator (SLFM) is shown in Fig. 4.1 (a). OXYZ is the inertial (global) frame of reference with origin at O. Coordinate axis OZ is perpendicular to the plane of motion of the manipulator. OB is the flexible link with a payload mass M_P and moment of inertia I_P. The link is fixed to its hub at O. The hub is fixed to a non-movable frame A. There is a revolute joint at O between the link and the hub. The link can be actuated by a motor at O which applies a torque τ at the hub. The mass of the motor at O is on the frame A. θ in Fig. 4.1 (a) represents the angular position of the link at any instant of time t. The instantaneous angular positions θ_i and θ_f of the link OB respectively at an initial time t_i and final time t_f are shown in Fig. 4.1 (b). The length of the link OB is l.

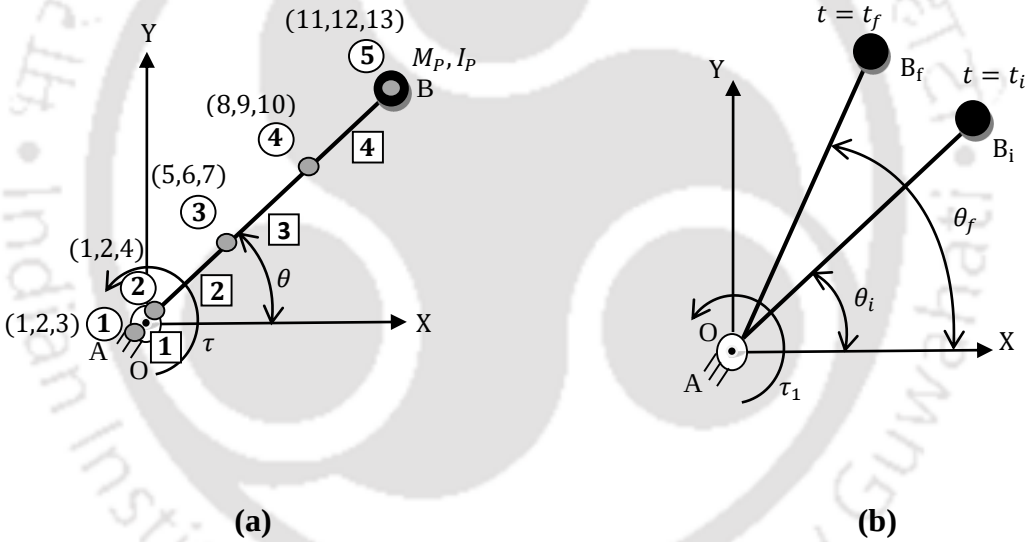

Figure 4.1: Finite element modeling of the manipulator: **(a)** Discretization scheme of the manipulator and **(b)** position of the manipulator with time.

The whole system is divided into n_e number of elements. The link is divided into $(n_e - 1)$ number of elements. For explanation purposes, n_e for the system in the figure has been taken as 4 only although n_e can be taken as any number in the actual finite element formulation of the system. The link OB is divided into 3 elements. The numbers in the circle in Fig. 4.1 (a) denote the node numbers while the number in square boxes represents finite elements (FEs) the system is divided into. The planar motion of the manipulator is considered. There exist 3 degrees of freedom at each

node. The numbers in parentheses in the figure represent the three nodal degrees of freedom (NDoF) associated with each node. For example, FE-3 has Node-3 at its origin and Node-4 at the distal end. The NDoF at Node-3 are (5,6,7) and that at node 4 are (8,9,10). The local Cartesian coordinates of FE-3 can be given as x_3, y_3, and z_3 with the local origin of the finite element at node 3. x_3 axis points towards node 4. The planar motion of the manipulator is considered so that the z_3 axis remains always parallel to the global Z axis. The first two numbers in parentheses at each node represent displacements at the node respectively in the x and y directions while the third numbers in the parentheses represent the flexural rotation of the cross-section at the node multiplied by the length of the finite element. The instantaneous angle of orientation for x is θ_n, $\theta_n = \theta$ where subscript n denotes the n^{th} finite element number. The finite element numbers FE-n, the node numbers of the elements, lengths of the FE-n, angle of instantaneous rotations of the element as well as nodal displacements at each node of the FE, as shown in Fig. 4.1 (a), can be summarised in Table 4.1.

Let h_n be the length of n^{th} finite element (FE-n), A_n be the area of its uniform cross-section. The modulus of elasticity, bending moment of inertia, and density of the n^{th} finite element is respectively E_n , I_n and ρ_n.

Table 4.1: Description of finite element modeling of the system

FE-n	On the structure	FE Nodes	Length of FE	θ_n	Nodal displacement
1	Hub and Link	1,2	l/n_e	θ	(1,2,3) & (1,2,4)
2	Link	2,3	l/n_e	θ	(1,2,4) & (5,6,7)
3	Link	3,4	l/n_e	θ	(5,6,7) & (8,9,10)
4	Link	4,5	l/n_e	θ	(8,9,10) & (11,12,13)

Let the nodal displacement of finite element (FE-n) in x_n direction be u_{mn} , where $m = i$ or j and the nodal displacement in y_n direction be v_{mn}. The flexural rotation of the elemental cross-

section at node m is ϕ_{mn}. The external load forces at node m in x_n and y_n directions are respectively, f_{mnx} and f_{mny}. The external bending moment at m is $\mathbb{T}_{mn}$. Let the distributed external loads on the n^{th} finite element due to the inertia of the element in x_n and y_n directions be respectively p_{nx} and p_{ny}.

The displacement d_{ne}, force F_{ne}, stiffness K_{ne}, and mass M_{ne} matrices in local coordinates of the n^{th} finite element (FE-n) are given below. The node numbers are i at the local origin, and j at the distal end of FE-n. Flexural bending is about the z-axis.

$$d_{ne} = [u_{in} \quad v_{in} \quad h_n\phi_{in} \quad u_{jn} \quad v_{jn} \quad h_n\phi_{jn}]^T \tag{4.1}$$

$$F_{ne} = \left[f_{inx} + p_{nx}\frac{h_n}{2} \quad f_{iny} + p_{ny}\frac{h_n}{2} \quad \mathbb{T}_{in} + p_{ny}\frac{h_n^2}{12} \quad f_{jnx} + p_{nx}\frac{h_n}{2} \quad f_{jny} + p_{ny}\frac{h_n}{2} \quad \mathbb{T}_{jn} + p_{ny}\frac{h_n^2}{12}\right]^T \tag{4.2}$$

$$K_{ne} = \begin{bmatrix} \frac{A_nE_n}{h_n} & 0 & 0 & -\frac{A_nE_n}{h_n} & 0 & 0 \\ 0 & \frac{12E_nI_n}{h_n^3} & \frac{6E_nI_n}{h_n^2} & 0 & \frac{-12E_nI_n}{h_n^3} & \frac{6E_nI_n}{h_n^2} \\ 0 & \frac{6E_nI_n}{h_n^2} & \frac{4E_nI_n}{h_n} & 0 & \frac{-6E_nI_n}{h_n^2} & \frac{2E_nI_n}{h_n} \\ -\frac{A_nE_n}{h_n} & 0 & 0 & \frac{A_nE_n}{h_n} & 0 & 0 \\ 0 & \frac{-12E_nI_n}{h_n^3} & \frac{6E_nI_n}{h_n^2} & 0 & \frac{12E_nI_n}{h_n^3} & \frac{6E_nI_n}{h_n^2} \\ 0 & \frac{-6E_nI_n}{h_n^2} & \frac{2E_nI_n}{h_n} & 0 & \frac{6E_nI_n}{h_n^2} & \frac{4E_nI_n}{h_n} \end{bmatrix} \tag{4.3}$$

$$M_{ne} = \frac{\rho_n A_n h_n}{420}\begin{bmatrix} 140 & 0 & 0 & 70 & 0 & 0 \\ 0 & 156 & 22h_n & 0 & 54 & -13h_n \\ 0 & 22h_n & 4h_n^2 & 0 & 13h_n & -3h_n^2 \\ 70 & 0 & 0 & 140 & 0 & 0 \\ 0 & 54 & 13h_n & 0 & 156 & -22h_n \\ 0 & -13h_n & -3h_n^2 & 0 & -22h_n & 4h_n^2 \end{bmatrix} \tag{4.4}$$

These elemental displacement vector, force vector, stiffness matrix, and mass matrix in elemental coordinate systems are transformed into global coordinate system with the help of the following equations:

$$d_{egn} = T_n d_{ne} \tag{4.5}$$

$$f_{egn} = T_n f_{ne} \tag{4.6}$$

$$K_{egn} = T_n^{'} K_{ne} T_n \tag{4.7}$$

$$M_{egn} = T_n^{'} M_{ne} T_n \tag{4.8}$$

where d_{egn}, f_{egn}, K_{egn} and M_{egn} are respectively the displacement vector, force vector, stiffness matrix, and mass matrix in the global coordinate system while T_n is the transformation matrix that transforms the coordinates of a point on n^{th} element in an elemental coordinate system to a global coordinate system at the hub and is given by

$$T_n = \begin{bmatrix} c_n & s_n & 0 & 0 & 0 & 0 \\ -s_n & c_n & 0 & 0 & 0 & 0 \\ 0 & 0 & 1 & 0 & 0 & 0 \\ 0 & 0 & 0 & c_n & s_n & 0 \\ 0 & 0 & 0 & -s_n & c_n & 0 \\ 0 & 0 & 0 & 0 & 0 & 1 \end{bmatrix} \tag{4.9}$$

where $c_n = \cos\theta_n$ and $s_n = \sin\theta_n$. θ_n is the instantaneous angle of orientation of x_n axis of n^{th} element. $T_n^{'}$ is the transpose of T_n.

Node 1 and node 2 are coincident but their flexural rotations are different due to the revolute joint at O. Joint at O is considered as flexible and is represented by a torsional spring between node 1 and node 2. The torsional stiffness of the spring is K_m. At node 5 a payload of mass M_p and rotational inertia I_p is attached.

On assembly of all elemental matrices in the global coordinates, the mathematical model of the whole system can be given as

$$M_{sys}\ddot{d}_{sys} + C_{sys}\dot{d}_{sys} + K_{sys}d_{sys} = F_{sys} \tag{4.10}$$

where M_{sys} is the system mass matrix, C_{sys} is the system damping matrix, K_{sys} is the system stiffness matrix, d_{sys} is the system displacement matrix, and F_{sys} is the system force matrix. The sizes of d_{sys} and F_{sys} are 13x1, and the sizes of M_{sys}, C_{sys} and K_{sys} are 13x13 for

the configuration shown in Fig. 4.1 (a). For example, $d_{sys}(9,1) = d_{sys9}$, which is the displacement of Node-4 in the y direction. $F_{sys}(9,1) = F_{sys9}$, which is the external force at Node-4 in the y direction. The indices in parentheses represent respectively row and column of the corresponding vector. The elemental force vectors in global coordinate with a size of 6x1 are assembled to obtain the system force vector (F_{sys}). For example, the nodal forces for node 4 are formed due to the distributed forces for FE-3 and FE-4. So, the following can be written for the elements of the nodal force vector, F_{sys}, corresponding to node 4:

$$F_{sys}(8,1) = p_{3_x}\frac{h_3}{2} + p_{4_x}\frac{h_4}{2} \tag{4.11}$$

$$F_{sys}(9,1) = p_{3_y}\frac{h_3}{2} + p_{4_y}\frac{h_4}{2} \tag{4.12}$$

$$F_{sys}(10,1) = p_{3_y}\frac{h_3^2}{12} + p_{4_y}\frac{h_4^2}{12} \tag{4.13}$$

where p_{n_x} and p_{n_y} are the distributed forces for FE-n respectively in the x and y direction in the local coordinate system and h_n is the length of the FE. The distributed inertia and gravity forces are given as

$$p_{n_x} = -\rho_n A_n h_n (a_{nmx} + g_x) \tag{4.14}$$

$$p_{n_y} = -\rho_n A_n h_n (a_{nmy} + g_y) \tag{4.15}$$

where a_{nmx} and a_{nmy} are respectively the components of acceleration of the mid-point of n^{th}element of the link of the flexible-joint flexible-link manipulator (FJFLM), and g_x and g_y are respectively the component of acceleration due to gravity g in X and Y-axis directions. a_{nmx} and a_{nmy} are given by the real part and imaginary part of the quantity which is obtained by differentiating twice the position vector $r_{nm} = R_{nm}e^{i\theta}$ of the midpoint of FE-n with respect to time. Here, R_{nm} is the absolute distance of a mid-point of FE-n on the link from the point O and $i = \sqrt{-1}$.

Global FE matrices with a size of 6x6 are assembled to obtain the system stiffness (K_{sys}) and the mass (M_{sys}) matrices. For example,

$$K_{sys}(9,8) = K_{eg3}(5,4) + K_{eg4}(2,1) \quad (4.16)$$

$$M_{sys}(9,8) = M_{eg3}(5,4) + M_{eg4}(2,1) \quad (4.17)$$

The combination of (9,8) exists in FE-3 and FE-4 as observed in Table 4.1. The combination of (9,8) is the combination of (5,4) for the FE-3 matrix and the combination of (2,1) for the FE-4 matrix.

4.2.1 Boundary Conditions

The flexible link of the manipulator is rigidly clamped to the hub at Node 1. Due to this Node 1 is considered to be fixed, so nodal displacements at the node are given as

$$d_{sys}(1,1) = 0 \quad (4.18)$$

$$d_{sys}(2,1) = 0 \quad (4.19)$$

$$d_{sys}(3,1) = 0 \quad (4.20)$$

In the case of joint flexibility also, only the above first two boundary conditions will be applicable. To account for the kinetic energy of the payload at the tip of the manipulator, M_P and I_P are added to the system mass matrix as follows

$$M_{sys}(11,11) = M_{eg4}(4,4) + M_P \quad (4.21)$$

$$M_{sys}(12,12) = M_{eg4}(5,5) + M_P \quad (4.22)$$

$$M_{sys}(13,13) = M_{eg4}(6,6) + I_P \quad (4.23)$$

To account for the joint flexibility, K_{m_1} is added to the system stiffness matrix as follows

$$K_{sys}(4,4) = K_{eg2}(3,3) + K_{m_1} \quad (4.24)$$

The inertia forces due to the payload mass are added for $F_{sys}(11,1)$, $F_{sys}(12,1)$ and $F_{sys}(13,1)$.

4.2.2 Application of Damping

The Rayleigh damping has been considered as

$$C_{sys} = \alpha M_{sys} + \beta K_{sys} \quad (4.25)$$

where α and β are damping coefficients.

4.2.3 Final Equation of Motion of the System

On application of boundary conditions to the system (4.10) and on consideration of Rayleigh damping the final system of equations for the FJFLM can be given as below.

$$M_f \ddot{d}_f + (\alpha M_f + \beta K_f)\dot{d}_f + K_f d_f = F_f \tag{4.26}$$

where the subscript 'f' denotes the final form of the respective quantities after the application of boundary conditions. The system of equations in Eq. (4.26) is in its coupled form which can be decoupled using modal analysis. Following modal analysis, the displacement vector d_f can be written as $d_f = \tilde{P}q$, where $\tilde{P}$ is the weighted modal matrix, and q is the modal displacement vector. Then, the i^{th} equation of the decoupled form of the system of equations (4.26) will be obtained as follows.

$$\ddot{q}_i + (\alpha + \beta\omega_i^2)\dot{q}_i + \omega_i^2 q_i = \tilde{f}_i \tag{4.27}$$

where ω_i is the i^{th} the natural frequency of vibration of the system, and $\tilde{f}_i$ is the i^{th} element of the vector $\tilde{P}^T F_f$. Once modal displacement vector q is obtained, n^{th} degree of freedom of the displacement vector of FJFLM can be obtained by the n^{th} element of the vector $\tilde{P}q$.

In the present case only the first three modes of vibration q_1, q_2 and q_3 have been considered. Writing Eq. (4.27) in matrix form using the three modes, one will get the following expression.

$$\ddot{q} + (\alpha + \beta\omega_{nf})\dot{q} + \omega_{nf}^2 q = \tilde{f} \tag{4.28}$$

where

$$q = [q_1 \quad q_2 \quad q_3]^T; \omega_{nf} = diagonal(\omega_1, \omega_2, \omega_3); \tilde{f} = [\tilde{f}_1 \quad \tilde{f}_2 \quad \tilde{f}_3]^T.$$

4.3 Control of the FLM and FJFLM

LQR is an optimal control technique in which an input control function is specified for a given dynamical system and a quadratic objective function is defined for the system which quantifies the cost of the control function and its effect on the system. In order to find the optimal control for the system, the objective function is optimized by the proper selection of weights given to the states of the system and the control inputs.

Let the modal coordinates q_1, q_2 and q_3 be written in terms of $q_1 = x_1,\ q_2 = x_2$ and $q_3 = x_3$ respectively and $\dot{q}_1 = x_4, \dot{q}_2 = x_5$, and $\dot{q}_3 = x_6$ where $x_i = x_i(t)$. Then, the system Eq. (4.28) in state-space form can be written as below.

$$\dot{x}(t) = Ax(t) + Bu_c(t) \tag{4.29}$$

$$y(t) = Cx(t) + Du_c(t) \tag{4.30}$$

where A is $n \times n$ matrix, B is $n \times m$ matrix, C is $p \times n$ matrix and D is $p \times m$ matrix. Here, $n = 6, m = 3$ and $p = 6$ and x, $\dot{x}$, A, B, C, and D are given as

$$x(t) = [x_1 \quad x_2 \quad x_3 \quad x_4 \quad x_5 \quad x_6]^T, \dot{x}(t) = [\dot{x}_1 \quad \dot{x}_2 \quad \dot{x}_3 \quad \dot{x}_4 \quad \dot{x}_5 \quad \dot{x}_6]^T, u_c(t) = \tilde{f},$$

$A = \begin{bmatrix} 0_{3\times3} & I_{3\times3} \\ -\omega_{nf}^2 & -(\alpha + \beta\omega_{nf}) \end{bmatrix}$; $B = \begin{bmatrix} 0_{3\times3} \\ I_{3\times3} \end{bmatrix}$; $C = I_{6\times6}$; and $D = 0_{6\times3}$. This is known as a continuous linear time-invariant system. Eq. (4.29) is called the state equation. Eq. (4.30) is called as output equation. The vector $x(t)$ is the state of the system at time t, the vector $\dot{x}(t)$ is the time-derivative of the state of the system at time t. Vector $u_c(t)$ is an independent input to the system. The vector $y(t)$ is the output of the system. The matrices A, B, C, and D are the matrices containing parameters of the overall system. C is a matrix that determines which components of the state are measurable. D denotes how the control affects this output. Typically, these matrices have only diagonal components of either 0 or 1.

One's main concern is to have control over the system of the form (4.29) and (4.30). Control will allow the system to converge toward a desired state. Control is handled through a feedback input, which depends upon the state of the system. One wishes to choose an input to drive the state of the system toward zero while also limiting the size of the input $u_c(t)$. More precisely, one wishes to minimize the cost function that is defined below.

$$J = \frac{1}{2}\int_0^{t_f} [x(t)^T Q x(t) + u_c(t)^T R u_c(t)]dt \tag{4.31}$$

where Q is a $n \times n$ symmetric positive semi-definite matrix and represents the cost penalty attributed to the state, R is a $m \times m$ symmetric positive definite matrix and represents the cost penalty attributed to the inputs. Cost function J is a quadratic function with respect to both state and control.

In the LQR control, the control u_c is chosen such that it minimizes the J over time. In order to minimize J, the Hamiltonian for the system when the terminal condition is $\lambda_c(t_f) = 0$, is defined as follows

$$H = -\frac{1}{2}\left(x(t)^T Q(t)x(t) + u_c(t)^T R(t)u_c(t)\right) + \lambda_c(t)^T\left(Ax(t) + Bu_c(t)\right) \tag{4.32}$$

where $\lambda_c(t)$ is the co-state vector.

Suppose $u_c(t) \in U$ is the optimal control and $x(t)$ is the state trajectory where U is the set of allowable controls dependent on the system. Then from the maximum principle for systems with quadratic cost, there is an adjoint trajectory $\lambda_c(t)$ such that x, u_c and λ_c satisfy

$$\frac{\partial H}{\partial u_c(t)} = 0 \Rightarrow \lambda_c(t)^T B - u_c(t)^T R = 0 \Rightarrow u_c(t) = R(t)^{-1}B(t)^T\lambda_c(t) \tag{4.33}$$

$$\frac{\partial H}{\partial \lambda_c(t)} = \dot{x}(t) \Rightarrow \dot{x}(t) = Ax(t) + Bu_c(t) \tag{4.34}$$

$$\frac{\partial H}{\partial x(t)} = -\dot{\lambda}_c(t) \Rightarrow \dot{\lambda}_c(t) = Q(t)x(t) - A^T\lambda_c(t) \tag{4.35}$$

$$x(0) = x_0 \tag{4.36}$$

$$\lambda_c(t_f) = 0 \tag{4.37}$$

In the above system of equations, there are $2n$ differential equations with $2n$ endpoint conditions and $2n$ unknown functions.

The system of differential equations consisting of Eqs. (4.34-4.35) is linear. $x(t)$ and $\lambda_c(t)$ depend linearly on x_0. Also, $\lambda_c(t)$ depends linearly on $x(t)$. Based on the above facts, the solution to $\lambda_c(t)$ can be assumed to be $\lambda_c(t) = -S(t)x(t)$, where $S(t)$ is a $n \times n$ matrix that is not known yet. Differentiating $\lambda_c(t)$ with respect to time, one will get

$$\dot{\lambda}_c(t) = -\dot{S}(t)x(t) - S(t)\dot{x}(t) \tag{4.38}$$

Substituting these expressions in the above differential equations

$$\dot{x}(t) = A(t)x(t) - B(t)R(t)^{-1}B(t)^T S(t)x(t) \tag{4.39}$$

$$-S(t)\dot{x}(t) - \dot{S}(t)x(t) = Q(t)x(t) + A^T(t)S(t)x(t) \tag{4.40}$$

Multiplying Eq. (4.39) by $S(t)$ and adding to Eq. (4.40)

$$\left[\dot{S}(t) + S(t)A(t) + A^T(t)S(t) - S(t)B(t)R(t)^{-1}B(t)^T S(t) + Q(t)\right]x(t) = 0 \quad (4.41)$$

The above expression will be satisfied for all $x(t)$ if

$$-\dot{S}(t) = S(t)A(t) + A^T(t)S(t) - S(t)B(t)R(t)^{-1}B(t)^T S(t) + Q(t) \quad (4.42)$$

and $S(t_f) = 0$ so that $\lambda_c(t_f) = 0 \ \forall \ x(t)$. Eq. (4.42) is quadratic in $S(t)$ and is called the differential Riccati equation with final condition $S(t_f) = 0$. $S(t)$ is symmetric $\forall\ t$. The solution to the Riccati differential equation can be obtained using backward integration starting at the time $t = t_f$ with the condition $S(t_f) = 0$. Once $S(t)$ is known, $\lambda_c(t)$ can be found $\forall\ x(t)$. Which, in turn, gives an expression for $u_c(t)$ as $u_c(t) = -R(t)^{-1}B(t)^T S(t)x(t)$ or $u_c(t) = -G(t)x(t)$ where $G(t) = R(t)^{-1}B(t)^T S(t)$is the feedback to the system.

If the matrices $A(t), B(t), Q(t)$, and $R(t)$ are constant and independent of time and also the final time t_f extends to infinity, then since the Riccati equation is integrated backward in time, the solution to the equation $S(t)$ is expected to become a constant matrix for t near 0. So that $\dot{S}(t)$ approaches 0. In this case, Eq. (4.42) becomes as follows.

$$S(t)A(t) + A^T(t)S(t) - S(t)B(t)R(t)^{-1}B(t)^T S(t) + Q(t) = 0 \quad (4.43)$$

Eq. (4.43) is called the algebraic Riccati equation. For control purposes the unique stabilizing solution of Eq. (4.43), $S(t)$ is obtained using the Schur Method [Laub (1979)] which gives stable eigenvalues $(A - BG)$ of the system. In this case the control $u_c(t) = -R^{-1}B^T Sx(t)$ or $u_c(t) = -Gx(t)$ where $G(t) = R^{-1}B^T S$ which gives the closed loop system with stable eigenvalues as follows.

$$\dot{x}(t) = (A - BG)x(t) \quad (4.44)$$

4.3.1 Stability Analysis

Here, the Lyapunov method is used to perform the stability analysis. Writing $x(t)$ as x and $u_c(t)$ as u_c for conciseness, one can define the Lyapunov function as follows.

$$V = x^T Sx \quad (4.45)$$

On differentiation of Eq. (4.45) with respect to time t and substituting Eqs. (4.29), $u_c = -R^{-1}B^T Sx$ and (4.43) into it, the following equation can be obtained.

$$\begin{aligned}\dot{V} &= \dot{x}^T Sx + x^T S\dot{x} \\ &= (Ax + Bu_c)^T Sx + x^T S(Ax + Bu_c) \\ &= x^T (A - BR^{-1}B^T S)^T Sx + x^T S(A - BR^{-1}B^T S)x \\ &= x^T (A^T S - S^T BR^{-1}B^T S)x + x^T (SA - SBR^{-1}B^T S)x \\ &= x^T (A^T S - S^T BR^{-1}B^T S + SA - SBR^{-1}B^T S)x \\ &= x^T \{(A^T S + SA - S^T BR^{-1}B^T S) - (SBR^{-1}B^T S)\}x \\ &= x^T \{(-Q) - (SBR^{-1}B^T S)\}x\end{aligned} \tag{4.46}$$

So that one gets the following expression for $\dot{V}$

$$\dot{V} = -x^T \{Q + S^T (BR^{-1}B^T)^T S\}x \tag{4.47}$$

Since matrices R, S are positive definite and Q is also semi-positive definite, one will have $\dot{V} < 0$ which guarantees the stability of the system.

4.4 Results and Discussions

For numerical simulation, the dimensions and material properties of the FJFLM as shown in Fig. 4.1 have been given in Table 4.2.

Table 4.2: Numerical values of the parameters used for FJFLM

Parameters	Values
Modulus of Elasticity E of link (in Pa)	2.1×10^{11}
Density ρ of link (in kg/m^3)	7850
Length (in m)	0.5
Width (in m)	5×10^{-2}
Thickness (in m)	2×10^{-3}
Weight of the payload (in kg)	0.1963
Spring constant K_m (in Nm/rad)	250
Number of Finite Elements n	100
Rayleigh damping coefficients	$\alpha = 0.0307, \beta = 3.8 \times 10^{-4}$
Constants taken in Newmark Method	$\gamma = 0.5, \eta = 0.25$
Time step size (in s)	0.01

The first 3 natural frequencies of the manipulator have been found for each of the cases: (a) when joint flexibility is not considered, and (b) when joint flexibility is also taken into account. In case (a), the first 3 natural frequencies are 3.83 Hz, 32.1 Hz, and 98.3 Hz, and in case (b) these are 3.52 Hz, 29.5 Hz, and 91.1 Hz.

The first 3 modes have been considered for the dynamic analysis of the manipulator. The modal coordinates are taken as $q_1(t), q_2(t)$, and $q_3(t)$. The initial conditions for the solution of Eq. (4.28) are: $q_1(t=0) = q_2(t=0) = q_3(t=0) = 0$ and $\dot{q}_1(t=0) = \dot{q}_2(t=0) = \dot{q}_3(t=0) = 0$. In order to carry out the dynamic analysis of the manipulator, a numerical solution of Eq. (4.28) has been obtained using Newmark numerical solution technique. For analysis of the dynamic behavior of the manipulator in the above-mentioned two cases, the following input has been given to the motor at the hub for a time duration of 2 seconds as described in the following expression, and tip deflection of the link has been observed.

$$\theta(t) = \begin{cases} (\theta_f - \theta_i)\left(\frac{t}{T_f} - \frac{1}{2\pi}\sin\frac{2\pi t}{T_f}\right) + \theta_i; \;\; 0 \le t \le 1\ s \\ 0; 1\ s \le t \le 2\ s \end{cases} \tag{4.48}$$

where $\theta(t)$ is the angular motion of the joint, θ_i is $\theta(t)$ at $t = 0$ s, θ_f is $\theta(t)$ at the end of the joint motion, $T_f = 2$ s is the final time of the motion. The same motion profile for the joint has been applied for all the cases and tip deflections of the manipulator have been observed in these cases. Initial time t_{in}, final time t_f and time step size t_{inc} has been taken as given below:

$t_{in} = 0$ s, $T_f = 2$ s and $t_{inc} = 0.01$ s; $\theta_i = \frac{\pi}{2}$ rad, $\theta_f = 0$ rad.

From the values of modal coordinates, tip displacements of the manipulator in the axial (X-axis) direction u_{tip} and that in the transverse (Y-axis) direction v_{tip} and slope at the tip of the manipulator ϕ_{tip} and their rate of changes with time t in both cases have been obtained and shown in Figs. 4.3.

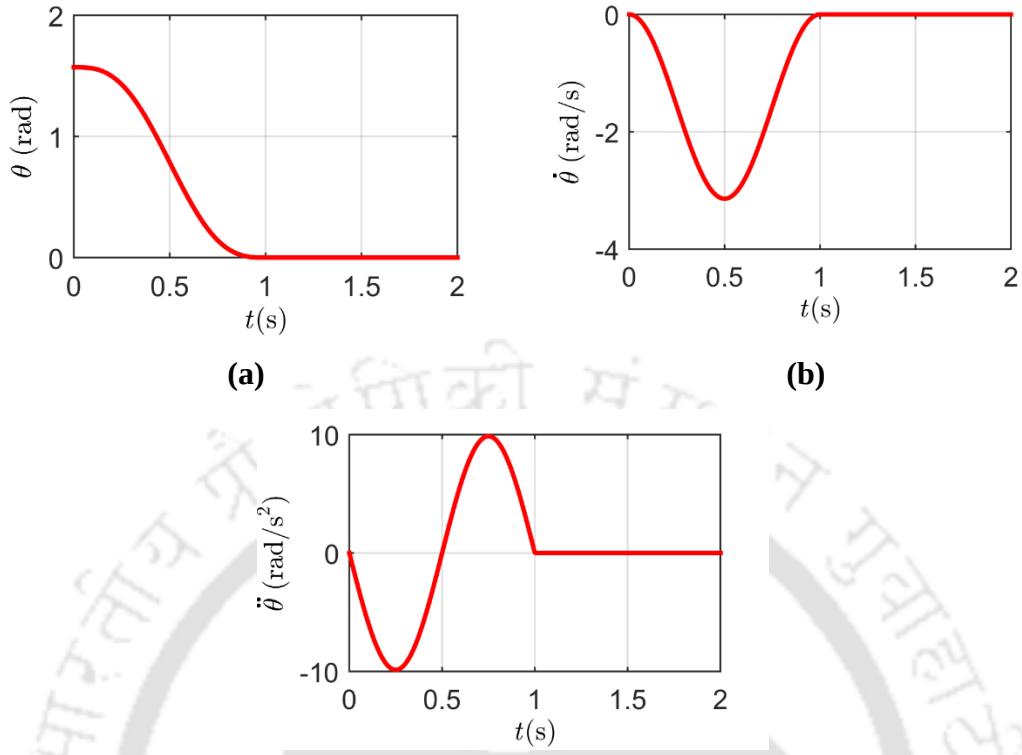

(a) **(b)**

(c)

Figure 4.2: Input given to the manipulator's joint: **(a)** angular displacement, **(b)** angular velocity, and **(c)** angular acceleration.

In the figures, the subscripts to the quantities in the legends represent the quantities obtained either for FLM or FJFLM case

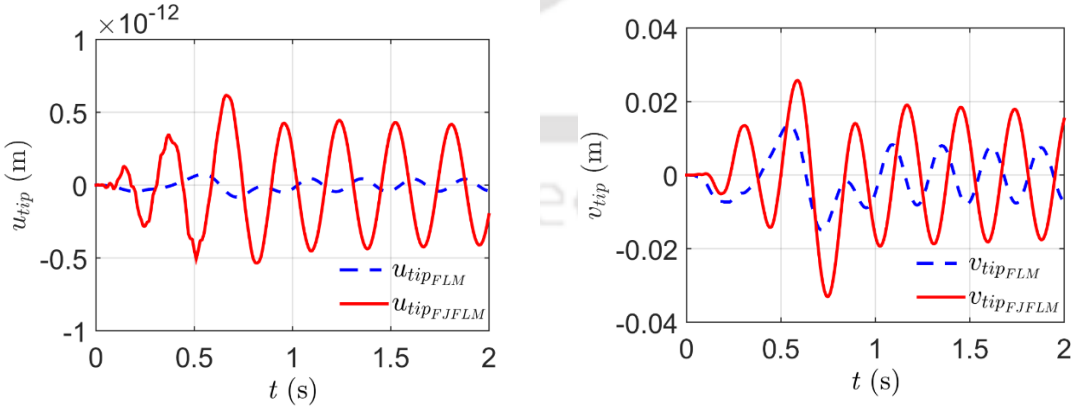

(a) **(b)**

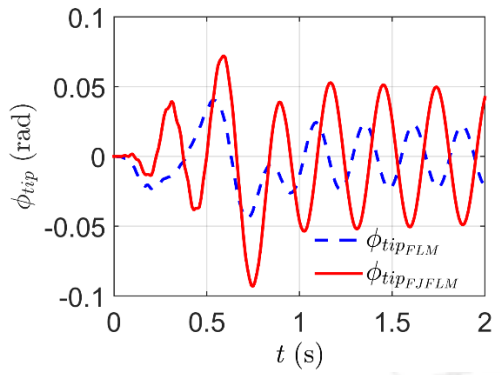
0.1
0.05
0
-0.05
-0.1
ϕ_{tip} (rad)
0
0.5
1
1.5
2
t (s)
$\phi_{tip_{FLM}}$
$\phi_{tip_{FJFLM}}$

(c)

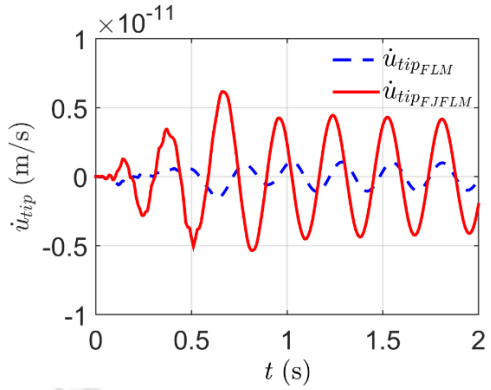
$\times 10^{-11}$
1
0.5
0
-0.5
-1
$\dot{u}_{tip}$ (m/s)
0
0.5
1
1.5
2
t (s)
$\dot{u}_{tip_{FLM}}$
$\dot{u}_{tip_{FJFLM}}$

(d)

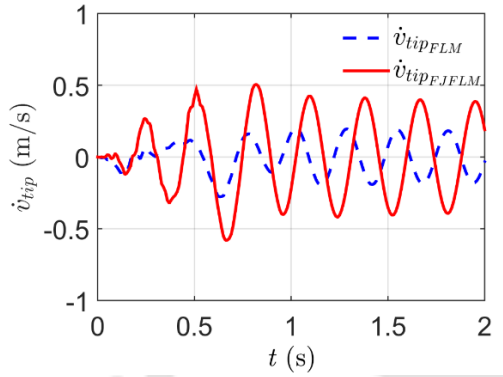
1
0.5
0
-0.5
-1
$\dot{v}_{tip}$ (m/s)
0
0.5
1
1.5
2
t (s)
$\dot{v}_{tip_{FLM}}$
$\dot{v}_{tip_{FJFLM}}$

(e)

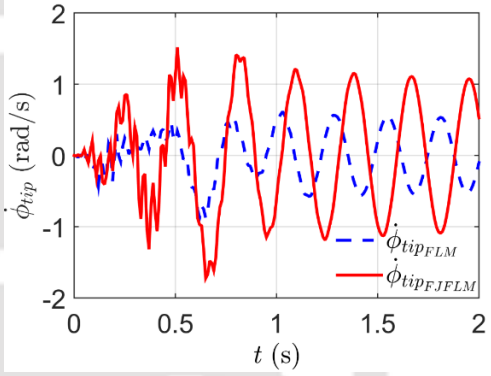
2
1
0
-1
-2
$\dot{\phi}_{tip}$ (rad/s)
0
0.5
1
1.5
2
t (s)
$\dot{\phi}_{tip_{FLM}}$
$\dot{\phi}_{tip_{FJFLM}}$

(f)

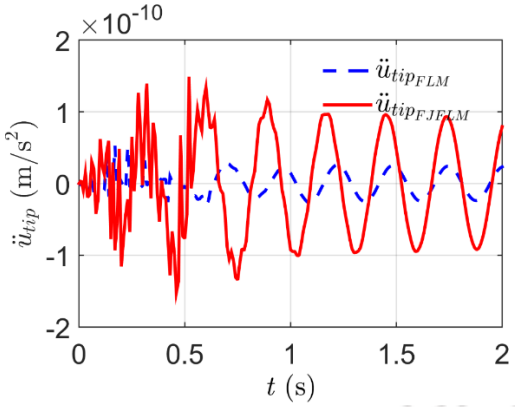
$\times 10^{-10}$
2
1
0
-1
-2
$\ddot{u}_{tip}$ (m/s^2)
0
0.5
1
1.5
2
t (s)
$\ddot{u}_{tip_{FLM}}$
$\ddot{u}_{tip_{FJFLM}}$

(g)

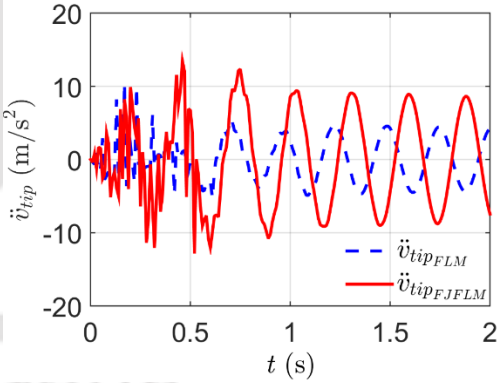
20
10
0
-10
-20
$\ddot{v}_{tip}$ (m/s^2)
0
0.5
1
1.5
2
t (s)
$\ddot{v}_{tip_{FLM}}$
$\ddot{v}_{tip_{FJFLM}}$

(h)

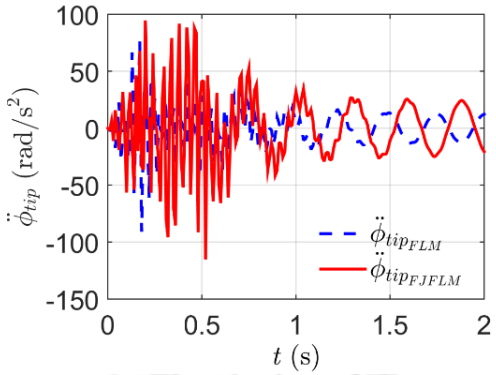

(i)

Figure 4.3: Tip motion of the FLM: **(a)** axial displacement, **(b)** transverse displacement **(c)** slope at the tip **(d)** axial velocity, **(e)** transverse velocity **(f)** time rate of change of slope at the tip **(g)** axial acceleration, **(h)** transverse acceleration **(i)** differentiation of slope at the tip twice with respect to time.

The natural frequencies of the first three modes of vibration and tip deflection values in transverse and axial directions for both the manipulators FLM and FJFLM have been given in Table 4.3. From Fig. 4.3 and values in Table 4.3, it can be observed that in the presence of joint flexibility, SLFM becomes more flexible. The presence of joint flexibility in the SLFM results in lower values of natural frequency and much higher values of tip deflections (2.3 times in transverse direction) as compared to the SLFM when joint flexibility is not considered. It is also observed that the tip deflection of the SLFM in the axial direction is negligibly small.

Table 4.3: Frequencies and tip deflection values of FLM and FJFLM

Quantities	FLM	FJFLM
Natural frequencies of the first three modes (in Hz)	3.83, 32.1, and 98.3	3.52, 29.5, and 91.1
Tip deflection values at the end of motion	$v_{tip} = -0.007539$ m at time $t = 1.88$ s, $u_{tip} = 4.12 \times 10^{-14}$ m at time $t = 1.88$ s.	$v_{tip} = -0.01734$ m at time $t = 1.89$ s,, $u_{tip} = 1.883 \times 10^{-13}$ m at time $t = 1.88$ s.

4.4.1 Verification of the Results

Results obtained from the dynamic analysis of the FJFLM have been verified with the numerical/analytical and experimental results of the work done by Malgaca et al. (2016) using the

same manipulator parameters and trajectory along with the same initial conditions as mentioned in the paper. The results obtained in this work have been compared with their simulation and experimental results. The dimensions and material properties of the FJFLM have been taken according to the paper mentioned above and have been given in Table 4.4.

Table 4.4: Analytical constants, dimensions, and material properties of FJFLM [Malgaca et al. (2016)]

Inertial Properties and Analytical constants	**Values**
Modulus of Elasticity E of link material (in GPa)	210
Density ρ of link material (in kg/m^3)	7850
Length (in mm)	500
Distance of the payload from the end point $d_{payload}$ (in mm)	20
Distance of receiving point from the center of the payload d_{sensor} (in mm)	70
Thickness (in mm)	4
Width (in mm)	80
Cross-sectional area (in mm^2)	320
The inertia of cross-section (in mm^4)	426.67
Number of Finite Elements	-
Newmark amplitude decaying factor	0.005
Weight of the sensor (in g)	0.054
Weight of the payload (in g)	0.62
Rayleigh damping coefficient	$4 \times 10^{-4}, 3.8 \times 10^{-4}$
Motor rotational spring constants (in Nm/rad)	16000
Time step size (in s)	0.005

The trapezoidal motion profile as shown in Fig. 4.4 has been given to the motor at the hub of the manipulator according to the paper by Malgaca et al. (2016). The manipulator moves from a starting position OB_i at $t = 0$ to an end position OB_f at $t = t_f$ as sown in Fig. 4.1(b), where t_f is the time of motion of the motor. The initial angular position is given as $\theta = \theta_i$ at $t = 0$. The angular position at the stopping time is given as $\theta = \theta_i + \theta_f$ at $t = t_f$. The motor at the joint follows the

trapezoidal velocity profile. The area under the velocity curve gives the corresponding motor rotation θ_f.

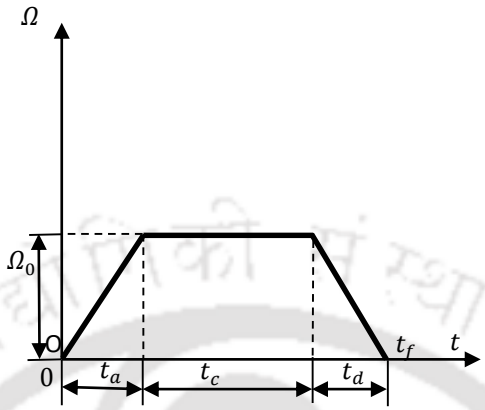

Figure 4.4: The trapezoidal angular velocity profile of the motor.

In Fig. 4.4, t_a, t_c, t_d are respectively time of accelerated, constant, and decelerated motions of the motor. Ω is the angular speed of running the motor and Ω_0 is the average angular speed of the motor during the time duration 0 to t_f. Considering the velocity profile of the motor, the following equations are obtained.

$$\Omega_0 = \frac{\vartheta_f}{0.5t_a + t_c + 0.5t_d} \tag{4.49}$$

$$\dot{\theta} = \begin{cases} \dfrac{\Omega_0 t}{t_a}, & 0 < t < t_a \\ \Omega_0, & t_a \le t < t_f - t_d \\ \dfrac{\Omega_0 (t_f - t)}{t_f - t_d}, & t_f - t_d \le t < t_f \\ 0, & t > t_f \end{cases} \tag{4.50}$$

$$\ddot{\theta} = \begin{cases} \dfrac{\Omega_0}{t_a}, & 0 < t < t_a \\ 0, & t_a \le t < t_f - t_d \\ -\dfrac{\Omega_0}{t_f - t_d}, & t_f - t_d \le t < t_f \\ 0, & t > t_f \end{cases} \tag{4.51}$$

$$\dot{\theta} = \frac{\Omega_0 t}{t_a}$$

(4.52)

$$\ddot{\theta} = \frac{\Omega_0}{t_a} \tag{4.53}$$

The initial conditions for the solution of Eq. (4.28) are: $q_1(t=0) = q_2(t=0) = q_3(t=0) = 0$ and $\dot{q}_1(t=0) = \dot{q}_2(t=0) = \dot{q}_3(t=0) = 0$. The angular motion of the motor is given as $\theta_i = 0, \theta_f = \frac{\pi}{2}$ rad. The motor is run for time $t_f = 2$ s and motion of the FJFLM is observed for $t = 6$ s.

The results obtained for the FJFLM with the payload for the above conditions as mentioned in Table 4.3 and Fig 4.4 are shown in Figs. 4.5. Fig. 4.5 shows the displacement and acceleration of the tip of the manipulator.

From modal analysis, the first three natural frequencies of the FJFLM were found to be 7.72 Hz, 67.2 Hz, and 202.0 Hz. In this work, the analysis of the dynamic behavior has been done for the condition when values of $[t_a,\ t_c,\ t_d,\ t_f] = [*,\ 2t_{1h},\ t_{1h},\ t_f]$, where '$*$' denotes time $t = t_f - t_c - t_d$ and $t_{1h} = \frac{1}{2f_{n_1}}$; f_{n_1} is the first natural frequency of the manipulator. From the comparison of the present analysis of the FJFLM and those of Figs. 7(e) and 7(g) in the work done by Malgaca et al. (2016), it can be concluded that they are in good agreement in both values and profile the tip motion with slight variations that may be due to different values of Newmark factor and some other manipulator constants taken by Malgaca et al. (2016). This fact proves the validity of the present work carried out.

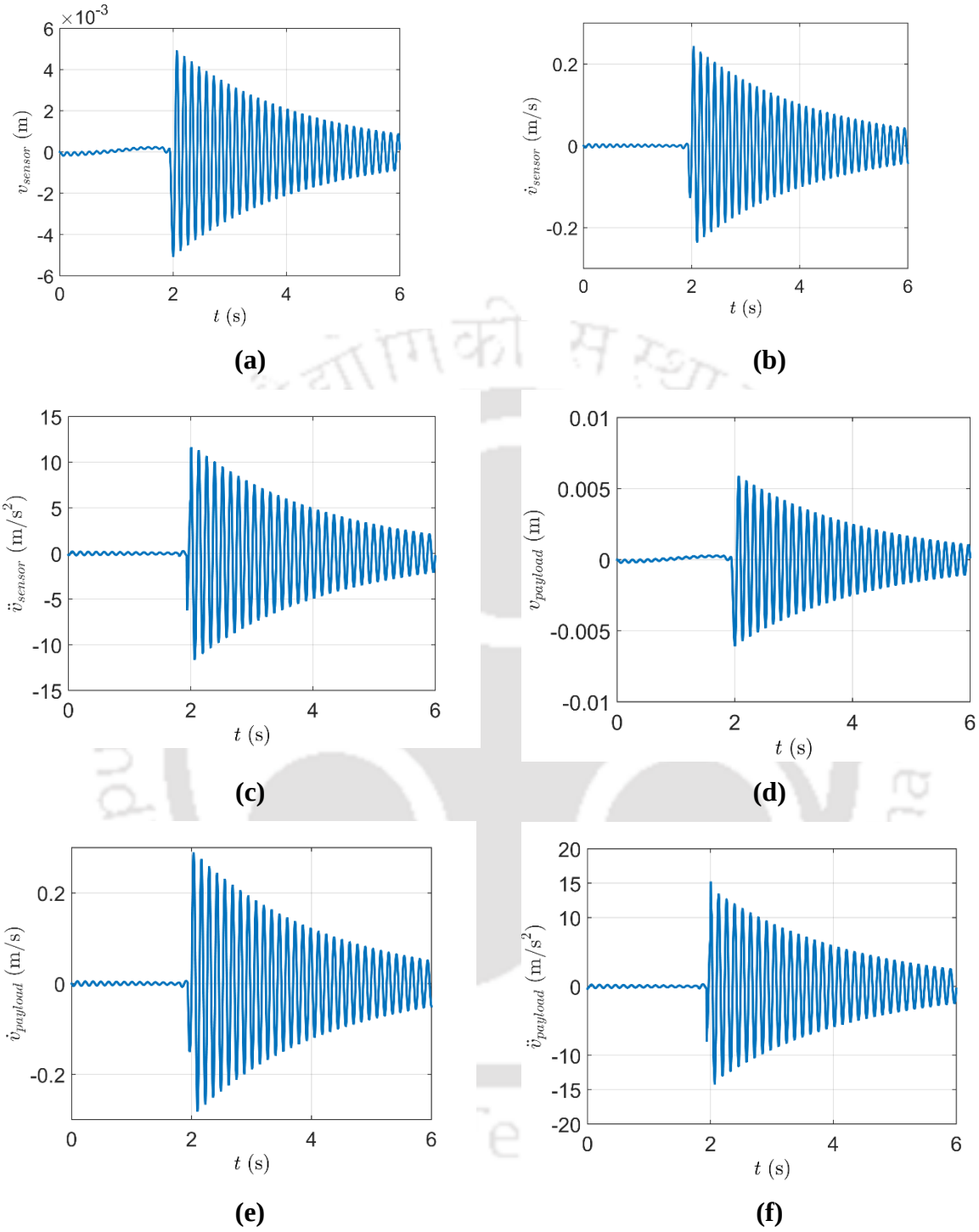

Figure 4.5: Motion of FJFLM at different points on the flexible link in transverse direction: **(a)** displacement at sensor point, **(b)** velocity at sensor point, **(c)** acceleration at sensor point, **(d)** displacement at payload point, **(e)** velocity at payload point and **(f)** acceleration at payload point.

4.4.2 Control of Tip Vibration

From Fig. 4.3 it can be observed that the oscillations of the tip of the manipulator still persist even after the motor is switched off (i.e., $\theta = 0$). Malgaca et al. (2016) applied the command shaping technique to control the tip vibrations that have been shown in the present work also in Fig. 4.5 of section 4.4.1. From the figure, it can be noticed that even after the length/duration of time that is twice the operating time of the manipulator, the oscillations of the manipulator are not subdued effectively which may prove too costly in actual industrial applications resulting in delayed task performance in the repetitive/cyclic types of jobs. Therefore, it necessitates applying some closed-loop types of controllers that can effectively attenuate the vibrations of the manipulator in desired intervals of time with optimum use of control input. With these requirements in mind, in the present work, LQR optimal control has been applied to eliminate the vibrations of the tip of the manipulator as mentioned in section 4.3.

From the dynamic analysis of the FJFLM it is observed from Fig. 4.6 that the first mode displacement is much higher than the other two modes for the input as given in Eq. (4.48).

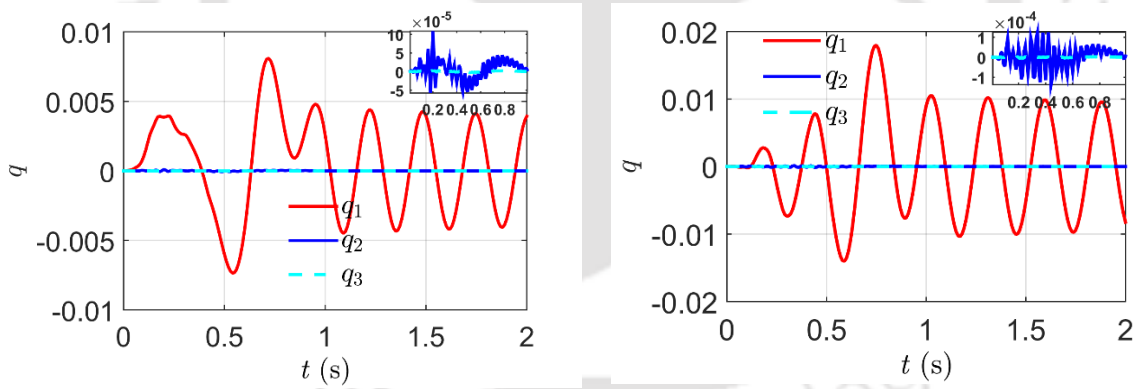

(a) **(b)**

Figure 4.6: Modal response for **(a)** FLM, and **(b)** FJFLM.

So, while selecting the cost penalty or weights to the states Q the higher weightage is given to the 1st mode q_1 and its rate of change with time $\dot{q}_1$.

Here, $Q_{6\times6} = diagonal(Q_1,\ Q_2,\ Q_3,\ Q_4,\ Q_5,\ Q_6)$ and $R_{3\times3} = diagonal(R_1,\ R_2,\ R_3)$ have been taken to be diagonal matrices. The values of the elements of Q and R have been selected by trial-and-error methods. A total of 15 sets of values of Q and R have been tried during the

simulation of the control, out of which the best 5 trial results and the corresponding sets of the values for both FLM and FJFLM have been presented here under the following five cases.

Case 1: the values of diagonal elements of Q and R have been taken as below:

$Q_1 = 0.0001, Q_2 = 1, Q_3 = 1, Q_4 = 0.0001, Q_5 = 1$, and $Q_6 = 1$; $R_1 = 0.001, R_2 = 1$ and $R_3 = 1$ for FLM and $Q_1 = 1, Q_2 = 0.01, Q_3 = 0.001, Q_4 = 1, Q_5 = 0.01$, and $Q_6 = 0.001$; $R_1 = 1, R_2 = 0.01$ and $R_3 = 0.001$ for FJFLM.

Case 2: the values of diagonal elements of Q and R have been taken as below:

$Q_1 = 10, Q_2 = 1, Q_3 = 1, Q_4 = 10, Q_5 = 1$, and $Q_6 = 1$; $R_1 = 0.001, R_2 = 1$, and $R_3 = 1$ for FLM; and $Q_1 = 10, Q_2 = 0.01, Q_3 = 0.001, Q_4 = 10, Q_5 = 0.01$, and $Q_6 = 0.001$; $R_1 = 1, R_2 = 0.01$ and $R_3 = 0.001$ for FJFLM.

Case 3: the values of diagonal elements of Q and R have been taken as below:

$Q_1 = 10, Q_2 = 1, Q_3 = 1, Q_4 = 10, Q_5 = 1$, and $Q_6 = 1$; $R_1 = 1, R_2 = 1$, and $R_3 = 1$ for FLM; and $Q_1 = 10, Q_2 = 0.01, Q_3 = 0.001, Q_4 = 10, Q_5 = 0.1$, and $Q_6 = 0.01$; $R_1 = 1, R_2 = 0.1$ and $R_3 = 0.01$ for FJFLM.

Case 4: the values of diagonal elements of Q and R have been taken as below:

$Q_1 = 30, Q_2 = 1, Q_3 = 1, Q_4 = 10, Q_5 = 1$, and $Q_6 = 1$; $R_1 = 0.1, R_2 = 1$, and $R_3 = 1$ for FLM; and $Q_1 = 30, Q_2 = 1, Q_3 = 1, Q_4 = 30, Q_5 = 1$, and $Q_6 = 1$; $R_1 = 1, R_2 = 1$, and $R_3 = 1$ for FJFLM.

Case 5: the values of diagonal elements of Q and R have been taken as below:

$Q_1 = 30, Q_2 = 1, Q_3 = 1, Q_4 = 30, Q_5 = 1$, and $Q_6 = 1$; $R_1 = 0.1, R_2 = 1$, and $R_3 = 1$ for both FLM and FJFLM.

The initial conditions for the control of both FLM and FJFLM have been taken to be $q_1 = 0, q_2 = 0, q_3 = 0, \dot{q}_1 = 0, \dot{q}_2 = 0$, and $\dot{q}_3 = 0$ while input given to the systems according to Eq. (4.48). The results of LQR control of the FLM have been presented in Fig. 4.7. The results of LQR control of the FJFLM have been presented in Fig. 4.8.

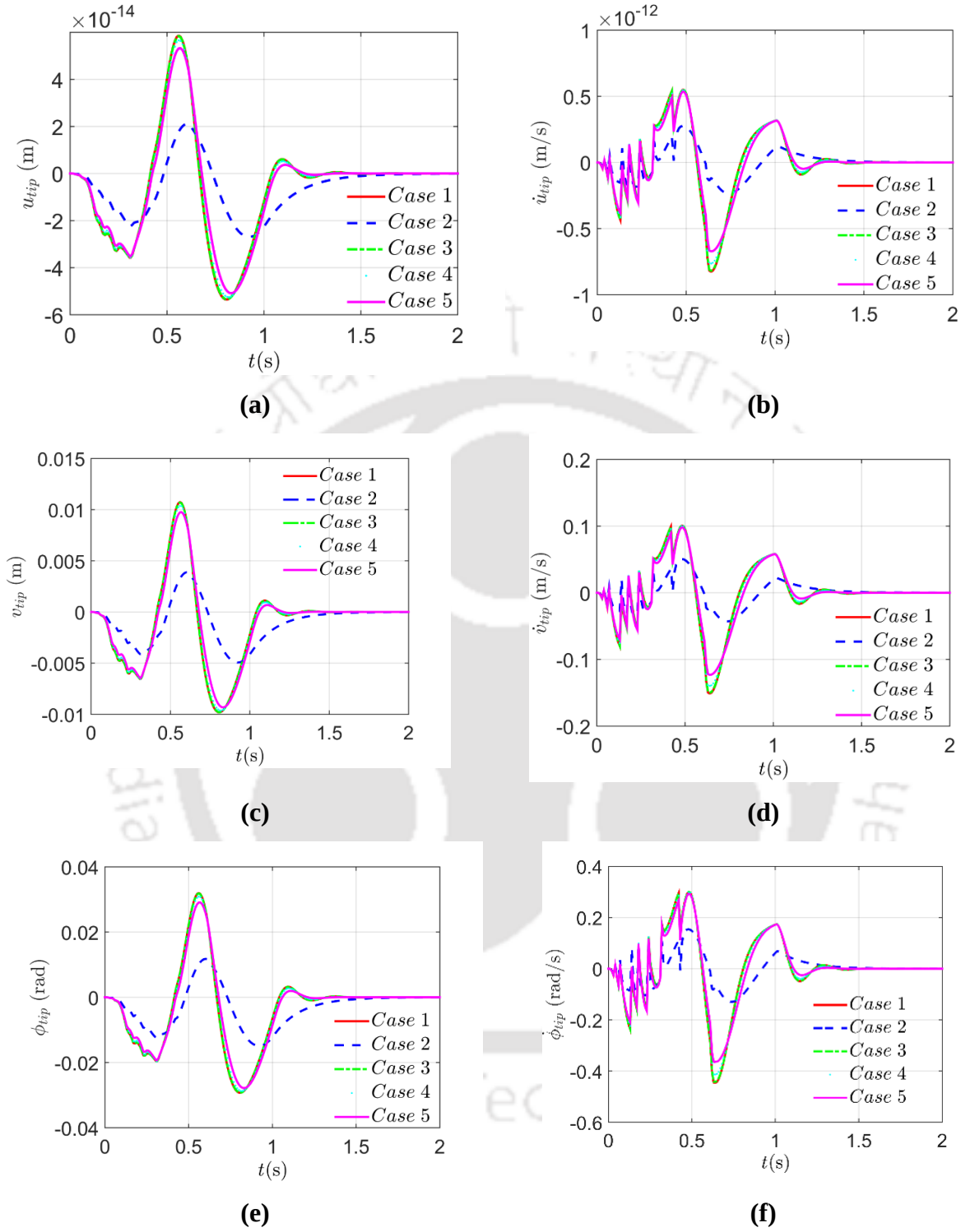

Figure 4.7: Motion control of Tip of the FLM using LQR optimal control: **(a)** axial displacement, **(b)** axial velocity, **(c)** transverse displacement, **(d)** transverse velocity, **(e)** slope at the tip and **(f)** rate of change of slope at the tip.

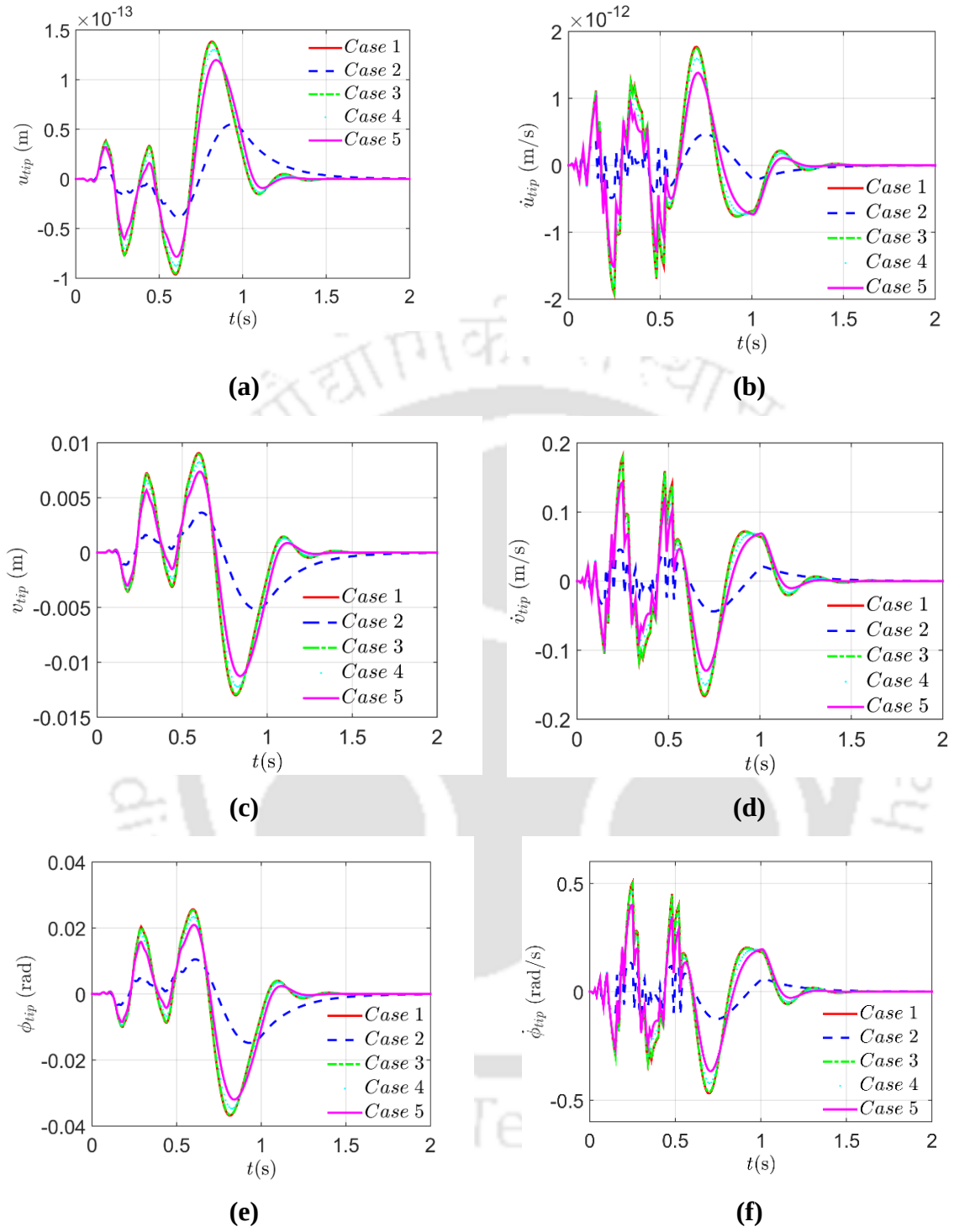

Figure 4.8: Motion control of Tip of the FJFLM using LQR optimal control: **(a)** axial displacement, **(b)** axial velocity, **(c)** transverse displacement, **(d)** transverse velocity, **(e)** slope at the tip and **(f)** rate of change of slope at the tip.

From Figs. (4.7) and (4.8) it can be observed that the application of LQR control to the system brings the system to the equilibrium state within a fraction of a second. Also, it can be observed that the set of values of Q and R in case 5 gives the minimum settling time and the least overshoot while those in case 4 require longer settling time but with no overshoot. This is because the values of Q with respect to first mode of vibration that is the most dominant component of vibration, have been taken to be the highest in case 5 while values of R corresponding to that mode have been kept relatively lower. In case 2, the values of Q_1 and Q_4 have been taken lower compared to case 5 but the values of R corresponding to that mode of vibration have been selected lower. The choice among the given sets of values of Q and R depends on the requirement of the operator of the manipulator or the performance of the manipulator may be further optimized with the careful selection of the values by the operator himself. Thus, with the help of LQR control and the mathematical modeling technique mentioned above for the physical system, a light manipulator can successfully be realized for the low production cost of the manipulator and its low operational cost advantages.

4.5 Conclusions

In this work, dynamic analyses have been carried out for the manipulator with both link-flexibility as well as joint-flexibility. The use of the Newmark technique results in the fast computation of the dynamic behavior of the FJFLM. Tip deflections for the FJFLM are considerably higher than those for FLM. Tip deflections in the axial direction are found to be negligibly small. With this method of dynamic modeling, there is no need for linearization of the system for the application of the LQR controller as joint angular displacement does not appear in the states of the system. Proper choice of the parameters of the LQR controller results in less overshoot and settling time which will yield smooth operation of the manipulator.

Chapter 5

Dynamic Analysis and Control of a String-Stiffened Single-Link Flexible Manipulator

5.1 Introduction

In this chapter, systematic mathematical modeling, analysis, and control of string-stiffened flexible-joint flexible-link manipulators have been carried out. As discussed in chapter 2, the use of a pair of strings will enhance the stiffness of the manipulator and hence reduce the tip deflection of the manipulator. As very less work is available in this field, a detailed analysis is carried out in this chapter.

This work is comprised of a total of 5 sections. Section 5.2 describes the modeling of the SSSLFM using the assumed mode method. The control of the manipulator is discussed in section 5.3. Here, adaptive PID control along with impedance control has been used to control the tip deflection. In section 5.4 the numerical results have been discussed and in section 5.5 the chapter is concluded.

5.2 Modelling

In this section, the modeling of the string-stiffened single-link manipulator with both link and joint flexibility has been carried out using the classical assumed mode method. Figures 5.1(a) and 5.1(b) respectively show the schematic diagram of a string-stiffened single-link flexible manipulator (SSSLFM) as viewed from the top and front. In order to provide extra stiffness to the flexible link, both ends of the link have been tied with a pair of strings on both sides of the link. On either side of the flexible link, two short supporting structures have been attached to the hub of the link to hold stiffening strings with other ends attached to the tip of the FLM as shown in Fig. 5.1. This configuration will reduce the addition of extra moment of inertia due to the attachment of strings to the overall moment of inertia of the FLM due to its proximity to the hub while maintaining its advantage of being lightweight.

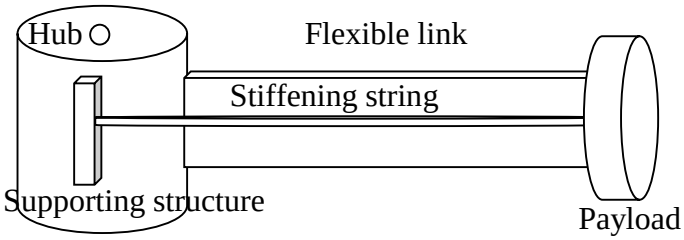

(a)

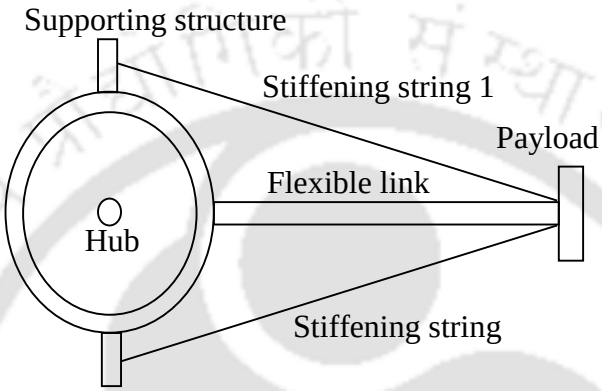

(b)

Figure 5.1: A schematic diagram of the SSSLFM: **(a)** as viewed from the front **(b)** as viewed from the top.

The CAD model of the manipulator in Solidworks 2019 has been shown in Figs. 5.2(a) and 5.2(b). It clearly illustrates how the flexible link is connected to the motor and the use of the strings to stiffen the flexible manipulator. In the next subsection, the mathematical modeling of the system has been presented by considering the forces acting on this structure.

5.2.1 Force Consideration

Forces acting on the flexible link system have been shown in Fig. 5.3. Here, T_1 and T_2 are tensions in the strings, γ_1 and γ_2 are the angles made by the strings with the flexible link. θ is the angular displacement and Ω is the angular velocity of the hub. The mass of the payload is M_p. F is the net radial force on the payload in the local frame. The payload is subjected to centrifugal

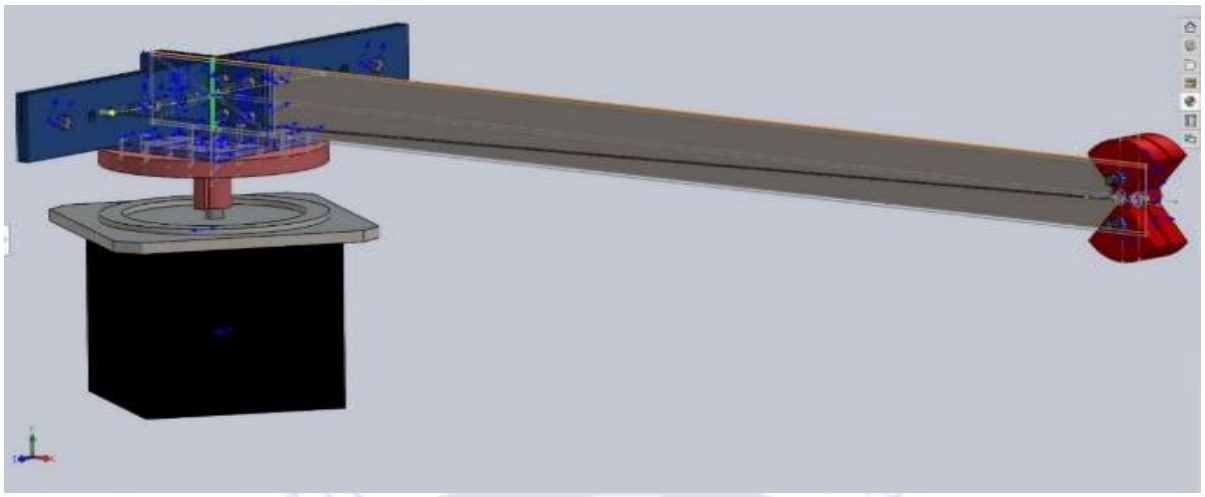

(a)

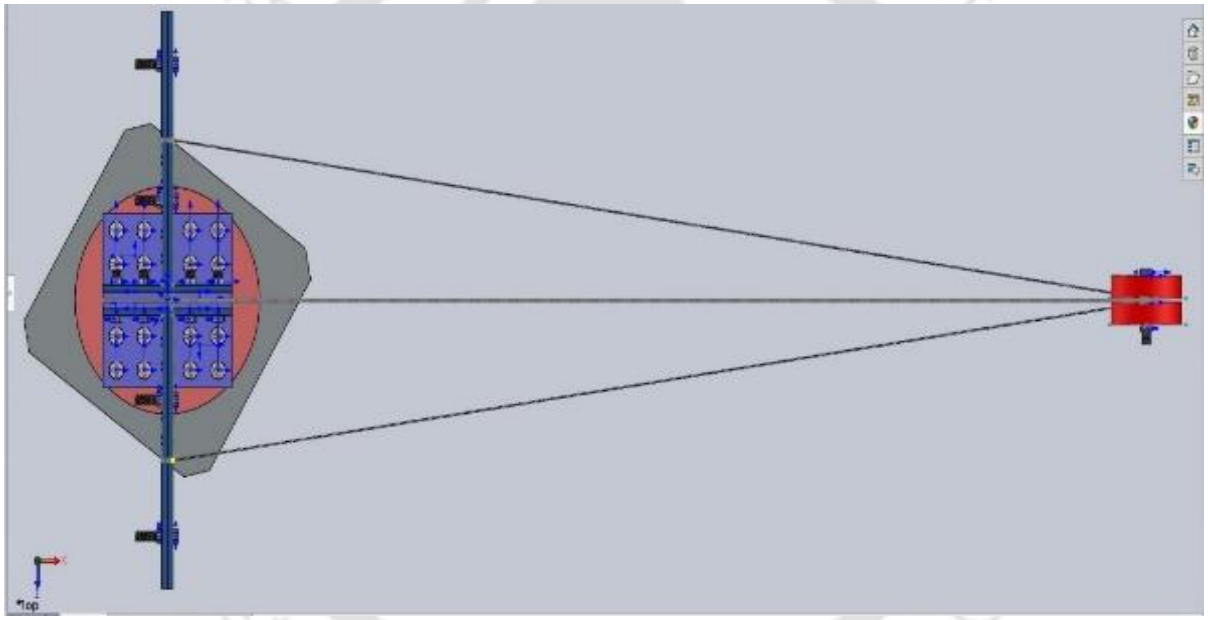

(b)

Figure 5.2: CAD model of the SSSLFM in Solidworks 2019 as viewed from **(a)** the front and **(b)** the top.

force along the radial direction away from the center and tangential force perpendicular to the radial direction and opposite to the direction of acceleration. The link is assumed to be subjected to a tensile force $T_1 \cos\gamma_1 + T_2 \cos\gamma_2$ along the link-length which may be achieved with the help of string-pulley arrangement. $M_p\Omega^2 l$ is the centrifugal force that acts on the payload during the motion of the manipulator. $T_1 \sin\gamma_1$ and $T_2 \sin\gamma_2$ are the forces acting at the tip of the manipulator due to the string tensions. $M_p\dot{\Omega}l$ is the force acting on the payload due to its inertia.

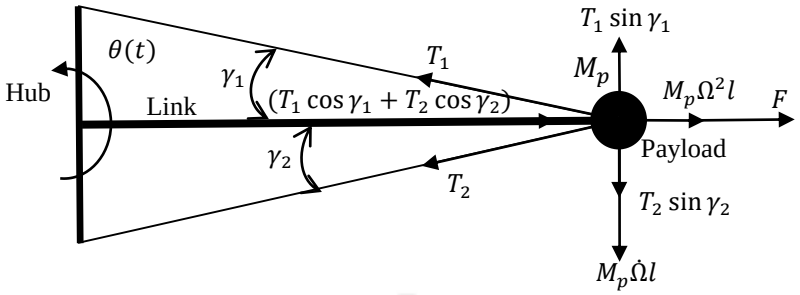

Figure 5.3: Forces acting on the flexible link with the payload.

The force balance as shown in Fig. 5.3 provides the following set of equations:

$$\mathrm{M_p}\Omega^2 l + T_1 \cos\gamma_1 + T_2 \cos\gamma_2 = F \tag{5.1}$$

$$\mathrm{M_p}\dot{\Omega} l = T_1 \sin\gamma_1 - T_2 \sin\gamma_2 \tag{5.2}$$

5.2.2 General Equation of Motion of a String-Stiffened Flexible Link

The link of SSSLFM as shown in Fig. 5.1 and Fig. 5.3 can be modeled as a cantilever beam subjected to axial load $P(x,t)$. The link is considered to be slender with a rectangular cross-section in the absence of deformation. The link undergoes small elastic deformation and can be considered as the Euler-Bernoulli beam. The assumed mode method (AMM) has been used to model this link. Let $f(x,t)$ be the external force per unit length of the link. At a distance x from the fixed end of the beam, a section of the beam of infinitesimal length dx has been considered whose deflection with the neutral axis of the beam is given by $w(x,t)$. The generalized equation for a uniform beam subjected to an axial loading [Rao (2011)] is given by

$$EI\frac{\partial^4 w}{\partial x^4} + \rho A\frac{\partial^2 w}{\partial t^2} - P\frac{\partial^2 w}{\partial x^2} = f \tag{5.3}$$

where E is the Young Modulus of elasticity, I is the moment of inertia of the cross-section of the beam, ρ is the density of the beam material, A is the cross-sectional area of the beam. In the case of free vibration of the beam, $f(x,t)$ is equal to zero. Then the solution of Eq. (5.3) can be found by separation of variable method as $w(x,t)$, where

$$w(x,t) = W(x)q(t) \tag{5.4}$$

$W(x)$ is the mode shape and $q(t)$ is the temporal variable given as $q(t) = A_n \cos \omega_n t + B_n \sin \omega_n t$. ω_n is the natural frequency, and A_n and B_n are constants for the n^{th} mode of vibration of the link, to be determined from the initial conditions of the vibration. Let $W(x) = Ke^{\beta x}$ where K and β are constants. Then, for free vibration of the link, using Eq. (5.4) into Eq. (5.3), the following roots can be obtained for Eq. (5.3)

$$\beta_{1,2}^2 = \frac{P}{2EI} \pm \sqrt{\frac{P^2}{4E^2I^2} + \omega_n^2 \frac{\rho A}{EI}} \tag{5.5}$$

So, $W(x)$ can be expressed as

$$W(x) = C_1 \cosh \beta_1 x + C_2 \sinh \beta_1 x + C_3 \cos \beta_2 x + C_4 \sin \beta_2 x \tag{5.6}$$

where C_1, C_2, C_3 and C_4 are the constants to be determined from the boundary conditions of the beam.

Depending upon different constraint conditions applied on the link, here, three cases can be considered:

Case I: when the tip of the link of the FLM is tied with a pair of strings on either side of the link. The other ends of the strings are tied to the supporting structure at the hub of the FLM. Here, the effect of string vibration on the tip deflection of the link is not considered.

Case II: Here the structure is the same as in case I. But the effect of the vibration of strings on the tip deflection of the link is considered in this case.

Case III: when the link of FLM is not tied with any string, i.e., when the system is that of a cantilever beam.

These three cases have been described in detail as follows:

Case I: when the tip of the link of the FLM is tied with a pair of strings on either side of the link. Without considering the effect of string vibrations, the following three types of boundary conditions have been discussed below.

Boundary conditions I(a):

With the attachment of the strings to the tip resisting the tip deflection, the flexible link will behave similarly to a clamped-pinned beam rather than a clamped-free beam. The following boundary conditions can be considered:

$$W(0) = 0; \frac{dW}{dx}(0) = 0; W(l) = 0; \frac{d^2W}{dx^2}(l) = 0 \tag{5.7}$$

The characteristic constants $\beta_1 l$ and $\beta_2 l$ are the roots of non-linear Eq. (5.6) and are given as,

$$\beta_1 l = \beta_2 l = \pm(2n-1)\frac{\pi}{2} \tag{5.8}$$

where $n = 1,2,3, \ldots\ldots, \infty$. From Eqs. (5.5) and (5.8), the natural frequency of beam vibration can be found to be

$$\omega_n = \left(\frac{EI}{\rho A}\right)^{\frac{1}{2}} \frac{\pi^2}{4l^2} \sqrt{(2n-1)^4 - (2n-1)^2 \left(\frac{2}{\kappa}\right)^2 \frac{P}{P_{Cr}}} \tag{5.9}$$

where P_{Cr} is the critical load of buckling for an axially loaded beam, given as $P_{Cr} = \frac{\pi^2 EI}{\kappa^2 l^2}$; κ is the effective length factor for the beam or link (*Buckling*, https://en.wikipedia.org/wiki/Buckling).

Thus, the solution for mode shapes is given as

$$W(x) = \sum_{n=1}^{\infty} \Big(C_n \big(\beta_{2_n} \cosh \beta_{1_n} x - \beta_{2_n} \cos \beta_{2_n} x \big) + D_n \big(\beta_{1_n} \sin \beta_{2_n} x - \beta_{2_n} \sinh \beta_{1_n} x \big) \Big) \tag{5.10}$$

where n is the number of modes, C_n and D_n are constants for n^{th} mode of vibration of the beam, given as $C_n = \frac{1}{\beta_{2_n}}$ and $D_n = \frac{\beta_{1_n}^2 \cosh \beta_{1_n} l + \beta_{2_n}^2 \cos \beta_{2_n} l}{\beta_{2_n} (\beta_{1_n}^2 \sinh \beta_{1_n} l + \beta_{1_n} \beta_{2_n} \sin \beta_{2_n} l)}$. Thus, a solution for the transverse displacement can now be given as follows.

$$w(x,t)=\sum_{n=1}^{\infty}\Big(\Big(C_n\big(\beta_{2_n}\cosh\beta_{1_n}x-\beta_{2_n}\cos\beta_{2_n}x\big)+D_n\big(\beta_{1_n}\sin\beta_{2_n}x-\beta_{2_n}\sinh\beta_{1_n}x\big)\Big)\big(A_n\cos\omega_n t+B_n\sin\omega_n t\big)\Big) \quad (5.11)$$

For $n=1$, the first mode of vibration of the flexible link is given as

$$W(s)=C(\beta_2\cosh\beta_1x-\beta_2\cos\beta_2x)+D(\beta_1\sin\beta_2x-\beta_2\sinh\beta_1x) \quad (5.12)$$

where C and D are constants for the mode of vibration of the link and are given as $C=\frac{1}{\beta_2}$ and $D=\frac{\beta_1^2\cosh\beta_1l+\beta_2^2\cos\beta_2l}{\beta_2(\beta_1^2\sinh\beta_1l+\beta_1\beta_2\sin\beta_2l)}$.

By plotting $W(x)$ vs. x for the first mode, one can find the point on the link where maximum deflection occurs on tying it with a pair of strings.

Boundary conditions I(b):

But, in actual practice, deflection of the tip of the string-stiffened link, although small, does take place despite the constraining tip movement with a pair of strings, partly because of the inertia of the payload at the tip of the link and partly due to the acute angle of the string with the link. In that case, boundary conditions on a cantilever beam subjected to an axial force because of string attachment are given by

$$w(0,t)=0;\ \frac{dw}{dx}(0,t)=0;\ \frac{d^2w}{dx^2}(l,t)=0;\ \text{and}\ \frac{d^3w}{dx^3}(l,t)+\frac{M_p\omega^2}{EI}w(l,t)-\frac{\mathrm{T}_1}{EI}\sin\gamma_1+\frac{\mathrm{T}_2}{EI}\sin\gamma_2=0 \quad (5.13)$$

Applying these boundary conditions in Eq. (5.6), the first mode of vibration of the flexible link is given by

$$W(x)=C(\beta_2\cosh\beta_1x-\beta_2\cos\beta_2x)+D(\beta_1\sin\beta_2x-\beta_2\sinh\beta_1x) \quad (5.14)$$

Then frequency equation on applying Boundary Conditions I(b), is given by the following equation:

$$C_1\left[-\beta_1(\beta_1^4+\beta_2^4)+(\beta_1^4\beta_2-\beta_1^2\beta_2^3)\sinh\beta_1 l\sin\beta_2 l-2\beta_1^3\beta_2^2\cosh\beta_1 l\cos\beta_2 l+\right.$$
$$\left.\frac{M_p\omega_n^2}{EI}\left\{\left(\beta_1\beta_2+\frac{\beta_1^3}{\beta_2}\right)\cosh\beta_1 l\sin\beta_2 l-(\beta_1^2+\beta_2^2)\sinh\beta_1 l\cos\beta_2 l\right\}\right]-\left(\frac{\mathrm{T}_1}{EI}\sin\gamma_1-\right.$$
$$\left.\frac{\mathrm{T}_2}{EI}\sin\gamma_2\right)(\beta_1^2\sinh\beta_1 l+\beta_1\beta_2\sin\beta_2 l)=0 \tag{5.15}$$

Here C_1 has been taken to be equal to 1.

Boundary conditions I(c):

If one assumes that the payload on the tip of the link is at all not allowed to move by the string forces that are normal to the link, then, in that case, boundary conditions on a cantilever beam subjected to an axial force because of strings are given by

$$w(0,t)=0;\frac{dw}{dx}(0,t)=0;\frac{d^2w}{dx^2}(l,t)=0;\text{ and }\frac{d^3w}{dx^3}(l,t)=0 \tag{5.16}$$

The frequency equation, in this case, will be given by

$$p_1(p_1^4+p_2^4)+2p_1^3p_2^2\cosh p_1\cos p_2+p_1^2p_2(p_2^2-p_1^2)\sinh p_1\sin p_2=0 \tag{5.17}$$

where $p_1=\beta_1 l$ and $p_2=\beta_2 l$.

Case II: Effect of String Vibration on the Vibration of Link

For a uniform string of length l_s under tension force T_s, the equation of motion for the vibration of the string is given as

$$T_s\frac{\partial^2 y}{\partial x^2}+f=\rho_s\frac{\partial^2 y}{\partial t^2} \tag{5.18}$$

where ρ_s is the mass of the string per unit length, f is the transverse force acting on the string and $y(x,t)$ is the transverse displacement of the string at x from the origin and at any time t. For free vibration, $f=0$, so that

$$c^2\frac{\partial^2 y}{\partial x^2}=\frac{\partial^2 y}{\partial t^2} \tag{5.19}$$

where $c=\sqrt{\frac{T_s}{\rho_s}}$ is the speed of the disturbance wave in the string. Equation (5.19) is known as the wave equation. The solution of Eq. (5.19) can be given as

$$y(x,t)=\phi(x)\psi(t) \tag{5.20}$$

where $\phi(x)$ is the mode shape of the string and $\psi(t)$ is the temporal variable for the string deflection. If ω_{ns} is the natural frequency of vibration of the string, then using Eq. (5.20) in Eq. (5.19), the solutions to the wave equation of the string for the first mode is

$$y(x,t) = \phi(x)\psi(t) = \left(A_s \cos\frac{\omega_{ns}}{c}x + B_s \sin\frac{\omega_{ns}}{c}x\right)(C_s \cos\omega_{ns}t + D_s \sin\omega_{ns}t) \tag{5.21}$$

where $A_s, B_s, C_s$and D_s are constants that can be found from the boundary and initial conditions. The ends of the stiffening string on any one side of the link have been shown in Fig. 5.4(a). Following boundary conditions can be applied to find constants A_s and B_s depending upon the conditions the string may be assumed to be subjected to:

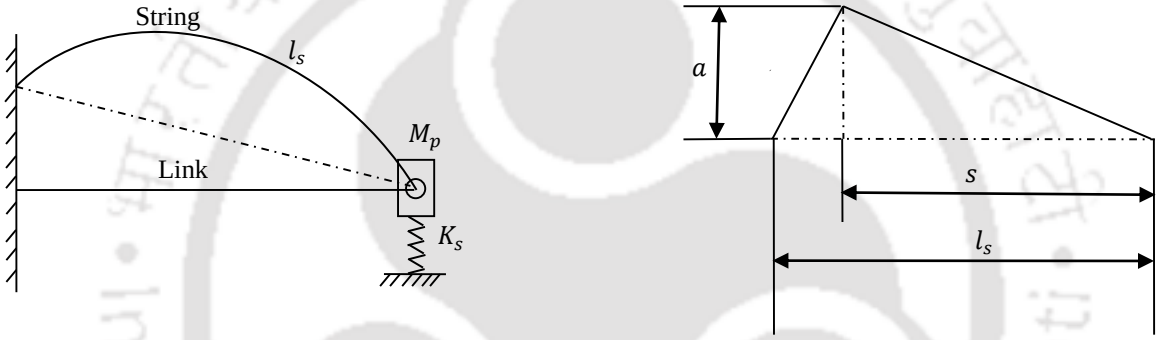

(a) **(b)**

Figure 5.4: Modelling of string oscillations: **(a)** boundary conditions at the end of the stiffening string **(b)** deflection of the string.

Boundary conditions II(a): one end of the string is attached to a rigid support and another end is attached to the tip of the flexible link modeled as a spring of stiffness K_s. If A_{ns}, B_{ns}, C_{ns} and D_{ns} are constants for solution $y(x,t)$ and ω_{ns} is the natural frequency of vibration of string in n^{th} mode, then, boundary conditions are

$$\phi(x=0) = 0 \text{ and } T_s\frac{\partial\phi}{\partial x}(l_s,t) = -K_s\phi(l_s,t) \text{ so that } \omega_{ns} = \frac{n\pi c}{l_s} \tag{5.22}$$

$$\phi_n(x) = A_{ns}\cos\frac{\omega_{ns}}{c}x \tag{5.23}$$

where n indicates the n^{th} mode of vibration of the string. Initial conditions have been taken as

$$y(x,0) = \frac{a}{s}x \text{ for } 0 \le x \le s;\ y(x,0) = \frac{a(l_s - x)}{(l_s - s)} \text{ for } s \le x \le l_s \text{ and } \dot{y}(x,0) = 0 \tag{5.24}$$

where a is the deflection of the string at a distance s from the end as shown in Fig. 5.4(b). Applying these conditions in Eq. (5.21), it follows that constants

$$D_{ns} = 0 \text{ while } C_{ns} = \frac{2a}{(l_s - s)}\left(\frac{c}{\omega_{ns}}\right)^2 \left(\frac{1}{s}\sin\frac{\omega_{ns}s}{c} - \frac{1}{l_s}\sin\frac{\omega_{ns}l_s}{c}\right) \tag{5.25}$$

$$\text{So that } y(x,t) = \sum_{n=1}^{\infty} B_{ns}\sin\frac{\omega_{ns}x}{c} C_{ns}\cos\omega_{ns}t \tag{5.26}$$

$$\frac{\partial y}{\partial x} = \sum_{n=1}^{\infty} \frac{\omega_{ns}}{c} B_{ns}\cos\frac{\omega_{ns}x}{c} C_{ns}\cos\omega_{ns}t \tag{5.27}$$

$$\frac{\partial y}{\partial x}(l_s,t) = \sum_{n=1}^{\infty} \frac{\omega_{ns}}{c} B_{ns}\cos\frac{\omega_{ns}l_s}{c} C_{ns}\cos\omega_{ns}t \tag{5.28}$$

Here only the first mode, i.e., for $n = 1$ has been considered. Transverse force on the string is given as $T_s \sin\vartheta = T_s\vartheta = T_s\frac{\partial y}{\partial x}(l_s,t)$, for small ϑ where ϑ is the instantaneous angle made by the string with the link tip on any one side. Instantaneous tension T_i along the string on using Binomial expansion is given as

$$\begin{aligned} T_i = T_s\cos\vartheta = T_s\sqrt{1-\sin^2\vartheta} = T_s\left(1 - \left(\frac{\partial y}{\partial x}(l_s,t)\right)^2\right)^{\frac{1}{2}} \\ = T_s\left(1 - \frac{1}{2}\left(\frac{\partial y}{\partial x}(l_s,t)\right)^2\right) \end{aligned} \tag{5.29}$$

At equilibrium, the equation of motion of the string is given as

$$T_s\frac{\partial y}{\partial x}(l_s,t) = K_s y(l_s,t) \tag{5.30}$$

where K_s is the spring constant of the link assumed as a spring and is given by $K_s = \frac{3EI}{l^3}$; E, I, l are respectively Young Modulus of elasticity, 2nd moment of inertia of the cross-section, and length of the link.

Boundary conditions II(b): one end of the string is attached to a rigid support and another end is attached to the tip of the flexible link modeled as a spring-mass system. Then, the equation of motion of the string is given as

$$T_s \frac{\partial y}{\partial x}(l_s, t) = M_p \ddot{y}(l_s, t) + K_s y(l_s, t) \tag{5.31}$$

The frequency equation for string vibration will be given as

$$\tan \alpha_s = \frac{\left(\frac{\alpha_s T_s}{K_s l_s}\right)}{1 - \frac{\alpha_s^2}{\left(\frac{\omega_s l_s}{c}\right)^2}} \tag{5.32}$$

where $\alpha_s = \frac{\omega_{ns} l_s}{c}$ and $\omega_s = \sqrt{\frac{K_s}{M_p}}$ is the circular frequency of the spring-mass system.

Boundary conditions II(c): here the link is not idealized as a spring. One end of the string is attached to a rigid support and another end is attached to the tip of the flexible link. Then, the equation of motion of the string is given as

$$T_s \frac{\partial y}{\partial x}(l_s, t) = EI \frac{\partial^3 y}{\partial x^3}(l_s, t) + \left(\rho A + M_p \delta(x - l)\right) \frac{\partial^2 y}{\partial t^2}(l_s, t) - P \frac{\partial^2 y}{\partial x^2}(l_s, t) \tag{5.33}$$

where ρ is the mass of the link per unit length and A is the area of the cross-section of the link. $\delta(\quad)$ is the Dirac-delta function of x. $P = T_{s1} + T_{s2}$, is the axial force the link is subjected to and T_{s1} and T_{s2} are initial tensions in the string on each side of the link. The frequency of vibration of the string can be found from the following characteristic equation

$$\tan \alpha_s = \frac{\frac{T_s l_s}{\alpha_s}}{\frac{EI\alpha_s^2}{l_s^2} - \left(\rho A + M_p \delta(x - l)\right) c^2 + P} \tag{5.34}$$

Case III: when the link tip is not tied with any string, the link is not subjected to any axial loading so that $P = 0$. The flexible link can be considered as a cantilever beam with one end fixed to a support while the other end is free to oscillate. The equation of motion for free vibration of the cantilever beam of the uniform cross-section and material properties is given as

$$EI\frac{\partial^4 w}{\partial x^4} + \rho A\frac{\partial^2 w}{\partial t^2} = 0 \tag{5.35}$$

Let the solution be found by the separation of the variable method. Let $w(s,t)$ be the solution of the above equation such that $w(x,t) = W(x)e^{i\omega_n t}$ where ω_n is the natural frequency of vibration of the link. Using this in Eq. (5.35), $W(x)$ will be given as

$$W(x) = C_1 \sin\beta x + C_2 \cos\beta x + C_3 \sinh\beta x + C_4 \cosh\beta x \tag{5.36}$$

Where $\beta = \left(\omega_n^2 \frac{\rho A}{EI}\right)^{1/4}$ and C_1, C_2, C_3 and C_4 are the constants to be determined from the boundary conditions of the beam.

Boundary conditions III: The boundary conditions for a cantilever beam of length l fixed at one end and carrying a payload of mass M_p at the other end are given as $W(0) = 0$; $\frac{dW}{dx}(0) = 0$; $\frac{d^2W}{dx^2}(l) = 0$; and $\frac{d^3W}{dx^3}(l) + \frac{M_p\omega^2}{EI}W(l) = 0$. Applying these boundary conditions, the mode shape of the link can be given as

$$W(x,t) = \sin\beta x - \mu\cos\beta x - \sinh\beta x + \mu\cosh\beta x \tag{5.37}$$

where $\mu = \frac{\sin\beta l + \sinh\beta l}{\cos\beta l + \cosh\beta l}$ and the frequency equation is given as

$$\bar{m}\beta l(\sinh\beta l\cos\beta l - \sin\beta l\cosh\beta l) + (1 + \cos\beta l\cosh\beta l) = 0 \tag{5.38}$$

where $\bar{m} = \frac{M_p}{\rho A l}$.

5.2.3 Dynamic Equation of Motion of the Single-Link Flexible Manipulator

Here, the manipulator is assumed to move in the horizontal plane. Hence, the effect of gravitational force has not been considered. The Euler-Lagrange formulation has been considered for the mathematical modeling of the manipulator. As shown in Fig. 5.2, torque can be applied at the joint through the servo motor to induce movement of the endpoint of the link along feasible trajectories.

The single-link flexible manipulator has been shown in Fig. 5.5. OA is the radius of the hub of the manipulator and AB is the flexible link. XOY is the inertial frame of reference while xoy is the

body-attached frame of reference. The hub radius is R_H and l is the length of the link. At the end of the link, there is a payload of mass M_p. u is the axial displacement while $w(s,t)$ is the deflection of the link in the y-direction in the body attached frame of reference at a distance s from the hub in the deflected condition. At any instant of time t, the link subscribes to an angle θ from the X-axis of the inertial frame at the hub-center.

The position vector r of any point P located at s on the flexible link can be expressed relative to the inertial frame of reference as

$$r = [r_x \quad r_y]^T \tag{5.39}$$

where the superscript T stands for transpose of the vector $[r_x \quad r_y]$ and r_x and r_y are given as

$$r_x = R_H \cos\theta + (s+u)\cos\theta - w\sin\theta \tag{5.40}$$

$$r_y = R_H \sin\theta + (s+u)\sin\theta + w\cos\theta \tag{5.41}$$

The link tip position where the payload is situated will be given by $r_{s=l} = [r_x \quad r_y]_{s=l}^T$.

Here inextensibility condition has been applied to account for the effect of the axial deformation on transverse deflections of a rotating flexible arm. Many researchers considered inextensibility conditions to account for axial displacement. Abe (2009) did trajectory optimization for the suppression of residual vibration of a two-link rigid-flexible manipulator. He used the inextensibility condition for finding the kinetic energy of the system. Zavodney and Nayfeh (1989) considered the non-linear terms up to third-order arising from inertia, curvature, and axial displacement caused by large transverse deflections of an Euler-Bernoulli's beam. Al-Bedoor and Hamdan (2001) employed the inextensibility condition to relate the axial and transverse deflections of a rotating flexible arm undergoing large planar flexural deformations. Martins et. al (2002) applied assumptions of the inextensibility of the neutral fiber, and moderate rotations of the cross-sections to account for the foreshortening of the beam due to bending.

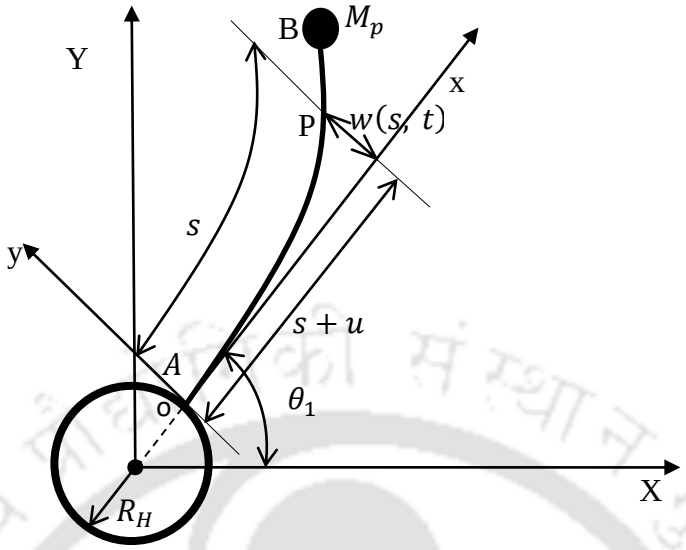

Figure 5.5: A single-link flexible manipulator.

Applying the inextensibility condition, the axial displacement u in terms of lateral displacement w can be given by the following relation

$$u = -\frac{1}{2}\int_0^s \left(\frac{\partial w}{\partial s}\right)^2 ds \tag{5.42}$$

The kinetic energy of the system can be expressed as

$$T = \frac{1}{2}\left[J_H\dot{\theta}^2 + \int_0^l \{\rho A + M_p\delta(s-l)\}\dot{r}^T\dot{r}ds\right] \tag{5.43}$$

in which $\dot{(\ )}$ denotes the derivative of the quantity with respect to time. J_H is the moment of inertia of the hub and M_p is the mass of the payload at the tip of the link. ρ, A, and l are respectively, the density, cross-sectional area, and length of the flexible link. $\delta(s-l)$ denotes the Dirac-delta function.

The potential energy V of the system is given by

$$V = \frac{1}{2}EI\int_0^l \mathcal{K}^2 ds = \frac{1}{2}EI\int_0^l \left[\left(\frac{\partial^2 w}{\partial s^2}\right)^2\left\{1+\left(\frac{\partial w}{\partial s}\right)^2\right\}\right]ds \tag{5.44}$$

Where $\mathcal{K}$ is the curvature of the neutral axis of the flexible link [Abe (2009)] is given by

$$\mathcal{K} = \frac{\partial^2 w}{\partial s^2}\left\{1 + \left(\frac{\partial w}{\partial s}\right)^2\right\}^{-\frac{1}{2}} \tag{5.45}$$

The term $\left[\left(\frac{\partial^2 w}{\partial s^2}\right)^2 \left(\frac{\partial w}{\partial s}\right)^2\right]$ in Eq. (5.44) represents the effect of the nonlinear curvature.

Lagrangian L of the manipulator system is given by

$$L = T - V \tag{5.46}$$

Using the Euler-Lagrange Equation of motion, the equation of motion for the single-link flexible manipulator can be given by the equations

$$\frac{d}{dt}\left(\frac{\partial L}{\partial \dot{\theta}}\right) - \frac{\partial L}{\partial \theta} = \tau \text{ and } \frac{d}{dt}\left(\frac{\partial L}{\partial \dot{q}}\right) - \frac{\partial L}{\partial q} = 0 \tag{5.47}$$

By substituting Eq. (5.46) into Eq. (5.47) and applying the above-mentioned Lagrangian formulation, the equations of motion of the system are obtained as follows:

$$\begin{bmatrix} M_{rr} & M_{rf}^T \\ M_{rf} & M_{ff} \end{bmatrix}\begin{bmatrix} \ddot{\theta} \\ \ddot{q} \end{bmatrix} + \begin{bmatrix} C_r \\ C_f \end{bmatrix} + \begin{bmatrix} 0 \\ K_f \end{bmatrix} + \begin{bmatrix} 0 \\ F_{str} \end{bmatrix} = \begin{bmatrix} \tau \\ 0 \end{bmatrix} \tag{5.48}$$

where $M_{rr} = (\alpha_{11} + \alpha_{Mp_{11}})$, $M_{rf}^T = (\alpha_{12} + \alpha_{Mp_{12}})$, $M_{rf} = (\alpha_{21} + \alpha_{Mp_{21}})$, $M_{ff} = (\alpha_{22} + \alpha_{Mp_{22}})$; $M = \begin{bmatrix} M_{rr} & M_{rf}^T \\ M_{rf} & M_{ff} \end{bmatrix}$ is the mass matrix; $C = \begin{bmatrix} C_r \\ C_f \end{bmatrix}$ is the torque due to Coriolis and centrifugal force vector; $C_r = (\alpha_{13} + \alpha_{Mp_{13}})\dot{\theta}^2 + (\alpha_{14} + \alpha_{Mp_{14}})\dot{q}^2 + (\alpha_{15} + \alpha_{Mp_{15}})\dot{\theta}\dot{q}$ and $C_f = (\alpha_{23} + \alpha_{Mp_{23}})\dot{\theta}^2 + (\alpha_{24} + \alpha_{Mp_{24}})\dot{q}^2 + (\alpha_{25} + \alpha_{Mp_{25}})\dot{\theta}\dot{q}$, where α_{ij} and $\alpha_{Mp_{ij}}; i = 1,2;\ j = 1,2,\ldots,5;$ are the coefficients of variables in Eq. (5.48) due to link motion and payload motion respectively; $K_f = EI\left(\int_0^l \left(\frac{\partial^2 w}{\partial s^2}\right)^2 dsq + 2\int_0^l \left(\frac{\partial^2 w}{\partial s^2}\right)^2 \left(\frac{\partial w}{\partial s}\right)^2 dsq^3\right)$ is the torque due to stiffness of the flexible link and $F_{str} = -P\int_0^l \left(\frac{\partial^2 w}{\partial s^2}\right)^2 dsq$ is the torque due to force applied by the pair of strings on the flexible link where $P = T_1\cos(\gamma_1) - T_2\cos(\gamma_2)$. τ is the torque applied on the joint. α_{ij} and $\alpha_{Mp_{ij}}$have been derived using symbolic calculations in the software package Matlab R2021a.

5.3 Control of the Flexible-Joint and Flexible-Link Manipulator

Strings stiffen the link to reduce the amplitude of vibration of the link tip; however, these also produce disturbances in the form of unwanted torque on joints that makes the joint of the manipulator oscillatory or flexible which excites the link to vibrate continuously. The oscillation of the tip, in the absence of any damping, still persists. As it is known that joint flexibility is more dangerous than link flexibility which poses greater difficulty in controlling the tip deflection. So, this complicates the problem to a much further extent than operating the manipulator without any string because, by this, one has to tackle not only link flexibility but also, joint flexibility at the same time. This poses problems in job handling. Therefore, control of tip vibration is necessary to take advantage of string stiffening. One of the very popular methods of control is to apply a proportional-integral-derivative (PID) controller for the task. However, controlling a flexible link is a very tedious task because of the highly nonlinear and strongly-coupled nature of the problem. Compared with the rigid manipulator, the dynamic characteristics of flexible manipulators are more difficult to control; they are more complex [Meng et al. (2018)]. In this work, adaptive PID control along with impedance control based on the work of Theodore and Ghosal (1995) and Spong (1989) has been applied in order to control the flexible-joint and flexible-link SSSLFM. However, the stress in this paper is to highlight the passive method of control of residual vibration of the flexible link manipulator using a pair of strings.

Let K_{P_x}, K_{I_x} and K_{D_x} be, respectively, the proportional, integral, and derivative gains for the X-coordinate of the tip and K_{P_y}, K_{I_y} and K_{D_y} be the same for the Y-coordinates of the tip. Similarly, K_{P_θ}, K_{I_θ} and K_{D_θ} be the respective quantities for link angular displacements. $K_{P_{\theta_m}}$, $K_{I_{\theta_m}}$ and $K_{D_{\theta_m}}$ are respectively, the proportional, integral, and derivative gains for the motor angular displacements. If θ_d and θ are respectively, the desired and the actual values of link angular displacement; x_d and x are respectively the desired and actual values of the X-coordinate while y_d and y are respective quantities for Y-coordinates of link tip motion, θ_{m_d} and θ_m are respectively the desired and actual angular displacement of the motor, then their errors at any time t are given as below:

$$e_\theta = \theta_d - \theta;\ e_x = x_d - x\ ;\ e_y = y_d - y \text{ and } e_{\theta_m} = \theta_{m_d} - \theta_m \tag{5.49}$$

5.3.1. Control of the SSSLFM When Joint Flexibility is Not Considered

If there is no effect of string-stiffening on the joint of the manipulator and also if joint defects such as looseness, misalignment, viscous damping, and backlash are neglected, the joint will behave as a rigid joint. Then rewriting Eq. (5.48) one will get the following set of equations.

$$\left(M_{rr} - M_{rf}^T M_{ff}^{-1} M_{rf}\right)\ddot{\theta} + C_r + M_{rf}^T M_{ff}^{-1}\left(-F_{str} - C_f - K_f\right) = \tau \tag{5.50}$$

and

$$\ddot{q} = M_{ff}^{-1}\left(-F_{str} - C_f - K_f\right) - M_{ff}^{-1} M_{rf}\ddot{\theta} \tag{5.51}$$

Joint torque is user-defined, so, to control the link oscillations, τ in Eq. (5.50) can be defined such that Eq. (5.50) can be written as

$$\tau = \left(M_{rr} - M_{rf}^T M_{ff}^{-1} M_{rf}\right)\tau_{CT} + C_r + M_{rf}^T M_{ff}^{-1}\left(-F_{str} - C_f - K_f\right) \tag{5.52}$$

so that

$$\ddot{\theta} = \tau_{CT} \tag{5.53}$$

Now τ_{CT} in Eqs. (5.52) and (5.53) are written as

$$\tau_{CT} = (I - Q)\tau_{pid_\theta} + Q\tau_{pid_{pos}} \tag{5.54}$$

where

$$I = 1 \text{ and } Q = \begin{cases} 0, & 0 \le t \le t_m \\ 1, & t_m < t \le t_f \end{cases} \tag{5.55}$$

t_m is the duration of time up to which the joint is given angular motion and t_f is the final time up to which the link motion is observed. τ_{pid_θ} is the unit torque applied for the joint angular motion during the motion of the manipulator while $\tau_{pid_{pos}}$ is the unit torque for position control of the tip of the manipulator. $\tau_{pid_{pos}}$ is given by the following equations.

$$\tau_{pid_{pos}} = J_{tip}^T \begin{bmatrix} F_{pid_x} \\ F_{pid_y} \end{bmatrix} \tag{5.56}$$

where J_{tip} is the Jacobian matrix for the motion of the link tip and J_{tip}^T is its transpose. F_{pid_x} and F_{pid_y} are the controlling force applied on the tip of the link and are given by the following expressions:

$$F_{pid_x} = K_{P_x}e_x + K_{I_x}\int e_x\,dt + K_{D_x}\dot{e}_x; \text{ and } F_{pid_y} = K_{P_y}e_y + K_{I_y}\int e_y\,dt + K_{D_y}\dot{e}_y \quad (5.57)$$

The controlling force at the tip is converted into joint torque using Eq. (5.56). The control input τ_{pid_θ} can be chosen for a specified joint trajectory as

$$\tau_{pid_\theta} = \ddot{\theta}_d + K_{P_\theta}e_\theta + K_{I_\theta}\int e_\theta\,dt + K_{D_\theta}\dot{e}_\theta \quad (5.58)$$

so that the error in the angular position of the link during time $0 < t < t_m$ satisfies

$$\ddot{e}_\theta + K_{P_\theta}e_\theta + K_{I_\theta}\int e_\theta\,dt + K_{D_\theta}\dot{e}_\theta = 0 \quad (5.59)$$

Now Eqs. (5.51) and (5.53) can be solved together to find the controlled motion of the angular displacement and the tip deflection of the flexible link of the manipulator. So, when the joint of the manipulator is not considered as flexible joint, with the help of Eqs. (5.51) and (5.53) joint angular displacement θ can be controlled to follow the desired trajectory θ_d and the oscillations of the tip of the manipulator can also be eliminated.

5.3.2 Control of the SSSLFM When Joint Flexibility is Considered

Here, in order to control the joint disturbances due to the string torques on the joint because of the oscillations of the link tip, the joint is modeled as a torsional spring of stiffness K_t. Let M_m be the mass of the motor at the joint and R_H be the radius of the motor so that the moment of inertia of the motor is given by $J_m = \frac{1}{2}M_mR_H^2$. Let the torque supplied by the motor be τ_m. Let θ_m and θ respectively be the angular displacements of the motor and link of the manipulator. Then, Eq. (5.48) is modified to get the equation of motion for a flexible-joint and flexible-link manipulator as below.

$$J_m\ddot{\theta}_m + K_t(\theta_m - \theta) = \tau_m \quad (5.60)$$

$$\begin{bmatrix} M_{rr} & M_{rf}^T \\ M_{rf} & M_{ff} \end{bmatrix}\begin{bmatrix} \ddot{\theta} \\ \ddot{q} \end{bmatrix} + \begin{bmatrix} C_r \\ C_f \end{bmatrix} + \begin{bmatrix} 0 \\ K_f \end{bmatrix} + \begin{bmatrix} 0 \\ F_{str} \end{bmatrix} = \begin{bmatrix} K_t(\theta_m - \theta) \\ 0 \end{bmatrix} \quad (5.61)$$

In case the joint is rigid, $K_t \to \infty$, this implies that $\theta_m \to \theta$ so that system of Eqs. (5.60)-(5.61) reduces to Eq. (5.48).

To know the dynamic behavior of this system the angular displacement of the motor θ_m is controlled to follow the desired trajectory by defining the motor torque τ_m such that one gets the following expression:

$$\ddot{\theta}_m = \ddot{\theta}_{m_d} + K_{P_{\theta_m}} e_{\theta_m} + K_{I_{\theta_m}} \int e_{\theta_m}\, dt + K_{D_{\theta_m}} \dot{e}_{\theta_m} \tag{5.62}$$

Eq. (5.61) can be rewritten as follows:

$$\begin{bmatrix} \ddot{\theta} \\ \ddot{q} \end{bmatrix} = M^{-1} \begin{bmatrix} K_t(\theta_m - \theta) - C_r \\ -C_f - K_f - F_{str} \end{bmatrix} \tag{5.63}$$

Now Eqs. (5.62) and (5.63) can be solved together to find the joint and link motion. Here, one thing has to be noted that in Eqs. (5.62), and (5.63), the joint flexibility is not controlled. Only the angular motion of the motor has been controlled to know that if the motor is forced to track the desired trajectory, will the angular as well as cartesian motion of the manipulator link follow the desired trajectory. So, the solution of Eqs. (5.62) and (5.63) give the behavior of the SSSLFM in the presence of joint flexibility.

To control the joint flexibility as well as link flexibility of the SSSLFM, represented by the system of Eqs. (5.60) and (5.61) together, so that the manipulator can follow the desired trajectory, it can be modeled as described below.

The motor torque τ_m in Eq. (5.60) is written such that

$$\tau_m = \tau_l(\theta, \dot{\theta}) + K_d(\dot{\theta} - \dot{\theta}_m) \tag{5.64}$$

where τ_l is the PID control law and K_d is a constant diagonal matrix whose diagonal elements are of the order of $\frac{1}{\epsilon}$, i.e., $O\left(\frac{1}{\epsilon}\right)$. Using Eq. (5.64) in Eq. (5.60) and subtracting $J_m\ddot{\theta}$ on both sides, the following expression is obtained.

$$J_m(\ddot{\theta}_m - \ddot{\theta}) + K_d(\dot{\theta}_m - \dot{\theta}) + K_t(\theta_m - \theta) = \tau_l(\theta, \dot{\theta}) - J_m\ddot{\theta} \tag{5.65}$$

Now putting $\dot{\theta}_m - \dot{\theta} = e_j$ in the above equation, one gets

$$J_m\ddot{e}_j + K_d\dot{e}_j + K_t e_j = \tau_l(\theta, \dot{\theta}) - J_m\ddot{\theta} \tag{5.66}$$

Multiplying both sides of Eq. (5.66) by K_t and putting $K_t e_j = \tau_j$ so that $K_t \dot{e}_j = \dot{\tau}_j$ and $K_t \ddot{e}_j = \ddot{\tau}_j$ one gets

$$J_m \ddot{\tau}_j + K_d \dot{\tau}_j + K_t \tau_j = K_t\left(\tau_l\left(\theta, \dot{\theta}\right) - J_m \ddot{\theta}\right) \tag{5.67}$$

If one chooses K_d and K_t such that $K_d = \frac{K_D}{\epsilon}$ and $K_t = \frac{K_P}{\epsilon^2}$ where $0 < \epsilon \ll 1$; then Eq. (5.67) becomes as follows.

$$\epsilon^2 J_m \ddot{\tau}_j + \epsilon K_D \dot{\tau}_j + K_P \tau_j = K_P\left(\tau_l\left(\theta, \dot{\theta}\right) - J_m \ddot{\theta}\right) \tag{5.68}$$

Now using $K_t e_j = \tau_j$ and Eq. (5.68), Eqs. (5.60), and (5.61) can be written together as

$$\epsilon^2 J_m \ddot{\tau}_j + \epsilon K_D \dot{\tau}_j + K_P \tau_j = K_P\left(\tau_l\left(\theta, \dot{\theta}\right) - J_m \ddot{\theta}\right) \tag{5.69}$$

$$M_{rr} \ddot{\theta} + M_{rf}^T \ddot{q} + C_r = \tau_j \tag{5.70}$$

$$M_{rf} \ddot{\theta} + M_{ff} \ddot{q} + C_f + K_f + F_{str} = 0 \tag{5.71}$$

The system of equations (5.69)-(5.71) is singularly perturbed. Variables τ_j and $\dot{\tau}_j$ are fast variables while the link variables θ and $\dot{\theta}$ are slow variables. Using the standard result from singular perturbation theory, one may approximate the flexible joint system (5.69)-(5.71) by a quasi-steady-state and a boundary layer system as follows. From Tichonov's theorem, the joint torque $\tau_j(t)$ and the link angles θ satisfy the following expressions:

$$\tau_j(t) = \bar{\tau}_j(t) + \gamma(\tau_t) + O(\epsilon) \text{ and } \theta(t) = \bar{\theta}(t) + O(\epsilon) \tag{5.72}$$

where the overbars indicate that the variables are defined at $\epsilon = 0$ and $\tau_t = \left(\frac{t}{\epsilon}\right)$ is the fast time scale and γ satisfies the equation

$$J_m \frac{d^2\gamma}{d\tau_t^2} + K_D \frac{d\gamma}{d\tau_t} + K_P \gamma = 0 \tag{5.73}$$

and the quasi-steady-state system are given by the following equations.

$$\bar{M}_{rr} \ddot{\bar{\theta}} + \bar{M}_{rf}^T \ddot{q} + \bar{C}_r = \bar{\tau}_j + \gamma\left(\frac{t}{\epsilon}\right) \tag{5.74}$$

$$\bar{M}_{rf} \ddot{\bar{\theta}} + \bar{M}_{ff} \ddot{q} + \bar{C}_f + \bar{K}_f + \bar{F}_{str} = 0 \tag{5.75}$$

where $\bar{\tau}_j(t) = \left(\bar{\tau}_l - J_m\ddot{\bar{\theta}}\right)$ and $\bar{M}_{rr} = M_{rr}(\bar{\theta}, q)$, $\bar{C}_r = C_r\left(\bar{\theta}, q, \dot{\bar{\theta}}, \dot{q}\right)$ etc., where the overbar indicates that the variables are defined at $\epsilon = 0$. It follows that the flexible-joint-flexible-link manipulator can be represented up to the order of $O(\epsilon)$ by the system of equations as written below.

$$J_m \frac{d^2\gamma}{d\tau_t^2} + K_D \frac{d\gamma}{d\tau_t} + K_P\gamma = 0 \tag{5.76}$$

$$(M_{rr}(\theta) + J_m)\ddot{\theta} + M_{rf}^T(\theta)\ddot{q} + C_r(\theta, \dot{\theta}) = \tau_l + \gamma\left(\frac{t}{\epsilon}\right) \tag{5.77}$$

$$M_{rf}\ddot{\theta} + M_{ff}\ddot{q} + C_f + K_f + F_{str} = 0 \tag{5.78}$$

From Eqs. (5.77) and (5.78) one can write the following equation

$$\left(M_{rr} - M_{rf}^T M_{ff}^{-1} M_{rf} + J_m\right)\ddot{\theta} + C_r + M_{rf}^T M_{ff}^{-1}\left(-F_{str} - C_f - K_f\right) = \tau_l + \gamma\left(\frac{t}{\epsilon}\right) \tag{5.79}$$

and

$$\ddot{q} = M_{ff}^{-1}\left(-F_{str} - C_f - K_f\right) - M_{ff}^{-1} M_{rf}\ddot{\theta} \tag{5.80}$$

Let us suppose that the control input vector is calculated using a nonlinear decoupling technique applied to joints and is given by

$$\tau_l = \left(M_{rr} - M_{rf}^T M_{ff}^{-1} M_{rf} + J_m\right)\tau_{CT} + C_r + M_{rf}^T M_{ff}^{-1}\left(-F_{str} - C_f - K_f\right) - \gamma\left(\frac{t}{\epsilon}\right) \tag{5.81}$$

so that

$$\ddot{\theta} = \tau_{CT} \tag{5.82}$$

The results and discussions of the dynamic analysis of the SSFLM and its verification along with the results of the control of the manipulator have been presented in the next section.

5.4 Results and Discussions

Dimensions and material properties of the SSSLFM as shown in Fig. 5.1 have been given in Table 5.1. The dynamic analyses of the single-link flexible manipulator have been studied one by one under various boundary conditions for each of the cases that have been described in Section 2. Also, the behaviors of the manipulator on applying different control techniques depending upon the modelings of the manipulator that have been described in Section 4, have been found out.

Table 5.1: Dimensions and material properties of SSSLFM

Description	**Length (m)**	**The thickness of the link (m)**	**The breadth of the link (m)**	**Diameter (m)**	**The density of the material (kg/m^3)**	**Young Modulus (Pa)**
Link	0.8	4.92×10^{-2}	2.028×10^{-3}	-	2690	69×10^9
String	0.60133	-	-	0.001	7850	210×10^9

In order to carry out the dynamic analysis of the manipulator, the numerical solution of Eq. (5.48) has been obtained using Range-Kutta's 4^{th}-5^{th} order numerical solution technique. The tension T_1 in the string on any one side of the link has been taken to be 25% of the critical load of buckling P_{Cr} of the link and tension T_2 in the string on the other side of the link has been taken to be 85% of T_1. The angle of the string on any one side of the link with the surface of the link in the undeflected condition is γ_1 and the angle of the string on the other side of the link with the surface of the link in the undeflected condition is γ_2 where $\gamma_2 = 0.95\gamma_1$. The tension values in strings and angles of strings with the link on either side have been taken to be different by considering uncertainty or difficulties in determining these values. The initial conditions for the solution of Eq. (5.48) are: $q_0 = 0$ and $\dot{q}_0 = 0$ where $q(t)$ is the temporal variable. A cycloidal motion profile as shown in Fig. 5.6 has been given to the motor at the hub for a time duration of 2 seconds as described in the following expression and tip deflection of the link has been observed.

$$\theta(t) = \begin{cases} (\theta_f - \theta_{in})\left(\frac{t}{T_f} - \frac{1}{2\pi}\sin\frac{2\pi t}{T_f}\right) + \theta_{in}; \;\; 0 \le t \le 1\ s \\ 0; 1\ s \le t \le 2\ s \end{cases} \tag{5.83}$$

where $\theta(t)$ is the angular motion of the joint, θ_{in} is $\theta(t)$ at $t = 0$ s, θ_f is $\theta(t)$ at the end of the joint motion, $T_f = 2$ s is the final time of the motion.

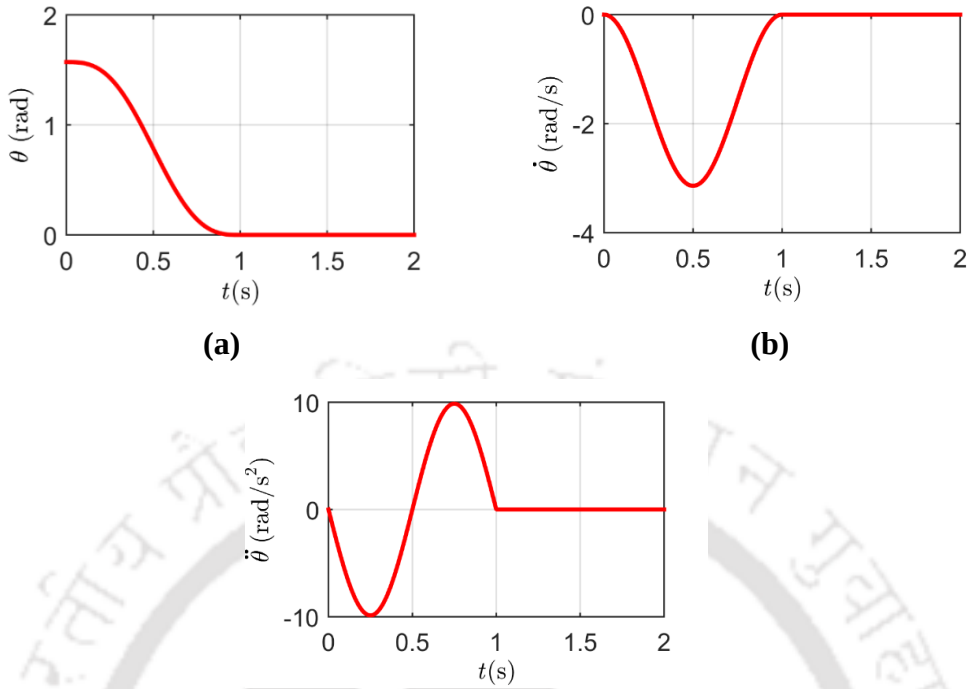

Figure 5.6: Input given to the manipulator's joint: **(a)** angular displacement, **(b)** angular velocity, and **(c)** angular acceleration.

The same motion profile for the joint has been applied for all the cases and tip deflections of the manipulator have been observed in these cases. Initial time t_{in}, final time t_f and time step size t_{inc} has been taken as given below:

$t_{in} = 0$ s, $T_f = 2$ s and $t_{inc} = 0.01$ s; $\theta_{in} = \frac{\pi}{2}$ rad, $\theta_f = 0$ rad.

For dynamic analysis of the manipulator, three different cases have been considered in section 2. These three cases consist of a total of seven boundary conditions (BCs) as described in the section. Eq. (5.48) will show the different dynamic behavior of the manipulator when subjected to these boundary conditions that have been discussed below.

Case 1: Applying boundary conditions I(a) under case I, that is, when the end of the link is assumed to be hinged support, the tip deflection is shown in Fig. 5.7 (a).

Case 2: when boundary conditions I(b) in case I for the link are considered, the tip deflection is as given in Fig. 5.7 (b).

Case 3: when the boundary conditions I(c) in case I for the link is taken, the tip deflection is given in Fig. 5.7 (c).

5.4.1 Taking the Effect of String Vibration

As the link will vibrate it will also vibrate the string attached to the tip of the link which, in turn, affects the tension force applied by the string on the link because, with the vibration of the link, the strings may become loose or tight depending on the tip deflection of the link. In that case, the tension in the string will vary as given by Eq. (5.29). However, the effect of string vibration is not so prominent on the tip deflection for small deflection. Because of this instead of finding the dynamic change of tension in the string during the motion of the link only the maximum value of change in the tension in any one of the two strings at a time has been considered. Here these effects have been found for hinge-supported beam, i.e. when Case 2 is considered for comparison. Therefore, 3 more cases arise depending upon the modeling of the string vibration problem that whether the end of the string that is attached to the link tip is modeled as the end attached to a spring or spring-mass system or directly to the link tip.

Case 4: when one of the ends of the string is fixed and the other is tied to a spring, then applying BCs II(a) in Eq. (5.48), the tip deflection is shown in Fig. 5.8(a).

Case 5: But, at the tip of the link there is a payload so that better way of modeling the string is to consider as one of the ends of the string is fixed and the other is tied to a spring-mass system as described in BCs II(b), then the link tip deflection is found to be as shown in Fig. 5.8(b).

Case 6: In this case, no idealization of the string ends has been considered and while one end of the string is fixed the other end is tied to the link tip which is also oscillating with its own dynamic behavior. In that case, BCs II(c) will be applied, and the tip deflection of the manipulator is as shown in Fig. 5.8(c).

From Fig. 5.7(b) and Fig. 5.8, it is noticed that not much difference is observed in the tip deflection of SSSLFM. So, it may be concluded that string vibration does not have much effect on link oscillations.

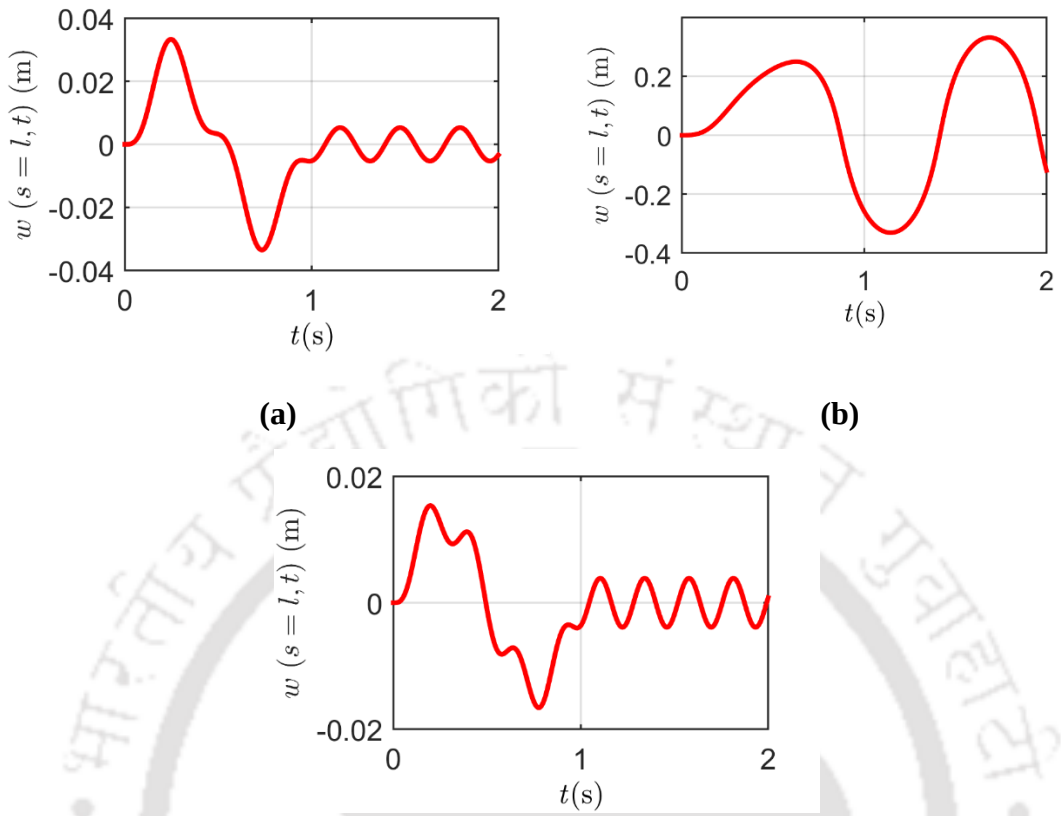

Figure 5.7: Tip deflection of the SSSLFM in **(a)** Case 1, **(b)** Case 2, and **(c)** Case 3.

Case 7: Using BC III under Case III in Eq. (5.48), i.e., when the flexible link is not stiffened with any string one gets the tip deflection of the link as shown in Fig. 5.9.

The tip deflection at steady state and natural frequencies of the oscillations of the link and the strings for each of these cases have been summarized in Table 5.2 below.

Here, it is observed that when the tip of the SSSLFM is assumed to be hinged supported, the SSSLFM has deflection much less compared to the flexible link of the same parameters but without any string stiffening, to the extent as low as around 102.83 times. The same is the case where the reduction in tip deflection is more than 140 times [Fig. 5.7(c)], when the payload at the tip of the SSSLFM, is assumed to be exactly balanced by the string forces in case 4 so that tip displacement is not allowed at all. In the case of Case 2 [Fig. 5.7(b)], it is seen that tip deflection is more compared to Case 1 and Case 3 which is expected because here no restriction for link tip movement

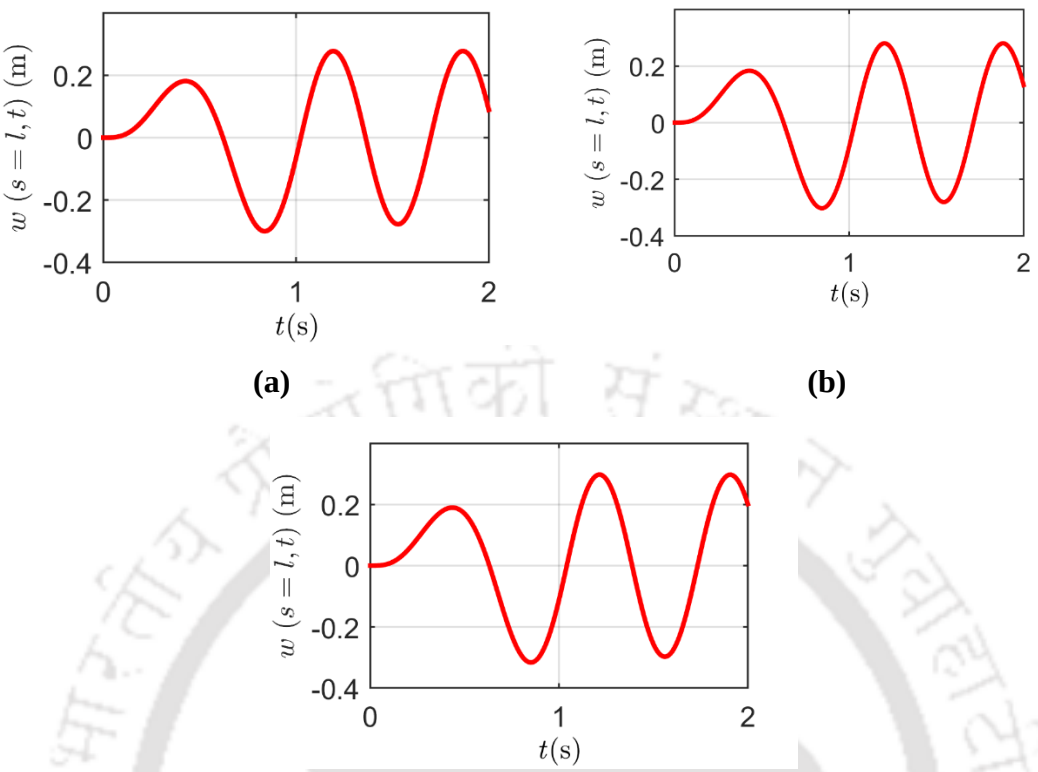

Figure 5.8: Tip deflections of the SSFLM in **(a)** Case 4, **(b)** Case 5, and **(c)** Case 6.

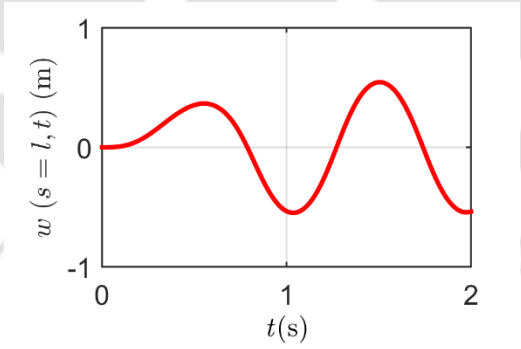

Figure 5.9: Tip deflection of the flexible link manipulator without any string stiffening.

has been applied in the boundary conditions. But, here also a reduction in tip deflection compared to case 7 is as high as 1.64 times. This also seems to be a more practical situation because in actual practice the link tip will not be constrained to have zero displacements. Even then, if one talks in terms of percentage reduction in residual vibration of the tip, where one strives for achieving a

percentage reduction in tip deflection from 5% to 25%, this technique of controlling tip vibration promises one 60.84% reduction in tip deflection for the values of γ_1 and γ_2.

This is a huge improvement in controlling the tip residual vibration which has also been shown experimentally by the work of Dixit and Kumar (2016). But they used the finite segment method for their analytical treatment of the problem. This analytical modeling of the problem will help in This is a huge improvement in controlling the tip residual vibration which has also been shown experimentally by the work of Dixit and Kumar (2016). But they used the finite segment method for their analytical treatment of the problem. This analytical modeling of the problem will help in

5.4.2 Verification of Results

Results obtained from the dynamic analysis of the manipulator with the boundary conditions I(a) and I(b) of Case I have been verified with the experimental result of the work done by Dixit and Kumar (2016) using the same manipulator parameters and trajectory along with the same initial conditions as mentioned in Dixit and Kumar (2016). The results obtained in this paper have been compared with their simulation and experimental results. The dimensions and material properties of the SSSLFM have been taken according to the paper mentioned above and have been given in Table 5.3. The same quintic polynomial has been taken for the input to the motor at the hub for time $t = 1$ s:

$$\theta(t) = a_0 + a_1 t + a_2 t^2 + a_3 t^3 + a_4 t^4 + a_5 t^5 \tag{5.84}$$

The initial and final positions of the link respectively at time $t = 0$ s and $t = 1$ s are as follows: $\theta(0) = 0$ rad, $\dot{\theta}(0) = 0$ rad/s, $\ddot{\theta}(0) = 0$ rad/s^2, $\theta(1) = \frac{\pi}{4}$ rad, $\dot{\theta}(1) = 0$ rad/s, $\ddot{\theta}(1) = 0$ rad/s^2. The link tip motion has been observed for $t = 2$ s. Initial time t_{in}, final time t_f and time step size t_{inc} has been taken respectively as $t_{in} = 0$ s, $T_f = 1$ s and $t_{inc} = 0.05$ s. From these conditions trajectory obtained for the link are as shown in Figs. 5.10(a), 5.10(b), and 5.10(c).

The initial conditions taken to solve Eq. (5.48) are $q = \dot{q} = 0$.

When the link is not stiffened with any string and the manipulator is not carrying any payload, the tip deflection and its speed have been shown in Figs. 5.11(a) and 5.11(b) respectively. Again, when

the link is not stiffened with any string and the manipulator is carrying a payload of 180×10^{-3} kg, the tip deflection, and its speed have been shown in Figs. 5.12(a) and 512(b) respectively.

Table 5.2: The Maximum tip deflection at the steady state and natural frequencies of the oscillations of the link and the strings

Case	Circular frequency ω_n (in rad/s)	Frequency f_n (in Hz)	Max. Tip deflection at steady state (in m)
1	$\omega_{n1_{link}} = 19.7991$	$f_{n1_{link}} = 3.1511$	0.005298
2	$\omega_{n1_{link}} = 9.6199$	$f_{n1_{link}} = 1.5311$	0.332
3	$\omega_{n1_{link}} = 19.4958$	$f_{n1_{link}} = 3.1029$	0.00389
4	$\omega_{n1_{link}} = 9.6480$ $\omega_{n1_{string\ 1}} = 13.4052$ $\omega_{n1_{string\ 2}} = 12.3590$	$f_{n1_{link}} = 1.5355$ $f_{n1_{string\ 1}} = 2.1335$ $f_{n1_{string\ 2}} = 1.9670$	0.2781
5	$\omega_{n1_{link}} = 9.6377$ $\omega_{n1_{string\ 1}} = 11.5299$ $\omega_{n1_{string\ 2}} = 11.4497$	$f_{n1_{link}} = 1.5339$ $f_{n1_{string\ 1}} = 1.8350$ $f_{n1_{string\ 2}} = 1.8223$	0.2806
6	$\omega_{n1_{link}} = 9.6199$ $\omega_{n1_{string\ 1}} = 2.1111$ $\omega_{n1_{string\ 2}} = 2.1369$	$f_{n1_{link}} = 1.5311$ $f_{n1_{string\ 1}} = 0.3360$ $f_{n1_{string\ 2}} = 0.3401$	0.2977
7 (Without any string)	$\omega_{n1_{link}} = 9.3454$ $\omega_{n2_{link}} = 78.3369$	$f_{n1_{link}}$ =1.4874 $f_{n2_{link}}$ =12.4677	0.5448

Table 5.3: Dimensions and material properties of SSSLFM [Dixit and Kumar (2016)]

Parameters	Value
Flexible link size	$500 \times 30 \times 1.5$ mm^3
The distance of cable attachment from the shaft axis	7.0×10^{-2} m
Mass of payload	0.18 kg
Density of link	7800 kg/m^3
Diameter of cable	0.8×10^{-3} m
Number of cables	1 pair
Cable material density	7800 kg/m^3
Target rotation	45°
Time duration	1s

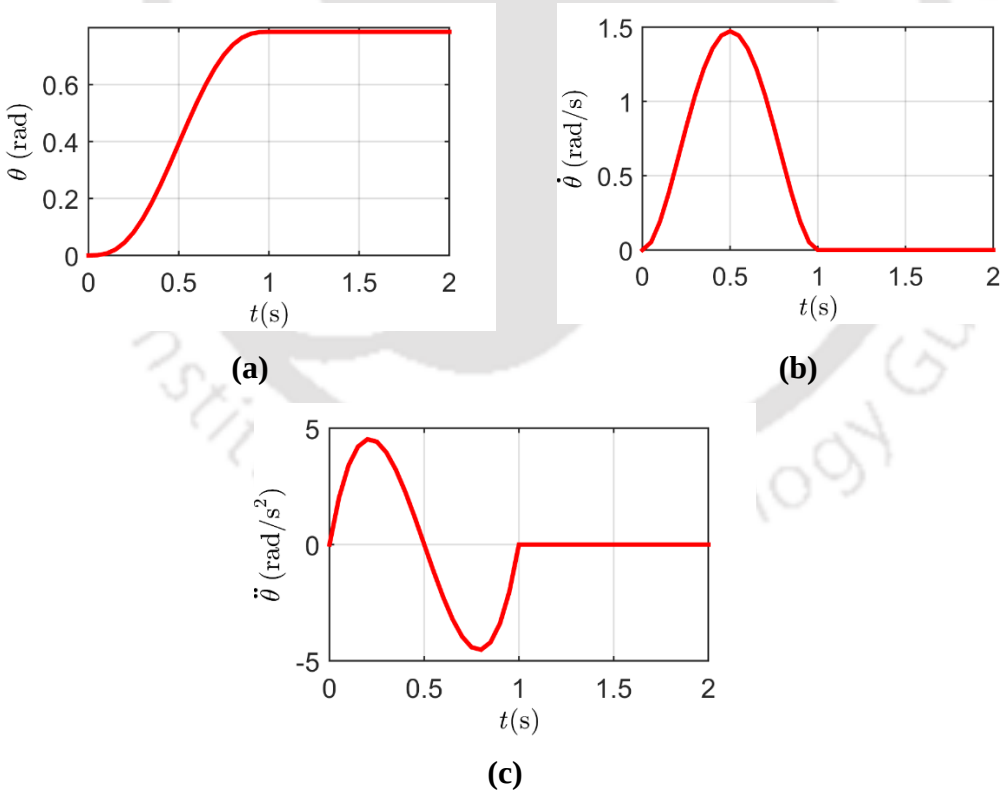

Figure 5.10: Input profile: **(a)** angular displacement, **(b)** angular velocity, and **(c)** angular acceleration of input given to motor.

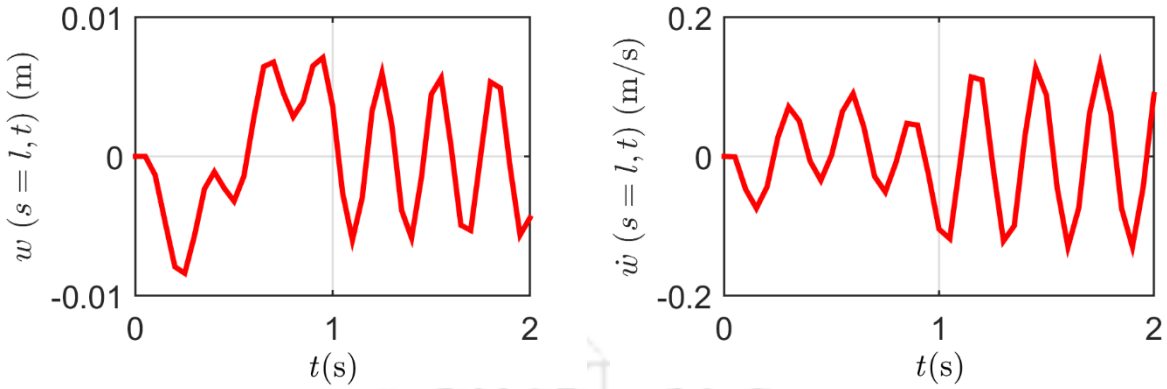

(a) **(b)**

Figure 5.11: Link tip deflection and rate of change of the deflection when no payload is applied and the link is without any string attachment: **(a)** link tip deflection **(b)** time rate of change of the tip deflection.

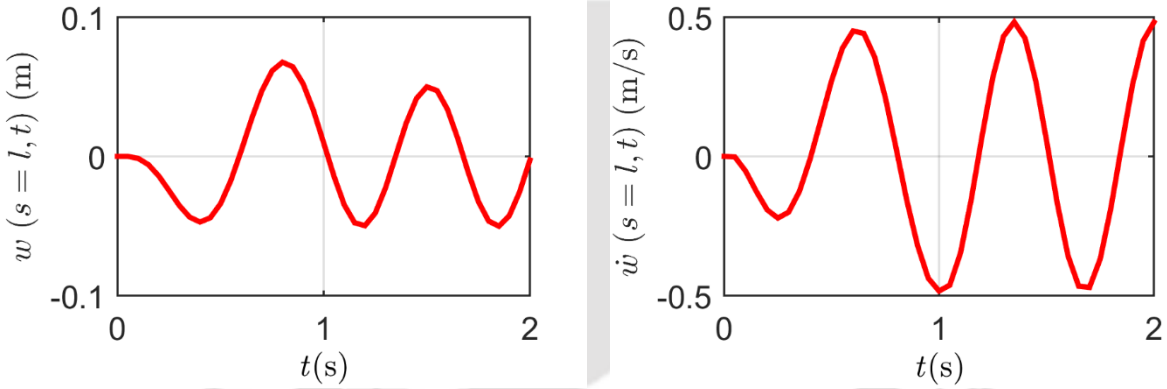

(a) **(b)**

Figure 5.12: Link tip deflection and its rate of change when a payload of 180×10^{-3} kg is applied, and the link is without any string attachment: **(a)** link tip deflection **(b)** time-rate of change of the tip deflection.

Values of tip deflections of the flexible link at the steady state and frequencies of vibration of the link when it is not stiffened with any string are given in Table 5.4.

The natural frequencies of vibration of the manipulator with the payload of mass 180×10^{-3} kg, has also been found in ANSYS using modal analysis which has been shown in

Table 5.4: Deflection and frequency without any string attachment

Conditions	Deflection of the link in 1st mode of vibration at a steady state (in m)	1st and 2nd mode frequencies (in Hz)
Without any payload at the tip of the link and without any string attachment	0.005649	4.9079 and 30.7575
Payload of 180×10^{-3} kg at the tip of the link and without any string attachment	0.05015	2.1516 and 22.6576

Fig. 5.13. The frequencies of the first two modes were found to be 2.0896 Hz and 22.773 Hz in ANSYS which match well with analytical values of 2.1516 Hz and 22.6576 Hz and can be seen from the figure below.

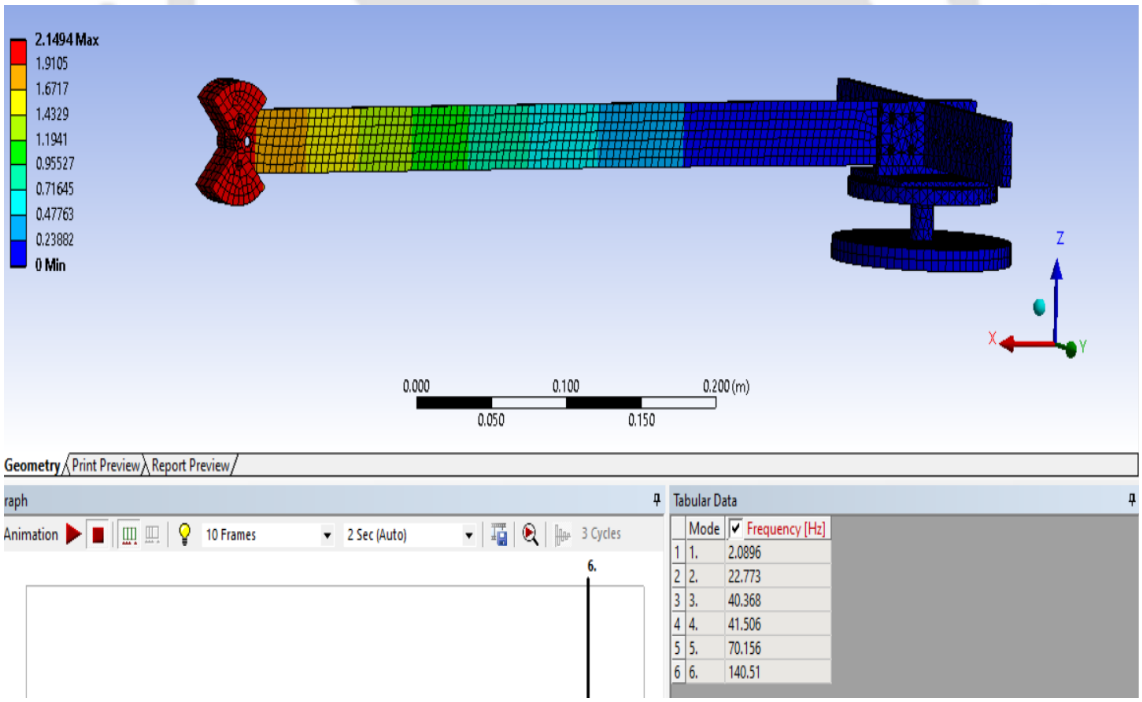

Figure 5.13: Modal analysis results of ANSYS for the FLM without string-stiffening.

When the tip of the link is assumed to be hinged supported due to string stiffening, the tip deflections of the link have been shown in Fig. 5.14 for different tension forces applied by the pair

of strings on the link. As the values of tensions in strings are not given in Dixit and Kumar (2016), results have been found here for several values of tensions in strings. Values of tip deflections of the flexible link near the end of the motion and frequencies of vibration of the link for BCs I(a) and I(b) of Case I for different tension forces in strings are given in Table 5.5.

Here it is seen that when tensions in strings are $T_1 = T_2 = 0.25P_{Cr}$, the deflection of the link tip is almost negligible but as the tensions in the strings increase from $0.25P_{Cr}$ to $0.30P_{Cr}$, the deflection of the tip is gradually increasing. This may be due to the foreshortening or snapping effect of tensions in the strings on the link. After that, the link remains in stable and stout conditions so that as the tensions in the strings increase from $0.30P_{Cr}$ to $0.60P_{Cr}$, the tip deflections reduce gradually with the increase in tensions. And from Table 5.5 and Fig. 5.14 (b) it is seen that at $T_1 = T_2 = 0.29P_{Cr}$, the deflection value and frequency of oscillations of the link closely match with those of the simulation result, shown in Fig. 5.4 and 5.13 of the paper, by Dixit and Kumar (2016). The in Fig. 5.14 in the same paper when the link tries to reach steady-state asymptotically after the time 2.4 s.

When the tip of the link is free to move in space consistent with the forces acting on the tip, boundary conditions I(b) of Case I are considered for obtaining tip deflections of the link. The tip deflections of the link obtained in this case for different tension forces applied by the pair of strings on the link tip are shown in Figs. 5.15 (a) to 5.15 (f). The frequencies and tip deflection the result also matches with the deflection and frequency values of the experimental result shown values of the manipulator at a steady state for different values of tensions in strings have been noted down in Table 5.5. The tensions in strings are expressed in terms of the percentage of critical load of the buckling of the link. Here also, it can be observed from Fig. 5.15 (a) and Table 5.5 that when the tension in strings are $T_1 = T_2 = 0.25P_{Cr}$, the tip deflection of the link closely matches with that of Fig. 5.15 of the experimental results in the paper by Dixit and Kumar (2016). Results obtained using BCs I(b) of Case I in this paper are more realistic than those using BCs I(a) of Case I because in actual practice it is almost impossible to achieve Fixed-Pinned boundary conditions

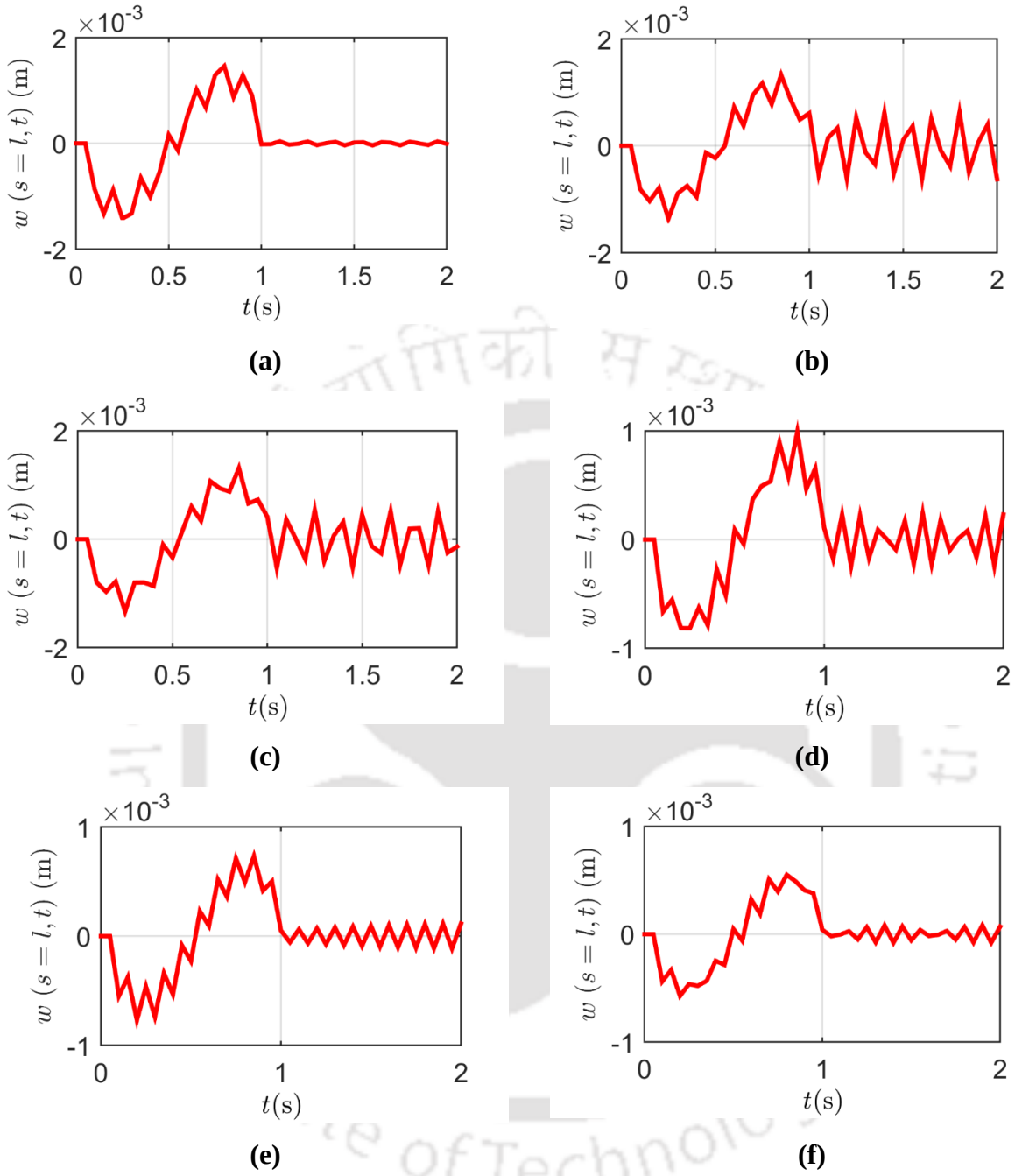

Figure 5.14: Tip deflections when boundary conditions I(a) of Case I have been applied to Eq. (5.49) when: (a) $T_1 = T_2 = 0.25P_{Cr}$, (b) $T_1 = T_2 = 0.29P_{Cr}$, (c) $T_1 = T_2 = 0.30P_{Cr}$, (d) $T_1 = T_2 = 0.40P_{Cr}$, (e) $T_1 = T_2 = 0.50P_{Cr}$ and (f) $T_1 = T_2 = 0.60P_{Cr}$.

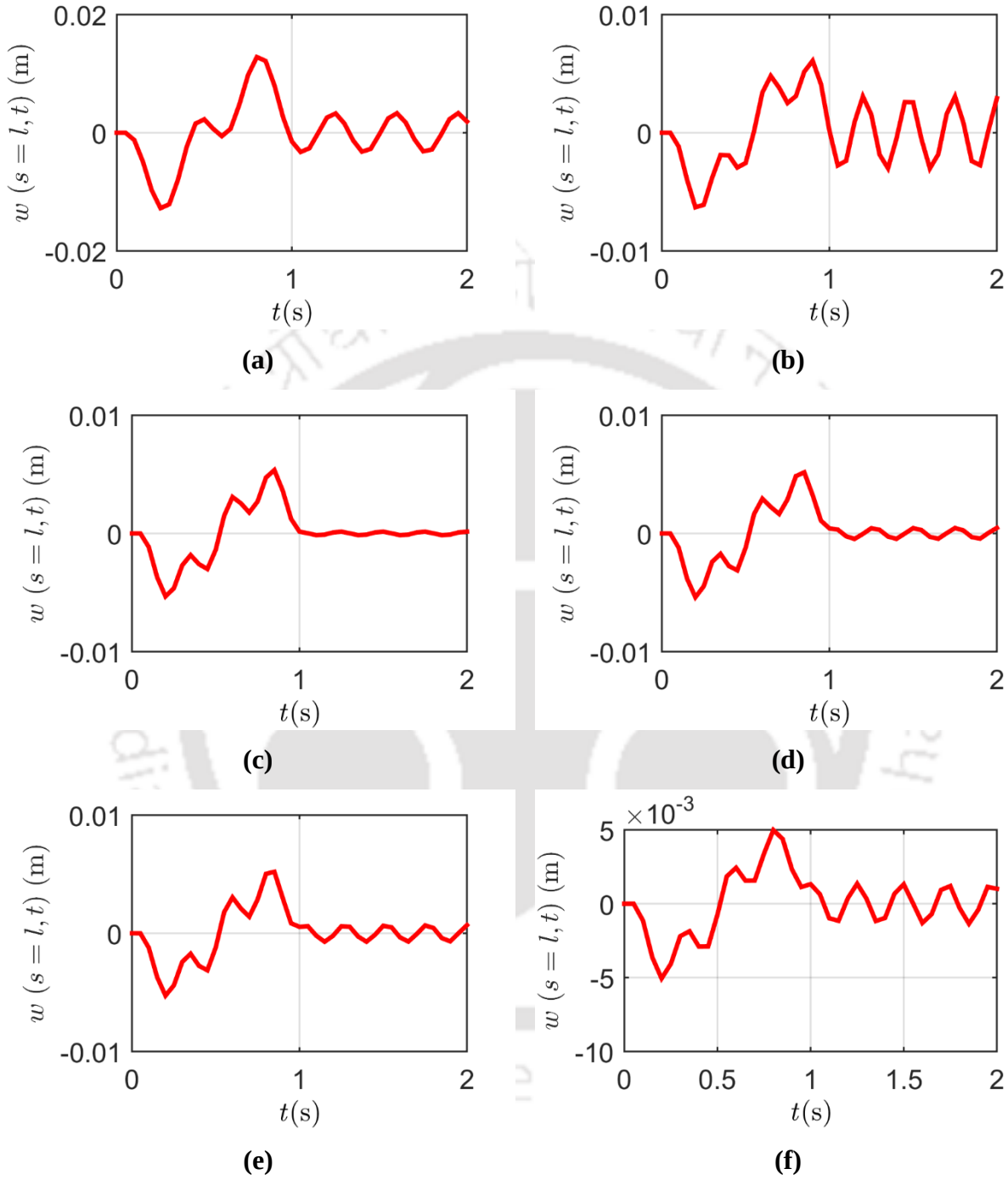

Figure 5.15: Tip deflections of the link for different values of tensions in strings when the tip is free to move: (a) $T_1 = T_2 = 0.25P_{Cr}$, (b) $T_1 = T_2 = 0.50P_{Cr}$, (c) $T_1 = T_2 = 0.60P_{Cr}$, (d) $T_1 = T_2 = 0.61P_{Cr}$, (e) $T_1 = T_2 = 0.62P_{Cr}$ and (f) $T_1 = T_2 = 0.65P_{Cr}$.

using arrangements as shown in Fig. 5.1 and what the experimental result of the paper by Dixit and Kumar (2016) reveals. This also explains why Dixit and Kumar are getting deflection values in the experiment one order of magnitude higher than that of their simulation result. This substantiates the effectiveness of the theoretical analysis of the problem of a string stiffened flexible link manipulator in the present paper.

5.4.3 The Effect of Axial Displacement and Load and Geometric Nonlinearity

Taking the fixed-free boundary conditions, here following three different cases have been considered depending on factors that have been neglected in obtaining Equation (5.48).

Case 8(a): when axial displacement is considered but geometric nonlinearity is not considered. In this case value of maximum tip deflection (MTD) was found to be -0.3347 m at $t = 1.18$ s.

Case 8(b): when axial displacement is not considered. The value of MTD is -0.2671 m at $t = 1.51$ s.

Case 8(c): when both axial displacement and geometric nonlinearity are not considered. The value of MTD is -0.2813 m at $t = 1.53$ s.

The results obtained in these cases have been shown in Fig 5.16 and compared with that of Case 2 of section 4 so that it can be observed that if the above-mentioned one or more factors in this section are not considered then how the results for tip deflection will vary. It is observed that compared to Case 2, there is an increase in the absolute value of tip deflection by 0.81% when geometric nonlinearity is neglected [Case 8(a)]. So, the stiffness of the flexible link decreases in this case. Compared to Case 2 the MTD decreases by 19.55% in Case 8(b) while by 15.27% in Case 8(c). From the above observation, it can be concluded that neglecting axial displacement due to axial load may prove dangerous as the underestimation of tip deflection value may result in a collision of the link tip with the environment.

Table 5.5: Values of tip deflections at steady state and first natural frequencies of vibration of the flexible link

Case I, BCs-I(a)			Case I, BCs-I(b)		
Tension in strings	**Frequency (Hz)**	**The maximum tip deflection (m)**	**Tension in strings**	**Frequency (Hz)**	**The maximum tip deflection (m)**
$T_1 = T_2 = 0.25P_{Cr}$	5.9630	3.214×10^{-5}	$T_1 = T_2 = 0.25P_{Cr}$	2.2161	0.003323
$T_1 = T_2 = 0.29P_{Cr}$	6.2729	4.918×10^{-4}	$T_1 = T_2 = 0.50P_{Cr}$	2.2836	0.002744
$T_1 = T_2 = 0.30P_{Cr}$	6.3480	5.043×10^{-4}	$T_1 = T_2 = 0.60P_{Cr}$	2.3115	0.0001482
$T_1 = T_2 = 0.40P_{Cr}$	7.0551	2.418×10^{-4}	$T_1 = T_2 = 0.61P_{Cr}$	2.3143	0.0004677
$T_1 = T_2 = 0.50P_{Cr}$	7.6976	1.137×10^{-4}	$T_1 = T_2 = 0.62P_{Cr}$	2.3171	0.0006901
$T_1 = T_2 = 0.60P_{Cr}$	8.2904	7.909×10^{-5}	$T_1 = T_2 = 0.65P_{Cr}$	2.3256	0.001354

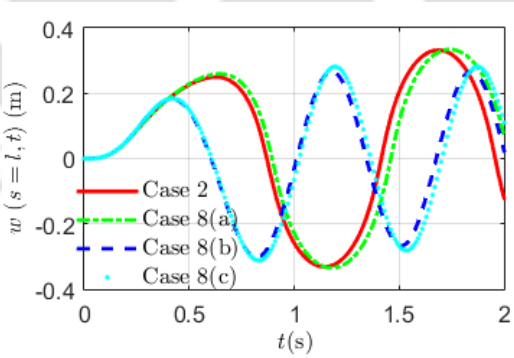

Figure 5.16: Tip deflection of the SSSLFM when a few of the above-mentioned factors are not considered.

5.4.4 Control of Tip Vibration

Despite using a pair of strings to control the tip deflection of the manipulator, it can be observed from Figs. 5.7 to 5.15 that although the amount of deflection is greatly reduced, the vibration of the tip in absence of any damping, still persists. This poses problems in job handling. Therefore, control of tip vibration is necessary to take advantage of string stiffening. Here adaptive PID control along with the impedance control has been applied to control both the joint trajectories and the tip position of the manipulator. The dimensions and material properties of the SSSLFM have been taken as given in Table 5.1. Gain factors for applying PID controller to the manipulator have been taken by trial and error method and are shown in Table 5.6.

Table 5.6: Controller gains

Controlled quantities	**Controller gains K_P, K_I and K_D values**		
X-coordinate	$K_{P_x} = 2000$	$K_{I_x} = 25$	$K_{D_x} = 100$
Y-coordinate	$K_{P_y} = 2000$	$K_{I_y} = 25$	$K_{D_y} = 150$
Joint angular displacement	$K_{P_\theta} = 750$	$K_{I_\theta} = 100$	$K_{D_\theta} = 200$
Motor angular displacement	$K_{P_{\theta_m}} = 750$	$K_{I_{\theta_m}} = 100$	$K_{D_{\theta_m}} = 200$

5.4.4.1 Control of the SSSLFM When Joint Flexibility is Not Considered

In this case, the effect of the tensions in the pair of strings on the joint of the SSSLFM has not been considered. The SSSLFM is considered as only a flexible link manipulator. Eqs. (5.51) and (5.53) will be applicable for such a type of manipulator. The desired trajectories of the joint θ_d and $\dot{\theta}_d$ are taken from Eq. (5.83) and as shown in Fig. 5.6. The initial conditions taken are: $\theta = \pi/2$ rad, $\dot{\theta} = 0$ rad/s, $q = 0$, $\dot{q} = 0$ and initial values of cumulative errors for θ, x and y equal to zero. Eq. (5.51) and (5.53) can be solved to control the tip deflection as shown in Figs. 5.17 (a, b, c, and d). Fig. 5.17(a) shows the tip deflection of the flexible link while Fig. 5.17(b) gives its speed. Figs. 5.17(c) and 5.17(d) represent the actual and desired values of joint angular displacement and

its angular speed respectively. From Fig. 5.17(a) it can be seen that manipulator tip motion reaches steady state quickly after the joint motion and tip oscillations also vanishes completely. The link tip is able to follow the desired tip motion. Fig. 5.17(b) shows that after the joint motion link becomes motionless after some time so that it can now be employed safely for job handling. From Fig. 5.17(c) it is seen that the desired joint trajectory is followed.

5.4.4.2 Flexible Joint Control

Here, in order to control the joint disturbances due to the string torques on the joint, the joint is modeled as a torsional spring of stiffness K_t. The motion imparted to the motor at the hub

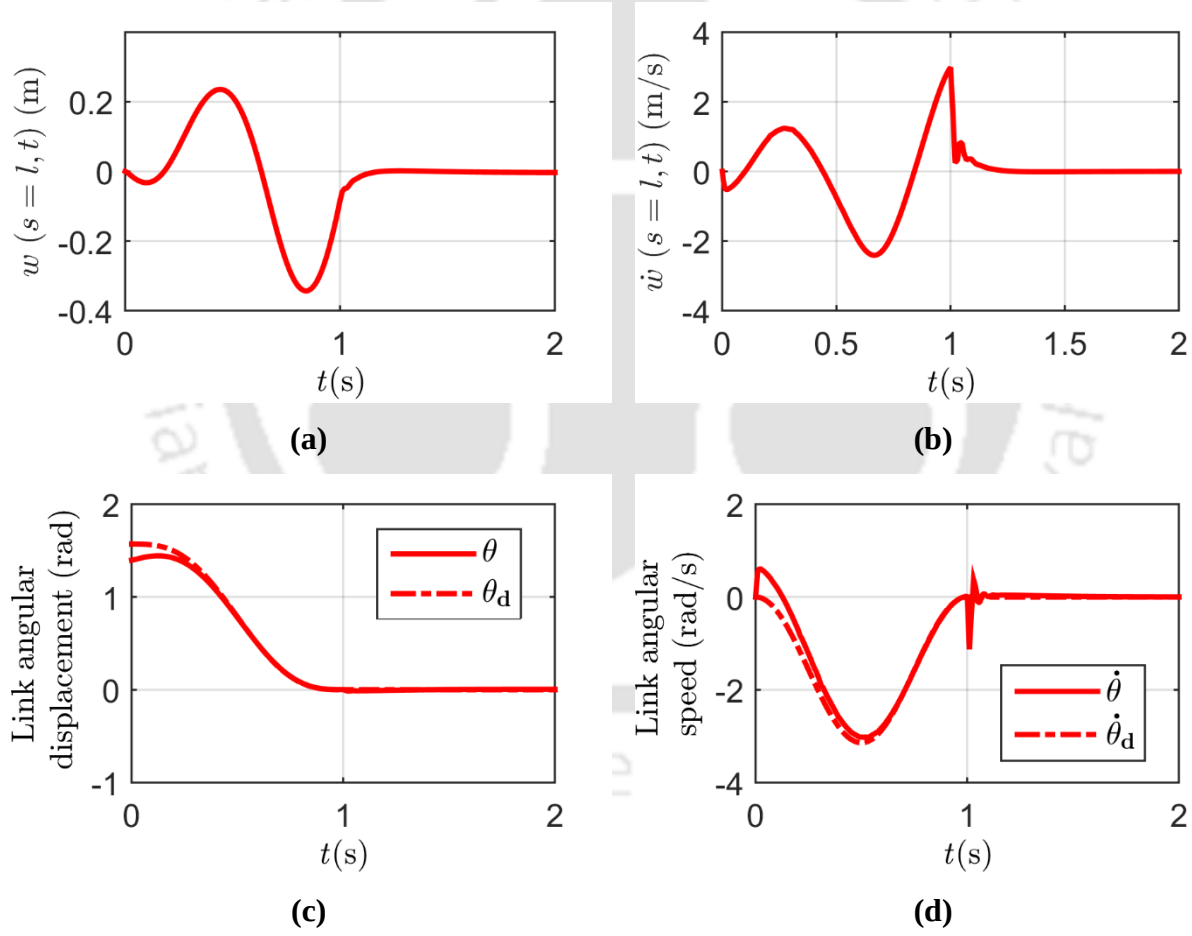

Figure 5.17: Tip deflection and joint motion control of the string stiffened flexible link manipulator **(a)** tip deflection, **(b)** rate of change of tip deflection, **(c)** joint angular displacement, and **(d)** joint angular speed.

is considered as the desired motion of the manipulator's joint. The motion of the joint motor is controlled so that it can follow the desired angular trajectory given by Eq. (5.83). Link angulardisplacement θ is expected to follow the motor angular displacement θ_m. Joint properties havebeen taken as given in Table 5.7. The PID gains for the control of the manipulator have been taken as shown in Table 5.6. In this case, no control has been applied to control the tip deflection of the flexible link. This allows one to see that in the presence of joint flexibility how the angular motion of the link and the cartesian motion of its tip behave.

With initial conditions taken as $\theta_m = \frac{\pi}{2}$ rad, $\theta = \frac{\pi}{2}$ rad, $q = 0$, $\dot{\theta}_m = 0$ rad/s $\dot{\theta} = 0$ rad/s $\dot{q} = 0$

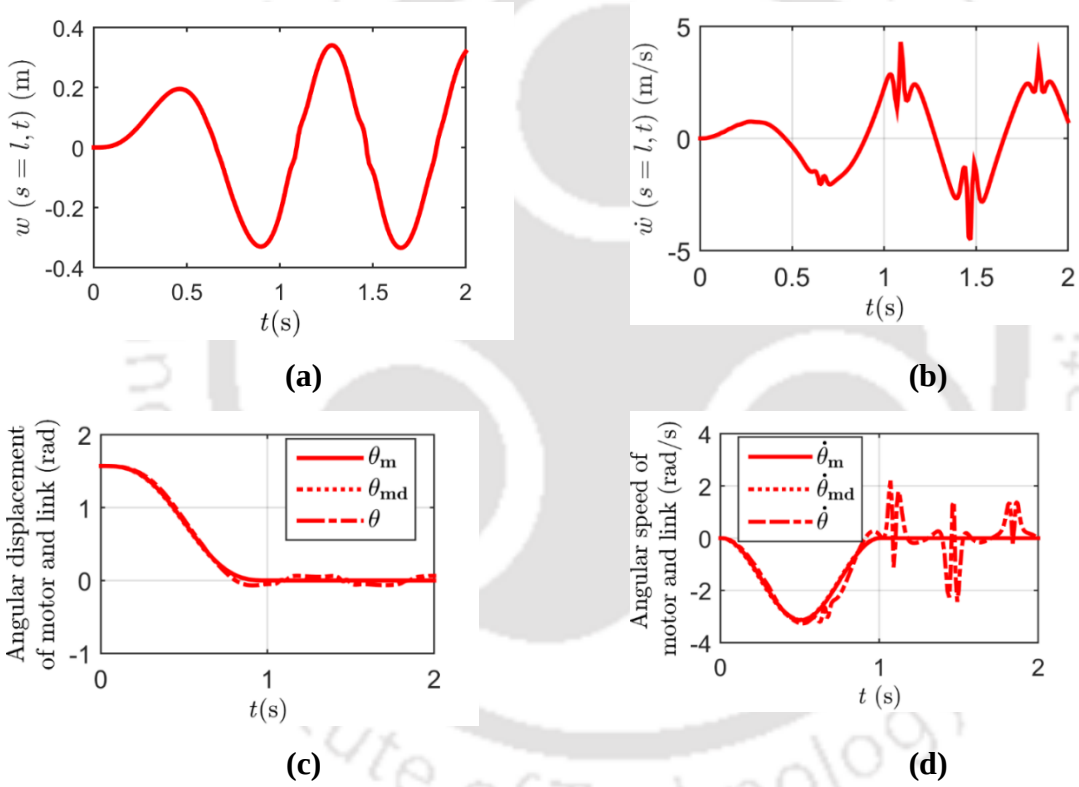

Figure 5.18: Tip deflection control of the flexible joint-flexible link string stiffened manipulator: **(a)** tip deflection, **(b)** rate of change of tip deflection, **(c)** joint angular displacement, and **(d)** joint angular speed.

and cumulative error for θ_m over the time t be equal to zero, Eqs. (5.62), and (5.63) can be solved to find results that have been shown in Figs. 5.18 (a, b, c, and d). From Figs. 5.18(c) and 5.18(d) it can be seen that while the motor angular displacement θ_m and its speed $\dot{\theta}_m$ are able to follow

Table 5.7: Joint properties

Joint stiffness (Nm/rad)	**Motor mass** (kg)	**The radius of gyration of the motor** (m)
$K_t = 100$	$M_m = 0.50$	$R_H = 0.025$

the desired trajectories θ_{md} and $\dot{\theta}_{md}$, the link angular displacement θ and $\dot{\theta}$ fluctuate about the corresponding quantities of the motor. Also, the link tip deflection and its speed as shown in Figs. 5.18(a) and 5.18(b) could not be controlled. The solution of these problems is given in the next section.

5.4.4.3 Flexible Joint and Flexible Link Control

In Fig. 5.18, it is seen that although the motor displacement has been controlled, the joint and link flexibilities have not been controlled. To control both angular and cartesian displacements of the link, here adaptive PID control along with impedance control have been applied.

Initial conditions taken to solve Eq. (5.76) are: $\gamma = \frac{\pi}{180}$ rad at $\tau_t = 0$ s and $\frac{d\gamma}{d\tau_t} = 0$ rad/s at $\tau_t = 0$ s and to solve Eqs. (5.80) and (5.82) the initial conditions are taken to be $\theta = \frac{\pi}{2}$ rad, $q = 0$; $\dot{\theta} = 0$

Table 5.8: Controller gains for controlling both joint and link flexibility

Controlled quantities	**Controller gains K_P, K_I and K_D values**		
X-coordinate	$K_{P_x} = 25$	$K_{I_x} = 5$	$K_{D_x} = 10$
Y-coordinate	$K_{P_y} = 25$	$K_{I_y} = 5$	$K_{D_y} = 10$
Joint angular displacement	$K_{P_\theta} = 50$	$K_{I_\theta} = 5$	$K_{D_\theta} = 20$

rad/s, $\dot{q} = 0$, initial cumulative errors for θ, x and y are taken to be zero. Time scaling factor ϵ has been taken to be equal to 0.1 and the damping factor ξ has been taken as $\xi = 1$ for critical damping. The controller gains have been suitably changed and shown in Table 5.8, to get the

steady-state quickly. Now solving Eqs. (5.76), (5.80) and (5.82) for q and θ, one gets the results as shown in Figs. 5.19(a) to 5.19(d). From Figs. 5.19(a) and 5.19(b), it is observed that whatever residual oscillations were present after stiffening the flexible link with strings, that too vanished on applying the control and the tip motion speed also became zero. Figs. 5.19(c) and 5.19(d) also show that the angular displacement and angular speed of the link of the SSSLFM are able to follow the desired trajectory. The link tip becomes still at the end of motion so that now it can be employed in handling any task without fear of any damage to the job or the manipulator.

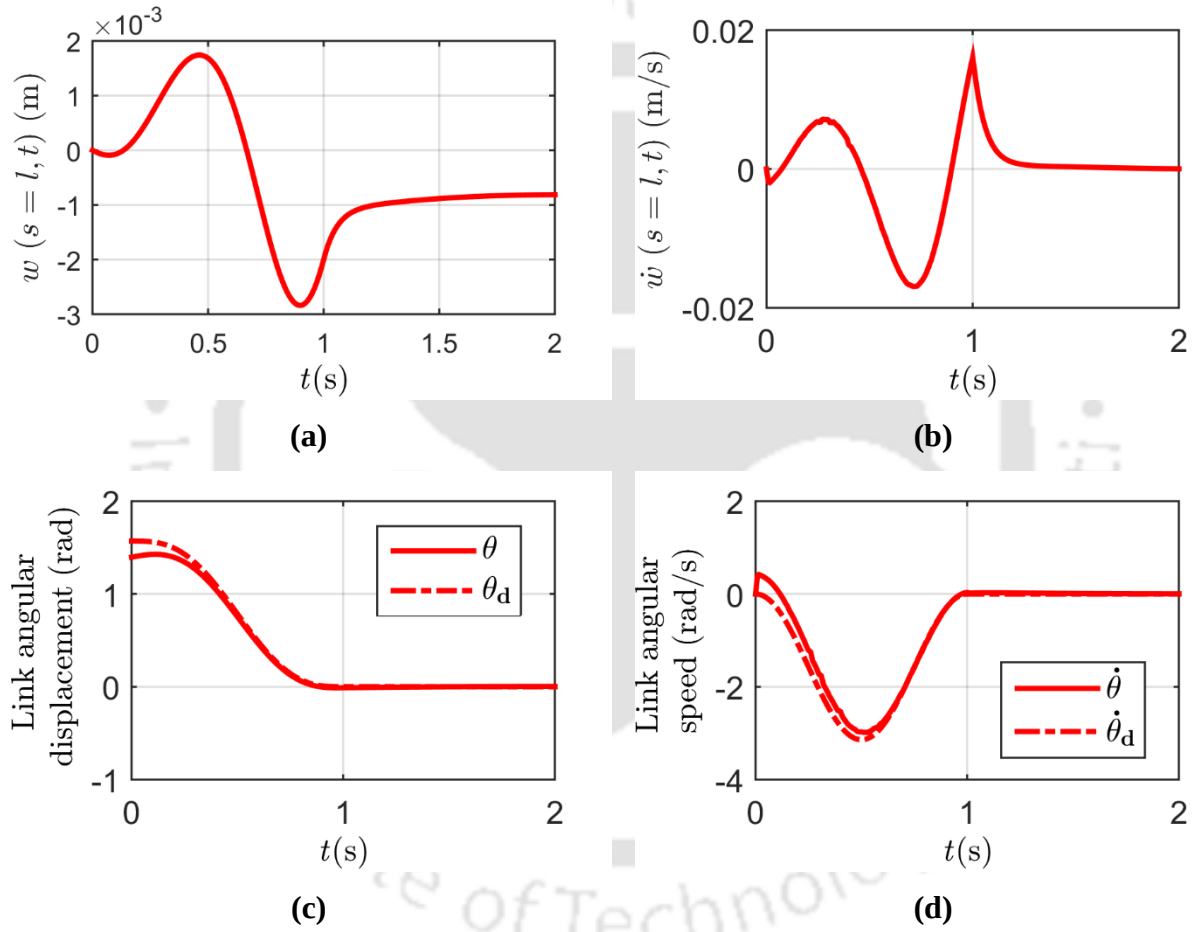

Figure 5.19: Tip deflection control of the flexible joint-flexible link string-stiffened single link manipulator: **(a)** tip deflection, **(b)** rate of change of tip deflection, **(c)** joint angular displacement, and **(d)** joint angular speed.

5.5 Conclusion

In this chapter, a systematic mathematical analysis of a string-stiffened single-link flexible manipulator has been carried out. It has been observed that by stiffening of a flexible link by application of a pair of strings can considerably reduce the tip deflection. Contrary to the assumption of Dixit and Kumar (2016) of the clamped-pinned beam, clamped-free boundary conditions for the link of the string-stiffened flexible link manipulator seems to be more practical as the theoretical result of the present work matches closely with the experimental result of Dixit and Kumar (2016). In this case, the tip deflection has been reduced by more than 60%.

However, due to the coupling effect of string vibration with that of the link, it may also introduce joint flexibility which has been controlled with the application of adaptive PID control technique. This makes it a promising technique for controlling tip deflection. By this method, with the addition of minimum weight to the manipulator, the stiffness of the flexible link can be increased considerably. This is especially important for aerospace applications like flapping wing aerial vehicles where weight management is one of the important factors that have to be considered.

Chapter 6

Dynamic Analysis and Control of a String-Stiffened Rigid-Flexible Two-Link Manipulator

6.1 Introduction

A single link manipulator has a limited workspace so that it may not be suitable in many practical applications. In this chapter, a string-stiffened rigid-flexible two-link manipulator (SSRFTLM) has been analyzed to find the tip deflection. In section 6.2, the mathematical modelling of the 2-link manipulator is carried out. In section 6.3 control has been applied. In section 6.4 results and discussions have been presented and finally in section 6.5 conclusions have been made.

6.2 Modelling

Here, a two-link planar rigid-flexible manipulator in which the first link is rigid while the second link is flexible has been considered. Similar to the work in the last chapter, here also, strings are used for stiffening the flexible link. To provide extra stiffness to the flexible link, the tip of the flexible link has been tied with a pair of strings on both sides of the link as shown in the schematic diagram of the SSRFTLM when viewed from top and front in Figs. 6.1(a) and 6.1(b) respectively. On either side of the flexible link, two string-fixers have been attached to the hub of the second link to hold stiffening strings. The three-dimensional (3D) model of the SSRFTLM has been shown in Fig. 6.2 which is modeled in CAD software package SOLIDWORKS 2019. At the tip of the second link, there is a payload. The two links are driven by two motors.

Forces acting on the flexible link and torques acting at the 2nd joint of the manipulator will be the same as given in section 5.2.1. The general equation of motion of the string-stiffened flexible link will be the same as given in Eq. (5.3) of section 5.2.2. Depending upon different constraint conditions applied on the link, here also, three cases can be considered:

Case I: when the tip of the link of the flexible link manipulator (FLM) is tied with a pair of strings on either side of the link. The other ends of the strings are tied to the supporting structure at the

hub of the FLM. Here, the effect of string vibration on the tip deflection of the link is not considered.

Case II: here the analysis of the flexible link has been done considering the effect of vibration of strings on the tip deflection of the link.

Case III: when the link of FLM is not tied with any string.

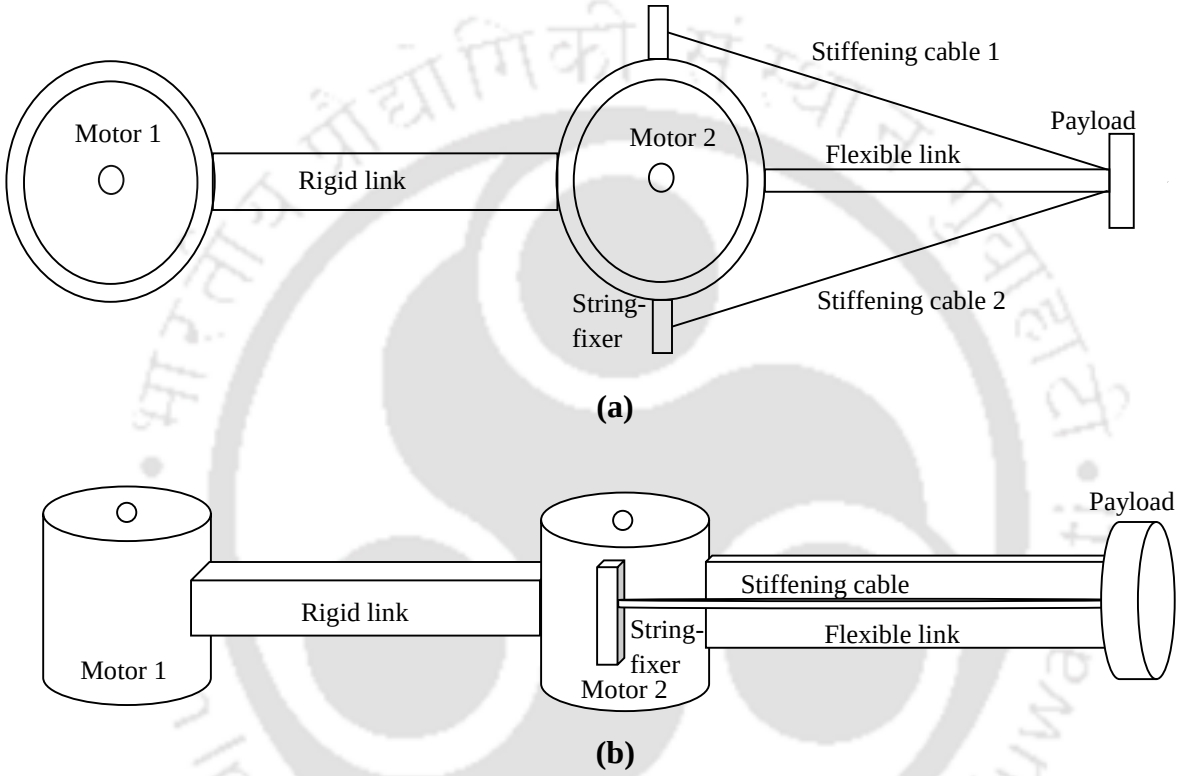

Figure 6.1: A schematic diagram of the string-stiffened rigid-flexible two-link manipulator (SSRFTLM) as viewed from (a) the top and (b) the front.

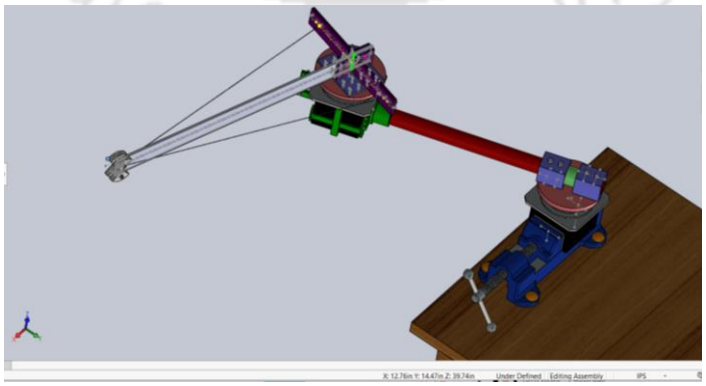

Figure 6.2: The 3D CAD model of the SSRFTLM obtained using SOLIDWORKS 2019.

All these conditions have been described in details in section 5.2.2 of chapter 5. In total seven boundary conditions mentioned in the same section of the chapter, have been considered to obtain mode shapes and frequencies of vibrations of the flexible link of the SSRFTLM. Eqs (5.3) to (5.38) are valid for current analysis also.

The inextensibility conditions and geometric nonlinearities considered in the works of Zavodney and Nayfeh (1989) and Abe (2009) have been taken to relate the axial displacement and the transverse deflection of the flexible link and its nonlinear curvature arising due to its large deflection. Further, the control of the tip deflection of the flexible-joint and flexible-link system is carried out using impedance control along with an adaptive PID controller.

6.2.1 Dynamic Equation of Motion of the Two-Link Rigid-Flexible Manipulator

The two-link rigid-flexible manipulator with OA as the rigid link and AB as the flexible link has been shown in Fig. 6.3. At the end of the second link, there is a payload of mass M_p. The hub of the second link of mass M_{H_2} acts as payload for link 1. XOY is the inertial frame of reference while xoy is the body-attached frame of reference.

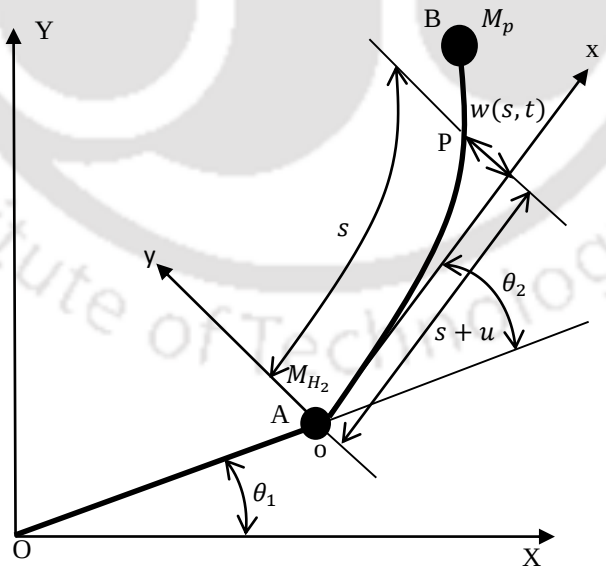

Figure 6.3: A two-link rigid-flexible manipulator.

P is a point on the flexible link at curvilinear distance s from the origin 'o'. u is the axial displacement while $w(x,t)$ is the deflection of the link in the y-direction in the body attached frame of reference. The first link subtends an angle θ_1 with the X-axis of the inertial frame at hub 'O' at any instant of time t while the second link makes an angle θ_2 with respect to the first link at the joint at 'o'. Taking l_r and l_f as the length of the rigid link and flexible link, respectively, the position vector r of any point P on the flexible link located at a curvature distance s from the hub 'o' can be expressed relative to the inertial frame of reference at hub 'O' as

$$r = \begin{bmatrix} r_x \\ r_y \end{bmatrix} \tag{6.1}$$

where

$$r_x = l_r \cos\theta_1 + (s+u)\cos(\theta_1+\theta_2) - w\sin(\theta_1+\theta_2) \tag{6.2}$$

$$r_y = l_r \sin\theta_1 + (s+u)\sin(\theta_1+\theta_2) + w\cos(\theta_1+\theta_2) \tag{6.3}$$

Applying the inextensibility condition, the axial displacement u in terms of lateral displacement w can be given by the following relation

$$u = -\frac{1}{2}\int_0^s \left(\frac{\partial w}{\partial s}\right)^2 ds \tag{6.4}$$

The kinetic energy of the system can be expressed as

$$T = \frac{1}{2}\left[J_{H_1}\dot{\theta}_1^2 + M_1 l_r^2\dot{\theta}_1^2 + J_{H_2}\dot{\theta}_2^2 + M_{H_2} l_r^2\dot{\theta}_1^2 + \int_0^{l_f}\{\rho A + M_p\delta(s-l_f)\}\dot{r}^T\dot{r}\,ds\right] \tag{6.5}$$

in which $\dot{(\ )}$ denotes the derivative of the quantity with respect to time. J_{H_1} and J_{H_2} are the moment of inertia of hub 1 and hub 2 respectively. While M_1 is the mass of the rigid link, ρ, A are respectively the density and cross-sectional area of the flexible link. δ denotes the Dirac-delta function.

The potential energy V of the system due to link flexibility is given by

$$V = \frac{1}{2}EI\int_0^{l_f}\mathcal{K}^2 ds = \frac{1}{2}EI\int_0^{l_f}\left[\left(\frac{\partial^2 w}{\partial s^2}\right)^2\left\{1+\left(\frac{\partial w}{\partial s}\right)^2\right\}\right]ds \tag{6.6}$$

where $\mathcal{K}$ is the curvature of the neutral axis of the flexible link [Zavodney and Nayfeh (1989), Abe (2009)] and is given by

$$\mathcal{K} = \frac{\partial^2 w}{\partial s^2}\left\{1 + \left(\frac{\partial w}{\partial s}\right)^2\right\}^{-\frac{1}{2}} \tag{6.7}$$

The term $\left[\left(\frac{\partial^2 w}{\partial s^2}\right)^2 \left(\frac{\partial w}{\partial s}\right)^2\right]$ in Eq. (6.6) represents the effect of the nonlinear curvature.

The virtual work δW done by the external torque τ_i, applied at the i^{th} joint and by the force P applied by the pair of the strings along the link as shown in Fig. 6.3 is given by

$$\delta W = \tau_1 \delta\theta_1 + \tau_2 \delta\theta_2 + P\delta u \tag{6.8}$$

Lagrangian L of the manipulator system is given by

$$L = T - V \tag{6.9}$$

Using the Euler-Lagrange equation of motion, the equation of motion for the manipulator can be given by the equations

$$\frac{d}{dt}\left(\frac{\partial L}{\partial \dot{\theta}_i}\right) - \frac{\partial L}{\partial \theta_i} = \tau_i \text{ and } \frac{d}{dt}\left(\frac{\partial L}{\partial \dot{q}}\right) - \frac{\partial L}{\partial q} = F_{str} \tag{6.10}$$

Using Eq. (6.10) into Eq. (6.9) the equations of motion of the system are obtained as follows.

$$\begin{bmatrix} M_{rr} & M_{rf}^T \\ M_{rf} & M_{ff} \end{bmatrix}\begin{bmatrix} \ddot{\theta} \\ \ddot{q} \end{bmatrix} + \begin{bmatrix} C_r \\ C_f \end{bmatrix} + \begin{bmatrix} 0_{n\times n} & 0_{n\times N} \\ 0_{N\times n} & K_f \end{bmatrix}\begin{bmatrix} \theta \\ q \end{bmatrix} = \begin{bmatrix} \tau \\ F_{str} \end{bmatrix} \tag{6.11}$$

where $\theta \in R^n$ is the vector of generalized joint variables, $q \in R^N$ is the vector of deformation. Here, for the SSRFTLM, $n = 2$, and $N = 1$. To write concisely one may take

$M = \begin{bmatrix} M_{rr} & M_{rf}^T \\ M_{rf} & M_{ff} \end{bmatrix}$, $C = \begin{bmatrix} C_r(\theta, q, \dot{\theta}, \dot{q}) \\ C_f(\theta, q, \dot{\theta}, \dot{q}) \end{bmatrix}$ and $K = \begin{bmatrix} 0_{n\times n} & 0_{n\times N} \\ 0_{N\times n} & K_f \end{bmatrix}$ where M is the $(n+N)\times(n+N)$ configuration dependent generalized mass matrix, C is the vector of size $(n+N)$ containing Coriolis and centrifugal terms, K is the $(n+N)\times(n+N)$ stiffness matrix of the flexural structure where $0_{n\times n}$, $0_{n\times N}$ and $0_{N\times n}$ are the null matrices of sizes $n\times n$, $n\times N$ and $N\times n$ and K_f is the matrix of size $N\times N$ corresponding to the deformation (flexible) variables, $\tau \in R^n$ is the vector of joint torques and $F_{str} \in R^N$ is the vector of generalized force on the link tip. It may be observed that Eq. (6.11) though seems to be similar to the governing equation of motion of a two-link manipulator, but the elements of the matrices are completely different due to the presence of the effect of the strings on the mode shapes of vibrations of the flexible link. Due to the

flexibility of the second link the tip will undergo vibrations. In the following section, the control of the tip vibration has been addressed.

6.3 Control of Tip Vibration

Although the use of strings as stiffening devices reduces the tip deflection of the manipulator greatly, oscillations of the tip, in the absence of any damping, will still persist. This poses problems in job handling. Therefore, control of tip vibration is necessary to take advantage of string-stiffened arms. One of the very popular methods of control is to apply a proportional-integral-derivative (PID) controller for the task. However, controlling a flexible link is a very tedious task because of the highly nonlinear and strongly coupled nature of the problem. Compared with the rigid manipulator, the dynamic characteristics of a flexible manipulator are more difficult and complex to control [Meng et al. (2018)]. Here, adaptive PID control along with impedance control has been applied to control the residual tip vibration of the planar two-link manipulator. Assuming the desired position of the end-effector to be (x_d, y_d) and the actual position as (x, y) at any time t for which the desired joint space coordinates are θ_{i_d} and actual joint angles are θ_i, where subscript $i = 1, 2$. The errors in tip positions (e_x, e_y) and link angular positions e_θ can be given in vector form as

$$e_\theta = \theta_d - \theta;\ e_x = x_d - x \text{ and } e_y = y_d - y \tag{6.12}$$

In the following subsections, 2 cases viz., flexible link control, and flexible-link and flexible-joint control have been considered. K_{P_j}, K_{I_j} and K_{D_j} are respectively, the proportional, integral, and derivative gains for the respective quantities denoted by the subscript j where $j = x, y, \theta_1, \theta_2$.

6.3.1 Flexible Link Control

Joint torque is user-defined, so, to control the link oscillations, τ in Eq. (6.11) is defined [Theodore and Ghosal (2003)] such that

$$\ddot{\theta} = (I - Q)\tau_{CT_\theta} + Q\tau_{pid_{pos}} \tag{6.13}$$

where $I = \begin{bmatrix} 1 & 0 \\ 0 & 1 \end{bmatrix}$ and $Q = \begin{cases} \begin{bmatrix} 0 & 0 \\ 0 & 0 \end{bmatrix}, & 0 \le t \le t_m \\ \begin{bmatrix} 1 & 0 \\ 0 & 1 \end{bmatrix}, & t_m < t \le t_f \end{cases}$

Here, t_m is the time of motion of joints and t_f is the final time of the motion of the tip of the manipulator up to which it is observed. τ_{CT_θ} is the computed torque applied for the joint angular motion during the motion of the manipulator while $\tau_{pid_{pos}}$ is the computed torque for position control of the tip of the manipulator and are given by the following equations, respectively:

$$\tau_{CT_\theta} = \ddot{\theta}_d + \tau_{pid_\theta} \tag{6.14}$$

$$\tau_{pid_{pos}} = J_{tip}^T \begin{bmatrix} F_{pid_x} \\ F_{pid_y} \end{bmatrix} \tag{6.15}$$

where J_{tip} is the Jacobian matrix for the motion of the link tip and J_{tip}^T is its transpose. τ_{pid_θ} is the torque applied at the joint and F_{pid_x} and F_{pid_y} are the controlling force applied on the tip of the link and are given by the following expressions:

$$\tau_{pid_\theta} = K_{P_\theta} e_\theta + K_{I_\theta} \int e_\theta \, dt + K_{D_\theta} \dot{e}_\theta;\ F_{pid_x} = K_{P_x} e_x + K_{I_x} \int e_x \, dt + K_{D_x} \dot{e}_x; \text{ and}$$
$$F_{pid_y} = K_{P_y} e_y + K_{I_y} \int e_y \, dt + K_{D_y} \dot{e}_y \tag{6.16}$$

The controlling force at the tip is converted into joint torque using Eq. (6.15).

From Eq. (6.11), one can write $\ddot{q}$ as following:

$$\ddot{q} = -\frac{1}{M_f}(C_f + K_f q - F_{str} + M_{rf}^T \ddot{\theta}) \tag{6.17}$$

Now Eqs. (6.13) and (6.17) can be solved together to find the controlled motion of the link joint and tip.

6.3.2 Flexible-Link and Flexible-Joint Control

Strings stiffen the link to reduce the amplitude of vibration of the tip of the link; however, these also produce disturbances in the form of unwanted torque on joints that makes the joint of the manipulator flexible which excites the link to vibrate continuously. The effects of imperfect joints on the dynamics of connected bodies and their dynamic modellings have been studied in

detail in the work of [Flores et al. (2006) and Marques et al. (2021)]. It is known that joint flexibility is more dangerous than link flexibility which creates greater difficulty in controlling the tip deflection. So, this complicates the problem to a much further extent than operating the manipulator without any string because, by this, one has to tackle not only link flexibility but also, joint flexibility at the same time.

Here, in order to control the joint disturbances due to the string torques on the joint, the joints are modeled as torsional springs of stiffnesses K_{t_i} where subscript $i = 1,2$ and denotes i^{th} the joint of the manipulator. Let M_{m_i} be the mass and R_{H_i} be the radius of motors at the i^{th} joint so that their moment of inertia will be given by $J_{m_i} = \frac{1}{2} M_{m_i} R_{H_i}^2$. θ_i denotes the i^{th} link angular displacement and θ_{im} denotes the i^{th} motor angular displacement, where subscript $i = 1,2$. In the presence of joint flexibility, Eq. (6.11) is modified to get the equations of motion in matrix form for the flexible-joint and flexible-link rigid-flexible 2-link manipulator as follows.

$$J_m \ddot{\theta}_m + K_t(\theta_m - \theta) = \tau \tag{6.18}$$

$$\begin{bmatrix} M_r & M_{rf}^T \\ M_{rf} & M_f \end{bmatrix} \begin{bmatrix} \ddot{\theta} \\ \ddot{q} \end{bmatrix} + \begin{bmatrix} C_r \\ C_f \end{bmatrix} + \begin{bmatrix} 0_{n\times n} & 0_{n\times N} \\ 0_{N\times n} & K_f \end{bmatrix} \begin{bmatrix} \theta \\ q \end{bmatrix} = \begin{bmatrix} K_t(\theta_m - \theta) \\ F_{str} \end{bmatrix} \tag{6.19}$$

Here, $\theta_m = [\theta_{1m}, \theta_{2m}]^T$.

In order to control both the joint flexibility as well as link flexibility, impedance control along with the adaptive proportional-integral-derivative (APID) control have been applied. The APID control that has been applied in Spong (1989) for control of a rigid-link manipulator, has been extended here for control of the SSRFTLM. Following Spong (1989) and the procedure mentioned in section 5.3.2 of chapter 5, the flexible-joint and flexible-link system described by Eqs. (6.18) and (6.19) have been modified to obtain the following expressions:

$$\frac{d^2\gamma}{d\tau_t^2} + 2\omega_{n_{Jt}}\xi \frac{d\gamma}{d\tau_t} + \omega_{n_{Jt}}^2 \gamma = 0 \tag{6.20}$$

$$\begin{bmatrix} M_r + J_m & M_{rf}^T \\ M_{rf} & M_f \end{bmatrix} \begin{bmatrix} \ddot{\theta} \\ \ddot{q} \end{bmatrix} + \begin{bmatrix} C_r \\ C_f \end{bmatrix} + \begin{bmatrix} 0_{n\times n} & 0_{n\times N} \\ 0_{N\times n} & K_f \end{bmatrix} \begin{bmatrix} \theta \\ q \end{bmatrix} = \begin{bmatrix} \tau + \gamma \\ F_{str} \end{bmatrix} \tag{6.21}$$

where $\omega_{n_{J_t}} = [\omega_{n_{Jt_1}} \quad \omega_{n_{Jt_2}}]^T$, $\omega_{n_{Jt_i}} = \epsilon\sqrt{\frac{K_{t_i}}{J_{m_i}}}$ for the i^{th} flexible joint; ξ is the damping factor; ϵ is the scaling factor; $\tau_t(t)$ is the fast time scale given as $\tau_t(t) = \frac{t}{\epsilon}$ and γ is a 1×2 vector that satisfies the Eq. (6.20) and is given as

$$\gamma = \left(\gamma_0 + \left(\left(\frac{d\gamma}{d\tau_t}\right)_{\tau_t=0} + \omega_{n_{Jt}}\gamma_0\right)\tau_t\right)e^{-\omega_{n_{Jt}}\tau_t} \tag{6.22}$$

In Eq. (6.21), τ are user-defined and taken to be equal to

$$\tau = (I - Q)\tau_{pid_\theta} + Q\tau_{pid_{pos}} \tag{6.23}$$

Now solving Eq. (6.21) for θ and q, joint, and link angular displacement can be controlled to get the steady-state solution.

6.4 Results and Discussions

The dimensions and material properties of the string stiffened rigid-flexible two-link manipulator (SSRFTLM) have been given in Table 6.1. The mass of the payload at the tip of the flexible link is equal to 0.5 times the mass of the flexible link.

The dynamic analyses of the manipulator have been carried out for various boundary conditions as described in section 6.2. Also, the behaviors of the manipulator on applying different control techniques depending upon the modeling of the manipulator that has been described in section 6.3, have been found out.

Table 6.1: Dimensions and material properties of the SSRFTLM

Description	Length (m)	Thickness of the link (m)	The breadth of the link (m)	Diameter (m)	Density (kg/m^3)	Young's Modulus (GPa)
1st link	0.8	NA	NA	-	NA	NA
2nd link	0.6	4.92×10^{-2}	2.028×10^{-3}	-	2690	69
String	0.601			1×10^{-3}	7850	210

In order to carry out the dynamic analysis of the manipulator, the numerical solution of Eq. (6.11) has been obtained using 4^{th}-5^{th} order Range-Kutta's method. The rotational inertia of motors at hubs and payload have been neglected here for finding the dynamic response. The tension T_1 in the string on any one side of the link has been taken to be 25% of the critical load of buckling P_{Cr} of the link and tension T_2 in the string on the other side of the link has been taken to be 85% of T_1. Here, the critical load of buckling $P_{Cr} = \frac{\pi^2 EI}{l_f^2}$ where κ is the effective length factor for the beam or link. The angle of the string on any one side of the link with the surface of the link in the undeflected condition is ϑ_1 and the angle of the string on the other side of the link with the surface of the link in the undeflected condition is ϑ_2 where $\vartheta_2 = 0.95\vartheta_1$. The tension values in strings and angles of strings with the link on either side have been taken to be different by considering uncertainty or difficulties in determining these values. The initial conditions for the solution of Eq. (6.11) are: $q_0 = 0$ and $\dot{q}_0 = 0$ where $q(t)$ is the temporal variable. Cycloidal motion profiles as shown in Fig. 6.4(a) have been given to motors at both joints for a time duration $t_m = 1$ second and observed up to the time $t_f = 2$ seconds as described below and tip deflection of the 2nd link $w_{Tip\,2}$ has been found out.

$$\theta_i(t) = \begin{cases} \left(\theta_{i_f} - \theta_{i_{in}}\right)\left(\frac{t}{t_m} - \frac{1}{2\pi}\sin\frac{2\pi t}{t_m}\right) + \theta_{i_{in}};\ 0 \le t \le 1\text{ s} \\ 0;\ 1\text{ s} \le t \le 2\text{ s} \end{cases} \tag{6.24}$$

where subscript $i = 1, 2$. $\theta_i(t)$ is the angular motion of the i^{th} joint, $\theta_{i_{in}}$ is $\theta_i(t)$ at $t = 0$, θ_{i_f} is $\theta_i(t)$ at the end of the joint motion, time step size t_{inc} taken as $t_{inc} = 0.01$s, $t_m = 1$ s is the time of the motion. The same motion profiles for both the joints have been applied for all the cases and tip deflections of the manipulator have been observed in all cases. $\theta_{1_{in}} = \frac{\pi}{2}$ rad, $\theta_{1_f} = 0$ rad, $\theta_{2_{in}} = \pi$ rad and $\theta_{2_f} = 0$ rad.

The inputs to the motors in the form of the angular displacement, velocity, and acceleration of the motors at joint 1 and joint 2 have been shown in Figs. 6.4(a), 6.4(b) and 6.4(c) respectively. The tip deflections of the 2nd link $w_{Tip\,2}$ for different cases that have been mentioned in section 6.2, have been shown in Figs. 6.5-6.7 under subsections 6.4.1-6.4.3 as follows. The observations have been discussed in the last of these subsections.

6.4.1 Tip Deflection of the Manipulator without any String Attachment

Case 1: When the flexible link is not stiffened with any string, the tip deflection is shown in Fig. 6.5.

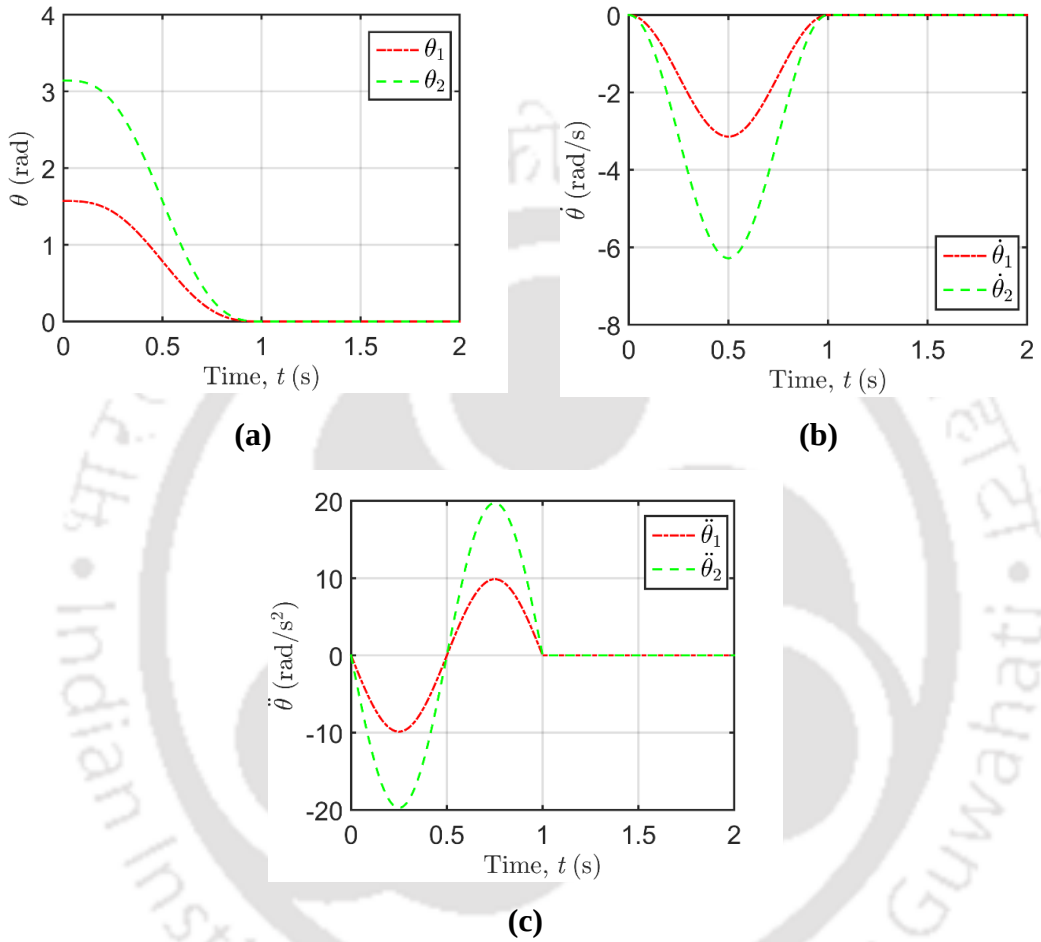

Figure 6.4: Motion of joint 1 and joint 2: **(a)** angular displacement, **(b)** angular velocity, and **(c)** angular acceleration.

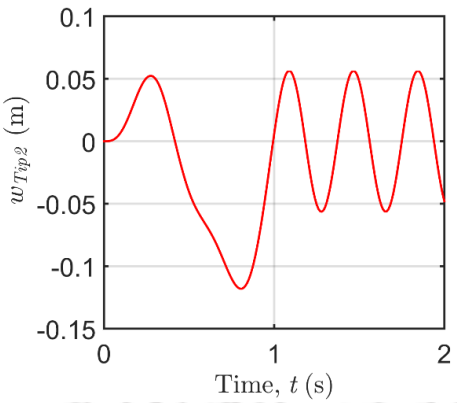

Figure 6.5: Tip deflection of the SSRFTLM with a payload but without any string - stiffening.

6.4.2 Tip Deflection of the String-Stiffened Manipulator without Considering String Vibration

Case 2: Applying boundary condition 1, that is, when the end of the 2nd link is assumed to be hinged support, the tip deflection is shown in Fig. 6.6(a).

Case 3: when boundary condition 2 for the flexible link is considered, that is, when the end of the 2nd link is assumed to be free to move in its plane of motion, the tip deflection is as shown in Fig. 6.6(b).

Case 4: when the boundary condition 3 for the 2nd link, that is, the tip of the 2nd link is not at all allowed to move, the tip deflection is given in Fig. 6.6(c).

6.4.3 Tip Deflection of the String-Stiffened Manipulator When String Vibration is Also Considered

When the link vibrates it will also vibrate the string attached to the tip of the link which, in turn, affects the tension force applied by the string on the link because with the vibration of the link the string may become loose or tight depending on the tip deflection of the link on any one side of the link. In that case, tension in the string will vary as given by Eq. (5.29) of Chapter 5. However, the effect of string vibration has not been found to be so prominent on the tip deflection for small deflection. Because of this, instead of finding the dynamic change of tension in the string

during the motion of the link only the maximum value of change in the tension in any one of the two strings has been considered. Here these effects have been found for hinge-supported beam, i.e., when Case 2, is considered for comparison. Therefore, 3 more cases arise depending upon the modeling of the string vibration problem that whether the end of the string that is attached to the link tip is modeled as the end attached to a spring or spring-mass system or directly to the link tip.

Case 5: when one of the ends of the string is fixed and the other is tied to the spring, the tip deflection is shown in Fig. 6.7(a).

Case 6: But at the tip of the 2nd link there is a payload so a better way of modeling the string is to consider as one of the ends of the string is fixed and the other tied to a spring-mass system. Then the link tip deflection is found to be as shown in Fig. 6.7(b).

Case 7: In this case, no idealization of the string ends has been considered and while one end of the string is fixed the other end is tied to the link tip which is also oscillating with its own dynamic behavior. In that case, the tip deflection of the manipulator is as shown in Fig. 6.7(c).

Here, it is observed that when the tip of the SSRFTLM is assumed to be hinged supported, the deflection of SSRFTLM [see Fig. 6.6(a) and Table 6.2] compared to the rigid-flexible 2-link manipulator of the same parameters but without any string stiffening has reduced by around 99%. The same is the case when the payload at the tip of the SSRFTLM is assumed to be exactly balanced by the string forces in Case 4 so that tip displacement is not allowed at all where the reduction in tip deflection [Fig. 6.6(c)] is found to be around 100%. In the case of Case 3 [Fig. 6.6(b)], it is seen that tip deflection is more compared to Case 2 and Case 4 which is expected because here no restriction for link tip movement has been applied in the boundary conditions. But, here also the reduction in tip deflection compared to Case 1 is as high as 96% approx.

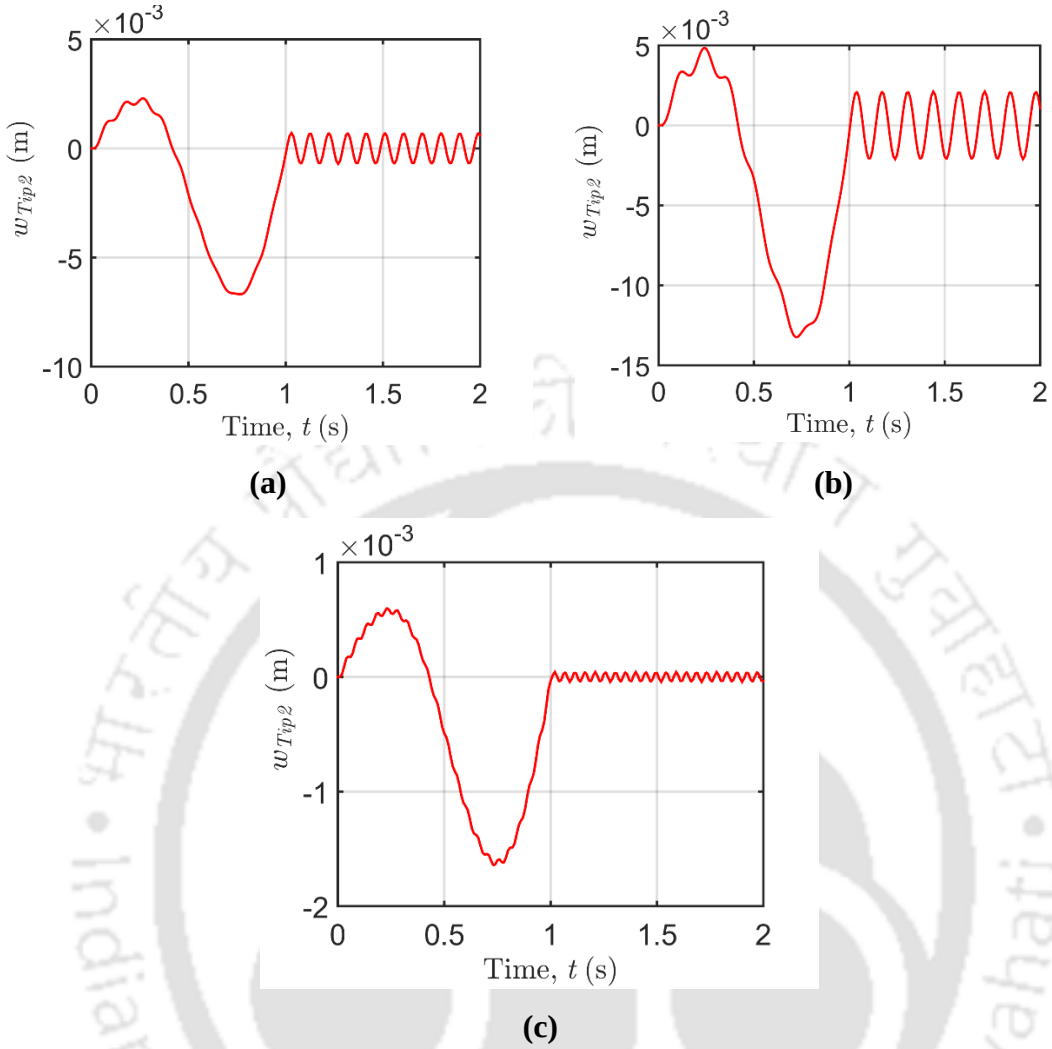

Figure 6.6: Tip deflection of the SSRFTLM in **(a)** Case 2, **(b)** Case 3, and **(c)** Case 4.

This also seems to be a more practical situation because in actual practice the link tip cannot be constrained to have zero displacements. This is a huge improvement in controlling the tip residual vibration which has also been shown experimentally for a single-link flexible manipulator by the work of [Dixit and Kumar (2016)]. The analytical modeling of the problem will help in the precise control of the link tip oscillations that may adversely affect the functioning of the manipulator. It is hard to understand by the authors of this paper that why the researcher's community did not take interest in the investigation of the advantage or disadvantages of the technique of string-stiffening of a flexible link manipulator for so long. This may be due to the reasons that strings in themselves are highly flexible and may pose another set of problems such as the problem of joint flexibility, foreshortening, instability, etc. But one cannot preclude their use in such applications because if

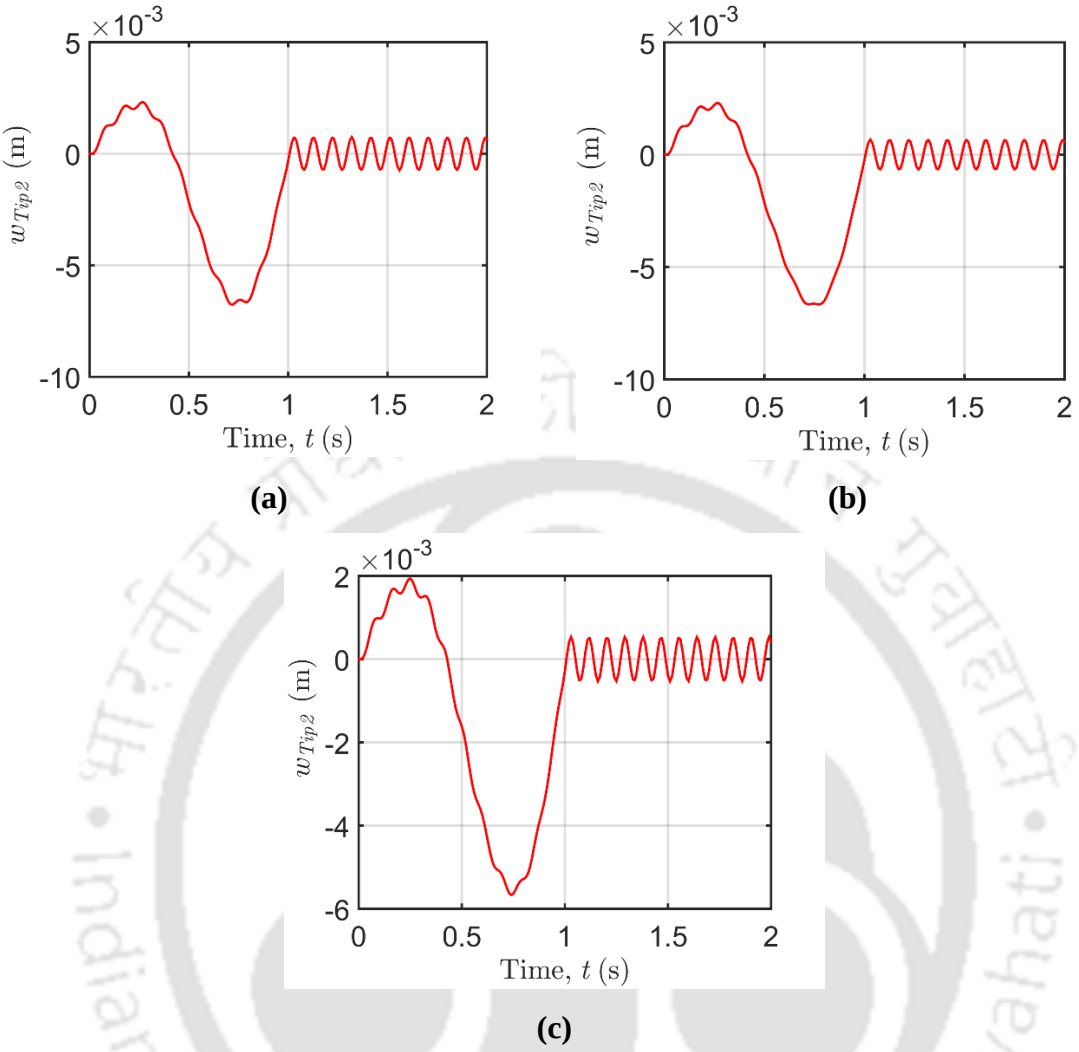

Figure 6.7: Tip deflections of the SSRFTLM in **(a)** Case 5, **(b)** Case 6, and **(c)** Case 7.

one does the proper systematic mathematical analysis of their behavior during operations of the manipulator; it may prove a promising technique for their (of strings) use in lightweight manipulators. Cables are already being used in bridge structures for supporting and vibration containment.

The tip deflections of the SSRFTLM near the end of the motion and the fundamental natural frequencies of its vibrations for each of the 7 Cases mentioned above have been given in Table 6.2. The percentage reductions in amplitudes of vibrations with respect to Case 1 have also been shown in the table.

Table 6.2: Values of tip deflections and first natural frequencies of vibration of the SSRFTLM

(PR1 = % reduction in amplitude of vibration with respect to Case 1, PR2 = Percentage reduction in amplitude of vibration with respect to Case 2)

Case	Fundamental frequency (in Hz)	Link 2 tip deflection $w_{Tip\,2}$ in (m)	PR1	PR2
Case 1	2.6442	5.627×10^{-2}		
Case 2	3.3650	6.896×10^{-4}	99	
Case 3	2.9709	2.113×10^{-3}	96	
Case 4	5.5162	4.137×10^{-5}	100	
Case 5	3.3639	7.036×10^{-4}	99	-2
Case 6	3.3641	6.532×10^{-4}	99	5
Case 7	3.3650	5.214×10^{-4}	99	24

6.4.4 Verification of Results

Results obtained from the dynamic analysis of the SSRFTLM have been verified with the experimental result of the work done by Dixit and Kumar (2016) using the same parameters for the flexible link and trajectory along with the same initial conditions. But here, the length and mass of the first link have been taken to be zero and both the joints have been given the same angular motion profiles so that the second hub coincides with the first hub. The dimensions and material properties of the flexible link of the SSRFTLM have been taken according to the paper mentioned above and have been given in Table 6.3.

The same quintic polynomial has been taken for the inputs to the motors at both the hubs for time $t = 1$ s so that hubs have coinciding motion:

$$\theta_i(t) = a_0 + a_1 t + a_2 t^2 + a_3 t^3 + a_4 t^4 + a_5 t^5 \tag{6.25}$$

The initial and final positions of the two links respectively at time $t = 0$ s and $t = 1$ s are as follows:

$\theta_i(0) = 0$ rad, $\dot{\theta}_i(0) = 0$ rad/s, $\ddot{\theta}_i(0) = 0$ rad/s^2, $\theta_i(1) = \frac{\pi}{4}$ rad, $\dot{\theta}_i(1) = 0$ rad/s, $\ddot{\theta}_i(1) = 0$ rad/s^2

Table 6.3: Dimensions and material properties of SSSLFM [Dixit and Kumar (2016)]

Parameters	**Value**
Length of the rigid link	0 m
Mass of the rigid link	0 kg
Dimension of the flexible link	$500 \times 30 \times 1.5$ mm^3
The distance of cable attachment from the shaft axis	7.0×10^{-2} m
Mass of payload	0.18 kg
Density of link	7800 kg/m^3
Diameter of cable	0.8×10^{-3} m
Number of cables	1 pair
Cable material density	7800 kg/m^3
Target rotation	45°
Time duration of the manipulator motion	1s

where subscript $i = 1,2$; against the quantities shows the values for the respective joint motions. The link tip motion has been observed for $t = 5$ s. From these conditions, trajectories obtained for the motions of joints are as shown in Figs. 6.8(a), 6.8(b), and 6.8(c).

The initial conditions taken to solve Eq. (6.11) are $q = \dot{q} = 0$. Equation (6.11) has been solved for the boundary conditions in which the tip of the flexible link is supposed to be hinge supported. That is, the boundary conditions I(a) is applied [as taken in the paper by Dixit and Kumar (2016)] with equal values of tensions in the strings T_1, T_2 and angles of strings with the link plane at its tip ϑ_1 and ϑ_2, i.e., $T_1 = T_2$; $\vartheta_1 = \vartheta_2 = \tan^{-1}\frac{70\times10^{-3}}{500\times10^{-3}}$. The tensions in the strings T_1, T_2 are expressed in terms of the critical load of buckling $P_{Cr} = \frac{\pi^2 EI}{l_f^2}$ where κ is the effective length factor for the beam or link. The results obtained for tip deflections for different values of tensions in the pair of strings have been shown in Fig. 6.9.

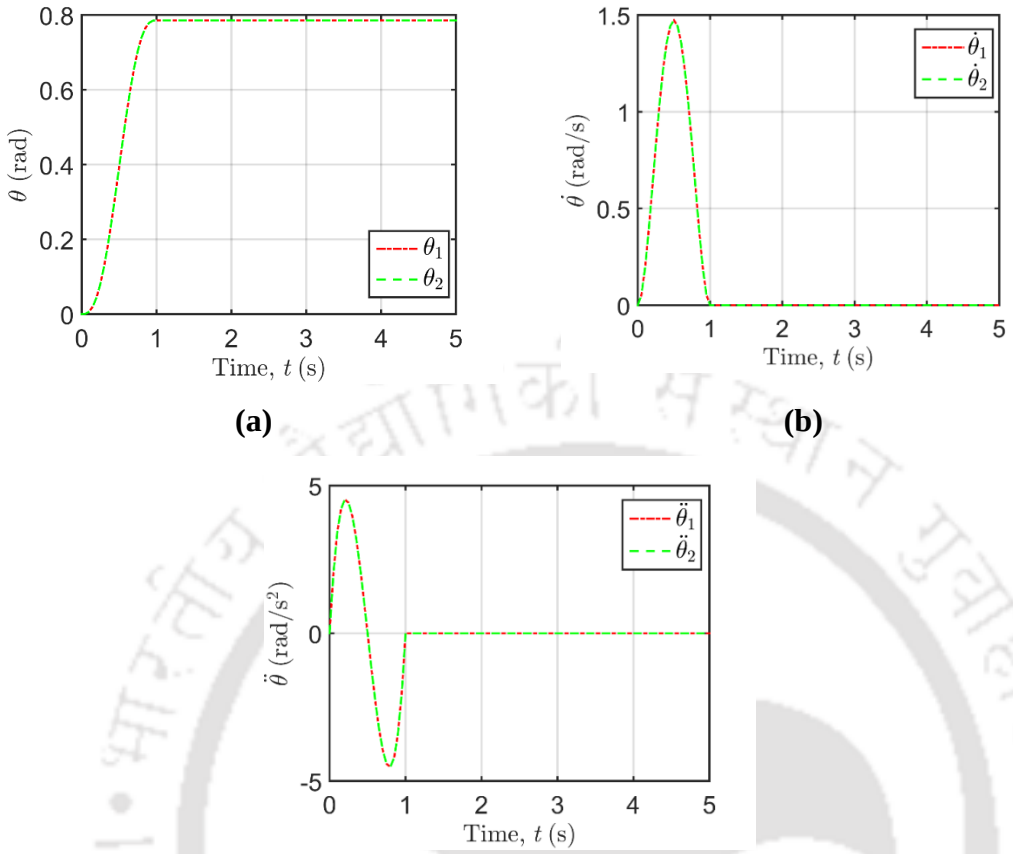

Figure 6.8: Motion of joint 1 and joint 2: **(a)** angular displacement, **(b)** angular velocity, and **(c)** angular acceleration.

The values of tip deflections $w_{Tip\,2}$ near the end of the motions of the manipulator and its frequencies of vibrations for different values of tensions in the pair of strings (in terms of the percentage of critical load of buckling of the link) have been noted down in Table 6.4. The maximum values of tip deflections of the manipulator at the steady state have been compared with the experimental result (i.e. Fig. 14) of the paper [Dixit and Kumar (2016)].

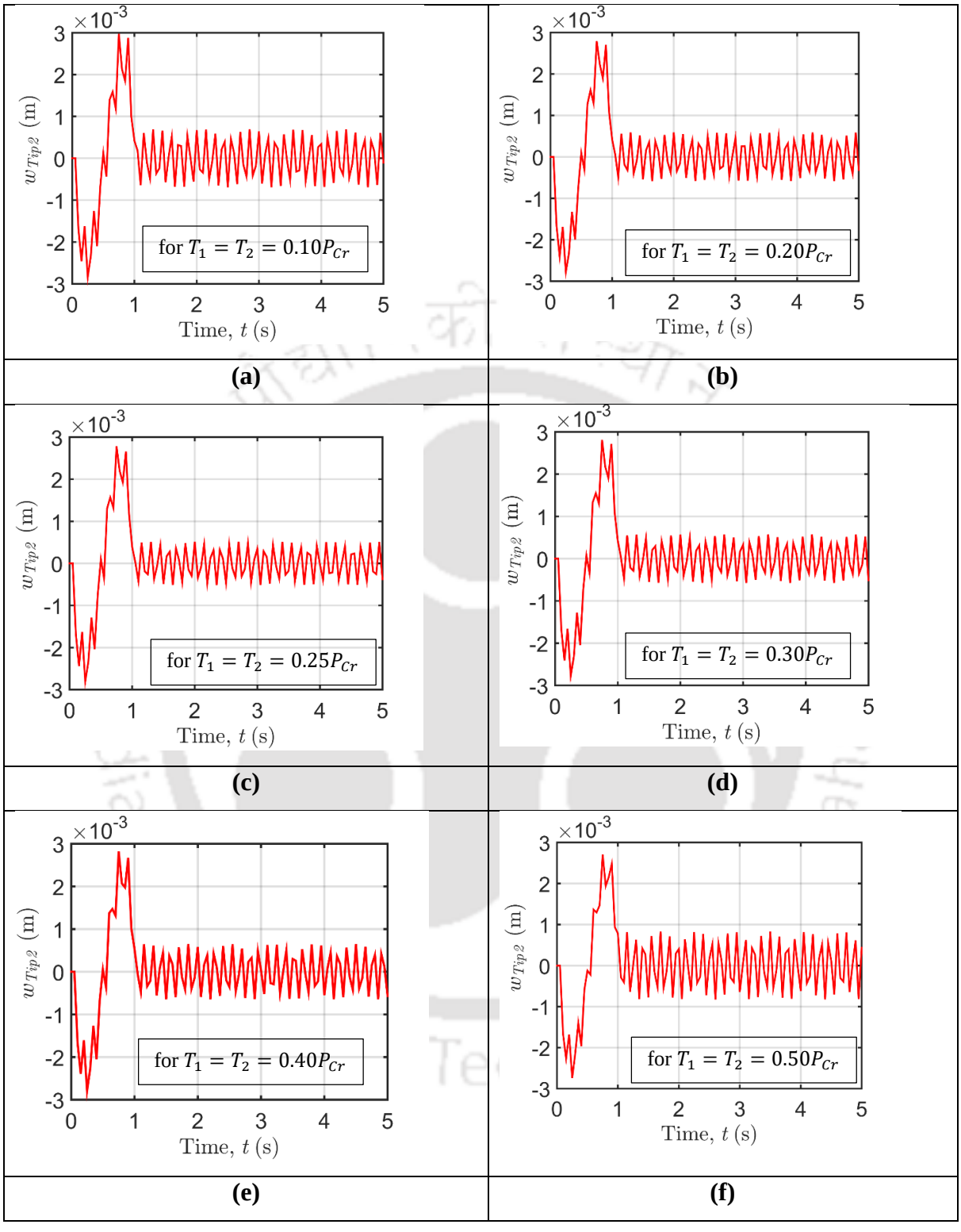
×10^-3
w_{Tip2} (m)
Time, t (s)
for $T_1 = T_2 = 0.10P_{Cr}$
(a)
for $T_1 = T_2 = 0.20P_{Cr}$
(b)
for $T_1 = T_2 = 0.25P_{Cr}$
(c)
for $T_1 = T_2 = 0.30P_{Cr}$
(d)
for $T_1 = T_2 = 0.40P_{Cr}$
(e)
for $T_1 = T_2 = 0.50P_{Cr}$
(f)

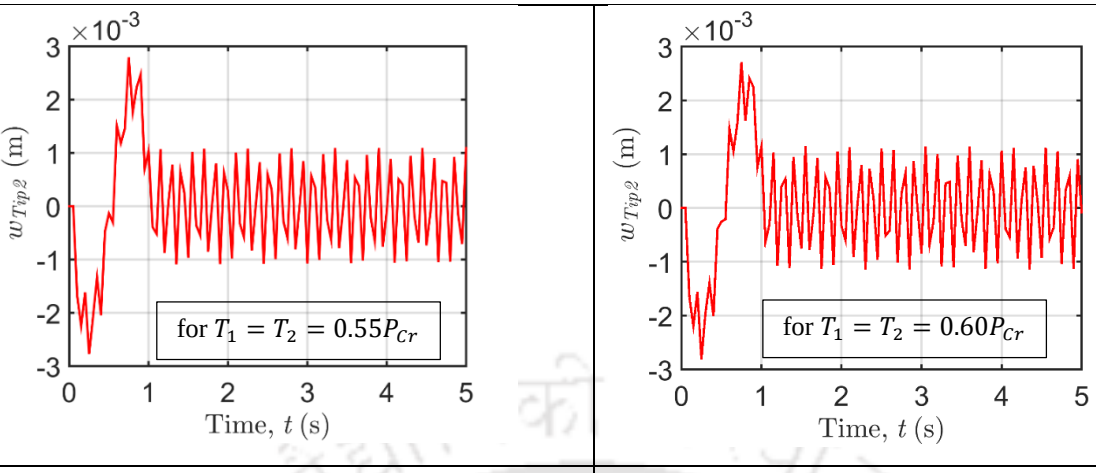

(g) **(h)**

Figure 6.9: Tip deflection $w_{Tip\,2}$ when tensions T_1 and T_2 in the strings are: **(a)** $T_1 = T_2 = 0.10P_{Cr}$, **(b)** $T_1 = T_2 = 0.20P_{Cr}$, **(c)** $T_1 = T_2 = 0.25P_{Cr}$, **(d)** $T_1 = T_2 = 0.30P_{Cr}$, **(e)** $T_1 = T_2 = 0.40P_{Cr}$, **(f)** $T_1 = T_2 = 0.50P_{Cr}$, **(g)** $T_1 = T_2 = 0.55P_{Cr}$, and **(h)** $T_1 = T_2 = 0.60P_{Cr}$.

Table 6.4: Values of tip deflections and frequencies of vibrations of the manipulator for different values of tensions in the pair of strings

Tension in strings	**Fundamental frequency (Hz)**	**Link 2 tip deflection $w_{Tip\,2}$ (m)**
$T_1 = T_2 = 0.10P_{Cr}$	4.6196	6.862×10^{-4}
$T_1 = T_2 = 0.20P_{Cr}$	5.5514	5.862×10^{-4}
$T_1 = T_2 = 0.25P_{Cr}$	5.9630	5.002×10^{-4}
$T_1 = T_2 = 0.30P_{Cr}$	6.3480	5.754×10^{-4}
$T_1 = T_2 = 0.40P_{Cr}$	7.0551	6.49×10^{-4}
$T_1 = T_2 = 0.50P_{Cr}$	7.6976	8.276×10^{-4}
$T_1 = T_2 = 0.55P_{Cr}$	7.9995	1.083×10^{-3}
$T_1 = T_2 = 0.60P_{Cr}$	8.2904	1.151×10^{-3}

Since the tension in the pair of cables has not been mentioned in [Dixit and Kumar (2016)], here, the values of tip deflections of the manipulator have been obtained for different values of the tensions in the strings and compared with their experimental result. It is seen from Table 6.4 that when the tensions in the strings $T_1 = T_2 = 0.30P_{Cr}$, the steady state value of tip deflection matches

well with that of Fig. 14 of the paper. Also, when the tensions in the strings are $T_1 = T_2 = 0.30P_{cr}$, the value of frequency of oscillations of the flexible link, 6.3480 Hz matches well with that (6.244 Hz) of the paper. It can also be seen from the present work that as tensions in the strings increase, the tip deflections decrease first and then again increase. This may be partly due to the foreshortening effect of string tensions and the combined effect of inertia force and buckling phenomena. Because of the inertia effect of the payload, the forces due to strings along the link shift away from the centroid of the cross-section of the flexible link, causing early yielding or buckling of the link. But, due to the tight holding of the link by the string from the opposite side, it can not deflect much. This observation highlights the importance of considering the effects of tension forces in the pair of strings that have not been found in the works of Dixit and Kumar (2016) and Tang et al. (2021). Changing of frequency of vibration of the flexible link with the tensions in strings shows that the stiffness of the flexible link can be varied according to the needs of a user.

6.4.5 Control of Tip Vibration

Despite using a pair of strings to control the tip deflection of the manipulator, it is observed that although the amount of deflection is greatly reduced, the vibration of the tip in the absence of any damping still persists. This poses problems in job handling. Therefore, control of tip vibration is necessary to take advantage of string stiffening. One of the very popular methods of control is to apply a proportional-integral-derivative (PID) controller for the task. However, controlling a flexible link is a very tedious task because of the highly coupled and nonlinear nature of the problem.

6.4.5.1. Flexible Link Control

Gain factors for applying PID controller to the manipulator with only link flexibility have been taken by trial and error method and are shown in Table 6.5. To control the flexible link along with the joints of the manipulator, first, the PID control has been applied at the joint level for up to 1 second when the manipulator is in motion. Thereafter, impedance control has been applied to control the flexible link vibration.

Table 6.5: Controller gains

Controlled quantities	**Controller gains K_P, K_I and K_D values**		
X-coordinate	$K_{P_x} = 2000$	$K_{I_x} = 25$	$K_{D_x} = 100$
Y-coordinate	$K_{P_y} = 2000$	$K_{I_y} = 25$	$K_{D_y} = 150$
Joint 1 angular displacement	$K_{P\theta_1} = 750$	$K_{I\theta_1} = 100$	$K_{D\theta_1} = 200$
Joint 2 angular displacement	$K_{P\theta_2} = 750$	$K_{I\theta_2} = 100$	$K_{D\theta_2} = 200$

θ_{id}, $\dot{\theta}_{id}$ and $\ddot{\theta}_{id}$ are taken from Eq. (6.24) and as shown in Fig. 6.4. With initial conditions $\theta_1 = \pi/2$ rad, $\theta_2 = \pi$ rad, $\dot{\theta}_1 = \dot{\theta}_2 = 0$ rad/s, $q = 0$, $\dot{q} = 0$ and initial values of cumulative errors for θ_i, x and y are equal to zero, Eqs. (6.13) and (6.17) can be solved together to find the controlled motion of the link tip as shown in Figs. 6.10(a-f). Figure 6.10(a) shows the tip deflection link 2, $w_{Tip\,2}$ while Fig. 6.10(b) gives the rate of change of the tip deflection $\dot{w}_{Tip\,2}$ with respect to (w.r.t.) time. Figs. 6.10 (c-d) represent the actual and desired angular displacements at joints 1 and 2 respectively while Figs. 6.10(e-f) give the actual and the desired angular speeds for these joints. From Fig. 6.10 it can be seen that the oscillations of the manipulator tip have vanished. $\dot{w}_{Tip\,2}$ became zero. The joint motions also try to follow the desired trajectories. This means that the SSRFTLM can now be used without any problem in job handling. Here, joint flexibility has not been introduced into the system. However, joint flexibility may not be avoidable in an SSRFTLM. The control of the SSRFTLM with both joint and link flexibilities has been mentioned in the next section.

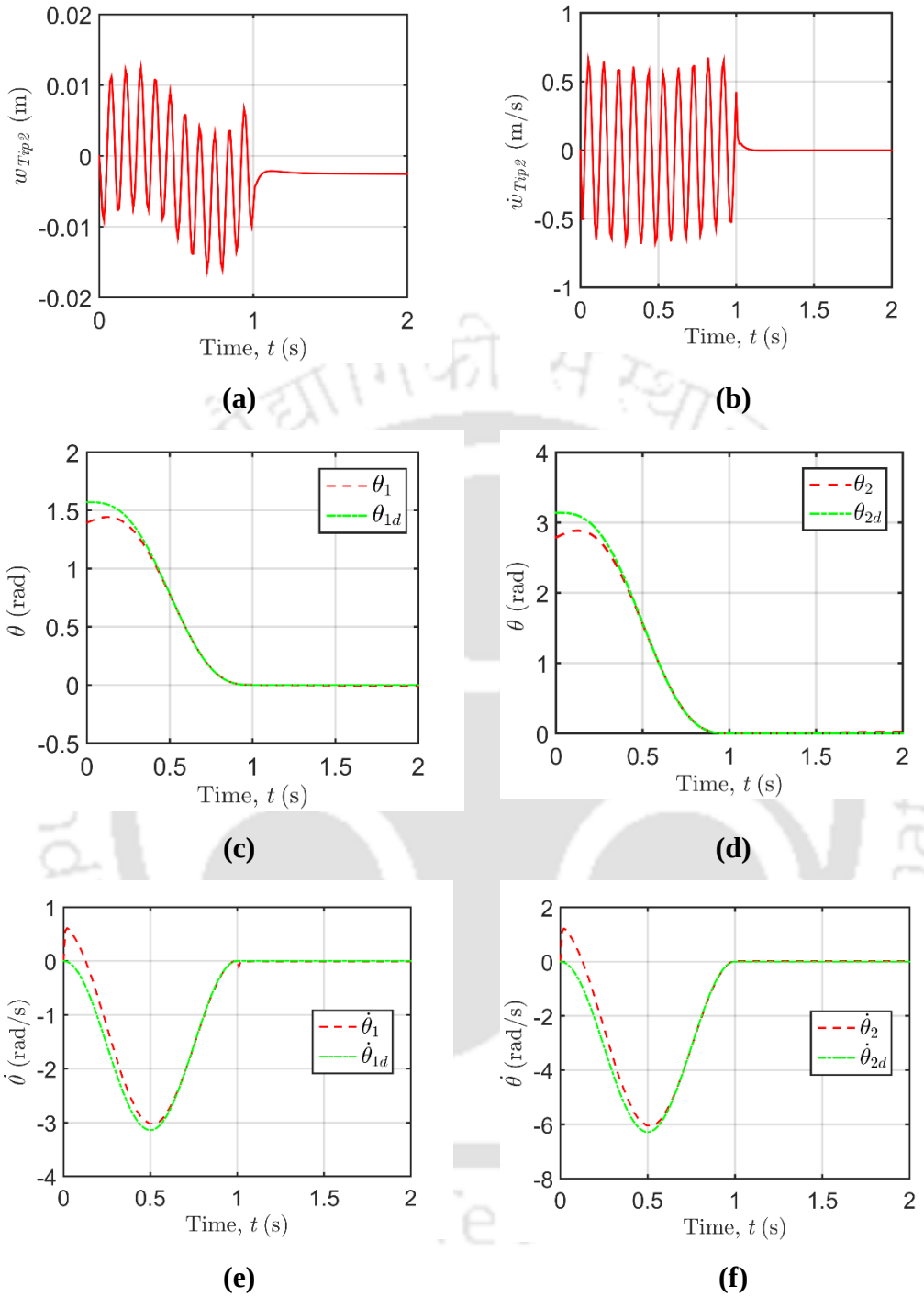

Figure 6.10: Tip deflection control of the SSRFTLM: **(a)** tip deflection of link 2 $w_{Tip\,2}$, **(b)** rate of change of tip deflection of link 2 $\dot{w}_{Tip\,2}$ w.r.t. time, **(c)** joint angular displacement of link 1, **(d)** joint angular displacement of link 2, **(e)** joint angular speed of link 1, and **(f)** joint angular speed of link 2.

6.4.5.2. Flexible Joint and Flexible Link Control

Here in addition to the link flexibility, flexibilities in both the joints also have been considered. The joint properties of the SSRFTLM have been taken as given in Table 6.6.

To control both the joint and link flexibilities simultaneously here impedance control along with the APID control have been applied. Initial conditions are taken to solve Eqs. (6.20), (6.21), and (6.22) are: $\gamma_1 = \gamma_2 = \frac{\pi}{180}$ rad at $\tau_t = 0$s, i.e., $\gamma_{10} = \gamma_{20} = \frac{\pi}{180}$ rad and $\frac{d\gamma_1}{d\tau_t} = \frac{d\gamma_2}{d\tau_t} = 0$ rad/s at $\tau_t =$ 0s, i.e., $\left(\frac{d\gamma_i}{d\tau_t}\right)_{\tau_t=0} = 0$ rad/s and $(\theta_1)_{t=0} = \frac{\pi}{2}$ rad, $(\theta_2)_{t=0} = \pi$ rad $q_0 = 0$; $\left(\dot{\theta}_1\right)_{t=0} = \left(\dot{\theta}_2\right)_{t=0} =$ 0 rad/s, $\dot{q}_0 = 0$, initial cumulative errors for θ_i, x and y are taken to be zero, where subscript $i = 1, 2$ for joint 1 and joint 2 respectively. The control gain factors have been kept unchanged as given in Table 6.5.

Table 6.6: Joint properties

Joint	Joint stiffness (Nm/rad)	Motor mass (kg)	The radius of gyration of the motor (m)	Moment of inertia of the motor (kg m^2)
Joint 1	$K_{t_1} = 150$	$M_{m_1} = 0.900$	$R_{H_1} = 0.0375$	$J_{m_1} = 6.3281 \times 10^{-4}$
Joint 2	$K_{t_2} = 100$	$M_{m_2} = 0.750$	$R_{H_2} = 0.0300$	$J_{m_2} = 3.3750 \times 10^{-4}$

Now solving Eqs. (6.20) and (6.21) for θ and q, one gets the results as shown in Figs. 6.11(a-f). Fig. 6.11(a) shows the tip deflection of link 2 $w_{Tip\,2}$ while Fig 6.11(b) shows the rate of change of tip deflection w.r.t. time. Figs. 6.11(c) and 6.11(d) represent the actual and desired values of joint angular displacements with respect to time t for joints 1 and 2 respectively. Figs. 6.11(e) and 6.11(f) give the actual and desired values of joint angular speeds for joints 1 and 2 respectively.

In Fig. 6.11 also, it can again be seen that oscillations of the manipulator tip disappeared. The joint motions of the SSRFTLM also can be seen to follow the desired trajectories in satisfactory manners. The problem with the APID control that has been used here is that it takes

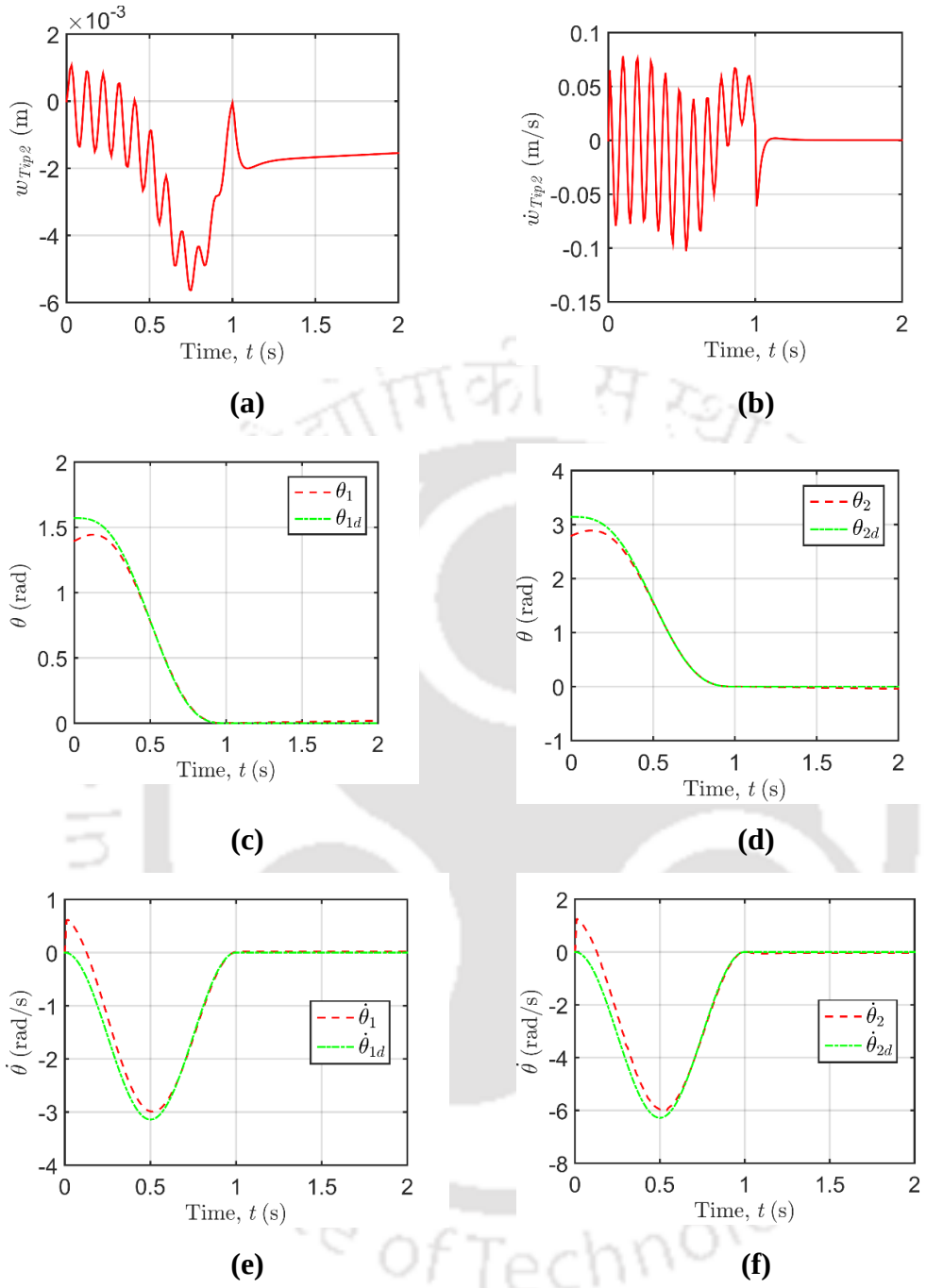

Figure 6.11: Tip deflection control of the SSRFTLM: **(a)** tip deflection of link 2 $w_{Tip\,2}$, **(b)** rate of change of tip deflection of link 2 $\dot{w}_{Tip\,2}$ w.r.t. time, **(c)** joint angular displacement of link 1, **(d)** joint angular displacement of link 2, **(e)** joint angular speed of link 1, and **(f)** joint angular speed of link 2.

an asymptotically longer to time to reach the equilibrium state. But, the problem of tip oscillation can still be controlled effectively.

6.5 Conclusions

In this work, a systematic mathematical analysis of a string stiffened rigid-flexible link manipulator (SSRFTLM) has been carried out. Since the string tensions may cause buckling at higher speeds of operations, the effects of geometric nonlinearities have been taken into account while modeling the flexible link. The axial displacement and nonlinear curvature resulting from large flexural deformation of the flexible link have been considered. For precise control of the SSRFTLM, accurate mathematical modeling and formulation of the problem have been tried to achieve by applying different boundary conditions. Also, the effect of tensions in the pair of strings has been investigated. It has been observed that how stiffening of a flexible link by a pair of strings can considerably reduce the tip deflection, as much as by 96.24%. However, due to the coupling effect of string vibration with that of the link, it may also introduce joint flexibility which has been tackled with the application of adaptive PID control. By this method with the addition of minimum weight to the manipulator, the stiffness of the flexible link can be increased considerably.

Chapter 7

Kinematic and Dynamic Analyses of Two 3R Co-ordinating Manipulators

7.1 Introduction

Many chemicals that are used in the laboratories or in pharmaceutical industries are found to be of dangerous nature that may potentially harm operator of such chemicals. For handling such chemicals coordinating manipulators which can cooperatively handle a given task can be employed to minimize the risk to the operators. For the coordination among these manipulators the first and foremost condition is that motions of these manipulators must be synchronized in terms of time of motion and their positions and orientations. Otherwise, instead of carrying the task properly, they may spoil the job. For example, in case of handling of chemicals, the manipulator holding the jar of chemical for pouring may pour it before the other manipulator with a collecting jar take the jar at right position and in right orientation and that too at proper time of pouring. Any fault in synchronization of motion and occurrence of events in handling of the chemical may lead to catastrophe rather than reducing the hazard. So, in this work synchronizations of motion, position and orientation of handling manipulators that work coordinately in cooperative manner have been considered. For this, one needs to model the forward and inverse kinematics along with dynamics of the coordinating manipulators.

In this work, kinematic and dynamic analyses of two similar kinds of 3R manipulators to handle chemicals cooperatively have been carried out. For this, it is necessary to determine and control the position and orientation of the liquid handling containers while the process is in operation. The position and orientation of the containers can be determined with the help of appropriate visual sensors that can be fitted on the manipulator end. Depending upon the required position and orientation of the containers, a suitable trajectory of the manipulator tip can be planned. The manipulators have to carry out the process smoothly without any spill or overflow of chemicals. For this, an accurate dynamic analysis has to be carried out for the exact estimation of torque on joints and load that manipulators will be subjected to. Point-to-point interpolation methods can be

applied for trajectory planning if paths are not known in advance or the continuous path method also can be employed if paths are well-defined. In the present work, a continuous path trajectory has been used for the task to be carried out. Here an elliptical path for the manipulator carrying a container full of chemicals and a path comprised of vertical and horizontal straight lines for the manipulator carrying a collecting container have been planned for an example. At the end of each section of trajectories for both manipulators, quintic polynomial trajectories have been applied in order to have smooth joint torques. The Euler- Lagrange method for the dynamic analysis of a 3-link manipulator has been applied considering rigid links and joints. Later, the effect of gear backlash also has been considered on the dynamic behavior of these manipulators. In the following sections, the kinematics, dynamics, and trajectory planning of the proposed two similar types of cooperative manipulators have been carried out.

7.2 Kinematics of the Manipulators

Fig. 7.1 shows the schematic diagram of two 3R manipulators A and B where manipulator A lifts a container with chemical and pours it into another container that is held by robotic manipulator B.

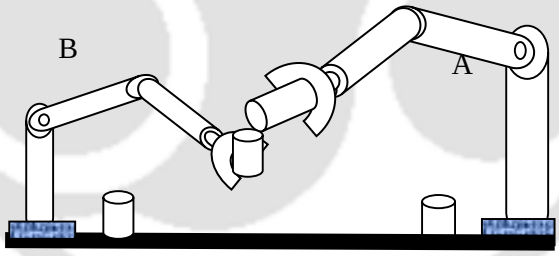

Figure 7.1: Schematic diagram of cooperative manipulators A and B handling hazardous chemicals.

The link coordinate system for the manipulators up to their grippers is shown in Fig. 7.2 which is similar to that of a PUMA 560 robot (Fu et. al. (1987)). The corresponding link coordinate parameters up to four axes have been given in Table 7.1 where θ_i and d_i are the joint angle and the joint offset distance while a_i and α_i are the link length and link twist angle, respectively for the i^{th} joint.

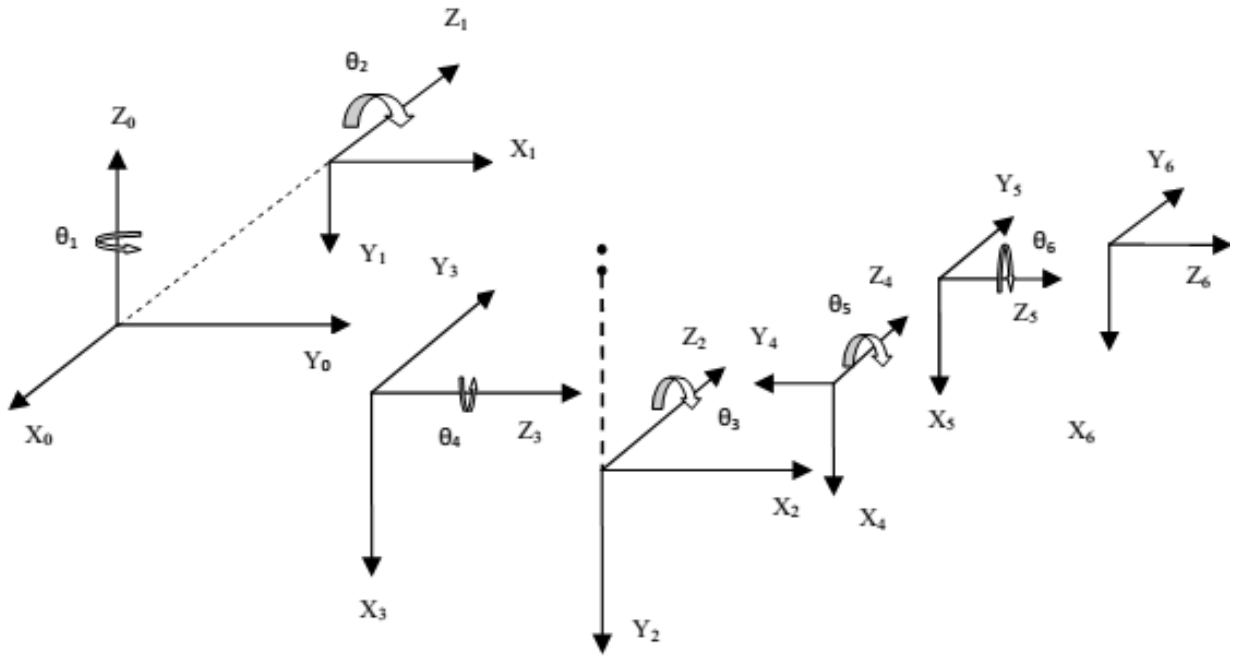

Figure 7.2: Link coordinate system for the two manipulators up to the gripper.

Table 7.1: Arm link coordinate parameters

Joint *i*	θ_i **(rad)**	d_i **(m)**	a_i **(m)**	α_i **(rad)**
1	θ_1	0	0	$-\frac{\pi}{2}$
2	θ_2	0.149.09	0.431.8	0
3	θ_3	0	-0.02032	$\frac{\pi}{2}$
4	θ_4	0.433.07	0	$-\frac{\pi}{2}$

The arm matrix equation [Schilling (2009)] can be given as

$$A_i^{i-1} = \begin{bmatrix} \cos\theta_i & -\cos\alpha_i \sin\theta_i & \sin\alpha_i \sin\theta_i & a_i \cos\theta_i \\ \sin\theta_i & \cos\alpha_i \cos\theta_i & -\sin\alpha_i \cos\theta_i & a_i \sin\theta_i \\ 0 & \sin\alpha_i & \cos\alpha_i & d_i \\ 0 & 0 & 0 & 1 \end{bmatrix} \quad (7.1)$$

Applying the respective values from the above table in the arm matrix above we get the following arm equation for the robotic manipulator. Using the arm matrix equations, the transformation

matrix for the wrist of the manipulator with respect to the base coordinate system can be given by Eq. (7.2) as follows

$$T = A_4^0 = \begin{bmatrix} n_x & s_x & a_x & p_x \\ n_y & s_y & a_y & p_y \\ n_z & s_z & a_z & p_z \\ 0 & 0 & 0 & 1 \end{bmatrix} \tag{7.2}$$

where

$n_x = c_1c_{23}c_4 - s_1s_4;\ \ n_y = s_1c_{23}c_4 + c_1s_4;\ \ n_z = -s_{23}c_4;\ \ s_x = -c_1s_{23};\ \ s_y = -s_1s_{23};\ \ s_z = -c_{23};\ \ a_x = -c_1s_4c_{23} - s_1c_4;\quad a_y = -s_1s_4c_{23} + c_1c_4;\ \ a_z = s_4s_{23};\ \ p_x = c_1(a_2c_2 + a_3c_{23} + d_4s_{23}) - d_2s_1;\ p_y = s_1(a_2c_2 + a_3c_{23} + d_4s_{23}) + d_2c_1;\ p_z = d_4c_{23} - a_3s_{23} - a_2s_2;$

Here c and s stand for the cosine and sine functions respectively and c_{ij}/s_{ij} and c_k/s_k denote $\cos(\theta_i + \theta_j)/\sin(\theta_i + \theta_j)$ and $\cos\theta_k/\sin\theta_k$ respectively. These equations are used for both the robots for trajectory planning and dynamic analysis.

7.2.1 Inverse Kinematics

Angles for each joint for each of the two manipulators through which the joints have to be moved during the course of handling the chemical have been found geometrically by applying inverse kinematics technique [Eqs. (2.3-47), (2.3-56) and (2.3-63) in Fu et. al. (1987)].

7.3 Dynamic Equations

The first three links before the wrist are like the human torso, upper arm, and forearm of a human being and together determine the end effector position. At the end of the forearm, a wrist is formed using three articulated joints which determine the end effector orientation. The dynamics of the first three joints pose the greatest problem for developing a control algorithm of an RRR-type manipulator because of the coupling between joints that results in highly coupled and nonlinear dynamics [Anderson (1988)]. That is why kinematic and dynamic modeling is one of the important tasks in robotics. The Dynamic equation of motion for a manipulator with n degrees of freedom using the Euler-Lagrangian method without considering the gear backlash effect is given as

$$\tau_i = \sum_{j=1}^{n} D_{ij}\ddot{q}_{ij} + \sum_{j=1}^{n}\sum_{k=1}^{n} C_{ijk}\dot{q}_j\dot{q}_k + G_i + M_i \qquad (7.3)$$

where $i = 1,2,3, \ldots\ldots\ldots, n$; n is the number of links.

$q_i, \dot{q}_i, \ddot{q}_i$ = generalized position, velocity, and acceleration of i^{th} joint respectively,

τ_i = torque acting on i^{th} joint,

D_{ii}, D_{ij} = effective and coupling inertias for i^{th} link including actuator inertia I_{a_i} and inertia of gear and pinion assembly I_{G_i} of i^{th} joint,

C_{ij} , C_{ijk} = centripetal and Coriolis forces for i^{th} joint,

G_i= gravity loading for i^{th} joint,

M_i= torque at i^{th} joint due to load applied at the wrist.

7.3.1 Effect of Joint Flexibility

Up to now, joint torque neglecting the effect due to gear assembly has been considered. In this section the effect of gear inertia and backlash during meshing of gear and pinion has been considered. The following assumptions have been made while considering the effect of gear inertia and backlash during the meshing of gear and pinion:

- These gears and pinions have their axes very close to joint axes and aligned along the joint axes.
- The coriolis and centrifugal effect of gear assembly have been neglected.
- The effective moment of inertia of gear and pinion assembly to be 20% of actuator inertia for the respective joint.
- Joint torques due to backlash stiffness to be within 5% of joint torque of the manipulator joint when backlash effect is not considered.

Let θ_{g_i}= angle subscribed by ith joint gear about the respective Z axis Z_i,

θ_{p_i}= angle subscribed by ith joint pinion about the respective Z axis Z_i,

$\dot{\theta}_{g_i}$= angular velocity of ith joint gear about the respective axis Z_i,

$\dot{\theta}_{p_i}$= angular velocity of ith joint pinion about the respective axis Z_i,

I_{g_i}= moment of inertia of ith joint gear about the respective axis Z_i,

I_{p_i}= moment of inertia of i[th] joint pinion about the respective axis Z_i,

N_i= gear ratio between pinion and gear for i[th] joint (assumed to be 3 for all 3 joints).

It is assumed that links are directly attached to the respective gears so that $\theta_{g_i} = \theta_i$.

The linear displacement of the mesh point of pinion and gear along the line of action can be given as

$$x_{p_i} = r_{p_i}\theta_{p_i};\ x_{g_i} = \beta_i r_{g_i}\theta_{g_i} \tag{7.4}$$

where, r_{p_i}, r_{g_i} are the distance of the mesh point from the axis of i^{th} joint pinion and gear respectively and β_i is the factor by which gear deviates along the line of action due to gear backlash. If K_i is the meshing stiffness due to gear backlash at i^{th} joint, then the potential energy of gear assembly due to gear meshing is

$$V = \frac{1}{2}\sum_{i=1}^{3} K_i \left(x_{p_i} - x_{g_i}\right)^2 \tag{7.5}$$

Using the above relations V can be given as

$$V = \frac{1}{2}\sum_{i=1}^{3} K_i {r_{p_i}}^2 {N_i}^2 (1-\beta_i)^2 {\theta_i}^2 \tag{7.6}$$

Let

$$K_i {r_{p_i}}^2 {N_i}^2 (1-\beta_i)^2 = K_{T_i} \tag{7.7}$$

so that

$$V = \frac{1}{2}\sum_{i=1}^{3} K_{T_i} {\theta_i}^2 \tag{7.8}$$

where i=1,2,3. Here θ_i is generalized coordinate q_i.

Thus, taking into account the effect of gear inertia and backlash during the meshing of gear and pinion joint torques for the two manipulators up to their wrist can be given below

$$\tau_i = \sum_{j=1}^{n} D_{ij}\ddot{q}_{ij} + \sum_{j=1}^{n}\sum_{k=1}^{n} C_{ijk}\dot{q}_j\dot{q}_k + G_i + K_{T_i}q_i + M_i \tag{7.9}$$

Quantities in Eq. (7.9) have already been mentioned above.

7.4 Results and Discussion

Inertial properties of different links and actuators of both manipulators which are of similar kinds have been taken from Zomaya [1993] for hint purpose only and considered exactly not to be the same. They are given in Table 7.2 and Table 7.3. But here mass of link is supposed to be comprised of link mass as well as joint (actuator and gear) masses also.

Table 7.2: Link mass and center of gravity

Link	Mass (kg)	X (m)	Y (m)	Z (m)
1	m_1=12.95	0	0.309	0.039
2	m_2=22.36	-0.329	0.005	0.2038
3	m_3=5	0.02	0.014	0.0037

Table 7.3: Actuator and link Inertia

Link	I_a (kg.m^2)	I_{xx} (kg.m^2)	I_{yy} (kg.m^2)	I_{zz} (kg.m^2)
1	0.7766	2.351	0.1968	2.3457
2	2.3616	1.3313	4.313	3.4116
3	0.5827	0.07582	0.07766	0.01038

7.4.1 Trajectory Planning

Fig. 7.1 shows two robotic manipulators A and B whose bases are placed 0.9 m apart. Robotic manipulator A lifts a container with chemical placed at (0.5, 0.25, 0.2) from the global coordinate system and pours it at (0.4, 0.25, 0.5) into another container that is held at (0.4, 0.25, 0.496) by robotic manipulator B. It is assumed that the manipulators are at rest and in their home positions just before the trajectory starts. Here, trajectory is planned only for up to third link of manipulators instead of up to gripper. Manipulator A moves the container in an elliptical path in order to have smooth movement of chemical in container through its course without any spill or overflow because of slowly changing slope of the path. It takes 5 seconds to bring the container from the table to the position of pouring liquid during which another manipulator also takes the collecting container immediate to the pouring container.

The equation of elliptical path can be found by using the information of the initial and the final positions as given below.

For time t, $0 \leq t \leq 5$ second:

$$\frac{(x-h)^2}{a^2}+\frac{(z-k)^2}{b^2}=1,\ y=250\times10^{-3} \tag{7.10}$$

where

$a=100\times10^{-3}$ m, $b=300\times10^{-3}$ m, $h=-500\times10^{-3}$ m and $k=200\times10^{-3}$ m.

Manipulator B tries to lift an empty container placed at (0.2, 0.25, 0.2) vertically up in the same X-Z plane at Y=0.250 m so that it may not collide with any other container on the table and moves it horizontally towards the second manipulator and thereafter lifts it again vertically up to the pouring container and hold it at the level 4 mm below the pouring container as can be seen in Fig. 7.3. The trajectory for the task can be given in terms of following equations:

For time t, $0\leq t\leq 1$second:

$$x=300\times10^{-3},\ y=250\times10^{-3}\text{ and }\quad z=200\times10^{-3}(1+t) \tag{7.11}$$

For time t, $1\leq t\leq 3$ seconds:

$$x=(250+50t)\times10^{-3},\ y=250\times10^{-3}\text{ and }z=400\times10^{-3} \tag{7.12}$$

And for time t, $3\leq t\leq 5$ seconds:

$$x=400\times10^{-3},\ y=250\times10^{-3}\text{ and }z=(256+48t)\times10^{-3} \tag{7.13}$$

where x, y and z are in meter.

Figure 7.3 shows the trajectory simulation for both the manipulators A and B. The values in parenthesis in Fig. 7.3 represent the position coordinates of different parts of the two manipulators in order to show the snapshots of motions of these manipulators.

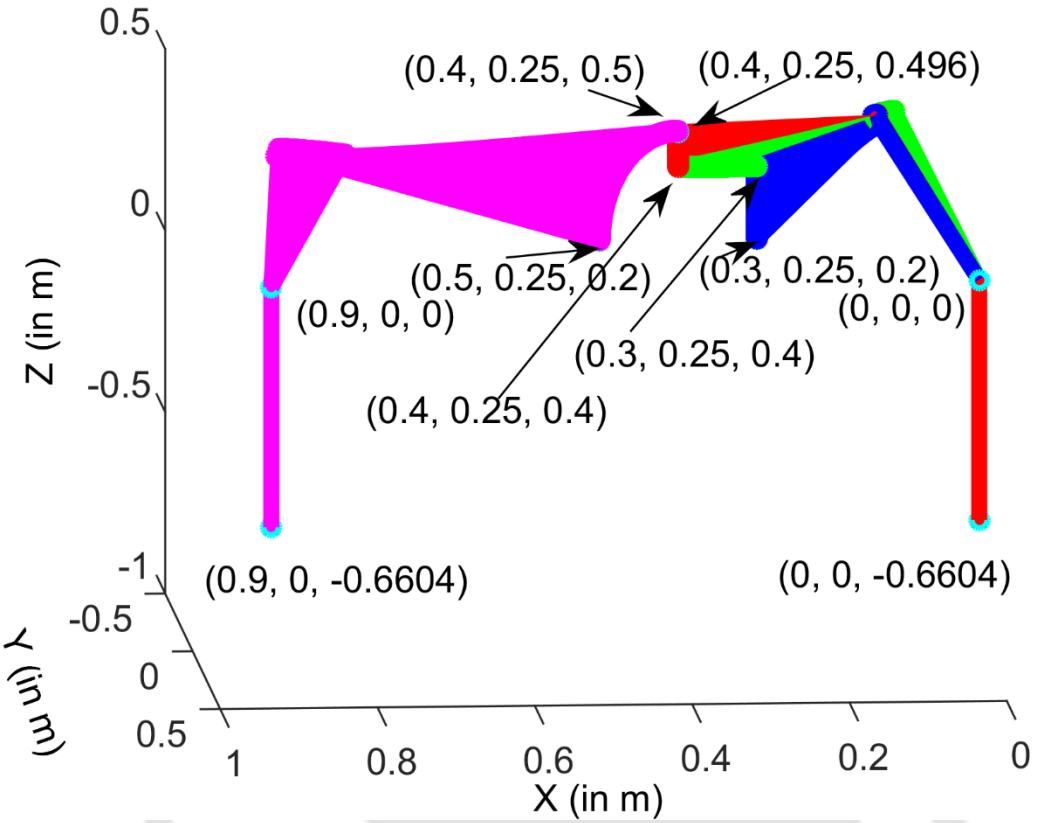

Figure 7.3: Two manipulators cooperatively handling hazardous chemicals (There is 4 mm of gap between the two containers at the time of pouring).

7.4.2 Calculation of External Load M_i on Wrist

Let the initial height of liquid in the pouring container be $h_0 = 0.20$ m. If a_0 be the average rate of pouring or collecting liquid and if it takes 60 seconds to empty a container full of liquid upto 0.20 m then

$$a_0 = \frac{(0.2-0)}{60} \text{ m/s} \tag{7.14}$$

The instantaneous height of liquid in a container or collecting container in meter can be given as

$$h = h_0 \pm a_0 t \tag{7.15}$$

where t is the time in seconds. Let $r = 0.025$ m be the radius of both the pouring and collecting container. The area of the container is

$$A = \pi \times r^2 \tag{7.16}$$

The instantaneous volume of liquid in the container

$$V = Ah \tag{7.17}$$

Water has been, for example, taken as the liquid chemical in the container whose density is $\rho = 1000$ kg/m^3. $\boldsymbol{g} = 9.81$ m/s^2 is the acceleration due to gravity. Let the mass of each container be $m_c = 0.075$ kg so that weight of each container is $\boldsymbol{w_c} = m_c\boldsymbol{g}$. Instantaneous gravitational force (in N) on end effector in X, Y, and Z-directions are

$$\boldsymbol{f_x} = \boldsymbol{w_c} + V\rho\boldsymbol{g}, \boldsymbol{f_y} = 0 \text{ and } \boldsymbol{f_z} = 0 \tag{7.18}$$

If $\boldsymbol{d_i}$ is the distance of the center of gravity of the container from the wrist in X, Y, and Z-directions, where $i = x, y, z$, then the moment on the wrist due to the container in X, Y, and Z-directions are respectively

$$\boldsymbol{M_x} = \boldsymbol{f_y} \times \boldsymbol{d_z}, \boldsymbol{M_y} = \boldsymbol{f_z} \times \boldsymbol{d_x} \text{ and } \boldsymbol{M_z} = \boldsymbol{f_x} \times \boldsymbol{d_y} \tag{7.19}$$

where quantities in bold letters show vector quantities. Here $\boldsymbol{d_y} = 0.075$ m has been taken for example.

The torques acting at the three joints of each of the manipulators A and B have been shown in Figs. 7.16-7.19 in which torque due to external loading have also been taken into account.

7.4.3 Kinematics and Dynamics of the Manipulators without Considering Joint Flexibility

First the kinematic and dynamic analyses have been carried out without considering effect of gear backlash and the analysis results are shown in Figs. 7.4 - 7.19. The angular displacements for the two manipulators have been shown in Figs. 7.4 and 7.6. But these displacements were giving very high and abrupt changes in angular velocities and accelerations at the start and end of each section of trajectories as can be seen in Figs. 7.8 and 7.10 for angular velocities and 7.12 and 7.14 for angular accelerations of joints which, in turn give rise to sudden and very high joint torques at the two ends as can be seen in Figs. 7.16 and 7.18. So, to minimize and produce smoothly varying torques as shown in Figs. 7.17 and 7.19, quintic polynomial trajectories has been applied at each end of trajectories as shown in Fig. 7.5 and 7.7 which give rise to smoothly varying angular joint velocities and accelerations as can be seen in Figs. 7.9 and 7.11 for velocities and 7.13 and

7.15 for accelerations. This resulted in reduction of maximum values of angular acceleration for elliptical path from 12.0929 rad/s^2 at second joint and 10.8193 rad/s^2 at third joint to respectively 0.3865 rad/s^2, and 0.5084 rad/s^2 as can be seen from Figs. 7.12 and 7.13. The maximum values of torques for the elliptical path have reduced from 59.3979 Nm to 12.9537 Nm for 2nd joint and from 6.1817 Nm to 0.4221 Nm for third joint which can be observed from Figs. 7.16 and 7.17. The reduction of maximum values of angular acceleration for path composed of vertical and horizontal lines from 147.533 rad/s^2 at second joint and 127.5507 rad/s^2 at third joint to respectively 5.4321 rad/s^2, and 5.2891rad/s^2 as can be seen from Figs. 7.14 and 7.15. The maximum values of torques for the elliptical path have reduced from 641.2638Nm to 19.0846 Nm for 2nd joint and from 95.0590 Nm to 4.7845 Nm for third joint which can be observed from Figs. 7.18 and 7.19.

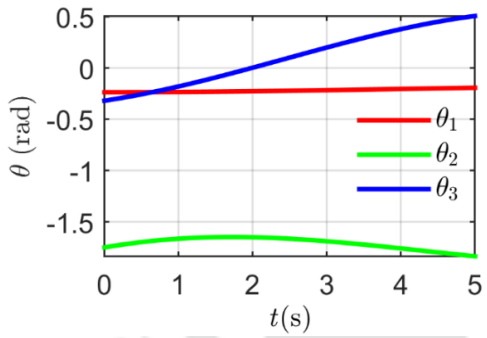

Figure 7.4: Joint angle of manipulator A before torque smoothening.

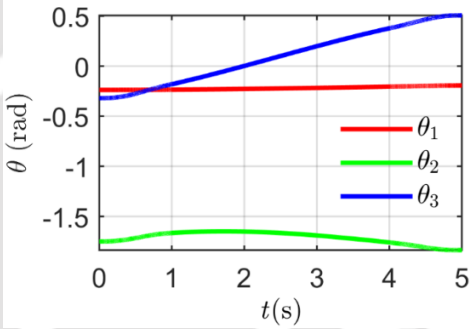

Figure 7.5: Joint angle of manipulator A after torque smoothening.

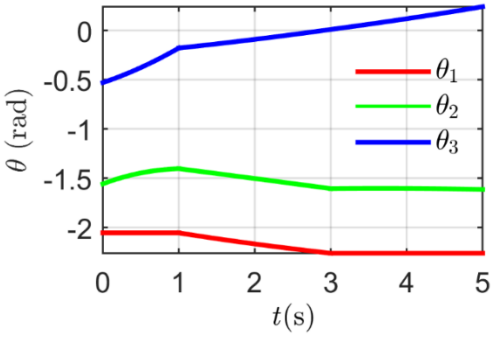

Figure 7.6: Joint angle of manipulator B before torque smoothening.

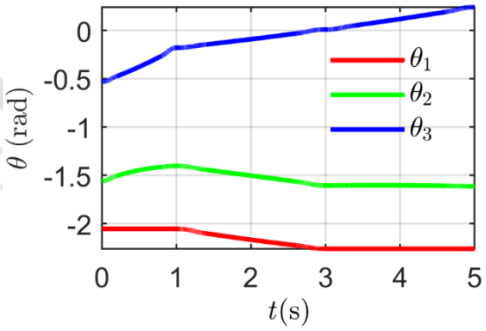

Figure 7.7: Joint angle of manipulator B after torque smoothening.

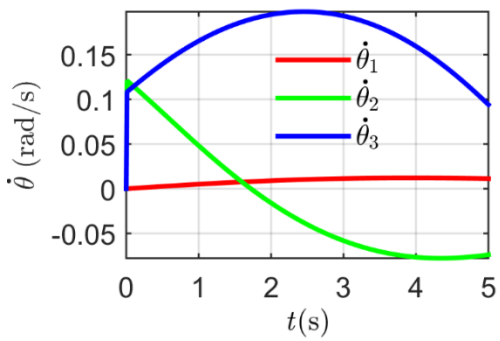

Figure 7.8: Joint velocity of manipulator A before torque smoothening.

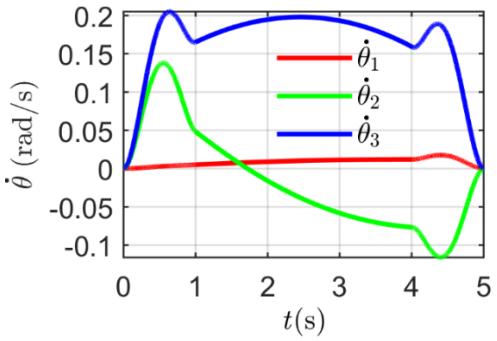

Figure 7.9: Joint velocity of manipulator A after torque smoothening.

By applying suitable quintic polynomial trajectories at each end of each section of trajectories for each of the manipulators, they can be started and stopped without violent motion.

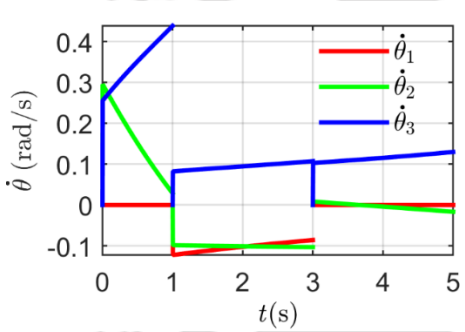

Figure 7.10: Joint velocity of manipulator B before torque smoothening.

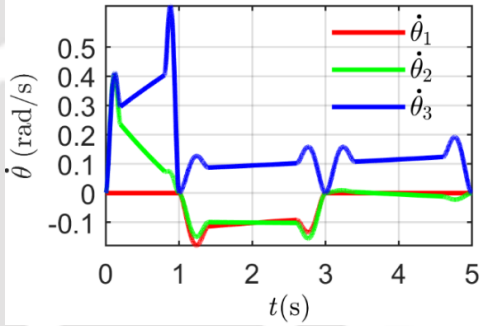

Figure 7.11: Joint velocity of manipulator B after torque smoothening.

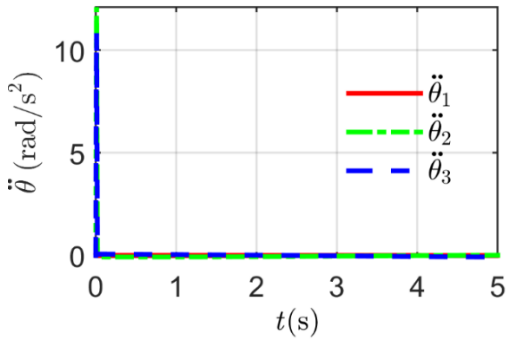

Figure 7.12: Joint angular acceleration of manipulator A before torque smoothening.

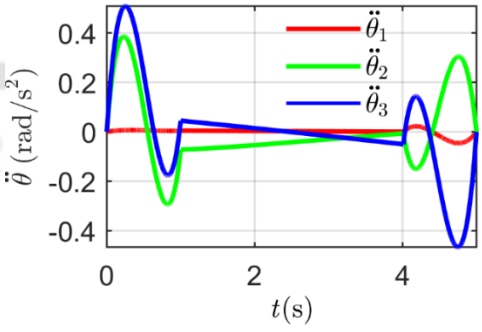

Figure 7.13: Joint angular acceleration of manipulator A after torque smotthening.

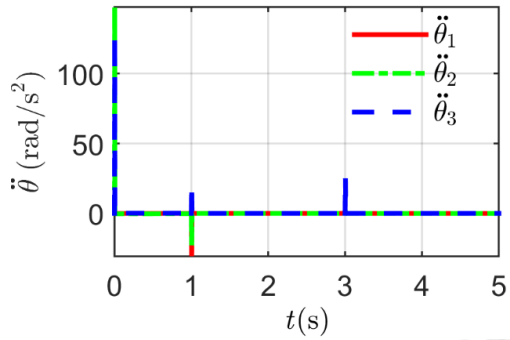

Figure 7.14: Joint angular acceleration of manipulator B before torque smoothening.

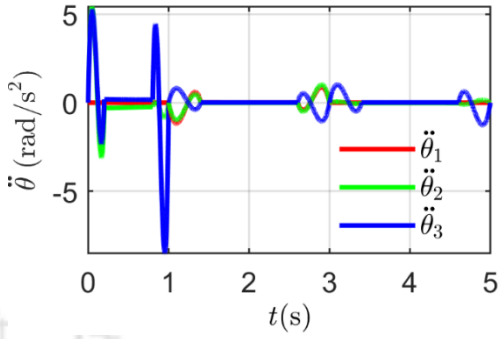

Figure 7.15: Joint angular acceleration of manipulator B after torque smoothening.

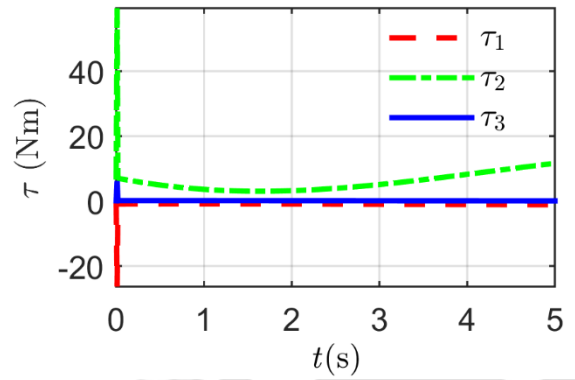

Figure 7.16: Joint torque of manipulator A before torque smoothening.

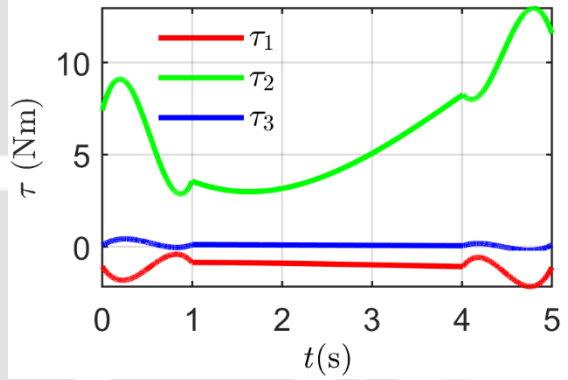

Figure 7.17: Joint torque of manipulator A after torque smoothening.

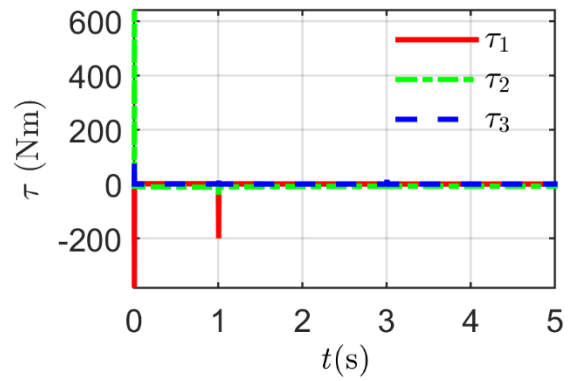

Figure 7.18: Joint torque of manipulator B before torque smoothening.

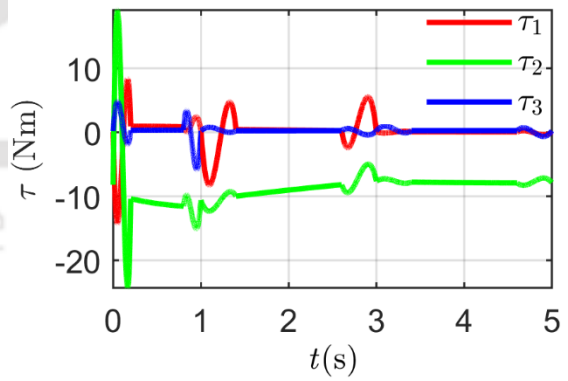

Figure 7.19: Joint torque of manipulator B after torque smoothening.

7.4.4 Effect of Joint Flexibility

Assuming I_i to be 20% of actuator inertia I_a for respective joint, and joint torques due to backlash stiffness to be within 5% of joint torque without considering backlash effect, the joint torques for the two manipulators A and B have been plotted for two values of K_T, i.e. $K_T =$ 0.175 and 0.275 Nm/rad as well as for the condition when joint flexibility has been not considered. The results are as shown in Figs. 7.20 and 7.21. From the figures, it can be observed that for the chosen values of K_T the torque due to the joint flexibility does not vary much compared to the condition when joint flexibility is not considered. Suitable experiments can be performed to find out the values of stiffness K_T and also factor β_i for respective joints.

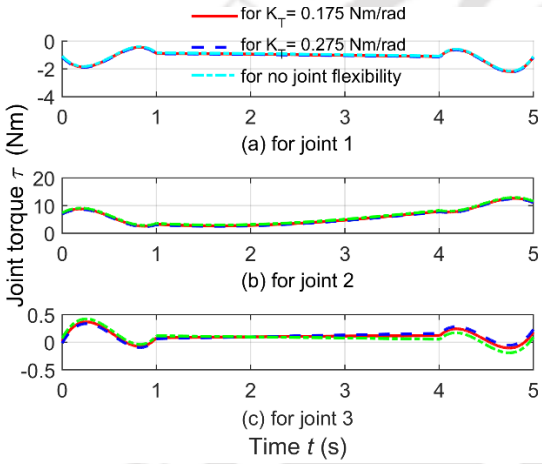

Figure 7.20: Variation of joint torque with time for manipulator A.

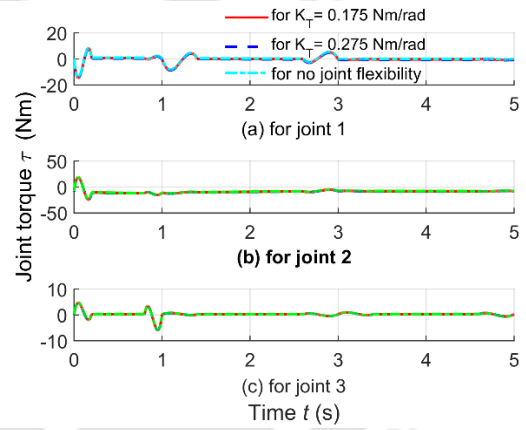

Figure 7.21: Variation of joint torque with time for manipulator B.

7.5 Conclusion

In this work, a systematic mathematical analysis of a group of two coordinating manipulators has been carried out. Path planning for the smooth performance of the given task of handling of hazardous chemical has been successfully carried out. Kinematic and dynamic analyses of the manipulators in operation have been performed. Jerk minimization with the application of quantic polynomial has been done. Joint flexibilities have been tried to be modelled.

Chapter 8

Conclusions and Scope of Future Work

8.1 Introduction

In this chapter, conclusions related to work done on flexible link manipulators and rigid manipulators have been presented. In the present work, kinematic and dynamic analyses of a manipulator with rigid link and flexible joint, manipulator with flexible links and manipulators with both link and joint flexibilities have been studied. Kinematic and dynamic modeling of flexible manipulators with finite element method and assumed mode method both have been done. First of all, it has been determined that how the dynamic behavior of a flexible link manipulator depends on various parameters of the manipulator. Transverse deflection, axial deflection, and flexural rotation in the modeling of the flexible link have been considered using both the finite element method and the assumed mode method. Thorough investigations of a string-stiffened flexible link manipulator have been done. Passive and active, both types of control have been applied to minimize the tip deflection of a flexible link manipulator.

Planar as well as three dimensional manipulators have been studied. Both single and multilink manipulators have been studied in the present work. In the study on coordinating manipulators for handling hazardous chemical, motion synchronization of coordinating manipulators with respect to time and position have been considered.

With regard to the above study a few general and specific conclusions can be made and are presented in the next sections. Further the scope of future works also has been highlighted at the end of this chapter.

8.2 General Conclusions

In this research work, five problems related to flexible manipulator have been investigated. In the first work, parametric studies of a two-link flexible manipulator, both the links of which are flexible, is studied. Kinematic and dynamic modeling has been done using finite element method.

The effects of different parameters of the manipulators: link length ratio, link diameter ratio, ratio of payload mass to the total mass of both links as well as the effect of different input torque profiles on the tip deflections, slopes at the tips, angular displacements and velocities of both the links of the manipulator have been investigated. The effects of torques due to gravity and centrifugal and Coriolis forces also have been studied. Time vs. tip deflection and joint response plots are obtained for different parameter ratios which will help designer to decide the optimal values of parameters of the manipulator for obtaining minimum tip deflection.

In the second problem, the dynamic analyses have been carried out for the manipulator with both link flexibility as well as joint flexibility using finite element method. The use of Newmark numerical integration technique results in much faster computation of the dynamic behaviour of the flexible-joint flexible-link manipulator (FJFLM). Tip deflections for the FJFLM have been found to be considerably higher than the those for flexible link manipulator (FLM). The residual vibrations of a single-link flexible-joint flexible-link manipulator (SLFJFLM) persisted even after the end of the joint motion of the FLM. Linear quadratic regulator (LQR) optimal control has been applied to control the tip vibrations of the FLM.

In the third and fourth problems, the tip deflections of a single-link and a rigid-flexible double-link flexible manipulator have been restrained with the help of a pair of strings tied on both sides of the flexible link. Kinematic and dynamic analysis of the string-stiffened flexible link manipulators are carried out in these works. Assumed mode method has been applied for discretization of the flexible link. Mode shapes of a cantilever beam with axial load has been used. The dynamic behavior of cables during the operation of the manipulator and their effect on the link vibration were obtained. The effects of pulling of link tip by the pair of cables on the joint of the manipulator have also been investigated. The axial deformation of the flexible link was taken care of. The buckling strength of the flexible link also has been considered. The effect of tension in the pair of strings on the tip deflection has been ascertained. The effect of geometric nonlinearities on the dynamic responses of the string-stiffened flexible link manipulators (SSFLMs) are found. Although the string-stiffening of the flexible manipulator minimized the tip deflections of the flexible link manipulators (FLMs), residual vibration of the links still persisted which have been eliminated by applying robust PID and impedance control.

In the fifth and the last problem, kinematic and dynamic analyses of two three-dimensional robotic manipulators, each of 3 axes, employed in cooperative handling of a job are carried out. Synchronization of motions of these manipulators with respect to time of motion and position of their end-effector (tip) has been carried out. Path planning of these robots also has been done. Jerk at the start and end of trajectories of the manipulators is eliminated.

8.3 Specific Conclusions

8.3.1 Parametric Study of a Two-Link Flexible Manipulator

In this section specific conclusions related to parametric study of a two-link flexible manipulator have been presented.

8.3.1.1 Effect of link length ratio δ on the dynamic response of the manipulator

- While the angular displacement of joint 2 increases with decrease in δ, the same for joint 1 depends on the combined inertia of both the links.
- Joint angular velocities of both joints are higher for lower link length ratio. This may be because lower inertia of the manipulators.
- Tip deflections and slopes at tips of link 1 and link 2 varies with the variation of δ in the same order. The reason for higher tip deflections and slopes of link 2 for higher δ is that higher δ increases the slenderness of the 2nd link which makes them more flexible and hence more tip deflection and slope. In case the 1st link this may be due to higher loads on tip of link 1 due to increased δ.

8.3.1.2 Effect of link diameter ratio ν on the dynamic response of the manipulator

- With respect to link-diameter ratio ν, the joint angular displacement θ_1 of the first joint depends on both the combined inertia of the manipulator and the amount of torque supplied that is proportional to ν. Here, θ_1 is highest for manipulator with ν_2.

- The angular displacement of joint 2 varies proportionally with ν. This is because, in this case, mass of the 2nd link and payload is the same for all ν but the torque applied at the 2nd joint is proportional to ν. Similar explanations hold for the joint angular velocities at both joints.
- Tip deflections and slopes at tip of link 1 varies with the diameter ratios ν in reverse order. This is because the lower ν makes the 1st links of these manipulators slender increasing flexibilities of the links while the payloads on the link 1 being the same.
- Tip deflections and slopes at tip of link 2 varies with the diameter ratios ν in the same order because of the same mass of the 2nd links for all ν but torques applied at the 2nd joint increases proportionally with ν.

8.3.1.3 Effect of payload mass (at the tip of 2nd link) on the dynamic response of the manipulator

- Angular responses of both the joints of the manipulator increase with the decrease in payload mass ratio. The corresponding links of these manipulators with different payload ratios are similar in lengths and diameters. So, this is due to less inertia offered by the links of the manipulator with less payload mass that tries to oppose any change in the state of motion of the links.
- But, the reverse conditions are found for tip deflections and slopes of both the links, i.e., these quantities increase with the increase in payload ratio.

8.3.1.4 Effect of torque profile on the dynamic response of the manipulator

- All the torque profiles give almost the same angular response profiles and their amplitudes. However, the triangular torque profile gives the marginally highest joint angular displacements and velocities and the bang-bang torque profile gives the least joint displacements and velocities.
- It was also observed that the sinusoidal torque profile gives the smoothest link tip motion while the bang-bang torque profile gives the jerky tip motion. This is because, in the bang-

bang torque profile, an abrupt change in torque amplitude takes place which results in oscillatory behavior of link tip motion at every change in values of the torque profile.

- The bang-bang profile also gives very high overshoots which may lead the link tip to collide with the surroundings.

8.3.1.5 Effect of torque due to gravity and the Coriolis and centrifugal forces on the dynamic response of the manipulator

- In the absence of gravity, it is observed that the angular response of joint 1 increases with δ while θ_2 for $\delta_3 > \theta_2$ for $\delta_1 > \theta_2$ for δ_2. This may be due to the manipulator with the least rotational inertia about joint 2 having a maximum response to the torque applied in the absence of gravitational force.
- Tip deflections of both the links increase with the link length ratios δ. This may be due to higher inertia experienced by these links. It is also noted that tip deflections in this case are lower than those in presence of gravity. This is due to no link and payload weight acting on these links due to absence of gravity.
- When both gravitational force and Coriolis and centrifugal forces are not considered, the same kind of behavior of joint angular displacements and tip deflections are displayed as in absence of gravity. However, the differences in this case can be observed after 2 seconds of joint motion, wherein the levels of attainment of θ are different compared to Case B. This difference in behavior after 2 seconds of joint motion can be attributed to the fact that the torque due to centripetal and Coriolis forces is much less than the torque supplied by the motor which operates for 0 to 2 second. After 2 seconds of motion the effects of centrifugal and Coriolis forces are clearly visible.

8.3.1.6 Effects of different parameters on the dynamic response of the manipulator

- With regard to the overshoots and the settling time, it is observed that these values increase with the increase in δ.
- The overshoots and settling time of the first link of the manipulator decrease with an increase in the diameter ratio while those for the 2^{nd} link increase with the increase in diameter ratio.

- As the payload ratio increases, the offshoots and the settling time increase and response time decreases.
- The sinusoidal and triangular torque profile gives the least overshoots, tip deflections, and settling time while the bang-bang torque profile gives the highest.

8.3.2 Dynamic Analysis and Control of a Single-Link Flexible Manipulator Using Finite Element Method

- The use of the Newmark numerical integration technique results in the much faster computation of the dynamic behavior of the FJFLM.
- The natural frequencies of the first three modes of vibration of FLM have been found to be 3.83 Hz, 32.1 Hz, and 98.3 Hz while those of the FJFLM were 3.52 Hz, 29.5 Hz and 91.1 Hz. This shows that joint flexibility results in further decrease in stiffness of the manipulator.
- Tip deflections for the FJFLM are considerably higher than those for FLM.
- The steady-state tip deflections in the transverse direction for FLM was $v_{tip} = -0.007539$ m time $t = 1.88$ s and for FJFLM was $v_{tip} = -0.01734$ m at time $t = 1.89$ s.
- Tip deflection in the axial direction for both FLM and FJFLM is negligible.
- There is no need for linearization of the system for the application of the LQR controller as joint angular displacement θ does not appear in the states of the system.
- Application of LQR control to the system bring the system to the equilibrium state within fraction of a second.
- It was observed that set of values of Q and R in case 5 gives the minimum settling time and the least overshoot while those in case 4 require longer settling time but with no overshoot. This is because that the values of Q with respect to first mode of vibration that is the most dominant component of vibration, have been taken to be highest in case 5 while values of R corresponding to that mode have been kept relatively lower.

8.3.3 Dynamic Analysis and Control of String-Stiffened Flexible Manipulator with Flexible Joint

- In this work, a systematic mathematical analysis of a string-stiffened single-link flexible manipulator (SSSLFM) has been carried out.
- Very few researchers only have been found to exploit the property of axial stiffness of a string for increasing the overall stiffness of a flexible link manipulator which results in the addition of minimum weight to the manipulator structure. However, they have not considered many aspects of the problem that have been considered here for example:
  (1) Mode shapes of a cantilever beam with axial load. (2) The dynamic behavior of cables during the operation of the manipulator and their effect on the link vibration. (3) The effect of pulling by the pair of cables on the joint of the manipulator. (4) The axial deformation of the flexible link. (5) The buckling strength of the flexible link. (6) The effect of tension in the pair of strings on the tip deflection. (7) The effect of geometric nonlinearities on the dynamic responses of the SSFLM. In the present work, an attempt has been made to consider all these points in the modeling of a string-stiffened flexible link manipulator.
- As against assumption of fixed-pinned boundary condition of Dixit and Kumar (2016), fixed-free boundary condition has been found to give more accurate results. This has been shown by their experiment also.
- With the use of a pair of strings as stiffeners, the tip deflections of the SSSLFM has been found to be reduced by 60.84%. In case of a string-stiffened two-link rigid-flexible manipulator (SSRFTLM), the stiffening of a flexible link by a pair of strings could reduce the tip deflection, as much as 26.63 times which is equal to a percentage reduction of 96.24%.
- The effect of string vibrations on the link vibrations have not been found to be significant.
- The tip deflections of SSSFLM and SSRFTLM depend on the values of tensions in the pair of strings.
- It is shown in case of SSSFLM that neglecting the effect of axial displacement will result in underestimation of tip deflection value by as much as 19.55 %. This may cause damage of link or job due to collision.

- The consideration of geometric nonlinearity results in the lower value of deflection of the flexible link.
- The coupling effects of strings and link vibrations on joint of the manipulator have been modelled.
- It is found that with the application of a suitable active control technique, smooth operation of SSSLFM and SSRFTLM even in presence of joint and link flexibilities can be achieved.
- Many of these points for an SSFLM have been analyzed for the first time in this work.
- The study is especially important for aerospace applications like flapping wing aircraft where weight management is one of the important factors that have to be considered.

8.3.4 Kinematic and Dynamic Analysis of Two 3R Coordinating Manipulators

- The synchronization of motion and position of coordinating robots has successfully have been achieved.
- The application of quantic polynomial at the start and end of a section of the trajectories of the two manipulators resulted in reducing the jerk by up to ten times which helps in carrying the hazardous chemical without any spill over.
- The application of quantic polynomial resulted in reduction of maximum values of angular acceleration for elliptical path from 12.0929 rad/s^2 at second joint and 10.8193 rad/s^2 at third joint to respectively 0.3865 rad/s^2, and 0.5084 rad/s^2.
- The maximum values of torques for the elliptical path have reduced from 59.3979 Nm to 12.9537 Nm for 2nd joint and from 6.1817 Nm to 0.4221 Nm for third joint with this technique.
- The reduction of maximum values of angular acceleration for path composed of vertical and horizontal lines from 147.533 rad/s^2 at second joint and 127.5507 rad/s^2 at third joint to respectively 5.4321 rad/s^2, and 5.2891 rad/s^2.
- The maximum values of torques for the elliptical path have reduced from 641.2638 Nm to 19.0846 Nm for 2nd joint and from 95.0590 Nm to 4.7845 Nm for third joint which can be observed from Figs. 7.18 and 7.19.

8.4 Scope of Future Work

In the present study, initially parametric study of a planar two-link flexible manipulator in which both the links are flexible has been done. There are many scopes to extend this work. Some of them are given below.

- Parametric study of three-dimensional flexible link manipulator with two or more links can be done.
- A full nondimensional analysis can be carried out to provide better insights.
- Multi-objective optimization techniques such as genetic algorithm, particle search method, etc. can be applied to determine the optimal value of different parameters to have the minimum tip deflection of the manipulator.
- Different types of robust control algorithms can be applied to make the operation of the manipulator robust to parametric uncertainties and external disturbances.

In Chapter 4, LQR control of a single-link flexible-joint flexible-link manipulator has been carried out. The scope of future work lies in

- Experimental verification of the control strategy.
- Investigation of improvement in the performance of the manipulator on applications of various optimal control algorithms can be carried out.

With regard to the work done in chapters 5 and 6 on string-stiffened flexible link manipulators (SSFLMs), the various scope of future works can be found as follows.

- Due to string-stiffening, foreshortening of flexible link may happen at higher speeds of the manipulator. More number of pairs of strings can be used to reduce the fore-shortening effect.
- The experimental assessment of effect of tensions in the pair of strings on the tip deflection can be carried out.
- Stability analysis of the string-stiffened flexible link manipulator can be carried out.
- The experimental validations of the results obtained for coupling effects of strings on joint and link vibrations of the manipulator can be done.

- The effect of considering geometric nonlinearity and axial displacements of the flexible link can be verified experimentally.
- The performance of various control strategies for the smooth performance of the SSFLM could be assessed experimentally.

With regard to the study done in chapter 7 on coordinating manipulators, there are many scopes to future works. A few of them are as follows.

- Flexible link manipulators can be employed to handle a job cooperatively.
- Manipulators with rigid links and flexible joints handling a task cooperatively can be studied.
- Manipulators handling a flexible object cooperatively can also be studied.

Bibliography

1. Abas, M. F. B., Rafie, A. S. B. M., Yusoff, H. B., Ahmad, K. A. B. (2016). Flapping wing micro-aerial-vehicle: Kinematics, membranes, and flapping mechanisms of ornithopter and insect flight. *Chinese Journal of Aeronautics*, 29(5): 1159-1177.
2. Abdelhedi B. F., Bouteraa, Y., and Medhaffar, H. (2013). Distributed sliding mode control of cooperative robotic manipulators. *10th International Multi-Conference on Systems, Signals and Devices, (SSD 2013).* doi: 10.1109/SSD.2013.6564140
3. Abe, A. (2009). Trajectory planning for residual vibration suppression of a two-link rigid-flexible manipulator considering large deformation. *Mechanism and Machine Theory*, 44, 1627-1639.
4. Abe, A. (2015). Nonlinear modeling and vibration control for a flexible manipulator. Paper presented at the *10th Asian Control Conference: Emerging Control Techniques for a Sustainable World, (ASCC 2015),* doi:10.1109/ASCC.2015.7244508
5. Abiko, S., and Yoshida, K. (2010). Adaptive reaction control for space robotic applications with dynamic model uncertainty. *Advanced Robotics, 24*(8-9), 1099-1126.
6. Abo-Shanab, R. F., and Sepehri, N. (2002). Effect of base compliance on the dynamic stability of mobile manipulators. *Robotica, 20*(6), 607-613.
7. Aghili, F. (2011). Self-tuning cooperative control of manipulators with position/orientation uncertainties in the closed-kinematic loop. Paper presented at the *IEEE International Conference on Intelligent Robots and Systems,* 4187-4193.
8. Aghili, F. (2013). Adaptive Control of Manipulators Forming Closed Kinematic Chain With Inaccurate Kinematic Model. *IEEE/ASME Transactions on Mechatronics,* 18(5).
9. Ahmad, M. A., Mohamed, Z., Ishak, H., and Nasir, A. N. K. (2008). Vibration suppression techniques in feedback control of a very flexible robot manipulator. Paper presented at the *Proceedings - 2nd Asia International Conference on Modelling and Simulation, AMS 2008,* 469-474.
10. Alandoli, E. A. and Lee, T. S. (2020). A critical review of control techniques for flexible and rigid link manipulators. *Robotica*, 38, 2239-2265. doi:10.1017/S0263574720000223.
11. Al-Bedoor, B. O., and Hamdan, M. N. (2001). Geometrically Non-linear Dynamic Model of a Rotating Flexible Arm. *Journal of Sound and vibration,* 240(1), 59-72.

12. Alexis, K., Nikolakopoulos, G., and Tzes, A. (2011). Switching model predictive attitude control for a quadrotor helicopter subject to atmospheric disturbances. *Control Engineering Practice, 19*(10), 1195-1207.
13. Amiri, M., Menhaj, M. B., and Yazdanpanh, M. J. (2008). A neural-network-based controller for a single-link flexible manipulator: Comparison of FFNN and DRNN controllers. Paper presented at the *Proceedings of the International Joint Conference on Neural Networks*, 1686-1691.
14. Anderson, G. P. (1988). Modelling and Simulation of a Puma 560 Manipulator for Control System Appraisal. *Thesis (ME). National Institute for Higher Education, Dublin*.
15. Angeles, J. (2003). Fundamental of Robotic Mechanical Systems: Theory, Methods, and Algorithms, *Springer, 2nd Ed.*, 2003.
16. Armstrong, B., Khatib, O., and Burdick, J. (1986). The Explicit Dynamic Model and Inertial Parameters of the PUMA 566 Arm. *Proceedings IEEE Int. Conference on Robotics and Automation, April 1986*, San Francisco, CA, pp. 510-518.
17. Asada, H., and Asari Y. (1988). The direct teaching of tool manipulation skills via the impedance identification of human motions. *Proceedings. 1988 IEEE International Conference on Robotics and Automation*, Philadelphia, PA, USA, 1988, vol.2, pp. 1269-1274. doi: 10.1109/ROBOT.1988.12235.
18. Ashrafiuon, H., and Nataraj, C. (1991). Effect on flexibility on manipulator dynamics. *In: Dwivedi, S.N., Verma, A.K., Sneckenberger, J.E. (eds) CAD/CAM Robotics and Factories of the Future '90. Springer*, Berlin, Heidelberg. https://doi.org/10.1007/978-3-642-58214-1_89
19. Ashwin, K. P., Mahapatra, S. K., Ghosal, A. (2021). Profile and contact force estimation of cable-driven continuum robots in presence of obstacles. *Mech. Mach. Theory*, 164, 104404.
20. Ata, A. A. (2010). Inverse dynamic analysis and trajectory planning for flexible manipulator. *Inverse Problems in Science and Engineering*, *18*(4), 549-566.
21. Ata, A. A. (2012). Trajectory selection for a rigid/flexible manipulator. Paper presented at the *2012 IEEE International Conference on Industrial Technology, ICIT 2012, Proceedings*, 36-41.
22. Ata, A. A., and Elkhoga, S. M. (1998). Effect of tip mass and actuator inertia on the behavior of a flexible arm robot. *Proceedings of the 1998 IEEE/RSI, Intl. Conference on Intelligent Robots and Systems, Victoria B. C., Canada*.

23. Ata, A. A., Haraz, E. H., Rizk, A. E. A., and Hanna, S. N. (2012). Kinematic analysis of a single link flexible manipulator. Paper presented at the *2012 IEEE International Conference on Industrial Technology, ICIT 2012, Proceedings*, 852-857.
24. Ata, A. A., and Johar, H. (2005). Dynamic analysis of a rigid-flexible manipulator constrained by arbitrary shaped surfaces. *International Journal of Modelling and Simulation, 25*(4), 259-268.
25. Augustynek, K., and Adamiec-Wójcik, I. (2012). Analysis of mechanisms with flexible beam-like links, rotary joints and assembly errors. *Archive of Applied Mechanics, 82*(2), 283-295.
26. Baigzadehnoe, B., Rahmani, Z., Khosravi, A., and Rezaie, B. (2017). On position/force tracking control problem of cooperative robot manipulators using adaptive fuzzy backstepping approach. *ISA Transactions, 70*, 432-446. doi:10.1016/j.isatra.2017.07.029
27. Bandopadhya, D., Dutta, A., and Bhattacharya, B. (2006). Active vibration control using terfenol-D with H-infinity filter. *International Journal for Engineering Modelling, 19*(1-4), 33-43.
28. Bascetta, L., and Rocco, P. (2002). Modelling flexible manipulators with motors at the joints. *Mathematical and Computer Modelling of Dynamical Systems, 8*(2), 157-183.
29. Basher, A. M. H. (2000). Dynamic behavior of a translating flexible beam with a prismatic joint. Paper presented at the *Conference Proceedings - IEEE SOUTHEASTCON*, 31-38.
30. Benzater H. and Chouraqui S. (2014). Puma 560 Trajectory Control using NSGAII Technique with Real Valued Operators. *International Journal of Soft Computing, Mathematics and Control (IJSCMC),* 3(3).
31. Bertrand, S., Guénard, N., Hamel, T., Piet-Lahanier, H., and Eck, L. (2011). A hierarchical controller for miniature VTOL UAVs: Design and stability analysis using singular perturbation theory. *Control Engineering Practice, 19*(10), 1099-1108.
32. Bertuccelli, L. F., Wu, A., and How, J. P. (2012). Robust adaptive markov decision processes: Planning with model uncertainty. *IEEE Control Systems, 32*(5), 96-109.
33. Bieze, T. M., Kruszewski, A., Carrez, B., and Duriez C. (2020). Design, implementation, and control of a deformable manipulator robot based on a compliant spine. *The International Journal of Robotics Research,* 2020, 1-16.

34. Bonarini, Andrea, Matteucci, Matteo, Migliavacca, Martino and Rizzi, Davide (2014). R2P: An open source hardware and software modular approach to robot prototyping, *Robotics and Autonomous Systems*, 62(7), 943-1084.
35. Bonitz, R. G., and Hsia, T. C. (1994). Force decomposition in cooperating manipulators using the theory of metric spaces and generalized inverses. Paper presented at the *Proceedings - IEEE International Conference on Robotics and Automation*, pp.1521-1527.
36. Bonitz, R. G., and Hsia, T. C. (1996). Internal force-based impedance control for cooperating manipulators. *IEEE Transactions on Robotics and Automation, 12*(1), 78-89.
37. Boscariol, P., Gasparetto, A., Giovagnoni, M., Moosavi, A. K., and Vidoni, R. (2012). Design and implementation of a simulator for 3D flexible-link serial robots. Paper presented at the *ASME 11th Biennial Conference on Engineering Systems Design and Analysis, ESDA 2012, 3*, 155-164.
38. Boscariol, P., Gasparetto, A., and Zanotto, V. (2010). Design and experimental validation of a hardware-in-the-loop simulator for mechanisms with link flexibility. Paper presented at the *ASME 10th Biennial Conference on Engineering Systems Design and Analysis, ESDA2010, 3*, 827-836.
39. Bossi, L., Rottenbacher, C., Mimmi, G., and Magni, L. (2011). Multivariable predictive control for vibrating structures: An application. *Control Engineering Practice, 19*(10), 1087-1098.
40. Brownbridg, Jason (2008). Teleoperation of Rescue Robots in Urban Search and Rescue Tasks: An Investigation of Factors which effect Operator Performance and Accuracy, *Honours Project Report 2008*, Department of Computer Science, University of Cape Town.
41. Bruhm, H., Deisenroth, J., and Schädler, P. (1989). On the design and simulation-based validation of an active compliance law for multi-arm robots. *Robotics and Autonomous Systems, 5*(4), 307-321.
42. Buckling.https://en.wikipedia.org/wiki/Buckling
43. Caccavale, F., Chiacchio, P., and Chiaverini, S. (1999). Stability analysis of joint space control law for a two manipulator system. *IEEE, Transaction on Automation. and Control*, 44, 1999, 85-88.
44. Caccavale, F., Chiacchio, P., and Chiaverini, S. (2000). Task-space regulation of cooperative manipulators. *Automatica*, 36, 2000, 879-887.

45. Callegari, M., Cammarata, A., Gabrielli, A., Ruggiu, M., and Sinatra, R. (2009). Analysis and design of a spherical micromechanism with flexure hinges. *Journal of Mechanical Design, Transactions of the ASME, 131*(5), 0510031-05100311.
46. Cambera, J. C., Feliu-Batlle, V. (2017). Input-state feedback linearization control of a single-link flexible robot arm moving under gravity and joint friction. *Robotics and Autonomous Systems*, 88 (2017) 24-36.
47. Cao, F., Liu, J. (2019). Boundary vibration control for a two-link rigid-flexible manipulator with quantized input. *Journal of Vibration and Control*, 25 (23-24), 2935-2945.
48. Cappelli, M., Castillo-Toledo, B., Di Gennaro, S., Memmi, F., and Sepielli, M. (2013). Digital nonlinear control for a pressurizer in a pressurized water reactor. Paper presented at the *International Conference on Nuclear Engineering, Proceedings, ICONE, 5*.
49. Carpenter, M. D., and Peck, M. A. (2009). Reducing base reactions with gyroscopic actuation of space-robotic systems. *IEEE Transactions on Robotics, 25*(6), 1262-1270.
50. Casalino, G., Simetti, E., Manerikar, N., Sperinde, A., Torelli, S., and Wanderlingh, F. (2015). Cooperative Underwater Manipulation Systems: Control Developments within the MARIS project. *IFAC-PapersOnLine*, 48(2), 001-007.
51. Casalino, G., and Turetta, A. (2003). Coordination and control of multiarm, non-holonomic mobile manipulators. Paper presented at the *IEEE International Conference on Intelligent Robots and Systems, 3*, 2203-2210.
52. Cascio, J., Karpenko, M., Gong, Q., Sekhavat, P., and Ross, I. M. (2009). Smooth proximity computation for collision-free optimal control of multiple robotic manipulators. Paper presented at the *2009 IEEE/RSJ International Conference on Intelligent Robots and Systems, IROS 2009*, 2452-2457.
53. Castri, C. D., and Messina, A. (2012). Exact modeling for control of flexible manipulators. *JVC/Journal of Vibration and Control, 18*(10), 1526-1551.
54. Celentano, L. (2012). An innovative method to modeling realistic flexible robots. *Applied Mathematical Sciences, 6*(73-76), 3623-3659.
55. Celentano, L., and Coppola, A. (2011). A wavelet based method to modeling realistic flexible robots. Paper presented at the *IFAC Proceedings Volumes (IFAC-PapersOnline), 18* (1), 929-937.

56. Cetinkunt, S., and Yu, W.-L. (1991). Closed-loop behavior of a feedback-controlled flexible arm:Acomparative study. *International Journal of Robotic Research.*, 10, 263-275.
57. Chalon, M., Wimböck, T., and Hirzinger, G. (2010). Torque and workspace analysis for flexible tendon driven mechanisms. Paper presented at the *Proceedings - IEEE International Conference on Robotics and Automation*, 1175-1181.
58. Chang, C.-F., and Fu, L.-C. (2006). Analysis of a behavior based nonholonomic wheeled mobile robot control with hybrid system approach. Paper presented at the *2006 SICE-ICASE International Joint Conference*, 646-651.
59. Chang, K., Holmberg, R., and Khatib, O. (2000). Augmented object model: Cooperative manipulation and parallel mechanism dynamics. Paper presented at the *Proceedings - IEEE International Conference on Robotics and Automation, 1*, 470-475.
60. Chang, L., and Fu, L. (1997). Nonlinear adaptive control of a flexible manipulator for automated deburring. Paper presented at the *Proceedings - IEEE International Conference on Robotics and Automation, 4*, 2844-2849.
61. Chang, W., Li, Y., and Tong, S. (2021). Adaptive Fuzzy Backstepping Tracking Control for Flexible Robotic Manipulator. *IEEE/CAA Journal of Automatica Sinica*, 8(12).
62. Chen, B., Huang, J., and Ji, J. C. (2019). Control of flexible single-link manipulators having Duffing oscillator dynamics. *Mechanical Systems and Signal Processing*, 121 (2019), 44-57.
63. Chen, W., Sun, Y., and Huang, Y. (2010). *A* collision detection system for an assistive robotic manipulator. Life System Modeling and Intelligent Computing Communications in Computer and Information Science, 97, 117-123.
64. Chen, W., Yu, Y., Zhang, X., and Su, L. (2006). Vibration controllability of underactuated robots with flexible links. Paper presented at the *IET Conference Publications*, (524), 1872-1878.
65. Chen, X., Deng, Y., and Jia, S. (2011). Rigid-flexible coupled dynamics modeling and analysis for a novel high-speed spatial parallel robot. *Advanced Science Letters, 4*(8-10), 2595-2599.
66. Chen, X., and Li, Y. (2006). Cooperative transportation by multiple mobile manipulators using adaptive NN control. Paper presented at the *IEEE International Conference on Neural Networks - Conference Proceedings*, 4193-4200.

67. Chen, Y., Liu, G. R., and Wu, W. J. (2013). *Stability analysis of elastic vibration of flexible manipulator arm based on routh criterion.* ISMSE 2013, Hong Kong, Nov. 1-2, 2013.
68. Chen, Z., and Chen, L. (2012). Robust neural network control of space robot system with flexible joints. Paper presented at the *Proceedings of the International Astronautical Congress, IAC, 8,* 6762-6767.
69. Chen, Z.-Y., and Chen, L. (2012). Robust control of flexible-joint space robot via flexibility compensation. *Gongcheng Lixue/Engineering Mechanics, 29*(11), 53-57.
70. Chen, Z., and Chen, L. (2011). Study on dynamics modeling and singular perturbation control of free-floating space robot with flexible joints. *Zhongguo Jixie Gongcheng/China Mechanical Engineering, 22*(18), 2151-2155.
71. Chhabra, R., and Emami, M. R. (2009). Concurrent synthesis of robot manipulators using hardware-in-the-loop simulation. Paper presented at the *Proceedings - IEEE International Conference on Robotics and Automation,* 568-573.
72. Chiacchio, P., Chiaverini, S., and Siciliano, B. (1996). Direct and inverse kinematics for coordinated motion tasks of a two-manipulator system. *Journal of Dynamic Systems, Measurement and Control, Transactions of the ASME, 118*(4), 691-697.
73. Chiacchio, P., Chiaverini, S., Sciavicco, L., and Siciliano, B. (1991). Global task space manipulability ellipsoids for multiple-arm systems. *IEEE Transactions on Robotics and Automation, 7*(5), 678-685.
74. Choi, D. H., Lee, S. J., Wickert, J. A., and Yoo, H. H. (2008). Tolerance analysis of a robot manipulator having uncertainties in joint clearance and axis orientation. Paper presented at the *2007 Proceedings of the ASME International Design Engineering Technical Conferences and Computers and Information in Engineering Conference, DETC2007, 5, PART C* 1911-1918.
75. Choi, J. S., Yoon, J. H., Park, J. H., and Kim, P. J. (2011). A numerical algorithm to identify independent grouped parameters of robot manipulator for control. Paper presented at the *IEEE/ASME International Conference on Advanced Intelligent Mechatronics, AIM,* 373-378.
76. Chowdhury, I., and Dasgupta, S. (2003). Computation of Rayleigh damping coefficients for large system. *The Electronic Journal of Geotechnical Engineering,* 43, 6855-6868.

77. Chu, M., Jia, Q.-X., Sun, H.-X., Zhang, X.-D., and Yao, F.-S. (2008). Coupling of the dynamics and control of the space flexible manipulative arm. *Beijing Youdian Daxue Xuebao/Journal of Beijing University of Posts and Telecommunications, 31*(3), 98-102.
78. Chung, S.-J., and Slotine, J.-J. E. (2009). Cooperative robot control and concurrent synchronization of Lagrangian systems. *IEEE Transactions on Robotics, 25*(3), 686-700.
79. Consolini, L., Gerelli, O., Guarino Lo Bianco, C., and Piazzi, A. (2009). Flexible joints control: A minimum-time feed-forward technique. *Mechatronics, 19*(3), 348-356.
80. Couceiro, M. S., Vargas, P. A., Rocha, R. P., and Ferreira, N. M. F. (2014). Benchmark of swarm robotics distributed techniques in a search task. *Robotics and Autonomous Systems, 62*(2), 200-213.
81. Craig, J. J. (2005). Introduction to Robotics: Mechanics and Control, *Pearson Education International*, Third Edition.
82. Crowe-Wright, I. J. P. (2018). Control theory: the double pendulum inverted on a cart. M. Sc. thesis in mathematics, The University of New Mexico Albuquerque, New Mexico. https://digitalrepository.unm.edu/math_etds/132
83. Czarnetzki, S., and Rohde, C. (2010). Handling heterogeneous information sources for multi-robot sensor fusion. Paper presented at the *IEEE International Conference on Multisensor Fusion and Integration for Intelligent Systems*, 133-138.
84. Daachi, B., Madani, T., and Benallegue, A. (2012). Adaptive neural controller for redundant robot manipulators and collision avoidance with mobile obstacles. *Neurocomputing, 79*, 50-60.
85. Dado, M. H. F., Al-Huniti, N. S., and Karim Eljabali, A. (2001). Dynamic simulation model for mixed-loop planar robots with flexible joint drives. *Mechanism and Machine Theory, 36*(4), 547-559.
86. De Luca, A., and Flacco, F. (2011). A PD-type regulator with exact gravity cancellation for robots with flexible joints. Paper presented at the *Proceedings - IEEE International Conference on Robotics and Automation*, 317-323.
87. Dellon, B., Matsuoka, Y. (2007). Prosthetics, exoskeletons and rehabilitation, Now and for Future. *Robotics and Automation Magazine, IEEE*, 14(1), March 2007.
88. Dentsoras, A. J., and Aspragathos, N. A. (1991). Modelling the Dynamic Characteristics of a Robot Arm Joint. *Robotics and Computer-Integrated Manufacturing*, 8(3), 157-161.

89. Diao, S., Sun, W., Su, S.-F., and Xia, J. (2021). Adaptive fuzzy event-triggered control for single- link flexible-joint robots with actuator failures. *IEEE Transactions on Cybernetics*.
90. Ding, X., Guo, P., Xu, K., and Yu, Y. (2019). A review of aerial manipulation of small-scale rotorcraft unmanned robotic systems. *Chinese Journal of Aeronautics*, 32(1): 200-214.
91. Dixit, R., and Kumar, R. P. (2014). Cable stiffened flexible link manipulator. *IEEE/RSJ International Conference on Intelligent Robots and Systems (IROS 2014)*, Chicago, IL, USA.
92. Dixit, R., and Kumar, R. P. (2016). Working and limitations of cable stiffening in flexible link manipulators. *Advances in Acoustics and Vibration*, 1-9. doi: 10.1155/2016/4503696
93. Dixit, U. S., Kumar, R., and Dwivedy, S. K. (2006). Shape optimization of flexible robotic manipulators. *J. Mech. Des.*, 128 (3), 559-565.
94. Dong, G., and Zhu, Z. H. (2018). Predictive visual servo kinematic control for autonomous robotic capture of non-cooperative space target. *Acta Astronautica*, 151 (2018), 173-181.
95. Dong, X., Li, D., Xiang J., and Wang, Z. (2020). Design and experimental study of a new flapping wing rotor micro aerial vehicle. *Chinese Journal of Aeronautics*, 33(12): 3092–3099.
96. Dong, X., Shi, K., Li, W. (2020). Residual vibration control of a single-link flexible manipulator with variable stiffness and damping magnetorheological joint. *J Phys Conf Ser*, 1678, 012005.
97. Dong, W., and Farrell, J. A. (2009). Decentralized cooperative control of multiple nonholonomic dynamic systems with uncertainty. *Automatica*, *45*(3), 706-710.
98. Dou, J., and Yu, Y. (2002). On the cooperation of flexible manipulators and inverse dynamic control algorithm. *Jixie Gongcheng Xuebao/Chinese Journal of Mechanical Engineering*, *38*(8), 14-18.
99. Du, X., and Cai, G.-P. (2009). Active control of two-link flexible manipulator. *Shanghai Jiaotong Daxue Xuebao/Journal of Shanghai Jiaotong University*, *43*(8), 1248-1253.
100. Du, Z., Yu, Y., and Yang, J. (2007). Analysis of the dynamic stress of planar flexible-links parallel robots. *Frontiers of Mechanical Engineering in China*, *2*(2), 152-158.
101. Duarte, F., Ballesteros, P., Ullah, F., and Bohn, C. (2015). Modeling and sliding mode control of a single-link flexible robot to reduce the transient response. Paper presented at

the *20th International Conference on Methods and Models in Automation and Robotics, MMAR 2015,* 235-240. doi:10.1109/MMAR.2015.7283879

102. Duchon, F., Hubinský, P., Hanzel, J., Babinec, A., and Tölgyessy, M. (2012). Intelligent vehicles as the robotic applications. *Procedia Engineering*, 48, 105 -114.
103. Dwivedy, S. K., and Eberhard, P. (2006). Dynamic analysis of flexible manipulators, a literature review. *Mechanism and Machine Theory, 41*(7), 749-777.
104. Dwivedy, S. K., Srinivasulu, M., Narayana, K. S., and Koushik, A. (2009). Dynamic analysis of composite flexible robotic manipulator with harmonic drives using finite element method. *Advances in Vibration Engineering, 8*(4), 313-320.
105. Elattar, S. M. S. (2008). Automation and robotics in construction: opportunities and challenges, *Emirates Journal for Engineering Research*, 13 (2), 21-26.
106. Erkaya, S. (2012). Investigation of joint clearance effects on welding robot manipulators. *Robotics and Computer-Integrated Manufacturing, 28*(4), 449-457.
107. Esakki, B., Bhat, R. B., and Su, C.-Y. (2013). Robust control of collaborative manipulators - flexible object system. *International Journal of Advanced Robotic Systems, 10, 257.*
108. Farid, M., and Salimi, I. (2001). Inverse dynamics of a planar flexible-link manipulator with revolute-prismatic joints. Paper presented at the *ASME International Mechanical Engineering Congress and Exposition, Proceedings, 2,* 347-352.
109. Fareh, R. (2019). Sliding Mode Fractional Order Control for a Single Flexible Link Manipulator. *International Journal of Mechanical Engineering and Robotics Research, 8(2).*
110. Feliu-Talegon, D., Feliu-Batlle, V. (2019). Passivity-based control of a single-link flexible manipulator using fractional controllers. *Nonlinear Dynamics*, 95, 2415-2441. doi:10.1007/s11071-018-4701-4
111. Feliu-Talegon, D., and Feliu-Batlle, V. (2022). Control of very lightweight 2-dof single-link flexible robots robust to strain gauge sensor disturbances: a fractional-order approach. *IEEE Transactions on Control Systems Technology*, 30(1).
112. Feliu-Talegon, D., Feliu-Batlle, V., Tejado, I., Vinagre, B. M., Hossein Nia, S. H. (2019). Stable force control and contact transition of a single link flexible robot using a fractional-order controller. *ISA Transactions*, 89 (2019) 139-157.

113. Feliu, V., Somolinos, J. A., and García, A. (2003). Inverse dynamics based control system for a three-degree-of-freedom flexible arm. *IEEE Transactions on Robotics and Automation, 19*(6), 1007-1014.

114. Ficuciello, F., Romano, A., Villani, L., and Siciliano, B. (2014). Cartesian impedance control of redundant manipulators for human-robot co-manipulation. Paper presented at the *IEEE International Conference on Intelligent Robots and Systems,* 2120-2125. doi:10.1109/IROS.2014.69428

115. Filaretov, V., Yukhimets, D., Zuev, A., Gubankov, A., and Mursalimov, E.(2014). An new approach for automatization of cutting of flexible items by using multilink manipulators with vision system. *International Symposium on Power Electronics, Electrical Drives, Automation and Motion, SPEEDAM 2014,* 1344-1349.

116. Flacco, F., Luca, A. D., Sardellitti, I. and Tsagarakis N. G. (2012). On-line estimation of variable stiffness in flexible robot joints. *The International Journal of Robotics Research,* 31(13), 1556-1577.

117. Flores, P., Ambro´sio, J., Claro, J. C. P., Lankarani, H. M., Koshy, C. S. (2006). A study on dynamics of mechanical systems including joints with clearance and lubrication. *Mech. Mach. Theory*, 41, 247-261.

118. Franitza, D. (2002). A convective description of flexible robot dynamics. Paper presented at the *American Society of Mechanical Engineers, Dynamic Systems and Control Division (Publication) DSC, 71,* 1037-1042.

119. Fratu, A., and Ilea, D. (2012). An Analysis of the Reciprocal Robots Collision Avoidance. *13th International Conference on Optimization of Electrical and Electronic Equipment (OPTIM),* Brasov, 24-26 May 2012, pp. 1511-1516.

120. Fu, K.S., Gonzalis, R. C., Lee, C.S.G. (1987). Robotics: Control, Sensing, Vision and Intelligence. *Mc. Graw Hill Book Company.*

121. Fujii S., and Kurono, S. (1975). Coordinated computer control of a pair of manipulators. *Proc. 4th IFToMM World Congress (Newcastle upon Tyne),* pp. 411-417.

122. Gao, H., and He, W. (2017). Fuzzy control of a single-link flexible robotic manipulator using assumed mode method. *31st Youth Academic Annual Conference of Chinese Association of Automation, Wuhan, China*, November 11-13, 2016.

123. Gao, Z., and Bian, Y. (2012). Resonance analysis of manipulators with flexible link and flexible joint. *Advanced Materials Research*, 383-390, pp. 2868-2874.

124. Gao, Z., Yu, J., and Bian, Y. (2011). Vibration suppression of the flexible joint manipulator based on controllable local degrees of freedom. *Source of the Document Applied Mechanics and Materials*. 66-68, pp. 989-994.

125. Garg, A., Vikram, C. S., Gupta, S., Sutar, M. K., Pathak, P. M., Mehta, N. K., Gupta, V. K. (2014). Design and development of in vivo robot for biopsy. *Mechanics Based Design of Structures and Machines, 42*(3), 278-295.

126. Gattulli, V., and Paolone, A. (1997). Planar Motion of a Cable-Supported Beam with Feedback Controlled Actions. *Journal of Intelligent Material Systems and Structures*, 8, 767-774.

127. Gattulli, V., and Lepidi, M. (2003). Nonlinear interactions in the planar dynamics of cable-stayed beam. *International Journal of Solids and Structures*, 40, 4729–4748.

128. Gattulli, V., and Lepidi, M. (2007). Localization and veering in the dynamics of cable-stayed bridges. *Computers and Structures*, 85, 1661-1678.

129. Gattulli, V., Lepidi. M., Macdonald, J. H. G., and Taylor, C. A. (2005). One-to-two global-local interaction in a cable-stayed beam observed through analytical, finite element and experimental models. *International Journal of Non-Linear Mechanics*, 40, 571-588.

130. Gavriloiu, V., Yurkevich, V., and Khorasani, K. (2009). Design of dynamic nonlinear control techniques for flexible-link manipulators. *Solid State Phenomena*, 144, 250-256.

131. Geng, D., Zhao, J., Zhang, L., and Zhao, Y. (2011). Study on bidirectional controllable flexible bending joints based on elongation artificial muscles. *Applied Mechanics and Materials*, 44-47, pp. 2877-2882.

132. Ghorbani, H., Alipour, K., Tarvirdizadeh, B., Hadi, A. (2019). Comparison of various input shaping methods in rest-to-rest motion of the end-effector of a rigid-flexible robotic system with large deformations capability. *Mech Syst Signal Process*, 118 (5), 584-602.

133. Ghosal, A. (2008). Robotics: Fundamental Concepts and Analysis, *Oxford University Press.*

134. Giorgio, I., and Del Vescovo, D. (2019). Energy-based trajectory tracking and vibration control for multilink highly flexible manipulators. Mathematics and Mechanics of Complex Systems, 7(2), 159-174. doi: 10.2140/memocs.2019.7.159

135. Gkountas, K., and Tzes, A. (2021). Leader/follower force control of aerial manipulators. *IEEE Access,* Vol. 9, 2021. doi: 10.1109/ACCESS.2021.3053654

136. González-Vázquez, S., and Moreno-Valenzuela, J. (2013). Time-scale separation of a class of robust PD-type tracking controllers for robot manipulators. *ISA Transactions, 52*(3), 418-428

137. Grandinetti, F. J., De S Soares, A. M., De Q Lamas, W., and Goes, L. C. S. (2012). Notes on vibration control of a micro/macromanipulator mounted on a flexible structure. *Proceedings of the Institution of Mechanical Engineers, Part K: Journal of Multi-Body Dynamics, 226*(1), 72-82.

138. Green, A., and Sasiadek, J. Z. (2005). Adaptive control of a flexible robot using fuzzy logic. *Journal of Guidance, Control, and Dynamics, 28*(1), 36-42.

139. Gu, Y.-K., Ni, F.-L., and Liu, H. (2011). Flexible-joint manipulator adaptive control based on recurrent elman neural networks and dynamic surface approach. *Kongzhi Yu Juece/Control and Decision, 26*(12), 1783-1790.

140. Gudino-Lau, J., Arteaga, M. A., Munoz, L. A., and Parra-Vega, V. (2004). On the control of cooperative robots without velocity measurements. *IEEE Transactions on Control Systems Technology, 12*(4), 600-608.

141. Gueaieb, W., Karray, F., and Al-Sharhan, S. (2003). A robust adaptive fuzzy position/force control scheme for cooperative manipulators. *IEEE Transactions on Control Systems Technology, 11*(4), 516-528.

142. Guidali, M., Keller, U., Klamroth-Marganska, V., Nef, T., and Riener, R. (2013). Estimating the patient's contribution during robot-assisted therapy. *Journal of Rehabilitation Research and Development, 50*(3), 379-394.

143. Guo, J., and Lee, K.-M. (2013). Compliant joint design and flexure finger dynamic analysis using an equivalent pin model. *Mechanism and Machine Theory, 70*, 338-353.

144. Guo, Y., and Sun, F. (2013). Nonlinear robust adaptive control for free-floating flexible space manipulator system. *Jixie Gongcheng Xuebao/Journal of Mechanical Engineering, 49*(23), 36-43.

145. Guo, Y.-S., and Chen, L. (2009). Backstepping control of coordinated motion of free-floating flexible space manipulator system. *Gongcheng Lixue/Engineering Mechanics, 26*(10), 165-170.

146. Hadian Jazi, S., Keshmiri, M., Sheikholeslam, F., Shahreza, M. G., and Keshmiri, M. (2012). Dynamic analysis and control synthesis of undesired slippage of end-effectors in a cooperative grasping. *Advanced Robotics, 26*(15), 1693-1726.
147. Halalchi, H., Laroche, E., and Bara, G. I. (2014). Flexible-link robot control using a linear parameter varying systems methodology regular paper. *International Journal of Advanced Robotic Systems, 11*(1).
148. Han, S. I., Lee, K. S., Park, M. G., and Lee, J. M. (2011). Robust adaptive deadzone and friction compensation of robot manipulator using RWCMAC network. *Journal of Mechanical Science and Technology, 25*(6), 1583-1594.
149. Hara, N., Handa, Y., and Nenchev, D. (2012). End-link dynamics of redundant robotic limbs: The reaction null space approach. Paper presented at the *Proceedings - IEEE International Conference on Robotics and Automation*, 299-304.
150. Hashemi, S. M., Abbas, H. S., and Werner, H. (2012). Low-complexity linear parameter-varying modeling and control of a robotic manipulator. *Control Engineering Practice, 20*(3), 248-257.
151. Hashemi, S. M., Gürcüoğlu, U., and Werner, H. (2013). Interaction control of an industrial manipulator using LPV techniques. *Mechatronics, 23*(6), 689-699.
152. Hatanaka, T., and Fujita, M. (2010). Passivity-based visual motion observer: From theory to distributed algorithms. Paper presented at the *Proceedings of the IEEE International Symposium on Computer-Aided Control System Design*, 1210-1221.
153. Hayden, H. W., Moffatt, W. G., and Wulff, J. (1965). The Structure and Properties of Materials, Vol. III, John Wiley, New York, 1965.
154. He, G., Lu, Z., and Wang, F. (2005). Internal resonance property of flexible under-actuated manipulators. *Beijing Hangkong Hangtian Daxue Xuebao/Journal of Beijing University of Aeronautics and Astronautics, 31*(8), 913-916.
155. He, G.-P., and Lu, Z. (2005). Nonlinear dynamic analysis of planar flexible underactuated manipulators. *Chinese Journal of Aeronautics, 18*(1), 78-82.
156. He, W., Mu, X., Chen, Y., He, X., and Yu, Y. (2018). Modeling and vibration control of the flapping-wing robotic aircraft with output constraint. *Journal of Sound and Vibration*, 423(2018), 472-483.

157. Heidari, H. R., Korayem, M. H., Haghpanahi, M., and Batlle, V. F. (2013). Optimal trajectory planning for flexible link manipulators with large deflection using a new displacements approach. *Journal of Intelligent and Robotic Systems: Theory and Applications, 72*(3-4), 287-300.

158. Hirschkorn, M., and Kövecses, J. (2013). The role of the mass matrix in the analysis of mechanical systems. *Multibody System Dynamics, 30*(4), 397-412.

159. http://www.andrew.cmu.edu/user/lingzhil/KDC/hw6/hw6.htm

160. http://www.jsme.or.jp/English/jsme%20roadmap/No-5.pdf

161. Hsu, P. (1993). Coordinated control of multiple manipulator systems. *IEEE Transactions on Robotics and Automation, 9*(4), 400-410.

162. Hu, F. L., and Ulsoy, A. G. (1994). Dynamic Modeling of Constrained Flexible Robot Arms for Controller Design. *Journal of Dynamic Systems Measurement and Control*, 116(1), 56-57. doi: 10.1115/1.2900681

163. Hu, Y.-R., Goldenberg, A. A., and Zhou, C. (1995). Motion and force control of coordinated robots during constrained motion tasks. *International Journal of Robotics Research, 14*(4), 351-365.

164. Huang, P., Yang, Q., Bao, G., and Zhang, L. (2013). Dynamic characteristic analysis of new pneumatic bending joint. *Applied Mechanics and Materials*, 271 (1), pp. 1742-1749.

165. Huang, Y., Chen, W., and Sun, Y. (2011). Safety design and realization of an assistive robotic manipulator based on collision detection. *Jiqiren/Robot, 33*(1), 40-45.

166. Hussain, I., Salvietti, G., Malvezzi, M., and Prattichizzo, D. (2017). On the role of stiffness design for fingertip trajectories of underactuated modular soft hands. *IEEE International Conference on Robotics and Automation (ICRA),* Singapore, May 29-June 3, 2017.

167. Hwang, Y.-L. (2008). Analysis of mechanical vibrations and forces using amalgamated decoupling method in multibody mechanical systems. *Communications in Numerical Methods in Engineering, 24*(11), 1553-1566.

168. Hwang, Y.-L. (2006a). Dynamic recursive decoupling method for closed-loop flexible mechanical systems. *International Journal of Non-Linear Mechanics, 41*(10), 1181-1190.

169. Hwang, Y.-L. (2006b). Nonlinear recursive formulation for kinematic and dynamic analysis of robotic manufacturing systems. *Material Science Forum, 505-507(Part 1), pp. 553-558.*

170. Hwang, Y.-L. (2003). Recursive method for the dynamic analysis of open-loop flexible multibody systems. Paper presented at the *Proceedings of the ASME Design Engineering Technical Conference, 5A*, 593-602.

171. Hwang, Y.-L. (2006c). Recursive newton-euler formulation for flexible dynamic manufacturing analysis of open-loop robotic systems. *International Journal of Advanced Manufacturing Technology, 29*(5), 598-604.

172. Hwang, Y.-L., and Wei, Z.-L. (2008). Dynamic analysis and control of 3D flexible mechanisms using nonlinear recursive method in multibody automation systems. *Journal of the Chinese Society of Mechanical Engineers, Transactions of the Chinese Institute of Engineers, Series C/Chung-Kuo Chi Hsueh Kung Ch'Eng Hsuebo Pao, 29*(2), 121-127.

173. Ikizoğlu, S., and Gürışık O. (2018). LQR based optimal control for single-joint flexible link robot. 6th International Conference on Control Engineering & Information Technology (CEIT), 25-27 October 2018, Istanbul, Turkey.

174. Incremona, G. P., De Felici, G., Ferrara, A., and Bassi, E. (2015). A supervisory sliding mode control approach for cooperative robotic system of systems. *IEEE Systems Journal*, 9(1), 263-272. doi: 10.1109/JSYST.2013.2286509

175. Jafarinasab, M., Sirouspour, S., and Dyer E. (2019). Model-based motion control of a robotic manipulator with a flying multirotor base. *IEEE/ASME Transactions on Mechatronics*, 24(5), 2328-2340. doi: 10.1109/TMECH.2019.2936760

176. Jayasuriya, S., and Choura S. (1991). On the finite settling time and residual vibration control of flexible structures. *Journal of Sound and Vibration*, 148(1): 117-136. https://doi.org/10.1016/0022-460X(91)90823-3.

177. Jeleni, G., and Crisfield, M. A. (2001). Dynamic analysis of 3D beams with joints in presence of large rotations. *Computer Methods in Applied Mechanics and Engineering, 190*(32-33), 4195-4230.

178. Jensen-Segal, S., Virost, S., and Provancher, W. R. (2008). ROCR: Dynamic vertical wall climbing with a pendular two-link mass-shifting robot. Paper presented at the *Proceedings - IEEE International Conference on Robotics and Automation*, 3040-3045.

179. Ji, H., and Hu, X. (2011). Design and characterization of a flexible micro-displacement manipulator. *Advanced Materials Research*, 221, 449-454.

180. Jia, Q., Huang, F., Chu, M., and Sun, H. (2013). Dynamic surface control of flexible joints based on extended state observer. *Gaojishu Tongxin/Chinese High Technology Letters, 23*(8), 819-826.

181. Jiang, T., Liu, J., and He, W. (2017). A robust observer design for a flexible manipulator based on a PDE model. *Journal of Vibration and Control*, 23(6) 871-882.

182. Jiang, Z.-H., and Goldenberg, A. A. (1999). Dynamic compensability and compensability measure for robot systems with structural flexibility. *Mechanism and Machine Theory, 34*(8), 1303-1317.

183. Jouybari, B. R., Osgouie, K. G., and Meghdari, A. (2016). Optimization of kinematic redundancy and workspace analysis of a dual-arm cam-lock robot. *Robotica* (2016), 34, 23-42. doi:10.1017/S0263574714000423

184. Kabanov, A. A., and Kramar, V. A. (2021). Cooperative control of underwater manipulators based on the sdre method. *2021 International Russian Automation Conference, RusAutoCon, 515-520.*

185. Kalyoncu, M. (2008). Mathematical modelling and dynamic response of a multi-straight-line path tracing flexible robot manipulator with rotating-prismatic joint. *Applied Mathematical Modelling, 32*(6), 1087-1098.

186. Kadge G. M. (2007). Influence of mode dependent Rayleigh damping on transient stress response. *Master's degree thesis*, Department of Mechanical Engineering, Blekinge Institute of Technology, Karlskrona, Sweden.

187. Kang, B., and Mills, J. K. (2002). Dynamic modeling of structurally-flexible planar parallel manipulator. *Robotica, 20*(3), 329-339.

188. Karagülle, H., Malgaca, L., Dirilmiş, M., Akdağ, M., Yavuz, Ş. (2017). Vibration control of a two-link flexible manipulator. *Journal of Vibration and Control*, 23 (12), 2023-2034.

189. Kasi, V., Mekhilef, S., Ghazilla, R. A. R., and Ahmad, N. (2014). Robotic system development for cooperative orthopedic drilling assistance. *Advances in Mechanical Engineering, 2014.* doi:10.1155/2014/437485

190. Katori, H. (2005). A note on the simulation of linkage mechanism. *Nihon Kikai Gakkai Ronbunshu, C Hen/Transactions of the Japan Society of Mechanical Engineers, Part C, 71*(7), 2253-2259.

191. Khatib, O., Yokoi, K., Chang, K., Ruspini, D., Holmberg, R., and Casal, A. (1996a). Coordination and decentralized cooperation of multiple mobile manipulators. *Journal of Robotic Systems, 13*(11), 755-764.

192. Khatib, O., Yokoi, K., Chang, K., Ruspini, D., Holmberg, R., and Casal, A. (1996b). Vehicle/arm coordination and multiple mobile manipulator decentralized cooperation. *IEEE International Conference on Intelligent Robots and Systems, 2,* 546-553.

193. Kim, D., Lee, S. J., and Kim, H. J. (2019). Trajectory Tracking for Cooperative Transportation with T3-multirotor. *19th International Conference on Control, Automation and Systems (ICCAS 2019),* Oct. 15-18, 2019, ICC Jeju, Jeju, Korea.

194. Kim, J.-S., and Uchiyama, M. (2000). Dynamic modeling of two cooperating flexible manipulators. *KSME International Journal, 14*(2), 188-196.

195. Ko, K.E., Park, S.-M., Park, J., and Sim, K.-B. (2011). A study on swarm robot-based invader-enclosing technique on multiple distributed object environments. *Journal of Electrical Engineering and Technology, 6*(6), 806-816.

196. Korayem, A. H., Azimirad, V., Binabaji, H., and Korayem, M. H. (2012). Sensitivity analysis of flexible joint nonholonomic wheeled mobile manipulator in singular configuration. *Acta Astronautica, 72,* 62-77.

197. Korayem, M. H., Davarpanah, F., and Ghariblu, H. (2006). Load carrying capacity of flexible joint manipulators with feedback linearization. *International Journal of Advanced Manufacturing Technology, 29*(3-4), 389-397.

198. Korayem, M. H., and Dehkordi, S. F. (2018). Derivation of motion equation for mobile manipulator with viscoelastic links and revolute-prismatic flexible joints via recursive Gibbs-Appell formulations. *Robotics and Autonomous Systems,*103, 175-198.

199. Korayem, M. H., Heidari, A., and Nikoobin, A. (2009). Effect of payload variation on the residual vibration of flexible manipulators at the end of a given path. *Scientia Iranica, 16*(4 B), 332-343.

200. Korayem, M. H., Shafei, A. M., and Shafei, H. R. (2012). Dynamic modeling of nonholonomic wheeled mobile manipulators with elastic joints using recursive Gibbs-Appell formulation. *Scientia Iranica, 19*(4), 1092-1104.

201. Krebs, H. I., Palazzolo, J. J., Dipietro, L., Ferraro, M., Krol, J., Rannekleiv, K., Volpe, B. T., Hogan, N. (2003). Rehabilitation Robotics: Performance-Based Progressive Robot-Assisted Therapy. *Autonomous Robots*, 15(1), 7-20.

202. Krikochoritis, T. E., and Tzafestas, S. G. (2001). Control of flexible joint robots using neural networks. *IMA Journal of Mathematical Control and Information, 18*(2), 269-280.

203. Laffranchi, M., Chen, L., Tsagarakis, N. G., and Caldwell, D. G. (2012). The role of physical damping in compliant actuation systems. Paper presented at the *IEEE International Conference on Intelligent Robots and Systems*, 3079-3085.

204. Lai, X., Hu, S., Ning, Z., Wang, X., and Jian, L. (2008). Modeling fuzzy belief with plausibility degree in intelligent systems. Paper presented at the *3rd International Conference on Innovative Computing Information and Control, ICICIC'08, 4603675.*

205. Laub, A. J. (1979). A Schur method for solving algebraic Riccati equations. *IEEE Transactions on Automatic Control,* AC-24(6). doi: 0018-9286/79/1200-0913%00.75

206. Le, T. -N., Battini, J. -M., and Hjiaj, M. (2012). Dynamics of 3D beam elements in a corotational context: A comparative study of established and new formulations. *Finite Elements in Analysis and Design, 61*, 97-111.

207. Lee, H.-H. (2005). Modeling and control of a horizontal two-link rigid/flexible robot. Paper presented at the *American Society of Mechanical Engineers, Dynamic Systems and Control Division (Publication) DSC, 74 DSC* (2 PART B), 1921-1927.

208. Lee, S. (1989). Dual redundant arm configuration optimization with task-oriented dual arm manipulability. *IEEE Transactions on Robotics and Automation, 5*(1), 78-97.

209. Lee, S., and Kim, S. (1990). Dual redundant arm system operational quality measures and their applications: Dynamic measures. *Proceedings of the IEEE Conference on Decision and Control, 2*, 1128-1130.

210. Lee, Su-Lin, Lerotic, Mirna, Vitiello, Valentina, Giannarou, Stamatia, Kwok, Ka-Wai, Visentini-Scarzanella, Marco, Yang, Guang-Zhong (2009). From medical images to minimally invasive intervention: Computer assistance for robotic surgery. *Computerized Medical Imaging and Graphics*, doi:10.1016/j.compmedimag.2009.07.007

211. Lee, Y.-H., and Lee, J.-J., (2003). Modeling of the dynamics of tendon-driven robotic mechanisms with flexible tendons. *Mechanism and Machine Theory, 38*(12), 1431-1447.

212. Li, C.-J. and Sankar, T. S. (1993). Systematic Methods for Efficient Modeling and Dynamics Computation of Flexible Robot Manipulators. *IEEE Transactions on Systems, Man, and Cybernetics*, 23(1), 77-95.

213. Li, H., Yang, Z., and Huang, T. (2009). Dynamics and elasto-dynamics optimization of a 2-DOF planar parallel pick-and-place robot with flexible links. *Structural and Multidisciplinary Optimization, 38*(2), 195-204.

214. Li, W., and Gao, C. (2010). Design and modeling of micro-displacement amplifying mechanism using revolute joints and flexible hinges. Paper presented at the *2010 International Conference on Intelligent Computation Technology and Automation, ICICTA 2010, 1*, 1147-1150.

215. Li, Y., Liu, X., Peng, Z., and Liu, Y. (2002). The identification of joint parameters for modular robots using fuzzy theory and a genetic algorithm. *Robotica, 20*(5), 509-517.

216. Li, Y., Tong, S., and Li, T. (2012). Fuzzy adaptive dynamic surface control for a single-link flexible-joint robot. *Nonlinear Dynamics, 70*(3), 2035-2048.

217. Li, Y., Tong, S., and Li, T. (2013). Adaptive fuzzy output feedback control for a single-link flexible robot manipulator driven DC motor via backstepping. *Nonlinear Analysis: Real World Applications, 14*(1), 483-494.

218. Li, Z., Melek, W. W., and Clark, C. (2009). Decentralized robust control of robot manipulators with harmonic drive transmission and application to modular and reconfigurable serial arms. *Robotica, 27*(2), 291-302.

219. Li, Z., Ren, H, Chiu, P. W. Y., Du, R., Yu, H. (2016). A novel constrained wire-driven flexible mechanism and its kinematic analysis. *Mechanism and Machine Theory,* 95 (2016), 59-75.

220. Lian, K.-Y., Chiu, C.-S., and Liu, P. (2002). Semi-decentralized adaptive fuzzy control for cooperative multi-robot systems with H-info motion/internal force tracking performance. *IEEE Trans. Syst. Man Cybern. - Part B: Cybernetics,* 32, pp. 269-280.

221. Liu, G., Liu, Y., and Goldenberg, A. A. (2011). Design, analysis, and control of a spring-assisted modular and reconfigurable robot. *IEEE/ASME Transactions on Mechatronics, 16*(4), 695-706.

222. Liu, S., Liu, K., and Li, Y. (2012). A new sliding mode control of manipulator handling a flexible payload based on distributed parameter system. Paper presented at the *Chinese Control Conference, CCC*, 3212-3217.

223. Liu, S.-Y, Liu, K. -P., and Li, Y.-C. (2013). Distributed parameter control for system of manipulator handling a flexible payload based on coupled sliding surface. *Jilin Daxue Xuebao (Gongxueban)/Journal of Jilin University (Engineering and Technology Edition), 43*(1), 267-272.

224. Liu, S., Wang, Z., Qiao, Y., Xie, M., and Li, Y. (2012). An energy-based position control and asymptotic stability analysis for manipulator handling a flexible payload. Paper presented at the *Proceedings of the World Congress on Intelligent Control and Automation (WCICA)*, 3617-3622.

225. Liu, X., Wang, Y., Geng, D., Zhao, Y., and Zhang, J. (2012). *Dynamics investigation on bidirectional active flexible bending joints*. Advanced Material Research, 422, 529-533.

226. Liu Y.-H., and Arimoto, S. (1998). Decentralized adaptive and nonadaptive position/force controller for redundant manipulators in cooperation. *International Journal of Robotic Research*, 17, pp. 232-243.

227. Liu, Y., and Yu, Y. (2003). Dynamic analysis of redundant flexible robots cooperating a rigid payload. *Proceedings of the International Symposium on Test and Measurement, 6*, 4509-4512.

228. Liu, Z., Sun, R., and Li, M. (2019). Research on Trajectory Tracking and Vibration Suppression of a Smart Flexible-joint-and-link Space Manipulator. *IOP Conf. Series: Journal of Physics: Conf. Series*, 1187(2019), 032076.

229. Long, P., Khalil, W., and Caro, S. (2014). Kinematic and dynamic analysis of lower-mobility cooperative arms. *Robotica*, http://dx.doi.org/10.1017/S0263574714001039

230. Low, K. H. (1997). A note on the effect of hub inertia and payload on the vibration of a flexible slewing link. *Journal of Sound and Vibration*, 204(5), 823-828.

231. Low, K. H., and Vidyasagar, M. (1988). A Lagrangian Formulation of the Dynamic Model for Flexible Manipulator Systems. *J. Dyn. Sys., Meas., Control*, 110(2), 175-181.

232. Lu, J.-W., Sun, X.-M., Vakakis, A. F., and Bergman, L. A. (2015). Influence of backlash in gear reducer on dynamic of single-link manipulator arm. *Robotica*, *33*(8), 1671-1685. doi:10.1017/S0263574714000915

233. Luca, A. de, and Siciliano, B. (1991). Closed-Form Dynamic Model of Planar Multilink Lightweight Robots. *IEEE Transactions on Systems, Man, and Cybernetics*, 21(4), 826-839.

234. Luca, A. de and Siciliano B. (1993). Regulation of Flexible Arms Under Gravity. *IEEE Transaction on Robotics and Automation*, 9(4), 463-467.

235. Luecke G. R., and Lai, K. W. (1997). A joint error-feedback approach to internal force regulation in cooperating manipulator systems. *J. Robot. Syst.*, 14, 1997, 631-648.

236. Ma, D., and Tang, Z. (2013). Vibration suppression for two manipulators handling a flexible payload based on observer. Paper presented at the *Proceedings - 2012 IEEE 2nd International Conference on Cloud Computing and Intelligence Systems, IEEE CCIS 2012, 3*, 1449-1453.

237. Meirovitch, L. (1967). Analytical Methods in Vibrations. *Macmillan USA, Facsimile edition.*

238. Madhusoodanan, K. R., and Ushakumari, S. (2012). Sliding mode control and fuzzy logic control of hydraulic robot manipulator. *Advances in Modelling and Analysis C*, *67*(1-2), 43-59.

239. Mahato, S., and Dixit, U. S. (2014). Parametric study of double link flexible manipulator. *Universal Journal of Mechanical Engineering*, 2(7), 211-219.

240. Malgaca, L., Yavuz, Ş., Akdağ, M., and Karagülle, H. (2016). Residual vibration control of a single link flexible curved manipulator. *Simulation Modelling Practice and Theory*, 67, 155-170.

241. Maouche, A. R., and Attari, M. (2007). Hybrid control strategy for flexible manipulators. *IEEE International Symposium on Industrial Electronics*, 50-55.

242. Marques, F., Roupa, I., Silva, M. T., Flores, P. (2021). Examination and comparison of different methods to model closed loop kinematic chains using Lagrangian formulation with cut joint, clearance joint constraint elastic joint approaches. *Mech. Mach. Theory*, 160, 104294.

243. Martin, A., and Emami, M. R. (2011). Dynamic load emulation in hardware-in-the-loop simulation of robot manipulators. *IEEE Transactions on Industrial Electronics*, *58*(7), 2980-2987.

244. Martin, E., Papadopoulos, E., and Angeles, J. (1998). Control scheme for the reduction of thruster-manipulator interactions in space robotic systems. Paper presented at the *IEEE International Conference on Intelligent Robots and Systems, 2*, 1352-1357.

245. Martins, J., Ayala Botto, M., and Da Costa, J. S. (2002). Modeling of flexible beams for robotic manipulators. *Multibody System Dynamics, 7*(1), 79-100.

246. Matei, Daniela-Maria Privantu (2012). The Study of Cooperative Robots Behaviors in Automatic Industrial Manufacturing. *International Conference on Applied and Theoretical Electricity, ICATE 2012 – Proceedings*, 6403470.

247. Matsuno, F., and Hatayama, M. (1995). Quasi-static cooperative control of two two-link flexible manipulators. *IEEE International Conference on Robotics and Automation,* 1, 615-620.

248. McPhee, J., Shi, P., and Piedbœuf, J.-C. (2002). Dynamics of multibody systems using virtual work and symbolic programming. *Mathematical and Computer Modelling of Dynamical Systems, 8*(2), 137-155.

249. Mechefske, C. K., Zhou, Z., and Xi, F. (2010). Modeling of configuration-dependent flexible joints for a parallel robot. *Advances in Mechanical Engineering, Vol. 2010, Art. ID 143961*.

250. Meng, D., She, Y., Xu, W., Lu, W., and Liang, B. (2018). Dynamic modeling and vibration characteristics analysis of flexible-link and flexible-joint space manipulator. *Multibody System Dynamics*, 43, 321-347.

251. Minakata, H., Ito, R., and Tadakuma, S. (2002). An experimental study of pseudo passive walking robot discussions about control parameters and expansion to flexible shoe system. Paper presented at the *International Workshop on Advanced Motion Control, AMC*, 449-454.

252. Mishra, N., and Singh, S. P. (2019). Hybrid vibration control of a two-link flexible manipulator. *SN Applied Science*, 1, 715.

253. Miyabe, T., Konno, A., Uchiyama, M., and Yamano, M. (2004). An approach toward an automated object retrieval operation with a two-arm flexible manipulator. *International Journal of Robotics Research, 23*(3), 275-291.

254. Moghanni-Bavil-Olyaei, M.-R., Ghanbari, A., Keighobadi, J. (2019). Trajectory tracking control of a class of underactuated mechanical systems with nontriangular normal form

based on block backstepping approach. *Journal of Intelligent & Robotic Systems* 96, 209-221.

255. Mohan, A., Singh, S. P., and Saha, S. K. (2010). A cohesive modeling technique for theoretical and experimental estimation of damping in serial robots with rigid and flexible links. *Multibody System Dynamics, 23*(4), 333-360.
256. Mordfin, T. G., and Tadikonda, S. S. K. (2000). Truth models for articulating flexible multibody dynamic systems. *Journal of Guidance, Control, and Dynamics, 23*(5), 805-811.
257. Munasinghe, S. R., Nakamura, M., Aoki, S., Goto, S., and Kyura, N. (1999). High speed precise control of robot arms with assigned speed under torque constraint by trajectory generation in joint co-ordinates. *IEEE International Conference on Systems, Man and Cybernetics, 2,* II-854 - II-859.
258. Munawar, K., and Uchiyama, M. (1997). Slip compensated manipulation with cooperating multiple robots. *IEEE Conference on Decision and Control, 2,* 1918-1923.
259. Murphy, S. H., Wen, J. T., and Saridis, G. N. (1991). Analysis of cooperative robot manipulators on a mobile platform. Paper presented at the *Proceedings of SPIE - the International Society for Optical Engineering, 1387* 14-25.
260. Na, K.-S, and Kim, J.-H. (2001). Dynamic analysis for the deployment of a multi-link flexible structure undergoing locking. *Collection of Technical Papers - AIAA/ASME/ASCE/AHS/ASC Structures, Structural Dynamics and Materials Conference*, 3, pp. 2173-2183.
261. Naganathan G., and Soni A. H. (1987). Coupling effects of kinematics and flexibility in manipulators. *The International Journal of Robotics Research*, 6(1):75-84. doi:10.1177/027836498700600106
262. Nakamura, Masatoshi, Iwanaga, Takuya, Goto, Satoru, and Kyura, Nobuhiro (2002). Trajectory Allowance under Torque and Speed Constraint: Trajectory Generation and Taught Data Generation. *Trans. of the Society of Instrument and Control Engineers*, Vol. E-2, No.1, pp.33-41.
263. Nakano E., Ozaki S., Ishida T., Kato I. (1974). Cooperational control of the anthropomorphous manipulator 'MELARM'. *Proc. 4th Int. Symp. on Industrial Robots,* Tokyo, pp, 251- 260.

264. Narula, N. S., Bhatnagar, A., Kumar, V., Rana, K. P. S. (2017) A teacher learning based optimization approach to tune backstepping controller for a single-link flexible-joint manipulator. *IEEE 2nd International Conference on Communication, Control and Intelligent Systems (CCIS 2017).*

265. Nataraj, C. (1993). Flexibility Effects in a Single Link Robotic Manipulator. *Proceedings of the ASME 1993 Design Technical Conferences. 14th Biennial Conference on Mechanical Vibration and Noise: Vibrations and Dynamics of Robotic and Multibody Structures*. Albuquerque, New Mexico, USA. September 19-22, 1993. pp. 115-122. https://doi.org/10.1115/DETC1993-0150

266. Ni, F., Liu, Y., and Dang, J. (2012). Fuzzy-sliding mode control for flexible-joint manipulator based on friction compensation. Paper presented at the *IEEE International Conference on Mechatronics and Automation, ICMA 2012,* 1868-1873.

267. Nikoobin, A., and Haghighi, R. (2009). Lyapunov-based nonlinear disturbance observer for serial n-link robot manipulators. *Journal of Intelligent and Robotic Systems: Theory and Applications, 55*(2-3), 135-153.

268. Niu, B. (2013). Parasitic torque pulsation suppression in drive train of flexible joint industrial robot. Paper presented at the *44th International Symposium on Robotics, ISR 2013.*

269. Njeri, W., Sasaki, M., and Matsushita, K. (2018.a). Two-degree-of-freedom control of a multilink flexible manipulator using filtered inverse feedforward controller and strain feedback controller. *Proceedings of 4th IEEE International Conference on Applied System Innovation 2018, ICASI,* 972-975.

270. Njeri, W., Sasaki, M., and Matsushita, K. (2018.b). Enhanced vibration control of a multilink flexible manipulator using filtered inverse controller. *Robomech Journal, 5(1): 28.* doi: 10.1186/s40648-018-0125

271. Njeri, W., Sasaki, M., and Matsushita, K. (2019). Gain Tuning for High-Speed Vibration Control of a Multilink Flexible Manipulator Using Artificial Neural Network. *Journal of Vibration and Acoustics, Transaction of the ASME,* 141(4). doi: 101115/1.4043241

272. Ollero, A., Tognon, M., Suarez, A., Lee, D., and Franchi, A. (2021). Past, present, and future of aerial robotic manipulators. *IEEE Transactions on Robotics*. doi:10.1109/TRO.2021.3084395

273. Omar, A., Ri, P., and Zhang, Y. (2016). Control algorithm trajectory planning for dual cooperative manipulators with experimental verification. *MATEC Web of Conferences*, 7, 05005, (2016). doi: 10.1051/matecconf/2016750500

274. Onen, U., Tinkir, M., Kalyoncu, M., and Botsali, F. M. (2010). Adaptive network based fuzzy logic control of a rigid - flexible robot manipulator. Paper presented at the *2nd International Conference on Computer and Automation Engineering, ICCAE 2010, 1, 102-106.*

275. Orin, D. E. and Oh, S. Y. (1981) Control of force distribution in robotic mechanisms containing of closed kinematic chains. *Trans. ASME J. Dyn. Syst. Meas. Contr.*, 102, 1981, 134-141.

276. Orlowski, C. T., and Girard, A. R. (2012). Dynamics, stability, and control analyses of flapping wing micro-air vehicles. *Progress in Aerospace Sciences*, 51 (2012), 18-30.

277. Ott, C., Albu-Schäffer, A., Kugi, A., and Hirzinger, G. (2003). Decoupling based cartesian impedance control of flexible joint robots. Paper presented at the *Proceedings - IEEE International Conference on Robotics and Automation, 3,* 3101-3107.

278. Otten, E. (2003). Inverse and forward dynamics: models of multi-body systems. *Philos Trans R Soc Lond B Biol Sci*, 358(1437), 1493–1500. doi: 10.1098/rstb.2003.1354

279. Ouyang, P. R., Dam, T., Huang, J., and Zhang, W. J. (2012). Contour tracking control in position domain. *Mechatronics, 22*(7), 934-944.

280. Ouyang, Y., He, W., and Li, X. (2017). Reinforcement learning control of a single-link flexible robotic manipulator. *IET Control Theory Appl.*, 11(9), 1426-1433.

281. Ouyang, Y., He, W., Li, X., Liu, J.-K., and Li, G. (2017). Vibration control based on reinforcement learning for a single-link flexible robotic manipulator. *IFAC PapersOnLine*, 50(1), 3476-3481.

282. Pai, D. K., Ascher, U. M., and Kry, P. G. (2000). Forward Dynamics Algorithms for Multibody Chains and Contact. *Robotics and Automation, 2000. Proceedings. ICRA '00. IEEE*. doi**:** 10.1109/ROBOT.2000.844157

283. Pan, B., Sun, J., and Yu, D.-Y. (2010). Modeling, control and simulation of space manipulators with flexible joints. *Xitong Fangzhen Xuebao / Journal of System Simulation, 22*(8), 1826-1831.

284. Panwar, V., Kumar, N., Sukavanam, N., and Borm, J. -H. (2012). Adaptive neural controller for cooperative multiple robot manipulator system manipulating a single rigid object. *Applied Soft Computing Journal, 12*(1), 216-227.

285. Park, C.-W., and Cho, Y.-W. (2003). Adaptive tracking control of flexible joint manipulator based on fuzzy model reference approach. *IEEE Proceedings: Control Theory and Applications*, 150(2), 198-204.

286. Park, J. B., Yoo, S. J., and Choi, Y. H. (2008). Output feedback dynamic surface control of flexible-joint robots. *International Journal of Control, Automation and Systems*, 6(2), 223-233.

287. Park, S. H., and Han, S. I. (2011). Robust-tracking control for robot manipulator with deadzone and friction using backstepping and RFNN controller. *IET Control Theory and Applications*, 5(12), 1397-1417.

288. Payo, I., Ramos, F., Cortázar, O. D., and Feliu, V. (2005). Experimental validation of nonlinear dynamic models for single-link very flexible arms. Paper presented at the *Proceedings of the 44th IEEE Conference on Decision and Control, and the European Control Conference, CDC-ECC '05, 2005*, 5304-5309.

289. Peng, J., Xu, W., Wang, F., Han, Y., and Liang, B. (2021). A hybrid hand-eye calibration method for multilink cable-driven hyper-redundant manipulators. *IEEE Transactions on Instrumentation and Measuremen*, 70. doi: 10.1109/TIM.2021.3078523

290. Peng, X., Yuan, J., Zhang, W., Yang, Y., and Song, Y. (2012). Kinematic and dynamic analysis of a serial-link robot for inspection process in EAST vacuum vessel. *Fusion Engineering and Design, 87*(5-6), 905-909.

291. Perdereau, V., and Drouin, M. (1996). Hybrid external control for two robot coordinated motion. *Robotica, 14*(2), 141-153.

292. Persad, P., Loutan Jr., K., and Maharaj, C. (2010). Dynamic stress analysis of a spring actuated manipulator with tip payload. Paper presented at the *Proceedings of the IASTED International Conference on Robotics, Robo 2010*, 141-147.

293. Peza-Solis, J. F., Silva-Navarro, G., Garcia-Perez, O. A., Trujillo-Franco, L. G. (2022). Trajectory tracking of a single flexible-link robot using a modal cascaded-type control. *Applied Mathematical Modelling* 104 (2022), 531-547.

294. Phung, A. S., Malzahn, J., Hoffmann, F., and Bertram, T. (2011). Data based kinematic model of a multi-flexible-link robot arm for varying payloads. *IEEE International Conference on Robotics and Biomimetics, ROBIO 2011*, 1255-1260.

295. Piltan, F., Emamzadeh, S., Hivand, Z., Shahriyari, F., and Mirzaei, M. (2012). PUMA-560 Robot Manipulator Position Sliding Mode Control Methods Using MATLAB/SIMULINK and Their Integration into Graduate/Undergraduate Nonlinear Control, Robotics and MATLAB Courses. *International Journal of Robotic and Automation, (IJRA)*, 6(3).

296. Pin, F. G., Parker, L. E., and De Piero, F. W. (1992). On the design and development of a human-robot synergistic system. *Robotics and Autonomous Systems, 10*(2-3), 161-184.

297. Potenza, F., Lepidi, M., Sabatinoa, U. D., and Gattulli, V. (2017). Nonlinear dynamics of a parametric analytical model for beam-cable-beam structures. *X International Conference on Structural Dynamics, EURODYN* 2017, Procedia Engineering, 199, 796-801.

298. Qian, Z., and Zhang, D. (2012). *Impact dynamics of multi-link robots with link and joint flexibility*. *Applied Mechanics and Materials*, 226-228, pp.685-692.

299. Qian, Z., Zhang, D., and Jin, C. (2018). A regularized approach for frictional impact dynamics of flexible multi-link manipulator arms considering the dynamic stiffening effect. *Multibody System Dynamics*, 43(3), 229-255. doi: 10.1007/s11044-017-9589-0

300. Qian, Z., Zhang, D., and Liu, J. (2013). Recursive formulation for dynamic modeling and simulation of multilink spatial flexible robotic manipulators. *Advances in Mechanical Engineering*, 2013. doi: 10.1155/2013/216014

301. Qiang, Y., Jing, F., Zeng, J., and Hou, Z. (2012). Dynamic modeling and vibration mode analysis for an industrial robot with rigid links and flexible joints. Paper presented at the *Proceedings of the 2012 24th Chinese Control and Decision Conference, CCDC 2012*, 3317-3321

302. Rafieian, F., Liu, Z., and Hazel, B. (2009). Dynamic model and modal testing for vibration analysis of robotic grinding process with a 6DOF flexible-joint manipulator. Paper presented at the *IEEE International Conference on Mechatronics and Automation, ICMA 2009*, 2793-2798.

303. Raju, E. M., Krishna, L. S. R., Mouli, Y. S. C., and Rao, V. N. (2015). Effect of link flexibility on tip position of a single link robotic arm. *Journal of Physics: Conference Series, 662*(1). doi:10.1088/1742-6596/662/1/012020

304. Ramalingam, S., Rasool, M. S., Manigandan, S., and Prem Anand, T. P. (2021). Hybrid polymer composite material for robotic manipulator subject to single link flexibility. *International Journal of Ambient Energy* 42(5), 514-521. doi: 10.1080/01430750.2018.1557551

305. Rao, S. S. (2003). *Mechanical Vibrations*. 4thed. India, Pearson Education.

306. Raţ, N. R., and Neagoe, M. (2009). Rigid vs. flexible links dynamic analysis of a 3DOF parallel robot. *3rd IEEE International Conference on Digital Ecosystems and Technologies, DEST '09*, 534-539.

307. Reddy, B. S., and Ghosal, A. (2015). Nonlinear dynamics of a rotating flexible link. *Journal of Computational and Nonlinear Dynamics, 10*(6) doi:10.1115/1.4028929

308. Reshmin, S. A. (2001). The dynamics of a manipulator with flexible joints. *Izvestiya Akademii Nauk.Teoriya i Sistemy Upravleniya*, (4), 168-176.

309. Ridao P. (2014). An Introduction to Applied Underwater Robotics, http://www.irs.uji.es/trident/files/SIE017-Seminario-PRidao.pdf, downloaded on 8-07-2014.

310. Rodriguez-Angeles, A. and Nizmeijer, H. (2004). Mutual synchronization of robots via estimated state feedback: a cooperative approach. *IEEE Trans. Contr. Syst. Technol.*, 12, 2004, pp. 542-554.

311. Rognant, M., Courteille, E., and Maurine, P. (2010). A systematic procedure for the elastodynamic modeling and identification of robot manipulators. *IEEE Transactions on Robotics, 26*(6), 1085-1093.

312. Saha, S. K. (2012). Introduction to Robotics, *Tata McGraw Hill Education Private Limited*, sixth reprint.

313. Samiei, E., and Shafiee, M. (2010). Descriptor modeling and response analysis of two rigid-flexible cooperative arms. *11th International Conference on Control, Automation, Robotics and Vision, ICARCV 2010*, 149-156.

314. Santos, C., and Ferreira, M. (2006). Ball Catching by a Puma Arm: A Nonlinear Dynamical Systems Approach. *Proceedings of the 2006 IEEE/RSJ*.

315. Sarkar, N., Yun, X., and Kumar, V. (1994). Control of a single robot in a decentralized multi-robot system. *Proceedings-IEEE International Conference on Robotics and Automation, 2*, 896-901.

316. Sawada, M., and Itamiya, K. (2012). A position control of 2 DOF flexible link robot arms based on computed torque method. *International Conference on Advanced Mechatronic Systems, ICAMechS 2012*, 547-552.

317. Schilling, R. J. (2009). Fundamental of Robotics: Analysis and Control, *Eastern Economy Publication*, Ed. 2009.

318. Schneider, S. A., and Cannon Jr., R. H. (1992). Object impedance control for cooperative manipulation: Theory and experimental results. *IEEE Transactions on Robotics and Automation, 8*(3), 383-394.

319. Seo, S. -W., Yang, H.-C., and Sim, K.-B. (2009). Behavior learning and evolution of swarm robot system for cooperative behavior. *IEEE/ASME International Conference on Advanced Intelligent Mechatronics, AIM*, 673-678.

320. Setoodeh, P., Sirouspour, S., and Shahdi, A. (2006). Discrete-time multi-model control for cooperative teleoperation under time delay. *IEEE International Conference on Robotics and Automation, 2006*, 2921-2926.

321. Sharifi, M., and Sayyaadi, H. (2015). Nonlinear robust adaptive Cartesian impedance control of UAVs equipped with a robot manipulator. *Advanced Robotics*, 29 (3), 171-186, http://dx.doi.org/10.1080/01691864.2014.1002529

322. Shi, Z. X., Fung, E. H. K., and Li, Y. C. (1999). Dynamic modelling of a rigid-flexible manipulator for constrained motion task control. *Applied Mathematical Modelling, 23*(7), 509-525.

323. Shitole, C., and Sumathi, P. (2015). Sliding DFT-based vibration mode estimator for single-link flexible manipulator. *IEEE/ASME Transactions on Mechatronics, 20*(6), 3249-3256. doi:10.1109/TMECH.2015.2391132

324. Shao, M., Huang, Y., and Silberschmidt, V. V. (2020). Intelligent manipulator with flexible link and joint, modeling and vibration control. *Shock and Vibration,* 2020, Article ID 4671358.

325. Shuai, G., Leying, D., Yuping, O., and Yefeng. (2009). The study of humanoid robot head motion planning. Paper presented at the *2009 IEEE International Conference on Robotics and Biomimetics, ROBIO 2009,* 376-379.

326. Siciliano, Bruno, Khatib, Oussama (Eds.) (2008). Springer Handbook of Robotics, Springer publication.

327. Simaan, N., Xu, K., Kapoor, A., Wei, W., Kazanzides, P., Flint, P., and Taylor, R. (2009). Design and integration of a telerobotic system for minimally invasive surgery of the throat**.** *International Journal of Robotic Research,* 28(9): 1134–1153. doi:10.1177/0278364908104278.

328. Singla, A., Tewari, A., and Dasgupta, B. (2015). Vibration suppression during input tracking of a flexible manipulator using a hybrid controller. *Sadhana - Academy Proceedings in Engineering Sciences, 40*(6), 1865-1898. doi:10.1007/s12046-015-0392-4

329. Spong, M. W. (1989). Adaptive control of flexible joint manipulators. *Systems and Control Letters* 13(1), 15-21.

330. Spong, M. W., Hutchinson, S., Vidyasagar, M. (2006). Robot Modeling and Control, *Wiley India Edition*, Ed. 2006.

331. Stolfi, A., Gasbarri, P., and Sabatini, M. (2018). A parametric analysis of a controlled deployable space manipulator for capturing a non-cooperative flexible satellite. *Acta Astronautica,* 148 (2018), 317-326.

332. Sujan, V. A., and Meggiolaro, M. A. (2004). Model predictive disturbance rejection during cooperative mobile robot assembly tasks. *Journal of the Brazilian Society of Mechanical Sciences and Engineering, 26*(3), 260-268.

333. Sun, B., Xu, W., and Yang, R. -. (2004). Dynamic modeling and analysis of a cleaning robot for hotline insulators. *Shanghai Jiaotong Daxue Xuebao/Journal of Shanghai Jiaotong University, 38*(8), 1304-1306.

334. Sun, D. and Mills, J. K. (2002). Adaptive synchrinised control for coordination of multirobot assembly tasks. *IEEE, Trans. Robot. Autom.*, 18, 2002, pp. 498-510.

335. Sun, H., Chu, M., and Jia, Q. (2010). Hybrid control using wavelet neural networks and robust method for flexible joint with friction and uncertainties compensation. *Jixie Gongcheng Xuebao/Journal of Mechanical Engineering, 46*(13), 68-75.

336. Sun, H., Wu, H., Shao, B., and Tian, F. (2009). The finite segment method for recursive approach to flexible multibody dynamics. Paper presented at the *2009 2nd International Conference on Information and Computing Science, ICIC 2009, 3,* 345-348.

337. Sun, H., Wu, H., Tian, F., and Shao, B. (2009). Dynamic software flow of the rigid-flexible coupling system based on spatial operator algebra theory. *Huazhong Keji Daxue Xuebao (Ziran Kexue Ban)/Journal of Huazhong University of Science and Technology (Natural Science Edition), 37*(12), 107-111.

338. Sun, Q., Sharf, I., and Nahon, M. (1999). Stability analysis of the force distribution algorithm for flexible-link cooperating manipulators. *Mechanism and Machine Theory, 34*(5), 753-763.

339. Sun, T., Song, Y. M., and Yan, K. (2011). Kineto-static analysis of a novel high-speed parallel manipulator with rigid-flexible coupled links. *Journal of Central South University of Technology (English Edition), 18*(3), 593-599.

340. Sun, Z., Yang, H., Ma, Y., Wang, X., Mo, Y., Li, H., and Jiang, Z. (2022). BIT-DMR: a humanoid dual-arm mobile robot for complex rescue operations. *IEEE Robotics and Automation Letters*, 7(2), 2022.

341. Suzuki, T., and Ebihara, Y. (2007). Casting control for hyper-flexible manipulation. Paper presented at the *Proceedings - IEEE International Conference on Robotics and Automation,* 1369-1374.

342. Suzuki, T., Ebihara, Y., and Shintani, K. (2005). Dynamic analysis of casting and winding with hyper-flexible manipulator. *International Conference on Advanced Robotics, ICAR '05, Proceedings, 2005,* 64-69.

343. Svinin, M., Goncharenko, I., and Hosoe, S. (2006). Motion planning of human-like movements in the manipulation of flexible objects. *Advances in Robot Control: From Everyday Physics to Human-Like Movements*, pp. 263-291.

344. Svinin, M. M., and Uchiyama, M. (1994). Coordinated dynamic control of a system of manipulators coupled via a flexible object. *Prepr. 4th IFAC Symp. on Robot Control, Capri*, pp. 1005-1010.

345. Taghirad, H. D., and Khosravi, M. A. (2003). Design and simulation of robust composite controllers for flexible joint robots. Paper presented at the *Proceedings - IEEE International Conference on Robotics and Automation, 3,* 108-3113.

346. Takase, K., Inoue, H., Sato, K., and Hagiwara, S. (1974). The design of an articulated manipulator with torque control ability. *Proc. 4th Int. Symp. Ind. Robots (Tokyo)*, pp. 261-270.

347. Tan, D. (2003). Dynamic simulations of space manipulators with flexible links. Paper presented at the *54th International Astronautical Congress of the International Astronautical Federation (IAF), the International Academy of Astronautics and the International Institute of Space Law*, *1*, 433-443.

348. Tan, W., Ding, F. Q., and Zhao, X. F. (2001). Stability analysis of the joint flexibility of direct-drive robots. *Shanghai Jiaotong Daxue Xuebao/Journal of Shanghai Jiaotong University*, *35*(1), 51-53.

349. Tang, L., Gouttefarde, M., Sun, H., Yin, L., and Zhou, C. (2021). Dynamic modelling and vibration suppression of a single-link flexible manipulator with two cables. *Mechanism and Machine Theory*, 162, 104347.

350. Tang, Z., Xu, J., Liu Keping, and Li, Y. (2012). An adaptive backstepping observer-controller design for manipulators cooperating flexible payload. *9th International Conference on Fuzzy Systems and Knowledge Discovery, FSKD 2012*, 2343-2347.

351. Tapia Herrera, R., Palacios Montúfar, C., Alcántara Montes, S., and Flores Campos, J. A. (2010). Dynamic analysis of an industrial robot manipulator using dual numbers. *IEEE Electronics, Robotics and Automotive Mechanics Conference, CERMA 2010*, 331-336.

352. Taylor, Russell H. (2001). Computer-Integrated Surgery: Coupling Information to Action in 21st Century Medicin. Invited address to the *Annual Meeting of the Society of Urological Engineers*, Anaheim, Ca. June 2, 2001.

353. Taylor, Russell H. (2003). Medical Robotics in Computer-Integrated Surgery. *IEEE Transactions on Robotics and Automation*, 19(5).

354. Thapa, S., Bai, H., and Acosta´, J. A. (2018). Force control in cooperative aerial manipulation. *2018 International Conference on Unmanned Aircraft Systems*, Dallas, TX, USA.

355. Theingi, Chen, I. -M., Li, C., and Angeles, J. (2006). The dynamic analysis of a planar parallel manipulator with joint-coupling. Paper presented at the *9th International Conference on Control, Automation, Robotics and Vision, ICARCV '06*,

356. Theodore, R. J., and Ghosal, A. (1995). Comparison of the assumed modes and finite element models for flexible multi-link manipulators. *The International Journal of Robotics Research*, 14(2), 91-111.

357. Theodore, R. J., and Ghosal, A. (2003). Robust control of multilink flexible manipulators. *Mechanism and Machine Theory*, 38, 367-377.

358. Tian, Q., Liu, C., Liu, L.-K., and Li, X.-G. (2013). Study on coupling dynamics and control of flexible capturing robot and solar panel. *Xitong Fangzhen Xuebao / Journal of System Simulation*, *25*(7), 1609-1616.

359. Tian, S.-X., and Wang, S.-Z. (2011). Dynamic modeling and simulation of a manipulator with joint inertia. *Communications in Computer and Information Science*, *86 CCIS*, pp. 10-16.

360. Tinós, R., Terra, M. H., and Ishihara, J. Y. (2006). Motion and force control of cooperative robotic manipulators with passive joints. *IEEE Transactions on Control Systems Technology*, *14*(4), 725-734.

361. Trivailo, P. M. (2006). Non-linear dynamic modelling of composite systems of multiple flexible robotic manipulators. Paper presented at the *AIAA 57th International Astronautical Congress, IAC 2006, 8*, 5133-5152.

362. Trivailo, P. M., Plotnikova, L. A., Gilbert, T. G., and Williams, P. (2005). Dynamic stress analysis of variable geometry telescopic multi-link flexible robotic systems during their reconfiguration. Paper presented at the *International Astronautical Federation - 56th International Astronautical Congress*, *5*, 2958-2983.

363. Ubertini, F. (2000). A contribution to the analysis of flexible link systems, *International Journal of Solids and Structures*, 37 (2000), 969-990.

364. Uchiyama, M. (1990). A unified approach to load sharing, motion decomposing, and force sensing of load sensing of dual arm robots. *Robotics Research: 5th Int. Symp., ed. by H. Miura, S. arimoto, MIT*, pp. 225-232.

365. Uchiyama, M., and Dauchez, P. (1988). A symmetric hybrid position/force control scheme for the coordination of two robots. *IEEE Int. conf. on Robotics and Automation*, Philadelphia, pp. 350-356.

366. Uchiyama, M., and Dauchez, P. (1993). Symmetric kinematic formulation and non master/slave control of two-arm robots. *Adv. Robot.*, 7(4), 361-383.

367. Uchiyama, M., and Kanamori, Y. (1992). Quadratic programming for dexterous dual-arm manipulation. *In: Robotics, Mechatronics and Manufacturing Systems, Trans. IMACS/SICE Int. Symp. On Robotics, Mechatronics and Manufacturing Systems*, Kobe, Japan, pp. 367-372.

368. Uchiyama, M., and Kanno, A. (1996). Modelling controllability and vibration suppression of 3D flexible robots. *Robotics Research, 7th Int. Symp.*, London, pp. 90-99.

369. Uchiyama, M., and Yamashita, T. (1991). Adaptive Load sharing for hybrid controlled two manipulators. *IEEE Int. Conf. on Robotics and Automation*, Sacramento, pp.986-991.

370. Udai, A. D., Salunkhe, D. H., Dutta, A., and Mukherjee, S. (2017). Force/position control of 3 DOF delta manipulator with voice coil actuator. *ACM International Conference Proceeding Series, Part F132085.* doi:10.1145/3132446.313489

371. Ueda, J., and Yoshikawa, T. (2004). Mode-shape compensator for improving robustness of manipulator mounted on flexible base. *IEEE Transactions on Robotics and Automation, 20*(2), 256-268.

372. Ulrich, S., Sasiadek, J. Z., and Barkana, I. (2012). Modeling and direct adaptive control of a flexible-joint manipulator. *Journal of Guidance, Control, and Dynamics, 35*(1), 25-39.

373. Urrea, C., and Coltters, J. P. (2015). Design and implementation of a graphic 3d simulator for the study of control techniques applied to cooperative robots. *International Journal of Control, Automation, and Systems*, 13(6), 1476-1485. doi: 10.1007/s12555-014-0278-y

374. Usoro, P. B., Nadira, R., and Mahil, S. S. (1986). A finite element/Lagrange approach to modeling lightweight flexible manipulators. *Journal of Dynamic Systems, Measurement, and Control* 108, 198-205.

375. Vakil, M., Fotouhi, R., Nikiforuk, P. N., and Salmasi, H. (2008). A constrained lagrange formulation of multilink planar flexible manipulator. *Journal of Vibration and Acoustics, Transactions of the ASME, 130*(3).

376. Vakil, M., Fotouhi, R., and Nikiforuk, P. N. (2012). A new method for dynamic modeling of flexible-link flexible-joint manipulators. *Journal of Vibration and Acoustics, Transactions of the ASME, 134*(1).

377. Vidoni, R., Boscariol, P., Gasparetto, A., and Giovagnoni, M. (2012). Kinematic and dynamic analysis of flexible-link parallel robots by means of an erls approach. Paper presented at the *Proceedings of the ASME Design Engineering Technical Conference, , 4*(PARTS A AND B) 1449-1458.

378. Vidoni, R., Gasparetto, A., and Giovagnoni, M. (2013). Design and implementation of an ERLS-based 3-D dynamic formulation for flexible-link robots. *Robotics and Computer-Integrated Manufacturing, 29*(2), 273-282.

379. Wai, R.-J., and Muthusamy, R. (2013). Fuzzy-neural-network control for robot manipulator via sliding-mode design. Paper presented at the *2013 9th Asian Control Conference, ASCC 2013,*

380. Wai, R.-J., and Yang, Z. -W. (2008). Adaptive fuzzy neural network control design via a T-S fuzzy model for a robot manipulator including actuator dynamics. *IEEE Transactions on Systems, Man, and Cybernetics, Part B: Cybernetics, 38*(5), 1326-1346.

381. Walker, I. D., Marcus, S. I., and Freeman, R. A. (1989). Distribution of dynamic loads for multiple cooperating robot manipulators. *J. Robot Syst.,* 6, pp. 35-47.

382. Walker, I. D., Freeman, R. A., and Marcus, S. I. (1991). Analysis of motion and internal force loading of objects grasped by multiple cooperating manipulators. *Int. J. Robot. Res.* 10(4), 396-409.

383. Walsh, A., and Forbes, J. R. (2012). Dynamic modelling and control of flexible robotic space manipulators with telescoping booms. Paper presented at the *Proceedings of the International Astronautical Congress, IAC, 8,* 5998-6008.

384. Wang, B., Yan, D., Fang, S., and Jin, Y. (2012). Dynamics modeling of slipping collision of robot and impact response under different stiffness. *Nongye Gongcheng Xuebao/Transactions of the Chinese Society of Agricultural Engineering, 28*(7), 51-56.

385. Wang, G. (2011). Simulations of the trajectory tracking and vibration suppression control of flexible-link robot arm. *International Conference on Intelligent System Design and Engineering Application, ISDEA 2010, 2,* 387-390.

386. Wang, H., and Xia, X. P. (2013). Simulation of manipulator with flexible joint. *Applied Mechanics and Materials,* 327, 999-1003.

387. Wang, J., Cui, X., Chen, W., and Jin, Y. (2012). Dynamic analysis of cable-driven humanoid arm based on lagrange's equation. Paper presented at the *Advances in Reconfigurable Mechanisms and Robots I,* 619-628.

388. Wang, Y., and Huston, R. L. (1994). A lumped parameter method in the nonlinear analysis of flexible multibody systems. *Computers and Structures* 50(3), 421-432.

389. Wang, Y., Ikeura, R., Sawai, H., and Hayakawa, S. (2010). Analysis of human arm characteristics in cooperative motion based on musculoskeletal model. Paper presented at the *3rd IEEE RAS and EMBS International Conference on Biomedical Robotics and Biomechatronics, BioRob 2010,* 301-306.

390. Wang, Z., Yi, Z., and Luo, Y. (2015). Energy-based formulation for nonlinear normal modes in cable-stayed beam. *Applied Mathematics and Computation,* 265, 176–186.

391. Wasfy, T. M., and Noor, A. K. (2003). Computational strategies for flexible multibody systems. *Applied Mechanics Reviews, 56*(6), 553-613.

392. Weia, M. H., Lin, K., Jin, L., and Zou, D. J. (2016). Nonlinear dynamics of a cable-stayed beam driven by sub-harmonic and principal parametric resonance. *International Journal of Mechanical Sciences,* 110, 78-93.

393. Wen, J. T., and Kreutz-Delgaudo, K. (1992). Motion and force control of multiple robotic manipulators. *Automatica*, 28(4), pp. 729-743.

394. Williams, D. and Khatib, O. (1993). The virtual linkage: a model for internal forces in multi-grasp manipulation. *IEEE Int. Conf. on Robotics and Automation*, Atlanta, 1993, pp. 1025-1030.

395. Wu, S.-T., Tang, S.-Q., Huang, K.-P. (2018). Vibration attenuation of a two-link flexible carried by a translational stage. *Journal of Vibration and Control,* 24 (23), 5650-5664.

396. Xia, Y., Fujino, Y. (2006). Auto-parametric vibration of a cable-stayed-beam structure under random excitation. *Journal of Engineering Mechanics*, 132 (3), 279-286.

397. Xu, G., and Sun, C. (2013). Dynamic modeling and stiffness coefficient analysis of a 3-DOF flexible joint space manipulator. *5th International Conference on Intelligent Human-Machine Systems and Cybernetics, IHMSC 2013, 2,* 171-174.

398. Xu, Q., Jing, Z., Hu, S. (2018). Stability analysis of nonlinear dynamic system with linear observer for a multilink flexible manipulator. *International Journal of Non-Linear Mechanics,* 103 (2018), 27-36.

399. Xu, W., Yan, L., Hu, Z., Liang, B. (2019). Area-oriented coordinated trajectory planning of dual-arm space robot for capturing a tumbling target. *Chinese Journal of Aeronautics*, 32(9), 2151-2163.

400. Xu, Y.-J., Li, Y.-C., and Zhao, X.-H. (2013). Modeling and trajectory tracking control of vehicle hydraulic rigid-flexible manipulator based on the expected joint angle compensation. *Jilin Daxue Xuebao (Gongxueban)/Journal of Jilin University (Engineering and Technology Edition), 43*(5), 1367-1374.

401. Yamakawa, Y., Odani, K., and Ishikawa, M. (2016). Sonic-speed manipulation of a bull whip using a robot manipulator. *IEEE International Conference on Advanced Intelligent Mechatronics (AIM), Alberta, Canada*, July 12-15, 201

402. Yamano, M., Kim, J.-S., Konno, A., and Uchiyama, M. (2004). Cooperative control of a 3D dual-flexible-arm robot, *J. Intell. Robot Syst*., 39, 1-15.

403. Yan, Z., Lai, X., Meng, Q., and Wu, M. (2021). A novel robust control method for motion control of uncertain single-link flexible-joint manipulator. *IEEE Transactions on Systems, Man, and Cybernetics: Systems*, 51(3).

404. Yang, C., Geng, S., Walker, I., Branson, D. T., Liu, J., Dai, J. S., and Kang, R. (2020). Geometric constraint-based modeling and analysis of a novel continuum robot with Shape Memory alloy initiated variable stiffness. *The International Journal Robotics Research*, 39(14), 1620-1634.

405. Yang, T., Yan, S., Ma, W., and Han, Z. (2016). Joint dynamic analysis of space manipulator with planetary gear train transmission. *Robotica*, 34(05), 1042-1058.

406. Yavuz, Ş. (2019). An enhanced method to control the residual vibrations of a single-link flexible glass fabric reinforced epoxy-glass composite manipulator. *Composites Part B*, 159 (2019), 405-417.

407. Yoo, S. J. (2014). Distributed adaptive containment control of networked flexible-joint robots using neural networks. *Expert Systems with Applications, 41*(2), 470-477.

408. Yoo, S. J., Choi, Y. H., and Park, J. B. (2007). Dynamic surface controller for flexible joint robots without velocity measurements. Paper presented at the *ICCAS 2007 - International Conference on Control, Automation and Systems*, 1098-1102.

409. Yoo, S. J., Choi, Y. H., and Park, J. B. (2008). A study on simple adaptive control of flexible-joint robots considering motor dynamics. *Journal of Institute of Control, Robotics and Systems, 14*(11), 1103-1109.

410. Yoo, S. J., Park, J. B., and Choi, Y. H. (2006). Adaptive dynamic surface control of flexible-joint robots using self-recurrent wavelet neural networks. *IEEE Transactions on Systems, Man, and Cybernetics, Part B: Cybernetics, 36*(6), 1342-1355.

411. Yoo, S. J., Park, J. B., and Choi, Y. H. (2008). Adaptive output feedback control of flexible-joint robots using neural networks: Dynamic surface design approach. *IEEE Transactions on Neural Networks, 19*(10), 1712-1726.

412. Yoshikawa, T., and Zheng, X. (1993). Coordinated dynamic hybrid position force control of multiple robot manipulators handling one constrained object. *Int. J. Robot. Res.*. 12, 1993, pp.219-230.

413. Yu, J., Liu, L., and Tan, M. (2007). Dynamic modeling of multi-link swimming robot capable of 3-D motion. Paper presented at the *Proceedings of the 2007 IEEE International Conference on Mechatronics and Automation, ICMA 2007,* 1322-1327.

414. Yu, J., Liu, L., and Wang, L. (2006). Dynamic modeling of robotic fish using schiehlen's method. Paper presented at the *2006 IEEE International Conference on Robotics and Biomimetics, ROBIO 2006,* 457-462.

415. Yu, S.-C., Yuh, J., and Kim, J. (2013). Armless underwater manipulation using a small deployable agent vehicle connected by a smart cable. *Ocean Engineering*, *70*, 149-159.

416. Yukawa, T., Uchiyama, M., Nenchev, D. N., and Inooka, H. (1996). Stability of control system in handling of a flexible object by rigid arm robots. Paper presented at the *Proceedings - IEEE International Conference on Robotics and Automation, 3,* 2332-2339.

417. Yurkevich, V. D. (2016). Multi-channel control system design for a robot manipulator based on the time-scale method. *Optoelectronics, Instrumentation and Data Processing*, 52(2), 196-202. doi: 10.3103/S875669901602013

418. Zavodney, L. D., and Nayfeh, A. H. (1989). The non-linear response of a slender beam carrying a lumped mass to a principal parametric excitation: theory and experiment. *Int. J. Of Non-Linear Mechanics*, 24(2), 105-125.

419. Zavrazhina, T. V. (2007). Influence of the flexibility of links on the dynamics of a multilink robot manipulator. *International Applied Mechanics, 43*(5), 577-585.

420. Zeng, H., and Sepehri, N. (2004). Design of a nonlinear position regulator for cooperating hydraulic manipulators handling a rigid object. Paper presented at the *American Society of Mechanical Engineers, Dynamic Systems and Control Division (Publication) DSC, 73*(1 Part A), 361-368.

421. Zeng, H., and Sepehri, N. (2005). Non-linear position control of cooperative hydraulic manipulators handling unknown payloads. *International Journal of Control, 78*(3), 196-207.

422. Zhai, A., Zhang, H., Wang, J., Lu, G., Li, J., and Chen, S. (2022). Adaptive neural synchronized impedance control for cooperative manipulators processing under uncertain environments. *Robotics and Computer-Integrated Manufacturing,* 75(2022), 102291.

423. Zhan, B., Jin, M., Yang, G., and Zhang, C. (2020). A novel strategy for space manipulator detumbling a non-cooperative target with collision avoidance. *Advances in Space Research, 66*(4), 785-799. doi: 10.1016/j.asr.2020.05.045

424. Zhang, C., and Yu, Y. (2003). Dynamic modeling and analysis for the cooperation of flexible manipulators. *Jixie Gongcheng Xuebao/Chinese Journal of Mechanical Engineering, 39*(5), 49-54.

425. Zhang, C.-X., and Yu, Y.-Q. (2004). Dynamic analysis of planar cooperative manipulators with link flexibility. *Journal of Mechanical Design, Transactions of the ASME, 126*(3), 442-448.

426. Zhang, D.-G., and Angeles, J. (2005). Impact dynamics of flexible-joint robots. *Computers and Structures, 83*(1), 25-33.

427. Zhang, D.-G., and Zhou, S.-F. (2006). Dynamic analysis of flexible-link and flexible-joint robots. *Applied Mathematics and Mechanics (English Edition), 27*(5), 695-704.

428. Zhang, L.-M., and Mei, J.-P. (2011). Optimization of dimension parameters of delta manipulator based on natural frequency. *Journal of Tianjin University Science and Technology,* 44(10), 901-906.

429. Zhang, Q., Zhang, X., and Liang, J. (2012). Dynamic analysis of planar 3-RRR flexible parallel robot. Paper presented at the *2012 IEEE International Conference on Robotics and Biomimetics, ROBIO 2012 - Conference Digest,* 154-159.

430. Zhang, Q.-H., and Zhang, X.-M. (2012). Elastodynamic analysis of planar 3-RRR and 3-PRR flexible parallel robots. *Huanan Ligong Daxue Xuebao/Journal of South China University of Technology (Natural Science), 40*(11), 52-57.

431. Zhang, Q.-H., and Zhang, X.-M. (2013). Dynamic modeling and analysis of planar 3-RRR flexible parallel robots. *Zhendong Gongcheng Xuebao/Journal of Vibration Engineering, 26*(2), 239-245.

432. Zhang, Y., Guo, D., Cai, B., and Chen, K. (2011). Remedy scheme and theoretical analysis of joint-angle drift phenomenon for redundant robot manipulators. *Robotics and Computer-Integrated Manufacturing, 27*(4), 860-869.

433. Zhang, L., and Liu, J. (2012). Nonlinear PDE observer design for a flexible two-link manipulator. Paper presented at the *Proceedings of the American Control Conference*, 5336-5341.

434. Zhang, L.-M., and Mei, J.-P. (2011). Optimization of dimension parameters of delta manipulator based on natural frequency. *Tianjin Daxue Xuebao (Ziran Kexue Yu Gongcheng Jishu Ban)/Journal of Tianjin University Science and Technology, 44*(10), 901-906.

435. Zhang, X., Mills, J. K., and Cleghorn, W. L. (2010). Investigation of axial forces on dynamic properties of a flexible 3-PRR planar parallel manipulator moving with high speed. *Robotica, 28*(4), 607-619.

436. Zhang, Z., Zheng, L., Chen, Z., Kong, L., and Karimi, H. R. (2021). Mutual-collision-avoidance scheme synthesized by neural networks for dual redundant robot manipulators executing cooperative tasks. *IEEE Transactions on Neural Networks and Learning Systems*, 32(3), 1052-1066.

437. Zhao, K., Wang, H., Chen, G., and Zhao, Y. (2010). Kineto-static stiffness mapping based on finite element analysis for robot manipulators. Paper presented at the *Proceedings of the ASME International Design Engineering Technical Conferences and Computers and Information in Engineering Conference, DETC2009, 7*(Part B), 1069-1077.

438. Zhao, Tiejun (2010). Design of a Redundant Arm for Yiren Humanoid Robot. *International Conference on Intelligent Control and Information Processing*, August 13-15, Dalian, China, 2010.

439. Zhao, T. (2010). Effect and Motion Planning of Waist for Humanoid Robot Dynamic Stability. *2010 International Conference, Wuhan, 26-28 June 2010,* 6146-6149.

440. Zhao, T. J. (2011). Dynamic cooperative manipulating pattern generation for mobile humanoid robot using waist moment compensation. *Advanced Materials Research,* 201-203, 1978-1982.

441. Zhao, Y., and Bai, Z. F. (2011). Dynamics analysis of space robot manipulator with joint clearance. *Acta Astronautica, 68*(7-8), 1147-1155.

442. Zheng K., Hua, Y., and Yu W. (2020). A novel parallel recursive dynamics modeling method for Robot with flexible bar-groups. *Applied Mathematical Modelling,* 77, 267-288.

443. Zheng, Y. F. (1989). Dynamic and Kinematic Behaviour of Two Coordinating Robots in Assembly. *Mathematical and Computer Modelling,* 12(1), 77-88.

444. Zheng, Y. F., and Chen, M. Z. (1993). Trajectory planning for two manipulators to deform flexible beams. Paper presented at the *Proceedings - IEEE International Conference on Robotics and Automation, Atlanta, 1,* 1019-1024.

445. Zheng, Y. F., and Luh, J. Y. S. (1989). Optimal load distribution for two industrial robots handling a single object. *Journal of Dynamic Systems, Measurement and Control, Transactions of the ASME, 111*(2), 232-237.

446. Zhengsheng, C., Minxiu, K., Ming, L., and Wei, Y. (2013). Dynamic modelling and trajectory tracking of parallel manipulator with flexible link. *International Journal of Advanced Robotic Systems, 10,* 328.

447. Zhicheng, Q. (2006). Dynamic characteristics' analysis of contact force response for the flexible joint manipulator system. Paper presented at the *Proceedings of the World Congress on Intelligent Control and Automation (WCICA), 1,* 1410-1414.

448. Zhiqian, W., Zhuangpeng, Y., and Yingshe, L. (2015). Energy-based formulation for nonlinear normal modes in cable-stayed beam. *Applied Mathematics and Computation,* 265(C), 176–186.

449. Zhong, Y., Hu, L., and Xu, Y. (2020). Recent advances in design and actuation of continuum robots for medical applications. *Actuators,* 9(142). doi:10.3390/act904014

450. Zhou, H., Yang, G., Lv, H., Huang, X., Yang, H., and Pang, Z. (2020). IoT-enabled dual-arm motion capture and mapping for telerobotics in home care. *IEEE Journal of Biomedical and Health Informatics, 24*(6), 1541-1549. doi:10.1109/JBHI.2019.295388

451. Zhou, J., and Yu, Y. (2011). Dynamic parameter identification of modular robot with flexible joints. *Jiqiren/Robot, 33*(4), 440-448.

452. Zhu, C.-X., Zhu, L.-D., Liu, Y.-X., and Cai, G.-Q. (2008). Stress analysis on flexible links of parallel machine tool based on ADAMS and ANSYS. *Dongbei Daxue Xuebao/Journal of Northeastern University, 29*(SUPPL. 2), 52-55.

453. Zhu, W.-H., Bien, Z., and De Schutter, J. (1998). Adaptive motion/force control of multiple manipulators with joint flexibility based on virtual decomposition. *IEEE Transactions on Automatic Control, 43*(1), 46-60.

454. Zi, B., Duan, B., and Du, J. (2007a). Dynamic modeling and numerical simulation of cable-driven parallel manipulator. *Jixie Gongcheng Xuebao/Chinese Journal of Mechanical Engineering, 43*(11), 82-88.

455. Zi, B., Duan, B.-Y., Du, J.-L., and Bao, H. (2007b). Modeling and active control of a cable-suspended parallel manipulator. *Zhendong Yu Chongji/Journal of Vibration and Shock, 26*(3), 96-100.

456. Zi, B., Qian, S., Ding, H., and Kecskeméthy, A. (2012). Design and analysis of cooperative cable parallel manipulators for multiple mobile cranes. *International Journal of Advanced Robotic Systems, 9*.

457. Zomaya, A. Y. (1993). Modelling and Simulation of Robot Manipulators: A Parallel Processing Approach, *World Scientific series in Robotics and Automated systems*, 8.

List of Publications

1. **Rajesh Ranjan and Santosha K. Dwivedy,** 'Dynamic analysis and control of a string-stiffened single-link flexible manipulator with flexible joint', *Mechanics Based Design of Structures and Machines*, 0 (0), 1-31, 2022. doi: 10.1080/15397734.2022.2040364 (A Q1 Journal, Impact factor-4.364 (2021)).

2. **Rajesh Ranjan and Santosha K. Dwivedy,** 'Dynamic analysis and robust control of a string-stiffened two-link rigid-flexible manipulator', (First review done in the journal *Mechanics Based Design of Structures and Machines*).

3. **Rajesh Ranjan and Santosha K. Dwivedy,** 'Parametric study of double link flexible manipulator under gravitational load'. (Submitted in the Journal: Applied Mathematical Modelling).
4. **Rajesh Ranjan and Santosha K. Dwivedy,** 'Finite element analysis and control of a string-stiffened single-link flexible manipulator with flexible joint', (to be submitted).

5. **Rajesh Ranjan and Santosha K. Dwivedy,** 'Dynamic analysis and optimal control of a single-link flexible manipulator', *Proceedings of the XVII Vibration Engineering & Technology of Machinery Conference, VETOMAC 2022, December 15 - 17, 2022, DMAE, IOE Pulchowk, Nepal (paper submitted).*

6. **Rajesh Ranjan, Saleendra Haribabu, and Santosha K. Dwivedy,** *'Dynamic analysis of flexible joint and single flexible link manipulator by using finite element analysis',* Proceedings of the XVI Vibration Engineering & Technology of Machinery Conference, VETOMAC 2021, Bengaluru, India, *December 16-18, 2021.*

7. **Rajesh Ranjan, Saleendra Haribabu, and Santosha K. Dwivedy**, *'Dynamic analysis of flexible joint and single flexible link manipulator by using finite element analysis',* Book Chapter, Springer Nature. *(Letter of acceptance received.)*

8. **Rajesh Ranjan and Santosha K. Dwivedy,** 'Forward dynamic analysis of a 3r manipulator', *iNaCoMM 2017, BARC, Mumbai, India*, Dec. 13-15, 2017.

9. **Rajesh Ranjan and Santosha K. Dwivedy,** 'Dynamic analysis of a single link flexible manipulator', *International Conference on Complex Dynamical Systems and Applications (CDSA)-2017, IIT Guwahati, Guwahati, India*, Dec. 4-6, 2017.
10. **Rajesh Ranjan and S. K. Dwivedy,** 'Kinematic and dynamic analyses of 3-link cooperative manipulators handling hazardous chemicals', *ICCMS Conference 2016, IIT Bombay, Mumbai, India*, June 27-July 1, 2016.